VOLUME 76 MAY 11, 1972 NUMBER 10

JPCHAx

THE JOURNAL OF PHYSICAL CHEMISTRY

PUBLISHED BIWEEKLY BY THE AMERICAN CHEMICAL SOCIETY

ANELASTIC RELAXATION IN CRYSTALLINE SOLIDS

by A. S. NOWICK, Henry Krumb School of Mines, Columbia Univ., N. Y., **and B. S. BERRY,** Thomas J. Watson Res. Center, IBM Corp., Yorktown Heights, N. Y.

CONTENTS: Characterization of Anelastic Behavior. Relations Among the Response Functions: The Boltzmann Superposition Principle. Mechanical Models and Discrete Spectra. Continuous Spectra. Internal Variables and the Thermodynamic Basis for Relaxation Spectra. Anisotropic Elasticity and Anelasticity. Point Defects and Atom Movements. Theory of Point-Defect Relaxation. The Snoek Relaxation. The Zener Relaxation. Other Point-Defect Relaxations. Dislocations and Crystal Boundaries. Dislocation Relaxations. Further Dislocation Effects. Boundary Relaxation Processes and Internal Friction at High Temperatures. Relaxations Associated with Phase Transformations. Thermoelastic Relaxation and the Interaction of Acoustic Waves with Lattice Vibrations. Magnetoelastic Relaxations and Hysteresis Damping of Ferromagnetic Materials. Electronic Relaxation and Related Phenomena. Experimental Methods. Appendices.

1972, 698 pp., $27.50

METHODS IN X-RAY CRYSTALLOGRAPHY

by J. W. JEFFREY, Dept. of Crystallography, Birkbeck College, Univ. of London

Dealing primarily with photographic methods, the book contains detailed descriptions of the construction and use of X-ray cameras and ancilliary equipment. This book also contains special features: a simple but novel energy analysis of X-ray diffraction which requires only the ideas of the addition of amplitudes for constructive interference, and of intensities in the case of random phases; and a chapter on the production and detailed interpretation of divergent beam photographs.

1971, 580 pp., $35.00

GROUP THEORY AND ITS APPLICATIONS

Volume 2

edited by ERNEST M. LOEBL, Polytechnic Inst. of Bklyn., N. Y.

CONTENTS: W. J. HOLMAN, III and L. C. BIEDENHARN: The Representations and Tensor Operators of the Unitary Groups. HAROLD V. McINTOSH: Symmetry and Degeneracy. CARL E. WULFMAN: Dynamical Agents in Atomic and Molecular Physics. STIG FLODMARK and ESKO BLOKKER: Symmetry Adaptation of Physical States by Means of Computers. JEAN-MARC LEVY-LEBLOND: Galilei Groups and Galilean Invariance.

1971, 328 pp., $18.50

IONIC INTERACTIONS

From Dilute Solutions to Fused Salts

edited by SERGIO PETRUCCI, Dept. of Chemistry, Polytechnic Inst. of Brooklyn, N. Y.

Volume 1/**EQUILIBRIUM AND MASS TRANSPORT**

CONTENTS: H. FALKENHAGEN and W. EBELING: Equilibrium Properties of Ionized Dilute Electrolytes. H. FALKENHAGEN, W. EBELING, and W. D. KRAEFT: Mass Transport Properties of Ionized Dilute Electrolytes. S. PETRUCCI: Statistical Thermodynamics of Ionic Association and Complexation in Dilute Solutions of Electrolytes. J. BRAUNSTEIN: Statistical Thermodynamics of Molter Salts and Concentrated Aqueous Electrolytes. C. T. MOYNIHAN: Mass Transport in Fused Salts.

1971, 421 pp., $19.50

Volume 2/**STRUCTURE AND KINETICS**

CONTENTS: C. H. LANGFORD: Complex .Formation and Solvent-Exchange Kinetics: A Dynamic Approach to Electrolyte Solutions. S. PETRUCCI: Kinetic Approach to the Study of Ionic Association and Complexation: Relaxation Kinetics. S. L. HOLT: Ultraviolet and Visible Spectra of Electrolyte Solutions and Fused Salts. D. E. IRISH: Vibrational Spectral Studies of Electrolyte Solutions and Fused Salts.

1971, 292 pp., $16.50

COMPUTER PROGRAMS FOR CHEMISTRY, Volume 4

edited by DeLOS F. DeTAR, Florida State Univ.

Computer Programs for Chemistry provides chemists with listings and descriptions of tested well-constructed FORTRAN programs-each of which performs a clearly defined calculation or other operation. The programs in Volume 4 will be of interest to many chemists—e.g., LSKIN2, CDORD, and EQCENT. In addition, there are programs that can be applied by anyone working with computers—GENLSS, FRS3, EDITQ, and EDITID. This volume also includes a number of FORTRAN subroutines for conversion between binary coded numbers and their integer or real representation, as well as packing and unpacking routines. A tape copy of the program in Volume 4 contains over 15,000 card images of programs and test data. This tape copy can be obtained from the publisher.

May 1972, about 300 pp., in preparation

CRYSTAL CHEMISTRY AND SEMICONDUCTION

In Transition Metal Binary Compounds

by JACQUES SUCHET, Instutut fur Anorganische Chemie, Stuttgart, Germany, on leave from Centre National de la Recherche Scientifique, Paris

Provides the chemist and physicochemist with a detailed introduction to the problems of semiconduction in transition metals and rare earth compounds. The book provides the knowledge of crystal chemistry and crystal physics that is necessary for understanding past work on the mixed valency oxides and presents investigations of the conduction process in crystals containing "magnetic" atoms—i.e., transition metal or rare earth atoms.

1971, 400 pp., $22.00

THE SCATTERING OF LIGHT

And Other Electromagnetic Radiation

by MILTON KERKER, Clarkson College of Tech., Potsdam, N. Y.

REVIEWS:

"... an excellent book presenting an impressive amount of useful information. The book should prove valuable to all who work on problems that involve electromagnetic scattering."—*Bulletin American Meteorological Society, April 1971*

"This is a book which will eminently serve to bring the pundit up to date in the theory and practice of electromagnetic scattering, and also provide a comprehensible account for the research worker who seeks to obtain an understanding of the phenomena."—*The Faraday Society, September 1971*

"... an excellent treatise of light scattering using the new results from many disciplines. This book is useful to anyone irrespective of his particular narrow field of interest."—*Journal of the Franklin Institute, October 1970*

1969, 666 pp., $33.50

ADVANCES IN HIGH TEMPERATURE CHEMISTRY

Volume 4

edited by LEROY EYRING, Dept. of Chemistry, Arizona State Univ., Tempe

CONTENTS: D. E. MILLIGAN and MARILYN E. JACOX: Infrared and Ultraviolet Spectroscopic Studies of a Number of Small Free Radicals and Molecular Ions in a Matrix Environment. R. F. PETERSON, Jr. and R. WOLFGANG: The Elementary Reactions of Atomic Carbon. W. L. WORRELL: Dissociation of Gaseous Molecules on Solids at High Temperature. G. L. DEPOORTER and T. C. WALLACE: Diffusion in Binary Carbides. G. A. SOMOBJAI and F. J. SZALKOWSKI: Auger Electron Spectroscopy on Surfaces. R. F. BARROW aud C. COUSINS: Spectroscopic Properties of ihe Gaseous Diatomic Sulfides. L. S. NELSON: Techniques for Studying Liquids and Solids at Extreme Temperatures. C. C. HERRICK: Automatic Data Acquisition and Its Treatment. A. L. BOWMAN and G. P. ARNOLD: High Temperature Neutron Diffraction Studies.

1972, 296 pp., $17.50

THE JOURNAL OF PHYSICAL CHEMISTRY

Volume 76

MAY—AUGUST 1972

PAGES 1389—2642

AMERICAN CHEMICAL SOCIETY

BOOKS AND JOURNALS DIVISION

JOHN K CRUM
Director

JOSEPH H. KUNEY
Head, Business Operations Department

RUTH REYNARD
Assistant to the Director

THE JOURNAL OF

PHYSICAL CHEMISTRY

 Published biweekly by the American Chemical Society at 20th and Northampton Sts., Easton, Pa. 18042. Second-class postage paid at Washington, D. C., and at additional mailing offices.

All manuscripts should be sent to *The Journal of Physical Chemistry*, Department of Chemistry, University of Minnesota, Minneapolis, Minn. 55455.

Additions and Corrections are published once yearly in the final issue. See Volume 75, Number 26 for the proper form.

Extensive or unusual alterations in an article after it has been set in type are made at the author's expense, and it is understood that by requesting such alterations the author agrees to defray the cost thereof.

The American Chemical Society and the Editor of *The Journal of Physical Chemistry* assume no responsibility for the statements and opinions advanced by contributors.

Correspondence regarding accepted copy, proofs, and reprints should be directed to Editorial Production Office, American Chemical Society, 20th and Northampton Sts., Easton, Pa. 18042. Manager: CHARLES R. BERTSCH. Assistant Editor: EDWARD A. BORGER.

Advertising Office: Century Communications Corporation, 142 East Avenue, Norwalk, Conn. 06851.

Business and Subscription Information

Remittances and orders for subscriptions and for single copies, notices of changes of address and new professional connections, and claims for missing numbers should be sent to the Subscription Service Department, American Chemical Society, 1155 Sixteenth St., N.W., Washington, D. C. 20036. Allow 4 weeks for changes of address. Please include an old address label with the notification.

Claims for missing numbers will not be allowed (1) if received more than sixty days from date of issue, (2) if loss was due to failure of notice of change of address to be received before the date specified in the preceding paragraph, or (3) if the reason for the claim is "missing from files."

Subscription rates (1972): members of the American Chemical Society, $20.00 for 1 year; to nonmembers, $60.00 for 1 year. Those interested in becoming members should write to the Admissions Department, American Chemical Society, 1155 Sixteenth St., N.W., Washington, D. C. 20036. Postage to Canada and countries in the Pan-American Union, $5.00; all other countries, $6.00. Single copies for current year: $3.00. Rates for back issues from Volume 56 to date are available from the Special Issues Sales Department, 1155 Sixteenth St., N.W., Washington, D. C. 20036.

This publication and the other ACS periodical publications are now available on microfilm. For information write to: MICROFILM, Special Issues Sales Department, 1155 Sixteenth St., N.W., Washington, D. C. 20036.

Notice to Authors last printed in the issue of December 23, 1971

THE JOURNAL OF

PHYSICAL CHEMISTRY

Volume 76, Number 10 May 11, 1972

JPCHAx 76(10) 1389–1510 (1972)

COMMUNICATIONS TO THE EDITOR

AUTHOR INDEX

In papers with more than one author the name of the author to whom inquiries about the paper should be addressed is marked with an asterisk in the by-line.

THE JOURNAL OF
PHYSICAL CHEMISTRY

VOLUME 76, NUMBER 10 MAY 11, 1972

Production of Triplet Methylene in the Reaction of Carbon Atoms with Hydrogen

by Timothy L. Rose[1]

Texas A&M University, College Station, Texas 77843 *(Received November 10, 1971)*

Publication costs assisted by the Petroleum Research Fund

The reactions of free carbon atoms in hydrogen–cyclopentadiene samples were studied using the nuclear recoil technique. A comparison of these hot-atom results with photochemical methylene studies shows that the carbon atoms react with hydrogen to produce methylene which is almost entirely in the triplet state.

Recently several papers have appeared concerning the reaction of carbon atoms with hydrogen.[2,3] Ground-state $C(^3P)$ atoms produced by photolysis of C_3O_2 react rapidly with hydrogen.[2a] It was assumed that vibrationally excited methylene (CH_2^*) was formed which is then collisionally stabilized. Carbon atoms produced by the nuclear recoil technique indeed react with hydrogen to give methylene. The spin state of the methylene produced was not identified although the importance of $^3CH_2$ was postulated.[3a] The present paper presents evidence that the methylene produced in the recoil system is almost entirely in the triplet state. This result is in contrast to the situation for hot carbon atoms reacting in alkane systems where the methylene formed is predominantly in the singlet state.[3b,4] The recoil technique with hydrogen present, therefore, may prove to be a useful source of triplet methylene for studies on the effect of spin state on methylene reactions, a subject of current interest in the literature.[5–8]

The nuclear recoil method[9] was used to produce hot radioactive carbon-11 atoms (20.5-min half-life) in a 20:1 hydrogen–cyclopentadiene (CPD) sample. Since the reactions of free ^{11}C with CPD have been characterized previously,[10] changes in the product spectrum were attributed to trapping by the CPD of radicals formed in the reaction of carbon with hydrogen. The products formed were identified and assayed by standard radio gas chromatographic techniques.[10–12] Absolute yields of the products were determined using ethane as an external monitor of the number of carbon atoms produced.[13] No determination was made of products having more than six carbon atoms.

Table I lists the products whose yields increased when hydrogen was added to the CPD. The other products formed which are not listed are attributed to the direct reaction of carbon with CPD.[10,12] The effect

(1) National Institutes of Health Predoctoral Fellow, 1965–1967.

(2) (a) W. Braun, A. M. Bass, D. D. Davis, and J. D. Simmons, *Proc. Roy. Soc., Ser. A*, **312**, 417 (1969); (b) F. F. Martinotte, M. J. Welch, and A. P. Wolf, *Chem. Commun.*, 115 (1968).

(3) (a) C. MacKay, J. Nicholas, and R. Wolfgang, *J. Amer. Chem. Soc.*, **89**, 5758 (1967); (b) R. F. Peterson, Jr., Ph.D. Thesis, Yale University, 1970.

(4) M. J. Welch and A. P. Wolf, *J. Amer. Chem. Soc.*, **91**, 6584 (1969).

(5) T. W. Eder and R. W. Carr, Jr., *J. Phys. Chem.*, **73**, 2074 (1969); *J. Chem. Phys.*, **53**, 2258 (1970).

(6) (a) P. S. T. Lee, R. L. Russell, and F. S. Rowland, *Chem. Commun.*, 19 (1970); (b) R. L. Russell and F. S. Rowland, *J. Amer. Chem. Soc.*, **90**, 1671 (1968).

(7) W. G. Clark, D. W. Setser, and E. E. Siefert, *J. Phys. Chem.*, **74**, 1670 (1970).

(8) D. F. Ring and B. S. Rabinovitch, *Int. J. Chem. Kinet.*, **1**, 11 (1969); *Can. J. Chem.*, **46**, 2435 (1968).

(9) (a) C. MacKay and R. Wolfgang, *Science*, **148**, 899 (1965); (b) A. P. Wolf, *Advan. Phys. Org. Chem.*, **2**, 210 (1964).

(10) T. Rose, C. MacKay, and R. Wolfgang, *J. Amer. Chem. Soc.*, **88**, 1064 (1966).

(11) R. Wolfgang and C. MacKay, *Nucleonics*, **16** (10), 69 (1958).

(12) T. Rose, Ph.D. Thesis, Yale University, 1967.

(13) (a) J. Dubrin, C. MacKay, M. L. Pandow, and R. Wolfgang, *J. Inorg. Nucl. Chem.*, **26**, 2113 (1964); (b) G. Stöcklin and A. P. Wolf, *J. Amer. Chem. Soc.*, **85**, 229 (1963).

Table I: Yields of ^{11}C-Labeled Products from Reactions of ^{11}C with Cyclopentadiene–Hydrogen Mixtures[a]

	Yields as % total ^{11}C atoms — Sample			
Products	CPD (30 cm)	CPD (4 cm) H_2 (76 cm)	CPD (0.4 cm) H_2 (7.6 cm)	CPD (3.8 cm) H_2 (76 cm) O_2 (0.2 cm)
Carbon dioxide	n.d.[b]	n.d.	n.d.	7.7 ± 2.1
Carbon monoxide	0.7 ± 0.4	0.3 ± 0.1[c]	3.2 ± 0.6[c]	11.0 ± 1.6
Methane		6.8 ± 0.6	4.6 ± 0.9	0.7 ± 0.1
3-Methylcyclopentene	<0.1	2.1 ± 1.3	10.2 ± 1.7	<0.2
Bicyclo[3.1.0]hex-2-ene	1.5 ± 0.1	13.3 ± 1.0	3.8 ± 0.2	1.3 ± 0.1
trans-1,3,5-Hexatriene	0.3 ± 0.1	2.0 ± 0.2	3.5 ± 0.7	0.5 ± 0.1
cis-1,3,5-Hexatriene	0.3 ± 0.1	2.4 ± 0.4	4.1 ± 0.2	0.5 ± 0.5
1,3-Cyclohexadiene	<0.5	1.4 ± 0.4	1.6 ± 0.1	<0.3

[a] The products shown are only those whose yields increased with the addition of hydrogen. See ref 12 for the complete product spectrum. [b] Not determined. [c] Arises presumedly from O_2 impurities in the sample and absorbed on the walls of the reaction vessel (ref 3b).

of reduced total pressure and scavenging by oxygen are shown in the last two columns of the table.

It is interesting to compare these results with those obtained from the reaction of photolytically produced methylene with CPD.[14] Methylene produced by the photolysis of diazomethane at 4358 Å was reacted with CPD, and the effects of changes in pressure and addition of oxygen scavenger were determined. Table II shows some typical results from the photolysis experiments.

Table II: Yields of C_6 Products from Reaction of Photochemically Generated CH_2 with Cyclopentadiene[a]

	Sample[b]		
Products	CPD (26.5 cm)	CPD (1 cm)	CPD (26.5 cm) + O_2 (3.0 cm)
Bicyclo[3.1.0]hex-2-ene	52.7	4.1	47.5
1-Methylcyclopentadiene	9.1	9.8	11.1
2-Methylcyclopentadiene	10.9	9.5	12.4
1,3-Cyclohexadiene	4.5	6.5	4.7
1,4-Cyclohexadiene	5.1	3.2	7.0
trans-1,3,5-Hexatriene	3.1	24.6	2.8
cis-1,3,5-Hexatriene	12.3	22.5	11.7
Benzene	1.4	18.2	2.0
A[c]	0.9	1.6	0.7

[a] See ref 14. [b] Cyclopentadiene pressure includes between 7 and 10% diazomethane. [c] This product is thought to be a C_6H_8 isomer but has not been identified.

Because of the difference in energy of the methylene in the recoil and photolysis experiments, a quantitative comparison is not justified. A qualitative comparison of the products and the trends of their yields, however, is very revealing. First, in the carbon atom case no methylcyclopentadiene isomers or 1,4-cyclohexadiene are observed, while these products constitute substantial yields in the photolysis experiment. On the other hand little, if any, methane or 3-methylcyclopentene is observed in the photolysis experiments. Second, oxygen almost totally eliminates the products in the recoil system but has only a slight effect on the relative product yields in the photolysis experiments. Finally, the *cis*-:*trans*-1,3,5-hexatriene ratio in the hot-atom sample is independent of pressure in the range covered, whereas in the photochemical work the ratio is pressure dependent with the cis:trans value decreasing from 3.8 at 30 cm of CPD to 1.2, the recoil value, at 2 cm of CPD and <1 at still lower pressures.[14]

On the basis of the photolysis work, the hot-atom products may be divided into two classes: (1) those arising from the reaction of methylene with CPD (the C_6H_8 isomers) and (2) those in which a methyl radical is involved (methane and 3-methylcyclopentene). A similar division was observed in the ^{11}C–H_2–C_2H_4 experiments.[3a,15] The following series of reactions is consistent with the observed results for the methylene products

$$C(^3P) + H_2 \longrightarrow {}^3CH_2^* \quad (1)$$

$${}^3CH_2^* \longrightarrow CH + H \quad (2)$$

$${}^3CH_2^* + M \longrightarrow {}^3CH_2 + M^* \quad (3)$$

$${}^3CH_2 + CPD \longrightarrow C_6H_8^* \quad (4)$$

$C_6H_8^* + M \longrightarrow$  $+ M^*$ (5)

$C_6H_8^* \longrightarrow$ 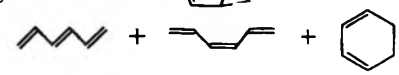 (6)

where $C_6H_8^*$ is an excited adduct of unspecified structure resulting from addition of $^3CH_2$ to a double bond of CPD. The work of Braun, *et al.*, indicates that at high pressures reaction (1) is rapid.[2a] Although the

(14) T. Rose, manuscript in preparation.

(15) In the ^{11}C–H_2–C_2H_4 experiments an additional product, pentene-1, was observed which was attributed to the reaction of methyne (CH). There was no indication of a methyne product in the CPD system, although by analogy with the ethylene work such a product would be a C_{11} molecule and would not have been observed in the analysis.

overall reaction of (1) and (2) is endothermic by about 20 kcal, conversion of some of the excess translational energy of the hot carbon atom will be available to overcome the energy deficit.[3a] Reactions (2) and (3) account for the reduced total yield of methylene products observed when the pressure is decreased. It is assumed that the methyne radical, CH, reacts further with hydrogen, eventually leading to the products attributed to the methyl radical.[3,16]

There are two compelling arguments indicating that the methylene formed in the recoil system is in the triplet state. First, there is the absence of the methylcyclopentadiene isomers which would be expected from insertion of a singlet methylene into the C–H bonds of CPD.[14] In the photolysis case, where about 80% of the methylene is in the singlet state,[17,18] these products constitute major yields.[19]

The other evidence for triplet methylene is the scavenging effect of oxygen in the recoil system. The yields of products attributed to direct reaction of triplet methylene, *i.e.*, the C_6H_8 compounds, are drastically reduced when oxygen is present, and there is a concurrent rise in labeled CO_2 and CO, known oxidation products of $^3CH_2$.[6b] The decrease is almost a factor of 10, much greater than the reduction by factors of 2–3 observed for products attributed to singlet methylene formed in hydrocarbon systems without hydrogen present. The products attributed to the methyne and methyl radical are also reduced but the oxidation products in these cases are not CO or CO_2.[20,21]

Russell and Rowland[6b] have suggested from their photochemical studies that the production of CO and CO_2 from triplet methylene is nearly quantitative. A similar situation occurs in the present case. The direct reaction of carbon atoms with oxygen yields CO as the only product.[22] The approximate relative reactivity of carbon atoms with cyclopentadiene, oxygen, and hydrogen is 20:20:1.[12] Taking into account the partial pressures of the reactants in the sample, about 2.5% of the carbon atoms will react directly with oxygen to give carbon monoxide. The corrected CO yield is then 8.5%, giving a total CO + CO_2 yield of 16.2%. This result may be compared with the value of 16.5% for the decrease of methylene products. The agreement is well within the uncertainties of the measurements. Our corrected ratio for CO/CO_2 of 1.1 also agrees with the average range of 1.2 ± 0.2 observed for four systems in the photochemical study.[6b]

At present the data are insufficient to draw any definite conclusion about the energy of the methylene. However, the pressure independence of *cis*-:*trans*-hexatriene ratio and the failure to observe any 1,4-cyclohexadiene, which is known to undergo unimolecular decay into benzene and hydrogen,[14,23] indicate that the methylene may be a very hot species. If this energy can be defined more quantitatively, the recoil technique may also find use in chemical activation studies.[24]

Acknowledgment. The author gratefully acknowledges the partial support of the Petroleum Research Fund, administered by the American Chemical Society, and the Atomic Energy Commission. The encouragement and help of Dr. Richard Wolfgang and Dr. Colin MacKay were also greatly appreciated.

(16) W. Braun, J. R. McNesby, and A. M. Bass, *J. Chem. Phys.*, **46**, 2071 (1967).

(17) B. M. Herzog and R. W. Carr, Jr., *J. Phys. Chem.*, **71**, 2688 (1967).

(18) (a) G. Z. Whitten and B. S. Rabinovitch, *ibid.*, **69**, 4348 (1965); (b) F. H. Dorer and B. S. Rabinovitch, *ibid.*, **69**, 1952, 1964 (1965).

(19) In the reaction of carbon atoms in the pure hydrocarbon system, a slight amount of singlet methylene produced would result in a yield of each methylcyclopentadiene isomer of only about 0.3%, as calculated by taking 10%, the value in the photolysis system, of the total C_6H_8 yield. This yield is below the upper limit of 0.4% set in our analysis (see ref 12).

(20) Reference 3b, pp 80, 81.

(21) M. Barber, J. Farren, and J. W. Linnett, *Proc. Roy. Soc., Ser. A*, **274**, 306 (1963).

(22) For unsaturated systems, no significant amount of radiolysis of ^{11}CO to $^{11}CO_2$ has been observed under radiation conditions similar to those employed in this work: J. Dubrin, Ph.D. Thesis, Yale University, 1965.

(23) R. J. Ellis and H. M. Frey, *J. Chem. Soc. A*, 553 (1966).

(24) (a) W. Simmons and G. W. Taylor, *J. Phys. Chem.*, **73**, 1274 (1969); G. W. Taylor and J. W. Simmons, *ibid.*, **74**, 464 (1970); (b) C. S. Elliot and H. M. Frey, *Trans. Faraday Soc.*, **64**, 2352 (1968); (c) B. S. Rabinovitch and D. W. Setser, *Advan. Photochem.*, **3**, 53 (1964), and references therein.

Mass Spectrometric Observations on the Reaction of Hydrogen Atoms with Iodine Cyanide

by G. P. Horgan, M. R. Dunn, C. G. Freeman, M. J. McEwan, and L. F. Phillips*

Chemistry Department, University of Canterbury, Christchurch, New Zealand *(Received December 28, 1971)*

Publication costs borne completely by The Journal of Physical Chemistry

The primary reaction is shown to be H + ICN → HCN + I (1), with a negligible contribution from H + ICN → HI + CN (6). The rate constant k_1 has been measured as (3.2 ± 1.0) × 10^{-14} cm^3 $molecule^{-1}$ sec^{-1}.

A previous communication[1] from this laboratory described the results of a photometric study of the reaction of H atoms with ICN. The formation of HCN as a major product and the observation of weak CN emission with intensity proportional to $[H]^2$ were accounted for by the reaction scheme

$$H + ICN \longrightarrow HCN^{\dagger} + I \quad (1)$$

$$H + HCN^{\dagger} \longrightarrow H_2 + CN \quad (2)$$

$$H + H + CN \longrightarrow H_2 + CN^* \quad (3)$$

$$CN + \text{wall} \longrightarrow \text{polymer} \quad (4)$$

$$I + \text{wall} \longrightarrow {}^1/_2I_2 \quad (5)$$

Here the HCN produced in reaction 1 and taking part in reaction 2 is assumed to be vibrationally excited. This is necessary if (2) is to be fast enough to produce significant amounts of CN for excitation by reaction 3, since the reaction with ordinary HCN is ~18 kcal endothermic. Goy, Shaw, and Pritchard[2] suggested the occurrence of reaction 1 when ICN was photolyzed in the presence of H_2. However, it was not possible, either in their work or in our photometric study, to rule out the alternative primary reaction

$$H + ICN \longrightarrow HI + CN \quad (6)$$

which would be followed by

$$CN + H_2 \longrightarrow HCN + H \quad (7)$$

and

$$H + HI \longrightarrow H_2 + I \quad (8)$$

On the basis of current estimates of the heats of formation of CN and ICN,[3,4] reaction 1 is exothermic to the extent of 47 kcal and could reasonably be expected to be fast; however, reaction 6, which is about 2 kcal endothermic, is not necessarily slow on this account. The present study was undertaken with the aim of establishing whether (1) or (6) is the major primary step and of measuring the rate of the primary reaction.

Experimental Section

The apparatus and procedures were as previously described.[4,5] The experiments were carried out at room temperature (23°), with the walls of the reaction tube coated with phosphoric acid. ICN was prepared by the method of Goy, Shaw, and Pritchard.[2] HCN was prepared by the reaction of 50% H_2SO_4 with KCN under vacuum, dried over P_2O_5, and further purified by trap-to-trap distillation. The sensitivity of the mass spectrometer for HCN was determined relative to that for argon using a known mixture of the two gases. Analytical reagent grade 66% HI solution was trapped with P_2O_5 at liquid air temperature; the gas released on warming was collected in an evacuated bulb.

Results and Discussion

We did not observe HI as a product at either short or long reaction times (10 or 100 msec), with either a large excess of H atoms or a small excess of ICN. (The amount of ICN which could be added was limited by its vapor pressure.) With H in excess, the absence of HI could be attributed to the occurrence of the fast reaction 8 (k_8 = 1.8 × 10^{-12} cm^3 $molecule^{-1}$ sec^{-1} [6]), but this does not account for the observations with excess ICN. The mass spectrometric sensitivity for HI at mass 128 was comparable with that for HCN at mass 27, and HCN was detected as a major product at both short and long reaction times. Production of HCN at short times is easily accounted for by reaction 1 but less easily by reactions 6 and 7 because of the relatively slow rate of reaction 7 (k_7 ~ 3 × 10^{-14} cm^3 $molecule^{-1}$

(1) R. F. C. Claridge, F. T. Greenaway, and M. J. McEwan, *J. Phys. Chem.*, **74**, 3293 (1970).

(2) C. A. Goy, D. H. Shaw, and H. O. Pritchard, *ibid.*, **69**, 1504 (1965).

(3) V. H. Dibeler and S. K. Liston, *J. Chem. Phys.*, **47**, 4548 (1967).

(4) M. R. Dunn, C. G. Freeman, M. J. McEwan, and L. F. Phillips, *J. Phys. Chem.*, **75**, 2662 (1971).

(5) C. G. Freeman and L. F. Phillips, *ibid.*, **72**, 3025 (1968).

(6) J. Sullivan, *J. Chem. Phys.*, **30**, 1292, 1577 (1959); **36**, 1925 (1962).

sec^{-1} [7]).[8] Thus it would appear that reaction 6 can be ruled out. Measurements of the ratio of HCN produced to ICN consumed in the reaction gave values between 0.89 and 0.95 (mean 0.93) with a six- to tenfold excess of H; values which ranged from 0.81 to 0.86 were obtained with an approximately equimolar reaction mixture. The difference of this ratio from unity with excess H is barely significant. The lower figures obtained with the equimolar mixture possibly result from incorporation of ICN in the wall layer; we return to this point shortly.

Table I contains the data from which the primary rate constant k_1 was evaluated, assuming 1:1 stoichiometry. The reaction is quite slow—we find a mean value of 3.2×10^{-14} cm^3 $molecule^{-1}$ sec^{-1} for k_1 at 296 K, with a standard deviation of 1×10^{-14}. It is notable that there is no marked dependence of the individual k_1 values on the ratio of H to ICN in the reaction mixture, although the sequence of reactions 5, 9

$$H + I_2 \longrightarrow HI + I \qquad (9)$$

($k_9 = 2.5 \times 10^{-11}$ cm^3 $molecule^{-1}$ sec^{-1} [6]) and 8 constitutes a chain which should rapidly remove H atoms, thereby causing low values to be obtained except at short reaction times and with a large excess of H. The absence of such an effect implies that the phosphoric acid coating on the walls is effective in largely preventing reaction 5, so that the stoichiometry at long reaction times is effectively that of reaction 1, plus a small additional consumption of H atoms by reaction 2. (If reaction 6 were the primary step the same overall stoichiometry would be obtained as the sum of reactions 6, 7, and 8.)

Although wall recombination of iodine atoms appears to have been unimportant during these experiments, some iodine was found to be present in the coating of "CN polymer" which gradually formed. After the wall coating had been allowed to accumulate for some time it was found that in the absence of ICN both the I^+ peak at mass 127 and the smaller HI^+ peak at mass 128 showed a marked increase when hydrogen atoms were produced by activating the discharge. (With ICN present in the gas phase the I^+ peak always decreased when the discharge was activated.) The size of the effect at mass 127 gradually decreased when the discharge was left running, typically with a half-life of about 1 hr, as the polymer layer was destroyed by reaction with H atoms. The iodine may have been incorporated in the polymer either as I_2 or as ICN.

Table I: Primary Rate of H and ICN Reaction[a]

$[ICN]_0$	[ICN]	$[H]_0$	t	$10^{14}k$
1.601	1.062	13.80	14.8	4.76
2.202	1.515	16.05	21.4	2.73
3.153	1.205	11.23	104.5	2.43
2.012	1.657	10.11	14.2	2.65
2.331	1.686	8.99	41.8	2.18
4.946	2.887	12.04	24.9	2.15
3.790	3.388	4.28	35.7	2.08
4.700	3.517	4.55	53.3	3.34
2.982	2.273	5.35	39.0	3.69
5.960	4.645	11.53	17.3	3.24
5.261	3.765	10.99	38.4	2.25
6.112	4.325	10.08	23.7	4.07
6.007	4.706	8.81	13.0	5.46
3.959	3.371	6.23	28.7	2.54
2.248	1.660	20.31	10.7	3.45
3.339	2.313	19.70	23.3	2.17
1.921	0.662	19.09	71.6	2.24
1.960	3.022	18.36	54.9	3.02
2.881	1.321	18.99	38.8	3.01

k(mean ± std dev) = $(3.2 \pm 1.0) \times 10^{-14}$ cm^3 $molecule^{-1}$ sec^{-1}

[a] Pressures are in millitorr, times t in msec. The subscript 0 indicates initial concentration. A correction for back-diffusion of reactant amounting to 2–5% of the time value has been applied.

Acknowledgment. This work was supported by the New Zealand Universities Research Committee and by Grant 71-2134 from the U. S. Air Force Office of Scientific Research.

(7) T. Iwai, D. W. Pratt, and H. P. Broida, *J. Chem. Phys.*, 49, 919 (1968).

(8) Since [CN] ~ 10^{11} per cm^3 or less[7] and $[H_2]$ typically ~10^{14} per cm^3, the rate of production of HCN by reaction 7 must have been less than 3×10^{11} cm^{-3} sec^{-1}. This is three orders of magnitude too small to account for the observed [HCN] at t = 100 msec.

Photocatalytic Reactions on Zinc Oxide. III. The Hydrogenation of Ethylene

by Ken-ichi Tanaka*[1] and George Blyholder

Department of Chemistry, University of Arkansas, Fayetteville, Arkansas 72701 *(Received September 22, 1971)*

Publication costs borne completely by The Journal of Physical Chemistry

The hydrogenation of ethylene taking place over zinc oxide was studied both under dark and illuminated conditions. The reaction rate and the adsorption were simultaneously measured during reaction. No photoeffects were observed on catalytic activity, adsorption of ethylene, or kinetics. The reaction rate is expressed by an equation, $r = kP_{H_2}^{1/2}[C_2H_4]_a$, where $[C_2H_4]_a$ is adsorbed ethylene, which is changed by the addition of propylene. The reactivity sequence of olefins on ZnO is $C_2H_4 \gg C_3H_6$, and the relative adsorption strength on ZnO is $C_2H_4 \ll C_3H_6$, which are the reverse of the sequences previously observed on Co_3O_4. These trends suggest that π complexes of olefins are favored on Co_3O_4 while allyl forms are favored on ZnO. It is concluded that the hydrogenation of ethylene on zinc oxide at room temperature is not directly related to the electronic band structure of the catalyst. It is suggested that reactions proceeding on interstitial zinc, Zn_i^0 or Zn_i^+ may be photosensitive, while those occurring on other sites or on strained sites are likely to be photoinsensitive.

Introduction

Since Dowden, MacKenzie, and Trapnell[2] found the activity sequence of the first transition metal oxides for the exchange reaction of H_2 and D_2, similar sequences have been reported for other reactions such as the exchange reaction of C_2H_4 and C_2D_4,[3] the hydrogenation of ethylene,[4] and the isomerization of *n*-butene.[5] As pointed out by Dowden, *et al.*, the sequence for H_2–D_2 exchange is difficult to explain by the electronic theory of catalysis.

However, from the viewpoint of the electronic theory of catalysis in which *n*-type oxides would be favored for hydrogen adsorption and catalysis, a number of researchers have studied the conductivity changes of zinc oxide with hydrogen adsorption. For the two types of chemisorption of hydrogen on zinc oxide,[6] it has been reported that the high-temperature adsorption is responsible for a conductivity increase but the low-temperature adsorption has a less pronounced effect on conductivity.[7] Others have found a more complicated relation between the adsorption and conductivity.[8] Doping effects on the catalytic activity of ZnO in the hydrogenation of ethylene suggested that the electronic structure of the catalyst is not an important factor for this catalytic process.[9]

On the other hand, Taylor, *et al.*,[10] observed a photoretardation of the high-temperature adsorption (300°), and Gray, *et al.*,[11] reported photo-promotion of the hydrogenation of propylene on doped zinc oxide even below 100°. We have shown that both the catalytic activities and the kinetics of the decomposition of nitrous oxide[12] and the oxidation of carbon monoxide with nitrous oxide and oxygen[13] taking place over zinc oxide are markedly influenced by illumination. In this paper, thermal catalysis and photoeffects for the hydrogenation of ethylene over zinc oxide near room temperature are studied.

Experimental Section

The apparatus and the light source used in these experiments are the same as reported in the previous papers.[12,13] The reactor was set in a water bath with a flat Pyrex glass bottom. The illumination was carried out from the bottom of the water bath using a front surface mirror. The temperatures inside the reactor were carefully calibrated under illumination to accurately include photoeffects. The analysis of ethylene, ethane, and propylene were carried out in an on-line gas chromatograph using a silica gel column. The adsorptions of hydrogen and ethylene during catalysis were computed from the material balance used by Tamaru[14] assuming ethane adsorption is negligible when ethylene is in the gas phase.

Ethylene and propylene were purified by being frozen

(1) To whom correspondence should be addressed at The Institute for Catalysis, Hokkaido University, Sapporo, Japan.

(2) D. A. Dowden, N. MacKenzie, and B. M. W. Trapnell, *Proc. Roy. Soc., Ser. A*, **237**, 245 (1956).

(3) A. Ozaki, H. Ai, and K. Kimura, *Proc. Int. Congr. Catal., 4th*, 708 (1968).

(4) D. C. Harrison, D. Nicholls, and H. Steines, *J. Catal.*, **7**, 359 (1967).

(5) Y. Kubokawa, T. Adachi, T. Tomino, and T. Ozawa, *Proc. Int. Congr. Catal., 4th*, 692 (1968).

(6) H. S. Taylor and C. O. Strother, *J. Amer. Chem. Soc.*, **56**, 586 (1934).

(7) Y. Kubokawa and O. Toyama, *J. Phys. Chem.*, **60**, 833 (1956).

(8) A. Cimino, E. Molinari, F. Cramarossa, and G. Ghersini, *J. Catal.*, **1**, 275 (1962).

(9) J. Aigueperse and S. J. Teichner, *Ann. Chim. (Paris)*, **7**, 13 (1962).

(10) V. Kesavulu and H. A. Taylor, *J. Phys. Chem.*, **66**, 54 (1962).

(11) T. J. Gray and D. C. Carpenter, *Proc. Int. Congr. Catal., 3rd*, 463 (1964).

(12) K. Tanaka and G. Blyholder, *J. Chem. Soc. D*, 1130 (1970); *J. Phys. Chem.*, **75**, 1037 (1971).

(13) K. Tanaka and G. Blyholder, *J. Chem. Soc. D*, 726 (1971).

(14) *Cf.* K. Tamaru, *Advan. Catal.*, **15**, 65 (1964).

at liquid air temperature and distilled at Dry Ice–methanol temperature. Hydrogen from a commercial cylinder was purified by passage through a liquid air trap. Zinc oxide, 2.00 g of Kadox-25, was oxidized at 410° overnight and then evacuated for several hours at that temperature. It has been shown that the irreversible part of adsorbed hydrogen on both ZnO and Co_3O_4 does not take part in the hydrogenation of ethylene and that the irreversible part of adsorbed hydrogen on ZnO slightly enhances the catalytic activity[15] while the irreversible adsorption on Co_3O_4 markedly reduces the catalytic activity.[16] Therefore, to get a stabilized surface, several reaction runs were carried out and followed by a 15–20-min evacuation under the reaction condition before the recorded experiments. A catalyst handled this way is denoted as ZnO(I). It was found that the hydrogenation of propylene on the stabilized catalyst caused a decrease in its activity for the hydrogenation of ethylene. The oxide that had been used for the hydrogenation of propylene was reoxidized and evacuated at about 410°. This retreated catalyst is denoted as ZnO(II).

Results

Figure 1 shows a typical time course of the reaction carried out over ZnO(II) catalyst at 26°. When the mixture of hydrogen and ethylene (initial pressures are P_{H_2} = 19.5 mm and $P_{C_2H_4}$ = 3.2 mm) is contacted over the catalyst, rapid adsorption of ethylene and hydrogen is observed in the initial stage of the reaction. As the reaction proceeds, the amount of adsorbed ethylene gradually decreases with time while the amount of adsorbed hydrogen gradually increases with time. The total amount of adsorbed ethylene and hydrogen is approximately constant within the experimental error (~0.05 ml) during the course of the reaction as shown in Figure 1 with a dotted line and is approximately equal to the saturated adsorption of ethylene shown in Figure 2A.

The slope of the C_2H_6 curve in Figure 1 indicates that the reaction rate slows down as the reaction proceeds. In this run, excess hydrogen was used so that the change of the hydrogen pressure in the course of the reaction had little influence on the reaction rate; accordingly, ethylene, either adsorbed or gaseous, should be responsible for the reaction rate slowing down. The relation between the amount of adsorbed ethylene during catalysis and the reaction rate obtained from tangents to the curve of C_2H_6 formation is shown in Figure 2B with crosses.

In order to examine the relative order of reactivity of different olefins, the hydrogenation of propylene, $P_{C_3H_6}$ = 2.2 mm, P_{H_2} = 19 mm, was also carried out over ZnO(I) at 26°. The hydrogenation of propylene was more than one order of magnitude slower than that of ethylene, and this relation was the same under illumination.

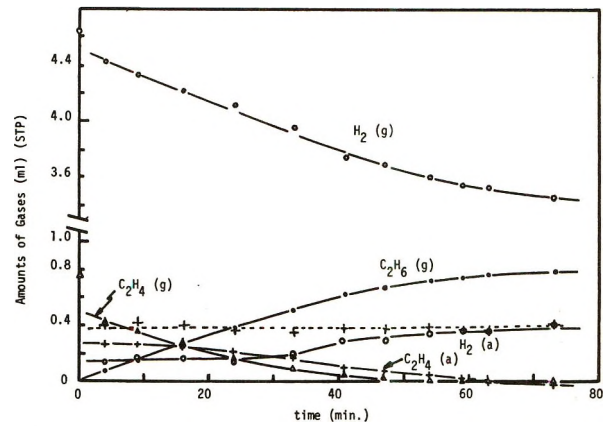

Figure 1. The hydrogenation of ethylene on ZnO(II) at 26° in the dark. Here (g) denotes gas phase concentrations and (a) denotes adsorbed species.

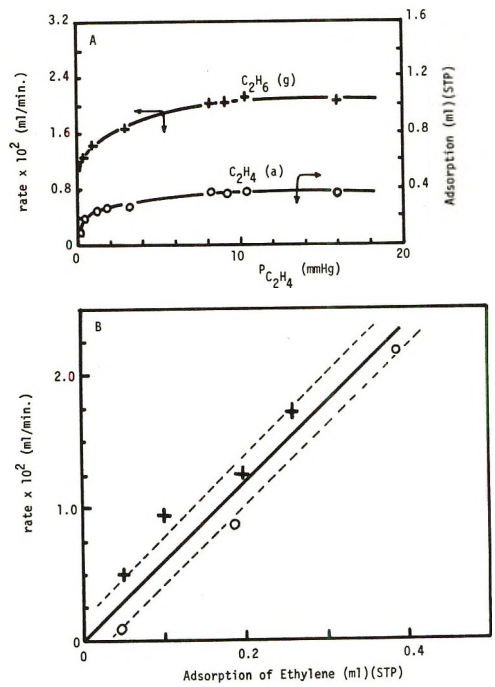

Figure 2. A, ethylene pressure dependence of the reaction rate and of adsorption during reaction on ZnO at 26° in dark. P_{H_2} = 18 ± 1 mm. B, a relation between reaction rate and adsorption of ethylene during catalysis: +, obtained from Figure 1; O, obtained from Figure 3.

It was found that propylene strongly retards the hydrogenation of ethylene. The activity of the catalyst was, however, restored by evacuation for more than 30 min at room temperature (10 hr of evacuation gave the same activity), and the restored activity was about 70% of the unpoisoned activity.

In order to examine the retardation effect of propylene in detail, adsorption was followed simultaneously with the reaction (Figure 3). When the gases at initial

(15) A. L. Dent and R. J. Kokes, *J. Phys. Chem.*, **73**, 3772, 3781 (1969).

(16) K. Tanaka, H. Nihira, and A. Ozaki, *ibid.*, **74**, 4510 (1970).

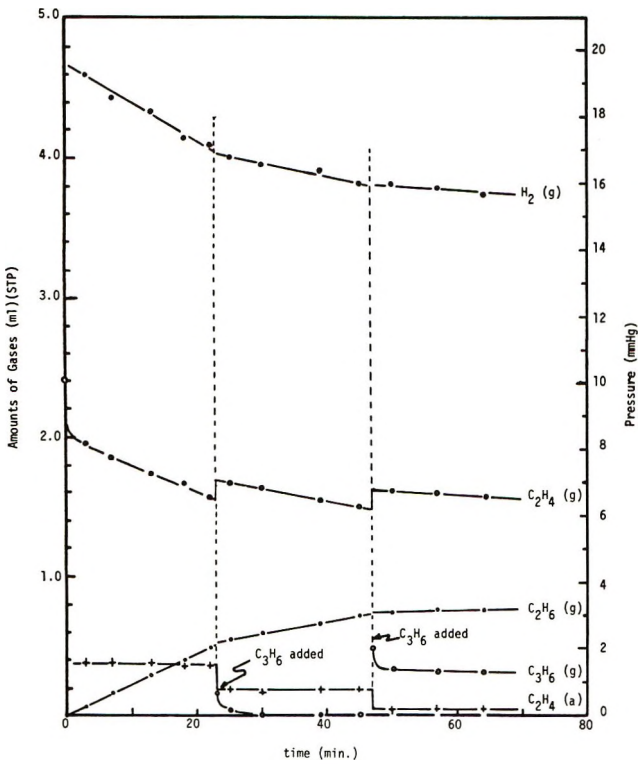

Figure 3. The effects of added propylene on the hydrogenation of ethylene over ZnO(II) at 26° in the dark.

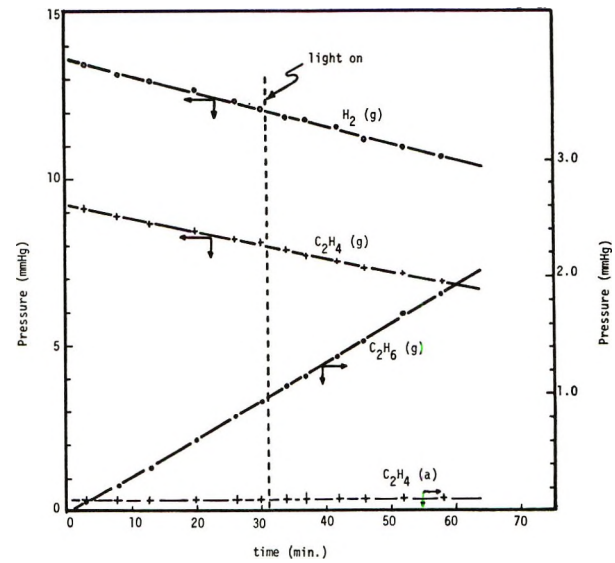

Figure 4. Illumination effects on reaction rate and adsorption taking place over ZnO(II) at 26°.

pressures of approximately P_{H_2} = 19.7 mm and $P_{C_2H_4}$ = 8.6 mm are contacted with ZnO(II) at 26°, about 0.4 ml (STP) of ethylene is adsorbed on the surface. This adsorption stays almost constant during the reaction until propylene is added. If a small amount of propylene is added to the reactants, abrupt changes are observed in the reaction rate, the adsorption of ethylene, and the pressures of ethylene. Almost all of the 0.17 ml of first added propylene is completely adsorbed on the catalyst and simultaneously about the same amount of ethylene is desorbed from the surface into the gas phase. Upon further addition of about 0.48 ml, again desorption of ethylene occurs to about the same amount as the added propylene adsorption. The relation between the reaction rates and the amount of adsorbed ethylene obtained during the competitive reaction is plotted in Figure 2B with open circles and a linear relation is established.

The reaction in dark was half order in hydrogen pressures and nearly zero order in ethylene pressures at higher pressures as shown in Figure 2A, which agree with previous work.[15] The pressure dependence of the reaction taking place over the illuminated zinc oxide was identical with that in the dark. Furthermore, the reaction rate and the adsorption of ethylene during the reaction were not influenced by illumination as is shown in Figure 4.

Discussion

Two types of hydrogen adsorption, one rapid and reversible (type I) and the other irreversible (type II), have been observed on ZnO[15] and on Co_3O_4[16] at room temperature. On both oxides type I hydrogen participates in the hydrogenation of ethylene but type II hydrogen does not participate in the hydrogenation reaction. Type II hydrogen on zinc oxide modifies the catalyst to enhance its activity for the hydrogenation of ethylene,[15] but type II hydrogen on Co_3O_4 markedly reduces the catalytic activity for the hydrogenation of ethylene.[16]

The adsorptions shown in Figure 1 are the amount of reversible adsorption on the catalyst. The constancy of the sum of hydrogen adsorption plus ethylene adsorption during reaction indicates that the active sites are competitively occupied by either ethylene or hydrogen during catalysis at the conditions adopted for Figure 1. As shown in Figure 2B, a linear relation between reaction rate and adsorption of ethylene during catalysis is established. A similar linear relation between rate and adsorption of ethylene was obtained by a static method in the absence of hydrogen by Dent and Kokes.[15] The establishment of the same linear relation in the presence of poisonous material, propylene, confirms that the isotherm of ethylene obtained during reaction (Figure 2A) represents the reactive intermediate.

The adsorption isotherm of type I hydrogen approaches a saturation value at pressures higher than about 30–40 mm,[15] but the reaction rate increased according to half-order kinetics in hydrogen pressures. The adsorption measurements during the reaction shown in Figure 1 also indicate that the reaction rate is less influenced by the amount of type I hydrogen than by the amount of adsorbed ethylene. This result is confirmed by the poisoning effect of propylene; the decrease of the reaction rate by the addition of propylene is well correlated with the decrease of adsorbed ethylene as shown in Figure 3 and Figure 2B (open

circles). Recently, Baranski and Cvetanovic[17] found that reactive hydrogen for ethylene hydrogenation is only a part of the type I hydrogen. These facts suggest that the amount of reactive hydrogen on zinc oxide may not be influenced by olefins adsorption and may not become saturated above 30–40 mm of hydrogen. This is in contrast to the poisoning brought about by water adsorption, which was explained as causing a reduction of type I hydrogen chemisorption.[15]

By a competitive hydrogenation of olefins over Co_3O_4, it was found that the reactivity sequence of olefins on Co_3O_4 catalyst is in the order of C_2H_4–$C_3H_6 > C_4H_8$ and the relative adsorption strength of the olefins on active sites is in the order of $C_2H_4 \gg C_3H_6 > C_4H_8$, suggesting a π-complex type adsorption.[18] The results obtained in this experiment present a striking contrast to those obtained on Co_3O_4 in that the reactivity is in the order of $C_2H_4 \gg C_3H_6$ and the adsorption strength is $C_2H_4 \ll C_3H_6$ (Figure 3).

Dent and Kokes[19] recently presented evidence of allyl type adsorption of propylene on ZnO at room temperature, and Tamaru, *et al.*,[20] demonstrated allyl type adsorption on zinc oxide by using micro-wave analysis of propylene-d_1. If propylene is rather easily dissociated on ZnO to form allyl species, the stronger adsorption and the slower hydrogenation of propylene over zinc oxide are as expected. The results suggest that π complexes of olefins on Co_3O_4 are favored while allyl forms are favored on ZnO, in spite of the fact that both oxides produce d_2-ethane selectively.[16,21]

It was desired to understand better the relation between the electronic structure of the catalyst and its catalytic activity for hydrogenation of ethylene. Teichner, *et al.*,[9] studied doping effects on the activity for the hydrogenation of ethylene and arrived at the conclusion that the electronic structure of the catalyst is not important for the reaction. Furthermore, Dent and Kokes[15] studied the poisoning effect of oxygen very carefully and showed that the poisoning effect of oxygen is not caused by the electronic processes usually considered but is caused by the reaction of oxygen with adsorbed hydrogen on zinc oxide.

The results shown in Figure 4 undoubtedly indicate that illumination does not influence either the adsorption of ethylene during reaction or the reaction rates. The electronic theory of catalysis predicts that n-type oxides such as zinc oxide are favorable for hydrogen adsorption and catalysis, and several investigators have reported photoeffects for hydrogen adsorption and/or catalysis. Recently, however, Leland and coworkers[22] have studied carefully photoeffects on the H_2–D_2 exchange reaction and on the adsorption of hydrogen on zinc oxide, and they concluded that these have no photoeffects if thermal effects are carefully eliminated. These results are quite consistent with the present observations on the hydrogenation of ethylene.

In the previous paper, the authors found that the illumination markedly changes the kinetics of the decomposition of N_2O[12] and the oxidation of CO with N_2O and O_2,[13] and some evidence was presented that the carbon monoxide oxidation on ZnO in the dark proceeds on the interstitial zinc atoms or ions, Zn_i^0 or Zn_i^+, while the reaction under illumination occurs on the sites, Zn^+ or Zn^+O^-, formed by illumination.[23] However, in the case of the hydrogenation of ethylene, no photoeffects were observed on either activity or kinetics. Furthermore, the number of adsorbed ethylene and hydrogen molecules during the reaction is undoubtedly larger than the number of interstitial zinc atoms or ions. Consequently, it may be concluded that the hydrogenation of ethylene on zinc oxide at room temperature is not related to the electronic band structure of the catalyst. Formic acid decomposition on zinc oxide, which may proceed on the whole surface,[24] also has no photoeffects.[25]

Acknowledgment. This investigation was supported in part by Research Grant No. 00818 from the Air Pollution Control Office, Environmental Protection Agency.

(17) A. Baranski and R. J. Cvetanovic, *J. Phys. Chem.*, **75**, 208 (1971).

(18) H. Nihira, T. Fukushima, K. Tanaka, and A. Ozaki, *J. Catal.*, in press.

(19) A. L. Dent and R. J. Kokes, *J. Amer. Chem. Soc.*, **92**, 1092, 6709 (1970).

(20) S. Naito, Y. Sakurai, H. Shimizu, T. Onishi, and K. Tamaru, *Bull. Chem. Soc. Jap.*, **43**, 2274 (1970); *Trans. Faraday Soc.*, **67**, 1529 (1971).

(21) W. C. Conner, R. A. Innes, and R. J. Kokes, *J. Amer. Chem. Soc.*, **90**, 6858 (1968); W. C. Conner and R. J. Kokes, *J. Phys. Chem.*, **73**, 2436 (1969).

(22) Private communication from T. W. Leland and his coworkers.

(23) K. Tanaka and G. Blyholder, submitted to *J. Phys. Chem.*

(24) Y. Noto, K. Fukuda, T. Onishi, and K. Tamaru, *Trans. Faraday Soc.*, **63**, 3081 (1967).

(25) Unpublished data.

Acid–Base Properties of the Radicals Produced in the Pulse Radiolysis of Aqueous Solutions of Benzoic Acid[1]

by M. Simic[2a] and Morton Z. Hoffman*[2b]

Pioneering Research Laboratory, U. S. Army Natick Laboratories, Natick, Massachusetts 01760 *(Received July 2, 1971)*

Publication costs borne completely by The Journal of Physical Chemistry

Hydrated electrons, produced by pulse radiolysis in aqueous solution, react with benzoic acid ($k = 1.6 \times 10^{10}$ M^{-1} sec^{-1}) and benzoate ($k = 3.2 \times 10^{9}$ M^{-1} sec^{-1}) to give transient species with pH-dependent optical absorption spectra. At pH 3.8, λ_{max} <290 (ϵ_{max} >16,000 M^{-1} cm^{-1}) and 420 (1600); at pH 9.1, λ_{max} 310 (25,000) and 435 nm (5200); at pH 13.2, λ_{max} 322 (27,000) and 445 nm (8000). The dependence of the spectra on pH show that the electron adduct transient species have pK_a values of 5.3 and 12.0. An extended Hückel molecular orbital calculation shows that the electron adds to the molecular π system with a large fraction of the electron density localized on the carboxylate carbon. Protonation takes place on the carboxylate oxygen atoms, not on the aromatic ring, producing absorption spectra that are completely different than that observed for the addition of H atoms to benzoic acid (λ_{max} 350 nm, ϵ_{max} <4200 M^{-1} cm^{-1}) forming the cyclohexadienyl radical, $\cdot C_6H_5(H)CO_2H$. The electron adduct can best be *represented* as a substituted benzyl radical, $C_6H_5C(OH)_2$. Electron addition to benzenesulfonate, on the other hand, yields a spectrum which resembles that of a cyclohexadienyl radical (325 nm, 3700 M^{-1} cm^{-1}), $\cdot C_6H_5(H)SO_3^-$. Hydroxyl radicals add to the benzoate aromatic ring to yield $\cdot C_6H_5(OH)CO_2H$ (350 nm, 3800 M^{-1} cm^{-1}) and $\cdot C_6H_5(OH)CO_2^-$ (330 nm, 3800 M^{-1} cm^{-1}) with pK_a = 4.4.

Introduction

The radiolysis of water generates e_{aq}^-, OH, and H as the reactive radical species. Depending on the concentrations of various solute scavengers, one or more of these radicals can be selectively removed producing a relatively clean reaction system. Pulse radiolysis techniques enables the detection and characterization of the reaction intermediates to be made in the micro- and submicrosecond region. Benzoic acid (pK_a = 4.19), as the archetype aromatic carboxylic acid, has been subjected to a number of pulse radiolytic studies in aqueous solution from which the transient optical absorption spectra have been determined. Sangster[3] found that at pH 12.8, the $e_{aq}^- + C_6H_5CO_2^-$ reaction resulted in an intense narrow absorption band at 322 nm and a much weaker one at 444 nm which was attributed to the cyclohexadienylcarboxylate radical, $\cdot C_6H_6CO_2^-$, proposed to have been formed upon the rapid protonation of the electron adduct to the aromatic ring. His examination of the pH dependence of the absorption did not extend below pH 11 where the spectral characteristics of the transient were apparently unchanged. In the presence of N_2O, where the e_{aq}^- is efficiently converted into OH (O^- at pH 12.8), a broad band was observed at 330 nm which was attributed to the O^- adduct to the ring. A further clarification of the spectra of the OH adduct, the hydroxycyclohexadienylcarboxylate radical, $\cdot C_6H_5(OH)CO_2^-$, was made by Dorfman who showed that $\epsilon_{330} = 3600 \pm 500$ M^{-1} cm^{-1} in neutral solution[4] but that at pH 3,[5] λ_{max} 347 nm with $\epsilon_{347} = 3600 \pm 500$ M^{-1} cm^{-1}. Thus, the spectra of the OH adducts to benzoic acid and benzoate ion show different λ_{max}. At pH 1 in the presence of CD_3OH,[5] where e_{aq}^- are converted into H and OH radicals are scavenged by the alcohol, the H adduct to benzoic acid, $\cdot C_6H_5(H)CO_2H$, exhibits λ_{max} 352 nm with $\epsilon_{352} = 3700 \pm 500$ M^{-1} cm^{-1}.

In this study we directed our attention to the following questions. (1) What is the spectrum of the electron adduct in other than highly alkaline solution? (2) Why are the spectra reported for the presumably protonated electron adduct to benzoate, $\cdot C_6H_6CO_2^-$, and the H adduct to benzoic acid, $\cdot C_6H_6CO_2H$, so strikingly different? (3) Keeping in mind that the pK_a for benzoic acid is 4.19, what are the pK_a values for the radicals produced in the radiolysis of benzoic acid and how do they arise?

Experimental Section

The details involving the Febetron 705 pulsed radiation source, detection systems, dosimetry, and solution handling techniques have been described previously.[6]

(1) Presented in part at the Fourth International Congress of Radiation Research, Evian, France, June 1970.

(2) National Academy of Sciences-National Research Council Senior Postdoctoral Research Associates at Natick. (a) Department of Zoology, Radiation Biology Laboratory, University of Texas, Austin, Texas 78712. (b) Department of Chemistry, Boston University, Boston, Mass. 02215.

(3) D. F. Sangster, *J. Phys. Chem.*, **70**, 1712 (1966).

(4) P. Neta and L. M. Dorfman, *Advan. Chem. Ser.*, **No. 81**, 222 (1968).

(5) R. Wander, P. Neta, and L. M. Dorfman, *J. Phys. Chem.*, **72**, 2946 (1968).

Table I: Spectral Characteristics, Acid–Base Properties, and Decay Rates of the Transients Produced in the Pulse Radiolysis of Benzoic Acid in Aqueous Solution

System	Reacting species	pH	Transient species	pK_a	λ_{max}, nm	ϵ_{max}, M^{-1} cm^{-1}	Decay rate constants: λ monitor, nm	Decay rate constants: $2k$, M^{-1} sec^{-1}	Decay rate constants: k, sec^{-1}
10mM $C_6H_5CO_2H$, 1 M *tert*-butyl alcohol	e_{aq}^-	3.8	$C_6H_5\dot{C}(OH)_2$	5.3	<290 420	>16,000 1,600	304	>8 × 10^8	...
2 mM $C_6H_5CO_2^-$ 1 M *tert*-butyl alcohol	e_{aq}^-	9.1	$C_6H_5\dot{C}(OH)O^-$	12.0	310 435	25,000 5,200	335	~7 × 10^8	...
2mM $C_6H_5CO_2^-$, 1 M *tert*-butyl alcohol	e_{aq}^-	13.2	$C_6H_5\dot{C}O_2^{2-}$	...	322 445	27,000 8,000	328 445	~5 × 10^8	4.6 × 10^2
10 mM $C_6H_5CO_2^-$, 1 M methanol	e_{aq}^-	13.0	$C_6H_5\dot{C}O_2^{2-}$	...	...	...	320	1.4 × 10^8	...
5 mM $C_6H_5SO_3^-$, 1 M *tert*-butyl alcohol	e_{aq}^-	9.0	$\cdot C_6H_5(H)SO_3^-$	...	325	3,700	...	...	...
1 mM $C_6H_5CO_2H$, 25 mM N_2O	OH	3.1	$\cdot C_6H_5(OH)CO_2H$	4.4	350	3,800	350	1.2 × 10^9	...
1 mM $C_6H_5CO_2^-$, 25 mM N_2O	OH	9.0 to 13.0	$\cdot C_6H_5(OH)CO_2^-$	>14	330	3,800	330	4.4 × 10^8	...
2 mM $C_6H_5CO_2H$, 1 M *tert*-butyl alcohol	H	1.0	$\cdot C_6H_5(H)CO_2H$	...	350	<4,200	350	1 × 10^9	...

Analytical reagent grade chemicals were used throughout and solutions were buffered using perchloric acid, potassium hydroxide, sodium tetraborate, and potassium phosphate. Spectral resolution using two high-intensity Bausch and Lomb monochromators was <2 nm. The concentrations of solutes were chosen on the basis of known radical–radical and radical–solute rate constants.[7] All values of ϵ and rate constants reported here were determined within ±20% error.

Results

The reaction of e_{aq}^- with benzoic acid or benzoate occurred in solutions containing alcohols such that >98% e_{aq}^- and <5% OH react with the substrate. Three distinct intermediate spectra as a function of pH were obtained <1 μsec after the pulse and are shown in Figure 1. The pH curves shown in the inserts were found to be identical for both absorption bands corresponding to deprotonation processes with pK_a values of 5.3 and 12.0. In the presence of 25 mM N_2O, only a very weak absorption remained. The decay of these transients followed second-order kinetics initially, becoming mixed or first order after several half-lives. In general, the second-order rate constant, $2k$, decreased as pH was increased. A summary of the decay data is given in Table I. Note that when methanol was used in the solution at pH 13, the initial decay rate constant (1.4 × 10^8 M^{-1} sec^{-1}) was smaller than that in *tert*-butyl alcohol solutions (~5 × 10^8 M^{-1} sec^{-1}).

The addition of 25 mM N_2O to a solution containing 10 mM benzoic acid and 1 M *tert*-butyl alcohol at pH 3.8 caused a diminution of the optical density of the absorption at 300 nm due to the competitive scavenging of the N_2O for e_{aq}^-. From a measure of such a decrease in OD, a value of the rate constant for the overall reaction of e_{aq}^- with all benzoic acid species was obtained (1.33 × 10^{10} M^{-1} sec^{-1}). From the known value of $k(e_{aq}^- + C_6H_5CO_2^-)$[7] and the pK_a of benzoic acid, the rate constant of e_{aq}^- + $C_6H_5CO_2H$ was calculated (1.6 × 10^{10} M^{-1} sec^{-1}; see Table II[8]).

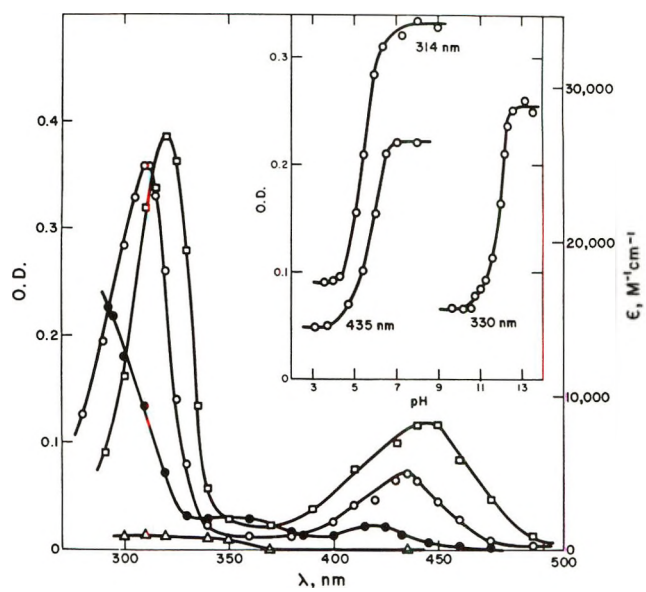

Figure 1. Transient absorption spectra produced in the reaction of e_{aq}^- with benzoic acid/benzoate. [Substrate] = 2–10 mM, [*tert*-butyl alcohol] = 1 M, 2.4 krad/pulse. ●, pH 3.8; ○, pH 9.1; □, pH 13.2; △, pH 9.1 in the presence of 25 mM N_2O. Insert: absorption at 314, 330 (2.4 krads/pulse), and 435 nm (8 krads/pulse) as a function of pH.

Under similar conditions, the transient absorption spectra from the reaction of e_{aq}^- with methyl benzoate

(6) M. Simic, P. Neta, and E. Hayon, *J. Phys. Chem.*, **73**, 3794 (1969).
(7) M. Anbar and P. Neta, *Int. J. Appl. Radiat. Isotopes*, **18**, 493 (1967).
(8) P. Neta and L. M. Dorfman, *J. Phys. Chem.*, **73**, 413 (1969).

Table II: Second-Order Rate Constants (in units of M^{-1} sec^{-1}) for the Reaction of e_{aq}^-, OH, and H with Benzoic Acid in Aqueous Solution

Solute, S	$k(e_{aq}^- + S)$	$k(H + S)$	$k(OH + S)$
$C_6H_5CO_2H$	1.6×10^{10}	1.0×10^{9} [a]	4.3×10^{9} [b]
$C_6H_5CO_2^-$	3.2×10^{9} [c]	...	6.0×10^{9} [b]

[a] Reference 8. [b] Reference 5. [c] Average value at pH 7.4–14 from ref 7.

were examined. In mildly acidic solution λ_{max} for the absorption was <300 nm. In neutral solution, λ_{max} 310 nm with $\epsilon_{310} = 27{,}000\ M^{-1}\ cm^{-1}$; a weak absorption at 440 nm was also observed. From the variation of the absorption as a function of pH, a pK_a value of 5.5 was obtained. Results in strongly alkaline solution are meaningless because of the base hydrolysis of the ester.

Completely different results were obtained for $e_{aq}^- + C_6H_5SO_3^-$. The spectrum of the transient in 1 *M* *tert*-butyl alcohol at pH 9 showed λ_{max} 325 nm with $\epsilon_{325} = 3700\ M^{-1}\ cm^{-1}$. There was no change in the spectrum even at pH 13.5.

Although the reaction of $OH + C_6H_5CO_2^-$ is fast ($6.0 \times 10^9\ M^{-1}\ sec^{-1}$),[5] O^- radicals appear to react more slowly. An apparent rate constant of $8.5 \times 10^7\ M^{-1}\ sec^{-1}$ was determined at pH 14 from the formation kinetics of the absorption at 330 nm. As Figure 2 shows, the transient spectra of the OH adduct is a function of pH although the spectrum in highly alkaline solution is the same as that of neutral pH. A summary of the spectral and decay characteristics is given in Table I.

The spectrum of the H adduct to benzoic acid, shown in Figure 3, was determined at pH 1 in 1 *M* *tert*-butyl alcohol; the convenience of using such conditions to study H-atom reactions has already been demonstrated.[9] At $[C_6H_5CO_2H] < 1.5$ m*M*, some H atoms are lost through radical recombination reactions and attack on *tert*-butyl alcohol while at $[C_6H_5CO_2H] > 10$ m*M*, the spectrum of the OH adduct begins to contribute. In the presence of 0.4 *M* 2-propanol, the spectrum of the H adduct disappears due to the preferential scavenging of the H atoms by this alcohol. This latter result demonstrates that any reaction of the *tert*-butyl alcohol radical with benzoic acid (if it indeed takes place) does not contribute towards the spectrum shown in Figure 3. Other H atom scavengers can also be added to benzoic acid at pH 1 in 1 *M* *tert*-butyl alcohol and from the decrease in the OD at 350 nm, provided, of course, that the H-atom transient from the added scavenger does not absorb at that wavelength, relative rates of H-atom attack can be established. For example, using this competitive method, $k(H + $ *tert*-amyl alcohol$) = 3 \times 10^6\ M^{-1}\ sec^{-1}$ was obtained. It may

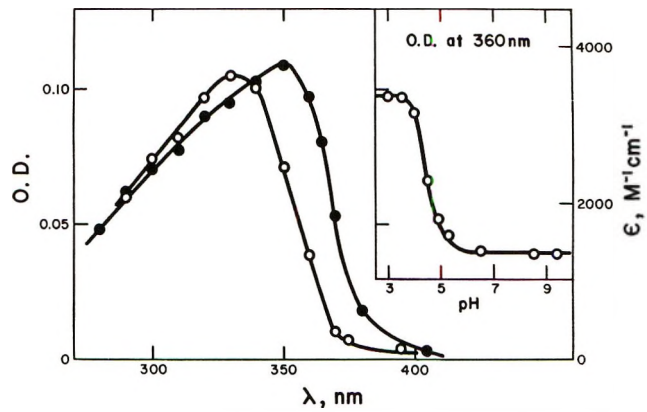

Figure 2. Transient absorption spectra produced in the reaction of OH with benzoic acid/benzoate. [Substrate] = 1 m*M*, $[N_2O] = 25$ m*M*, 2.4 krads/pulse. ●, pH 3.0; ○, pH 9.3. Insert: absorbance at 360 nm as a function of pH.

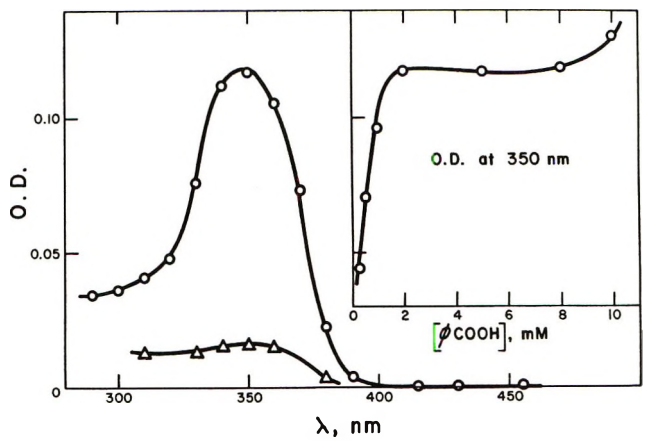

Figure 3. Transient absorption spectrum produced in the reaction of H atoms with 2 m*M* benzoic acid at pH 1 in the presence of 1 *M* *tert*-butyl alcohol (4 krads/pulse), ○; in the presence of 0.4 *M* 2-propanol, △. Insert: absorbance at 350 nm as a function of [benzoic acid].

be useful to note that $k(OH +$ *tert*-amyl alcohol), as determined by the CNS^- competitive method,[10] is $1.6 \times 10^9\ M^{-1}\ sec^{-1}$ making this alcohol a convenient scavenger for both H and OH. The radical produced from the abstraction of an H atom from this alcohol has a weak absorption in the ultraviolet (λ_{max} 225 nm; $\epsilon_{225} = 1100\ M^{-1}\ cm^{-1}$) which disappears *via* second-order kinetics ($2k = 1.1 \times 10^9\ M^{-1}\ sec^{-1}$). The spectrum is independent of pH up to pH 14 indicating that this β-hydroxy radical has a $pK_a > 14$.

Discussion

OH (or O^-) + Benzoic Acid. The values of λ_{max}, ϵ_{max}, and $2k$ are in very close agreement with those al-

(9) M. Simic and M. Z. Hoffman, *J. Amer. Chem. Soc.*, 92, 6096 (1970).

(10) G. E. Adams, J. W. Boag, J. Currant, and B. D. Michael in "Pulse Radiolysis," M. Ebert, J. P. Keene, A. J. Swallow, and J. H. Baxendale, Ed., Academic Press, New York, N. Y., 1965, p 131.

ready reported[5] for $\cdot C_6H_5(OH)CO_2H$ and $\cdot C_6H_5(OH)CO_2^-$, the cyclohexadienyl radicals formed by OH addition to the ring. The observed pK_a value of 4.4 for the change of spectra as a function of pH is taken to represent the acid–base equilibrium

$$\cdot C_6H_5(OH)CO_2H \rightleftharpoons H^+ + \cdot C_6H_5(OH)CO_2^-$$

Thus, the presence of the radical on the ring has little effect on the acidity of the carboxylic acid side chain as compared to the parent acid. In comparison, it should be noted that although the pK_a of an aliphatic carboxylic acid radical is about the same as the parent acid,[11] the pK_a of an α-carboxy-α-hydroxyalkyl radical appears to be higher than that of the parent, often by more than one pK unit.[12] This latter effect has been attributed[12] to the delocalization of the unpaired electron by the OH group at the α position so that the inductive effect of the OH group on the dissociation of the acid is reduced.

The radiolysis of benzoic acid yields all three hydroxy derivatives in varying ratios depending on the presence of other scavengers.[13] Eiben and Fessenden[14] have concluded, on the basis of esr data with benzoate, that the meta and para adducts are produced at the same rate and the ortho at about half the rate per position on the ring. They attribute the lower rate in the ortho position to steric factors. Thus, the broad OH adduct spectrum shown in Figure 2 could be a composite of the overlapping spectra of the three isomers and the observed pH dependence could be a similar composite. Since the pK_a values for *o*-, *m*-, and *p*-hydroxybenzoic acid are 2.97, 4.06, and 4.48, respectively, it is possible that the observed pK_a of 4.4 represents an acidity lower or equal to those of the hydroxy acids indicating the reduction of the inductive effect of the OH group. It is not clear from the steady-state radiolysis data whether the state of protonation of the benzoic acid affects the position of attack of the OH radical. It has been proposed,[13d] in fact, that the OH radical does not attack a specific position on the ring but is rather a complex between the radical and the aromatic electronic system. The specificity of position then arises as a result of the one-electron oxidation step leading to the final, stable products. However, neither pulse nor steady-state radiolysis studies have yet clarified that suggestion.

The second-order decay constants for $\cdot C_6H_5(OH)CO_2H$ and $\cdot C_6H_5(OH)CO_2^-$ are in agreement with those expected from the Debye relationship[15] for the bimolecular reaction of 0 and -1 charged species in aqueous solution. The independence of the spectrum and decay kinetics on pH between 9 and 13 strongly suggests that the hydroxy group on the radical is not ionized even in highly basic solution. This must be contrasted with the pK_a of 11.9 for the free OH radical[16] and the acidity constants for the –OH group in the *o*-, *m*-, and *p*-hydroxybenzoic acids of 13.4, 9.9, and 9.3, respectively. However, it must be remembered that the ring in the $\cdot C_6H_5(OH)CO_2^-$ radical is no longer aromatic and that the hydroxy group is bonded to a tetracoordinated carbon atom forming a secondary alcohol. Thus, the pK_a for cyclohexanol is >14; the pK_a for the β-, γ-, and δ-hydroxycyclohexyl radicals is expected to be this high, as well.[6]

The reaction of $O^- + C_6H_5CO_2^-$ is very much slower than that of $OH + C_6H_5CO_2^-$. The apparent rate constant for the formation of the transient absorption at high pH values consists of a contribution from O^- and OH radicals which are in equilibrium. By taking this equilibrium into account,[17] a value of $k(O^- + C_6H_5CO_2^-)$ 4×10^7 M^{-1} sec^{-1} is obtained which is almost an order of magnitude higher than the previously given upper limit obtained indirectly from competition kinetics.[18] This diminished reactivity is attributed to the unfavorable interaction of O^- with the aromatic π system reflecting the diminished electrophilicity of the attacking radical. A similar diminution of the rate has been observed for $O^- + C_6H_5CH_2CO_2^-$ (as compared to the OH reaction) although in this case the effect is accompanied by a change in the spectrum of the transient species which reflects transition from OH addition onto the ring to H abstraction by O^- from the methylene group.[17]

We have already shown[19] that attack of OH radicals on benzoate coordinated to Co^{III}, in the form of the $(NH_3)_5CoO_2CC_6H_5^{2+}$ complex, results in OH addition to the aromatic ring with the formation of a transient species that absorbs at λ_{max} 340 nm with a pH-independent spectrum (pH 3–7). The transient decays in a second-order manner with a rate consistent with its charge. These results provide further evidence that the state of protonation or coordination of the carboxylic acid moiety has little effect on the nature of the reaction of OH radicals with the aromatic ring.

H + Benzoic Acid. The details of the spectrum of the $\cdot C_6H_5(H)CO_2H$ radical likewise correspond well with those reported before.[5] Furthermore, the similarities between this radical and the OH adducts, similarities that have been noted before between cyclohexadienyl and hydroxycyclohexadienyl radicals in

(11) P. Neta, M. Simic, and E. Hayon, *J. Phys. Chem.*, **73**, 4207 (1969).

(12) M. Simic, P. Neta, and E. Hayon, *ibid.*, **73**, 4214 (1969).

(13) (a) A. M. Downes, *Aust. J. Chem.*, **11**, 154 (1958); (b) W. A. Armstrong, B. A. Black, and D. W. Grant, *J. Phys. Chem.*, **64**, 1415 (1960); (c) O. Volkert and D. Schulte-Frohlinde, *Tetrahedron Lett.*, 2151 (1968); (d) K. F. Nakken, T. Brustad, and A. K. Hansen, *Advan. Chem. Ser.*, **81**, 251 (1968).

(14) K. Eiben and R. W. Fessenden, *J. Phys. Chem.*, **75**, 1186 (1971).

(15) P. Debye, *Trans. Electrochem. Soc.*, **82**, 265 (1942).

(16) J. Rabani and M. S. Matheson, *J. Phys. Chem.*, **70**, 761 (1966); J. L. Weeks and J. Rabani, *ibid.*, **70**, 2100 (1966).

(17) P. Neta, M. Z. Hoffman, and M. Simic, *ibid.*, **76**, 847 (1972).

(18) B. L. Gall and L. M. Dorfman, *J. Amer. Chem. Soc.*, **91**, 2199 (1969).

(19) M. Z. Hoffman and M. Simic, *ibid.*, **92**, 5533 (1970).

general,[8] strengthens the belief that the H atom adds to a specific position on the ring and that the unpaired electron is similarly localized. Thus, the broad transient spectrum may be the result of the existence of the three substituent isomers, a possibility that an examination of the products of the continuous radiolysis has not yet uncovered. We would predict that the pK_a of $\cdot C_6H_5(H)CO_2H$ would be very similar to that of the parent acid and the $\cdot C_6H_5(OH)CO_2H$ radical.

As with the reaction of OH with coordinated benzoate, H atoms at pH 1 react with $(NH_3)_5CoO_2CC_6H_5^{2+}$ to give a transient spectrum with λ_{max} 350 nm which has been identified with addition to the ring.[19]

e_{aq}^- + Benzoic Acid. Despite the fact that e_{aq}^- reacts very slowly with benzene ($k = 1.4 \times 10^7\ M^{-1}$ sec^{-1})[20] and carboxylate ions such as formate and acetate ($k < 10^6\ M^{-1}\ sec^{-1}$),[20] the reaction of e_{aq}^- with $C_6H_5CO_2^-$ is quite fast, thereby demonstrating the extremely strong interaction between the ring and the carboxylic side chain which provides accessible molecular orbitals for the incoming electron. Protonation of the carboxylate group removes resonance stabilization, increases electrophilicity, and establishes an orbital system with strong carbonylic character thus causing the rate of e_{aq}^- reaction to increase to nearly the diffusion controlled limit. This effect is known for aliphatic carboxylic acids;[20] we have demonstrated here that benzoic acid behaves in the same way. It is not clear how these rate constant values can be applied to the Hammett $\rho\sigma$ relationship as given by Anbar and Hart[21] since the σ_{para} values for $-CO_2H$ and $-CO_2^-$ are 0.45 and 0.0, respectively.[22] Perhaps the analogy between the rate of e_{aq}^- reactions and σ values from nucleophilic substitution is questionable, as Anbar and Hart have in fact suggested.[21]

The reduction of benzoic acid by metallic sodium at 77°K generates a species which exhibits an esr spectrum of transient nature;[23] a similar spectrum is obtained from the action of Na in liquid NH_3 on benzoic acid.[24] On the basis of these spectra, a conclusion was reached that the transient species was the radical-anion resulting from the addition of an electron to the benzoic acid and could be best *represented* as a substituted benzyl radical. The product of this reduction in liquid NH_3 in the presence of proton donors such as methanol and ethanol is 1,4-dihydrobenzoic acid.[25] This product has not been identified in the radiation chemistry of benzoic acid in aqueous solution.[13] Presumably its radical precursor from e_{aq}^- addition can undergo secondary reactions, particularly with OH adduct radicals, to yield the hydroxybenzoic acids as the major products. The radiolysis of benzoic acid in the absence of OH radicals has apparently not yet been accomplished.

The reaction of e_{aq}^- and benzoic acid (benzoate) gives three discrete pH-dependent absorption spectra with pK_a values of 5.3 and 12.0. *None of the transient absorptions resembles that of the H adduct at pH 1.* The e_{aq}^- would be expected to enter the lowest vacant molecular orbital available which might be considerably delocalized due to the overlap of the π systems of the aromatic ring and the carboxylic side chain. Thus the initial reaction is best described as

$$e_{aq}^- + C_6H_5CO_2H/C_6H_5CO_2^- \longrightarrow (C_6H_5CO_2H)^-/(C_6H_5CO_2^-)^-$$

An extended Hückel molecular orbital calculation[26] shows that the carboxylate carbon in ground state benzoate has a significant partial positive charge while the locus of negative charge is at the oxygen atoms (Table III). The aromatic ring, with its smeared-out electron density, is relatively neutral. Note that protonation of benzoic acid has relatively little effect on the electron charge distribution. It is possible to rationalize the fact that the reactivities of benzoic acid and benzoate with e_{aq}^- are orders of magnitude greater than for benzene in terms of the $\delta+$ contribution of the carboxylate carbon. It is possible that a substantial fraction of the electrons which attack benzoate are initially associated with the carboxylate carbon. The MO calculation also provides insight into the symmetry and distribution of the orbital into which the electron has been promoted. The added electron will be in a π system conjugated throughout the molecule rather than in the σ framework. The greatest contribution to the electron density of the new orbital (~30%) comes from the carboxylate carbon with correspondingly less from the bridgehead carbon and ortho/para positions. The smallest contribution arises from the meta positions indicating that the benzoate radical-anion still remains strongly meta directing towards nucleophilic substitution. The carboxylate oxygens still remain the locus of negative charge in the radical-anion. Because of this negative charge, protonation will take place at the carboxylate moiety. It must be kept in mind that the

(20) E. J. Hart and M. Anbar, "The Hydrated Electron," Wiley-Interscience, New York, N. Y., 1970.

(21) M. Anbar and E. J. Hart, *J. Amer. Chem. Soc.*, **86**, 5633 (1964).

(22) D. H. McDaniel and H. C. Brown, *J. Org. Chem.*, **23**, 420 (1958).

(23) J. E. Bennett and L. H. Gale, *Trans. Faraday Soc.*, **64**, 1174 (1968).

(24) A. R. Buick, T. J. Kemp, G. T. Neal, and T. J. Stone, *J. Chem. Soc. A*, 2227 (1970).

(25) H. Plieninger and G. Ege, *Angew. Chem.*, **70**, 505 (1958); M. E. Kuehne and B. F. Lambert, *J. Amer. Chem. Soc.*, **81**, 4278 (1959).

(26) Calculations were performed on Boston University's IBM 360-50 computer using programs obtained from the Quantum Chemistry Program Exchange (QCPE), Indiana University. Extended Hückel calculations were made as described by R. Hoffmann, *J. Chem. Phys.*, **39**, 1397 (1963), with a program modified by E. B. Moore, W. C. Cook, and A. R. M. Rom, Boeing Scientific Research Laboratories, Seattle, Wash. (QCPE64). The authors thank Professor R. H. Mann of Boston University for his assistance with these computations.

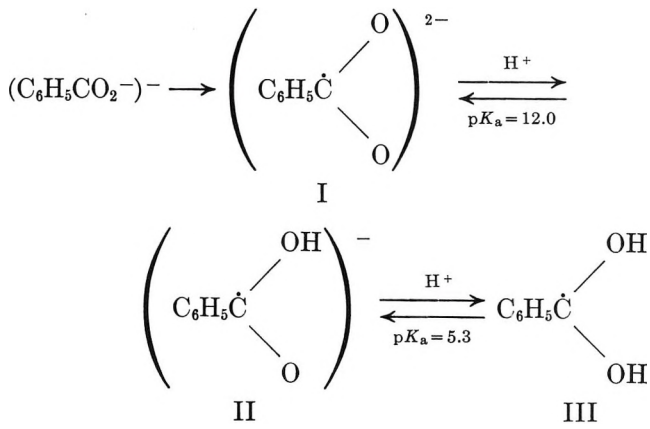

structures are *representations* and in no way can completely describe the electronic nature of the radical.

Table III: Extended Hückel Calculations on Benzoate Ion and Benzoic Acid[a]

Atom	Charges: Benzoate ion	Charges: Benzoic acid	Squares of coefficients of the lowest unfilled molecular orbital[b]: Benzoate ion	Squares of coefficients of the lowest unfilled molecular orbital[b]: Benzoic acid
Carboxylate carbon	+1.405	+1.403	0.433	0.474
Bridgehead carbon	−0.025	−0.011	0.134	0.099
Ortho ring carbons	−0.067	−0.050	0.133	0.140
Meta ring carbons	−0.094	−0.096	0.020	0.014
Para ring carbon	−0.059	−0.046	0.207	0.178
Oxygen 1	−1.233	−1.231	0.094	0.102
Oxygen 2 (H)	−1.233	−0.807	0.094	0.083

[a] The bond lengths and interbond angles for benzoic acid and benzoate were taken from G. A. Sim, J. M. Robertson, and T. H. Goodwin, *Acta Crystallogr.*, **8**, 157 (1955), and J. M. Skinner, G. Stewart, and J. C. Speakman, *J. Chem. Soc.*, 180 (1964), respectively. [b] The coefficients are for the p_z atomic orbitals, since the lowest-lying unfilled molecular orbital is a π orbital.

We wish to propose that the spectrum observed at pH 13.2 is of species I. The very high ϵ value observed for I reflects the high oscillator strength for the $\pi \rightarrow \pi^*$ transition of this strongly resonating species. Partial protonation to form II results in a slight shift to shorter wavelengths. Complete protonation apparently changes the orbital configuration sufficiently to shift λ_{max} to <290 nm. Such spectral shifts to shorter wavelength with increasing state of protonation have been observed before for carboxy radicals.[12]

Further evidence can be cited to support our contention that electron addition to benzoate does not produce a cyclohexadienyl radical. In the first place, the pK_a for III → II is more than 1 pK unit higher than the parent acid which is a good indication that III is not simply a cyclohexadienyl radical with a normal carboxylic acid substituent group. Furthermore, *the spectra of III and the H adduct are completely different despite the fact that these species are stoichiometrically equivalent.* Finally, benzoate is isoelectronic with nitrobenzene which has been shown[27] to add e_{aq}^- to the nitro group. Thus, the spectra of the electron adduct and H adduct to nitrobenzene are very different.[27]

We attempted to measure the rate of protonation of the transient at pH 3.3–6 by observing the formation of the absorption under conditions where e_{aq}^- was scavenged by the substrate in <0.1 μsec. The equilibration reaction was over in 1–4 μsec and was dependent on pH with $k = 1.2 \times 10^6$ sec^{-1} at pH 4.5 and 7.2×10^5 sec^{-1} at pH 5.5. It appears that protonation proceeds not only *via* reaction with H_3O^+, but also through reaction with the solvent or the substrate. These protonation rates are considerably slower than those expected for protonation of the electron adduct with the charge localized on the ring.[28]

The proposed structures of the transient species are consistent with the observed pK_a values. Thus, species II, $(C_6H_5\dot{C}O_2H)^-$, is a considerably weaker acid than benzoic acid which is to be expected on electrostatic grounds. The difference of almost seven orders of magnitude in the values of the dissociation constants is observed in the successive dissociation of common dibasic acids. Similarly, the pK_a value for protonated benzoic acid, $[C_6H_5C(OH)_2]^+$ is estimated to be *ca.* −7.[29]

The values of the initial second-order decay constants for the electron adducts follow the general trend expected for species of these charges. Unfortunately, absolute kinetic evidence cannot be provided because of the possible reactions of the adducts with the *tert*-butyl radicals also present.[30] Note that the decay of I at pH >13 in the presence of CH_3OH as an OH scavenger is measurably slower than in *tert*-butyl alcohol. Here the reaction between two I species should be considerably slower than the reaction of two $\cdot CH_2O^-$ radicals ($2k = 9.0 \times 10^8$ M^{-1} sec^{-1})[6] on electrostatic grounds. The observed decay rate for I of $2k = 1 \times 10^8$ M^{-1} sec^{-1} is thus consistent with its charge. The first-order decay component which is present at the end of the initial second-order decay was not investigated in detail and is believed to be associated with the further reactions of the product of the adduct–adduct or adduct–alcohol radical reaction. Decarboxylation of the electron adduct must be a less probable process based on the low yields of CO_2 in the continuous radiolysis.[13] It is easy to see that the bimolecular disproportionation of III will yield benzoic acid and a species which, through proton transfer, leads to 1,4-dihydrobenzoic acid.

(27) K. D. Asmus, A. Wigger, and A. Henglein, *Ber. Bunsenges. Phys. Chem.*, **70**, 862 (1966).

(28) S. Arai and L. M. Dorfman, *J. Chem. Phys.*, **41**, 2190 (1964).

(29) E. Vander Donckt and G. Porter, *Trans. Faraday Soc.*, **64**, 3215 (1968).

(30) *tert*-Butyl alcohol radicals do not appear to be deprotonated in this pH range; see ref 6.

e_{aq}^- + Related Compounds. The spectral and acid–base characteristics of the electron adduct to methyl benzoate are virtually identical with those of the parent acid leading to the conclusion that here too the transient can be represented as a substituted benzyl radical.

$$e_{aq}^- + C_6H_5CO_2CH_3 \longrightarrow$$

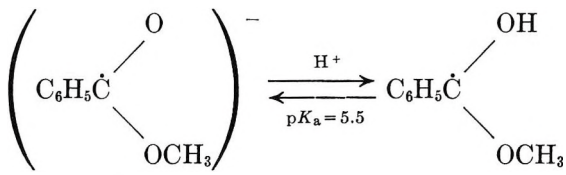

Inasmuch as protonation of benzoate does not have any significant effect on the charges of the atoms other than the carboxylate oxygen (Table III), esterification should likewise have little effect. Thus, in methyl benzoate, the carboxylate carbon would have a significant positive charge and could serve as the site of initial attack by e_{aq}^-. In the case of $(NH_3)_5CoO_2CC_6H_5^{2+}$, where the carboxylate oxygen is bound directly to the Co^{III} metal center, reaction with e_{aq}^- is very rapid ($k = 8 \times 10^{10}\ M^{-1}\ sec^{-1}$).[31] However, it is apparent that the molecular orbital populated provides facile intramolecular electron transfer into the metal center inasmuch as no electron adduct spectrum is observed within the time resolution of the pulse apparatus.[19]

The presence of substituents on the benzoic acid ring would be expected to show the effect of variation of orbital interaction between ring and side chain. Thus, the electron adduct to *o*-phthalate at pH 11 has λ_{max} 335 nm with $\epsilon_{335} = 1 \times 10^4\ M^{-1}\ cm^{-1}$. However, in the case of *m*-phthalate in basic solution, λ_{max} 325 nm with $\epsilon_{325} = 1.3 \times 10^4\ M^{-1}\ cm^{-1}$ with a weaker absorption at 450 nm. Evidently the presence of another carboxylate group in the ortho position gives the transient properties intermediate between that of the cyclohexadienyl radical with the charge localized on the ring and the benzyl type radical with the charge localized on the side chain. With the meta-directing substituents re-enforcing each other, the electron adduct resembles the benzoic acid radical even more.

As Table I shows, the electron adduct to $C_6H_5SO_3^-$ exhibits a spectrum that appears to be characteristic of cyclohexadienyl radicals with λ_{max} 325 nm and $\epsilon_{325} = 3.7 \times 10^3\ M^{-1}\ cm^{-1}$. With no apparent pH dependence of the spectrum up to pH 13.5, we conclude that the vacant orbital into which the electron adds must be strongly localized on the ring; the subsequent rapid protonation of the ring would occur even in alkaline solution.[28]

$$e_{aq}^- + C_6H_5SO_3^- \longrightarrow (\cdot C_6H_5SO_3)^{2-} \xrightarrow[\text{fast}]{H^+} \cdot C_6H_5(H)SO_3^-$$

It is worth mentioning that the electron adduct to benzene has been searched for unsuccessfully in aqueous solution.[32] On the other hand, the electron adduct to biphenyl (λ_{max} 405 nm)[28] can be readily seen to decay rapidly by first-order kinetics in aqueous solution even at pH 9 through protonation. The detailed nature of electron addition to aromatic systems, the ultimate in nucleophilic substitution, is still poorly characterized and requires further experimental and theoretical investigations before these details will be known to the same extent as are the rates of e_{aq}^- attack.

Acknowledgment. The authors thank Dr. E. Hayon for his interest in this work and for his hospitality during the tenure of our associateships.

(31) M. Simic and M. Z. Hoffman, manuscript in preparation.
(32) E. J. Hart, private communication.

Further Evidence on Free-Radical Decay in γ-Irradiated Alkyl Halide and Hydrocarbon–Alkyl Halide Glasses[1]

by Colin R. Roy and John E. Willard*

Department of Chemistry, University of Wisconsin, Madison, Wisconsin 53706 *(Received November 24, 1971)*

Publication costs assisted by the U. S. Atomic Energy Commission

This paper extends experimental information on factors which affect the decay rates of free radicals produced from alkyl halides in hydrocarbon glasses and in pure glassy and polycrystalline alkyl halides by γ irradiation. Effects of radical structure are illustrated by differences in the decay rates of the isomeric butyl radicals in solutions of the butyl chlorides in glassy 3-methylpentane-d_{14} (3MP-d_{14}) and by a decrease in decay rates with increasing chain length of alkyl radicals produced from *n*-alkyl iodides in 3MP-d_{14}. Effects of matrix structure are illustrated by the decay rates of the radicals in glassy ethyl, *n*-propyl, *n*-butyl, and *n*-amyl halides (RCl < RBr < RI) and by comparison of the relative decay rates of the isomeric butyl radicals in the glassy parent chloride matrices, with the relative rates in glassy 3MP-d_{14}. C_2H_5, CH_3CD_2, CD_3CH_2, and C_2D_5 radicals decay at the same rate in glassy 3MP-d_{14} but at different rates in their parent ethyl iodide matrices, the rates decreasing with the extent of deuteration. When γ-irradiated polycrystalline C_2H_5I at 77°K, giving the previously studied complex 1000-G esr spectrum, is warmed to 125°K, the central spectrum, attributable to C_2H_5 radicals, grows slowly with accompanying decrease of the lines on the wings. Photobleaching in the 375-nm region causes a decrease in all parts of the spectrum. On increase of the temperature to 134°K in the dark, the central signal increases by threefold in 10 min, accompanied by a decrease of the signal on the wings and followed by rapid decay of the central signal, indicating that the growth reaction does not have a sharp temperature threshold as previously suggested. Radical decays in polycrystalline ethyl and propyl chlorides and bromides have been compared.

Introduction

The kinetics of decay of free radicals formed by ionizing radiation or photochemical processes in organic glasses are informative about both the spatial distribution of the radicals and the role which the solvent plays in radical recombination processes. CH_3 and CD_3 radicals produced from CH_3I, CH_3Br, CH_3Cl, and CD_3I by dissociative electron capture and CH_3 formed by photodissociation of CH_3I in 1 mol % solutions in 3-methylpentane (3MP) glass at 77°K all decay by a pure first-order process with the same 16-min half-life.[2,3] In other glasses, such as 2-methylpentane (2MP) and methylcyclohexane (MCHx), the half-life is different and plots of the logarithm of the radical concentration *vs.* time show curvature convex toward the origin.[3] However, plots for samples having widely different initial concentrations as a result of different doses are superimposable after normalization for initial concentration, *i.e.*, the fractional decay per unit time is independent of initial concentration. These pure first-order and "composite first-order" decays, together with other evidence, have led to the conclusion that each radical must combine with its geminate halide ion or halogen atom partner. Similar kinetics have been observed for alkyl radicals produced from alkyl halides in a number of other systems, including γ irradiation of pure C_2H_5I glass at 77°K.[4] Of particular significance is the finding that radical decay by geminate recombination in a perdeuterated glassy matrix at 77°K is much slower than in the corresponding perprotiated matrix,[3-5] whereas the rate of decay is not influenced by deuteration of the decaying radical.[2] This and related evidence indicate that the rate-determining step in radical decay by geminate recombination is controlled by vibrations and/or rotations of the matrix molecules, or groups on the matrix molecules, which assist the trapped radical to gain the configuration necessary for combination with the partner with which it is caged.

In the present paper the investigation of free radical decay rates has been extended to a series of systematically chosen systems for the purpose of learning more about the relative roles of radical structure and matrix structure in determining such rates.

Experimental Section

The alkyl halides used were Eastman White Label. 3-Methylpentane-d_{14} (3MP-d_{14}), C_2D_5I, CD_3CH_2Br, and CH_3CD_2I (stated isotopic purities 98%) were from Merck Sharp and Dohme. All of these compounds were used

(1) This work has been supported in part by the U. S. Atomic Energy Commission under Contract AT(11-1)-171 and by the W. F. Vilas Trust of the University of Wisconsin.

(2) R. F. C. Claridge and J. E. Willard, *J. Amer. Chem. Soc.*, 87, 4992 (1965).

(3) W. G. French and J. E. Willard, *J. Phys. Chem.*, 72, 4604 (1968).

(4) H. W. Fenrick, N. B. Nazhat, P. J. Ogren, and J. E. Willard, *ibid.*, 75, 472 (1971).

(5) H. W. Fenrick and J. E. Willard, *J. Amer. Chem. Soc.*, 88, 412 (1966).

as received following degassing and distillation from P_2O_5 on the vacuum line. CD_3CH_2I was made by the reaction of CD_3CH_2Br with AlI_3 under vacuum. All samples were distilled to 3-mm i.d. Suprasil esr tubes on the vacuum line.

Glassy samples were formed by immersion in liquid nitrogen. Polycrystalline C_2H_5I and C_3H_7Cl were prepared by warming the glass until spontaneous crystallization occurred followed by recooling to 77°K. C_2H_5Br and C_3H_7Br crystallized on immersion at 77°K. A point of interest is that although the esr signal from γ-irradiated glassy C_2H_5I is isotropic with respect to rotation around its vertical axis in the esr cavity, γ irradiation of the polycrystalline sample formed spontaneously from the glass gives an anisotropic signal[4,5] which, however, becomes isotropic when the sample is pulverized.[6]

In the case of C_2H_5I, it was shown that a sample which had been held at 77°K for 17 days prior to γ irradiation gave the same rate of radical decay (within 5%) as an unannealed sample.

Esr measurements were made with the sample tubes in a Varian liquid nitrogen esr dewar using a Varian 4500 X-band spectrometer operating at a modulation frequency of 100 kHz and a power of 7 mW. γ-Irradiations were made at 77°K with a ^{60}Co source at a dose rate of 4×10^{18} eV g^{-1} min^{-1}.

Results

Confirmation of Composite First-Order Decay. Composite first-order decay of ethyl radicals in γ-irradiated ethyl iodide has been demonstrated.[4] The similarity of the decay curves of other alkyl radicals in their γ-irradiated alkyl iodide matrices implies similar kinetics.[4] Our experiments have confirmed the composite first-order decay of C_2H_5 radicals in γ-irradiated C_2H_5I glass and have shown that the decay curves for n-C_4H_9 radicals in samples of n-C_4H_9Cl glass at 77°K, which differ in concentration by a factor of 8 (0.5- and 4-min irradiations), are superimposable after normalization for the initial concentration, indicating further the generality of composite first-order kinetics for the decay of alkyl radicals produced by γ irradiation of glassy alkyl halides.

Relative Decay Rates of Isomeric Butyl Radicals. To compare the decay rates of the four isomeric butyl radicals when produced by the same mechanism in identical matrices, we have γ-irradiated 1 mol % solutions of n-C_4H_9Cl, *sec*-C_4H_9Cl, i-C_4H_9Cl, and *tert*-C_4H_9Cl in 3MP-d_{14} at 77°K. The outer lines of the *ca.* 150-G wide spectra of the protiated radicals are easily observed without interference from the *ca.* 50-G wide spectrum of the C_6D_{13} matrix radical. The irradiations were 1 min in duration. All four radicals decayed less than 1% per 10 min at 77°K. About 10 min after the end of irradiation, the sample was transferred to liquid argon (87°K) contained in the Varian esr dewar in the cavity. Decay measurements were initiated 40 sec after the transfer by allowing the Fieldial unit to repetitively scan one of the outer peaks of the radical spectrum at 30-sec intervals. A time of 40 sec after immersion in the liquid argon is taken as zero time on Figure 1, which shows that the decay rates of *sec*-C_4H_9, i-C_4H_9, and *tert*-C_4H_9 are similar, while that of n-C_4H_9 is much slower.

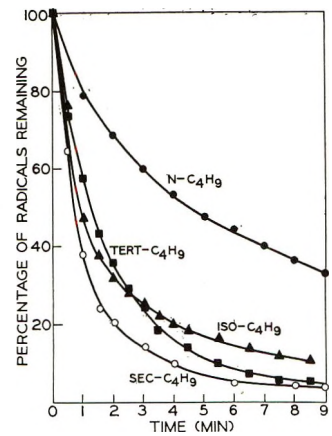

Figure 1. Decay of isomeric butyl radicals formed by dissociative electron capture by 1 mol % butyl chlorides in 3MP-d_{14}. γ dose at 77°K, 3.5×10^{18} eV g^{-1}. Decay measured at 87°K starting 40 sec after transfer of sample from 77°K.

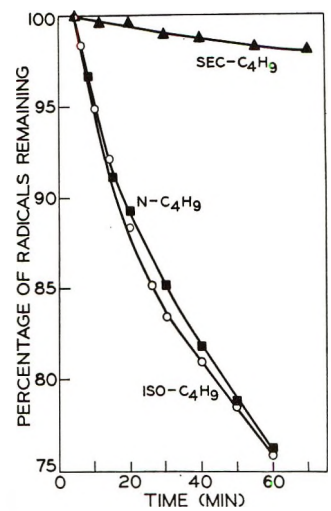

Figure 2. Decay of isomeric butyl radicals in isomeric glassy butyl chlorides at 77°K. γ dose, 3.6×10^{18} eV g^{-1}.

Comparison of Figure 2 with Figure 1 shows that the nature of the matrix in which decay occurs, or temperature, affects the relative decay rates of the isomeric radicals. The data of Figure 2 are for the isomeric radicals decaying at 77°K in the γ-irradiated parent isomeric compounds. The normal and iso radical decays are essentially equal in rate, while the secondary radical decays much more slowly. *tert*-Butyl chloride could not be obtained as a glass.

(6) R. J. Egland, P. J. Ogren, and J. E. Willard, *J. Phys. Chem.*, 75, 467 (1971).

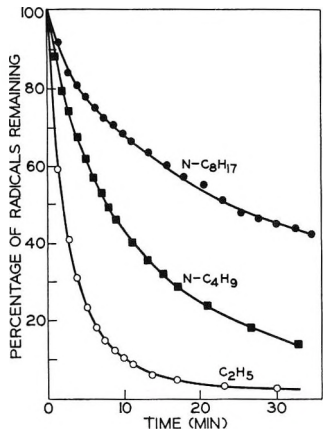

Figure 3. Decay of C_2H_5, n-C_4H_9, and n-C_8H_{17} radicals formed by dissociative electron capture by 1 mol % alkyl iodides in 3MP-d_{14}. γ dose at 77°K, 10^{18} eV g^{-1}. Decay measured at 87°K starting 40 sec after transfer of sample from 77°K.

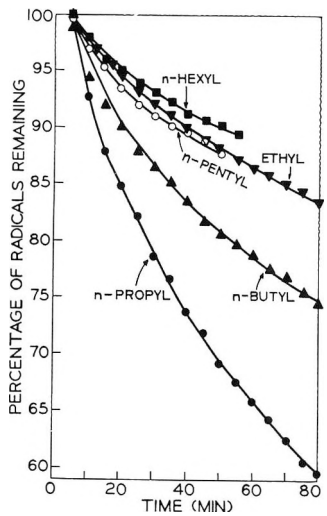

Figure 4. Decay of C_6H_{13}, C_5H_{11}, C_4H_9, C_3H_7, and C_2H_5 radicals in glassy n-$C_6H_{13}Cl$, n-$C_5H_{11}Cl$, n-C_4H_9Cl, n-C_3H_7Cl, and C_2H_5Cl, respectively, following formation by γ irradiation at 77°K. γ dose, 3.6 × 10^{18} eV g^{-1}.

Effect of Chain Length on Radical Decay in 3MP. When 1 mol % solutions of C_2H_5I, n-C_4H_9I, and n-$C_8H_{17}I$ in 3MP-d_{14} are γ irradiated at 77°K and then raised to 87°K, the C_2H_5, C_4H_9, and C_8H_{17} radicals formed decay at rates which decrease with increasing chain length (Figure 3). The data of Figure 3 start at a time 40 sec after immersion of the sample in liquid Ar at 87°K.

Variation of Radical Decay Rates with C Number in n-Alkyl Halide Glasses. In the homologous series of alkyl chloride glasses, the decay rates of the alkyl radicals produced by γ irradiation decrease in going up the series (Figure 4), except for ethyl chloride, which falls between pentyl and hexyl. 100% C_2H_5Cl does not form a glass. Therefore, the glassy sample of Figure 4 was prepared with addition of 10 mol % n-$C_6H_{13}Cl$.

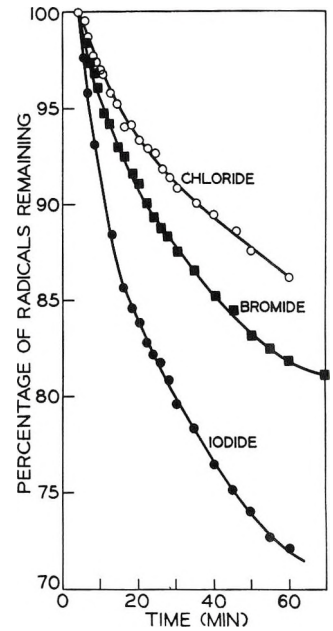

Figure 5. Decay of C_5H_{11} radicals in glassy n-$C_5H_{11}Cl$, n-$C_5H_{11}Br$ and n-$C_5H_{11}I$ at 77°K. γ dose, 3.6 × 10^{18} eV g^{-1}.

An experiment with n-C_3H_7Cl, which forms a glass easily in the pure state, showed that 10% of such an additive does not significantly alter the decay rate of the radical of the major component. Further evidence that ethyl halide glasses have a structure less conducive to radical decay than C_3, C_4, and C_5 halides was found with the glassy n-alkyl bromide and iodide series, where again the decay rates of the ethyl compounds fell between the pentyl and hexyl. In the pure glassy alkyl halides, two factors influence the relative rates of decay of the different radicals, one being the structure of the radical (as is also the case when they decay in 3MP-d_{14}, Figures 1 and 3), and the other the change in structure of the matrix with change in C number.

Relative Decay Rates in Alkyl Chlorides, Bromides, and Iodides. The rates of decay of alkyl radicals have been compared in their glassy chloride, bromide, and iodide matrices, as illustrated in Figure 5 for the pentyl compounds. For the ethyl, propyl, butyl, and pentyl halides, decay in the iodide matrices was faster than in the bromide, which was faster than in the chloride. For the hexyl halides, the order was I > Cl > Br.

Comparison of Radical Decay in C_2D_5I, CD_3CH_2I, CH_3CD_2I, and C_2H_5I, C_2H_5Br and CD_3CH_2Br. C_2D_5 radicals produced in C_2D_5I glass at 77°K by γ irradiation decay much more slowly (12 days for 50% decay) than C_2H_5 radicals in C_2H_5I (150 min for 50% decay).[4] In a 50%–50% mixture of C_2D_5I and C_2H_5I, C_2H_5 and C_2D_5 decay equally, at a rate which is intermediate between the rates in the isotopically pure matrices, indicating that the differences in rate result from the deuteration of the matrix rather than the deuteration of the decaying radicals.[4] To test the hypothesis that the deuteration effect might be due predominantly to slowing

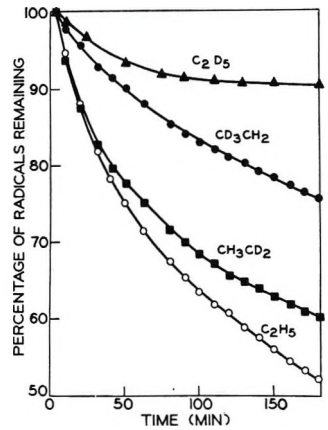

Figure 6. Decay of isotopic ethyl radicals in γ-irradiated glassy ethyl iodides at 77°K during first 170 min after irradiation. γ dose, 5.4×10^{18} eV g^{-1}.

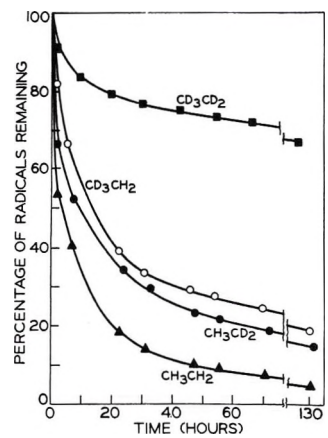

Figure 7. Decay of isotopic ethyl radicals in γ-irradiated glassy ethyl iodides at 77°K during 130 hr after irradiation. γ dose, 5.4×10^{18} eV g^{-1}.

of motions of the relatively light CH_3 groups, with relatively little effect from deuteration of the heavy CH_2I group, we have compared ethyl radical decay rates in CD_3CH_2I and CH_3CD_2I with those in C_2D_5I and C_2H_5I (Figures 6 and 7). During the first 150 min of decay, illustrated in Figure 6, the ethyl radical signal heights were scanned every minute; all of the data fell on the lines shown in the figure.

Another effect of deuteration is indicated by the data of Table I, which show that the rates of decay of CD_3CH_2 radicals in glassy CD_3CH_2I and CD_3CH_2Br are nearly identical, whereas the rates of decay of C_2H_5 in C_2H_5I and C_2H_5Br differ by a factor of more than 2. Deuteration of the methyl group of the iodide has a much greater effect on the rate of radical decay than deuteration of the methyl group of the bromide.

Radical Decay in Polycrystalline Alkyl Halides. A comparison of radical decays in four γ-irradiated polycrystalline alkyl halides is given in Table II. It suggests the conclusion that for equal T_D/T_M, decay is faster in the ethyl and *n*-propyl bromides than in the corresponding chlorides and faster in the ethyl than the propyl matrices. This is in contrast to the glassy systems, where ethyl decay falls out of the carbon number sequence, being slower than that of propyl, butyl, or pentyl in their matrices.

Table I: Effect of Methyl Group Deuteration on Relative Decay Rates of Ethyl Radicals in Glassy Ethyl Iodide and Ethyl Bromide

Radical (matrix)	Time, min, for the % decay indicated 5%	10%	15%	20%
CD_3CH_2 (CD_3CH_2Br)	16	41	67	107
CD_3CH_2 (CD_3CH_2I)	18	46	78	126
Ratio of times	0.9	0.9	0.9	0.9
CH_3CH_2 (CH_3CH_2Br)	7	24	43	71
CH_3CH_2 (CH_3CH_2I)	~4	11	20	31
Ratio of times	~2	2.2	2.2	2.2

Table II: Decay of Alkyl Radical in Polycrystalline Alkyl Halides

Radical (matrix)	Mp (T_M), °K	Temp of decay study (T_D), °K	T_D/T_M	Time for 50% decay, min
C_2H_5Cl (C_2H_5Br)	134	125	0.92	24
C_2H_5Br (C_2H_5Br)	154	133	0.86	11
C_3H_7Cl (C_3H_7Cl)	150	145	0.97	37
C_3H_7Br (C_3H_7Br)	163	153	0.94	20

Postirradiation Radical Growth and Decay in Polycrystalline C_2H_5I. γ-Irradiated polycrystalline C_2H_5I gives a complex 1000-G esr spectrum of *ca.* 40 lines[5-7] (Figure 8), the origin of which is not yet understood. When samples giving this spectrum are warmed from 77 to 147°K for 1 min and reexamined at 77°K, the multiline spectrum on the wings is found to have decreased in intensity accompanied by growth of the central signal attributed to C_2H_5 radicals.[5] During further exploration of this phenomenon, we have found that the spectrum (1) shows little decay in the dark at 121°K over 15 min; (2) decays at about 1–2%/min when the sample is exposed at 121°K to radiation of *ca.* 375 nm at an intensity of 5×10^{14} photons sec^{-1}, with similar bleaching observed at other wavelengths; and (3) shows a large rapid growth of the central signal accompanied by decay of the signal on the wings when the

(7) P. J. Ogren and J. E. Willard, *J. Phys. Chem.*, **75**, 3359 (1971).

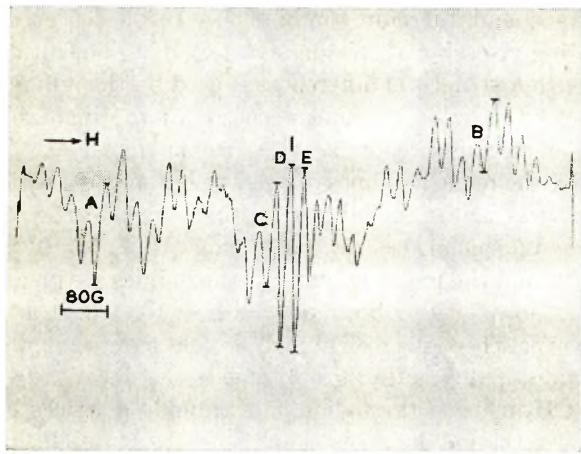

Figure 8. Esr spectrum of γ-irradiated polycrystalline ethyl iodide at 77°K: γ dose, 8×10^{19} eV g^{-1}; power, 7 mW; modulation amplitude, 800; signal level, 100; recorder setting, 60 mV.

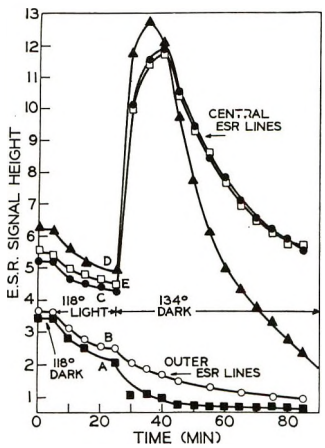

Figure 9. Growth and decay of central esr spectrum (C, D, E) and wing spectrum (A, B) in γ-irradiated polycrystalline C_2H_5I. Each lettered curve represents the decay (growth) of the correspondingly lettered line in Figure 8. γ dose at 77°K, 8×10^{19} eV g^{-1}. The conditions were changed with time as follows: (1) 0–5 min, 110°K in the dark; (2) 5–25 min, 118°K and exposed to 375-nm light; (3) 25–85 min, 134°K in the dark.

temperature is raised to 134°K, followed by decay of the central signal (Figure 9). This decay has an initial half-life of about 20 min, in contrast to the complete decay of C_2H_5 radicals in C_2H_5I glass in less than 5 min at 102°K.[8] Slow growth of the central signal was also observed when C_2H_5I glass irradiated at 77°K was warmed to 125°K. Confirming previous work, no growth occurred in samples of polycrystalline C_2H_5I frozen slowly at the melting point using a seed crystal. Likewise, there was no growth in a sample crystallized from a glass if the crystals were warmed to 145°K before γ irradiation at 77°K. The slow growth at temperatures as low as 125°K shows that the earlier suggestion that the growth is dependent on a strain release with a very sharp temperature threshold at about 147°K is not correct.

Systematic efforts to induce growth of the central signal by photobleaching such as reported earlier[9] were unsuccessful.[10] These utilized several sources of light including the unfiltered radiation of 660–1000 nm with 6×10^{16} photons sec^{-1} on the sample (Cary ir source), and filtered radiation of 320–680 nm with 2×10^{16} photons sec^{-1} on the sample (high-pressure Hg lamp). Photobleaching was done at both 77 and 121°K. The light exposure caused decrease in both the central and outer lines of the 1000-G spectra, the decrease being greater in the outer region.

The optical spectra of both polycrystalline[9] and glassy[11] ethyl iodide which have been γ-irradiated contain four absorption peaks in the 300–800-nm range which appear to represent at least three species. The results suggest that no single one of these is responsible for the absorption which leads to the observed photobleaching, but that an unresolved absorption must be involved.

Other Postirradiation Changes in Free-Radical Esr Spectra. When the esr spectra of samples of γ-irradiated 3MP-d_{14} glass containing 1 mol % alkyl halide were observed at 77°K both before and after immersion for 30 sec in liquid argon at 87°K, the line height of the second spectrum was usually 40% or more higher than the first. In the case of *tert*-butyl chloride, the line height doubled while the line width at maximum slope decreased by 10%.

The compounds yielding radicals which showed peak height increases as a result of the 30-sec treatment at 87°K included CH_3CD_2I, CD_3CH_2I, CD_3CH_2Br, *n*-C_4H_9I, *sec*-C_4H_9I, and *tert*-C_4H_9I. In each case, a second 30-sec treatment at 87°K lowered the peak height, as did subsequent 3- and 4-min treatments.

Discussion

In their extensive survey of esr spectra of γ-irradiated alkyl halide solids at 77°K, Ayscough and Thompson[12] showed that the spectra are consistent with the conclusion that bond rupture is predominantly at the carbon–halogen bond and that line widths and line heights are conditioned by constraints which the molecules of the matrix place on the configuration of the radical, and on rotations of its groups. Subsequent work[2-4,13] suggests that a major fraction of the carbon–halogen bond rupture occurs by dissociative electron capture, and that the free radicals decay by recom-

(8) P. J. Ogren, Ph.D. Thesis, University of Wisconsin, 1968.

(9) R. J. Egland, Ph.D. Thesis, University of Wisconsin, 1968.

(10) This fact has been reported in a previous paper,[6] p 469. By error, the abstract of that paper retained a statement that conversion of the complex spectrum to the central spectrum is induced by photobleaching.

(11) R. F. C. Claridge and J. E. Willard, *J. Amer. Chem. Soc.*, **88**, 2404 (1966).

(12) P. B. Ayscough and C. Thompson, *Trans. Faraday Soc.*, **58**, 1477 (1962).

(13) M. Shirom and J. E. Willard, *J. Phys. Chem.*, **72**, 1702 (1968).

bination with the geminate halide ion partner. For methyl radicals it is well established that this rate of recombination is dependent on the nature of the matrix and the temperature[3] but not on the nature of the halide partner or on whether the radical is CH_3 or CD_3.[2] It has earlier been shown that CH_3 and CD_3 decay at the same rates in a mixed CH_3OH–CD_3OH matrix, but that decay is slower in CD_3OH than CH_3OH.[14] The present work has confirmed the independence of decay rate on the nature of the geminate partner and the extent of deuteration of the radical by showing (within the accuracy of the data) that n-C_4H_9 radicals decay at the same rate in glassy 3MP-d_{14} at 87°K whether Cl^- or I^- is the geminate partner, and that the rates of ethyl radical decay in 3MP-d_{14} at 87°K are the same for C_2H_5, CH_3CD_2, CD_3CH_2, and C_2D_5 and for Br^- or I^- as the geminate partner. (The absence of an esr signal for the paramagnetic species RX^- formed on recombination is attributed to line broadening which makes it unobservable.)

If, as postulated,[3,4] the rate of free-radical decay is determined by the rate at which radicals retrieve the configuration necessary for combination with their geminate partners, this might be expected to vary for radicals of different isomeric structures. Such variation is illustrated by the difference between the rate of n-C_4H_9 decay in 3MP-d_{14} and the rates of the other butyl radical isomers (Figure 1). Likewise, the rate of decay decreases with increasing chain length of the alkyl group when the decays are examined in the same matrix (Figure 3).

The slowness of *sec*-C_4H_9 decay in glassy *sec*-C_4H_9Cl relative to the decays of n-C_4H_9 and i-C_4H_9 in their parent matrices, as compared to the slowness of n-C_4H_9 relative to the other radicals when examined as solutes in 3MP-d_{14}, indicates that isomerism of the *matrix* molecules greatly influences decay rates. The matrix effect is further illustrated by comparing the relative decay rates of the n-alkyl radicals in 3MP-d_{14} with those in the parent glassy chlorides. In 3MP-d_{14} the rate for C_2H_5 is faster than the decay rates of radicals with higher carbon number, whereas the C_2H_5 rate falls between that of n-C_5H_{11} and n-C_6H_{13} in the parent matrices (Figure 4).[15]

The data of Figure 5 for the amyl halides and similar data for the ethyl, n-propyl, and n-butyl show that in each case the initial decay rates of the alkyl radicals fall in the sequence I > Br > Cl, in contrast to the independence of the rates on the nature of the halide partner when the halides are dissolved in 3MP-d_{14}. This is in the order of decreasing melting points of the halide crystals, and therefore probably in the order of decreasing viscosity of the glasses at 77°K. Thus it appears that structural differences caused by the different sizes of the halogen atoms account for the increasing ease of recombination as the size is increased. At 293°K the molar volumes of the five bromides in which decay was tested are all greater than those of the corresponding chlorides (by an average of 7×10^{-3} l. mol^{-1}) and the molar volumes of the iodides are greater than those of the bromides (10×10^{-3} l. mol^{-1}). However, the data of Table I, which show that deuteration of the methyl group affects the decay rate of CD_3CH_2 in both the iodide and bromide matrices but more in the iodide, show that the deuteration effect is stronger than that of molecular volume in this case.

The differences in decay rates of C_2H_5, CH_3CD_2, CD_3CH_2, and C_2D_5, as measured in their respective iodide matrices (Figures 6 and 7), cannot be attributed to decay by hydrogen abstraction from matrix molecules, with a higher activation energy for abstraction of D than H, because: (a) no new radicals are formed replacing those which decay (such alkyl radicals would be readily observable) and (b) the activation energy would have to be of the order of 6 kcal/mol^{-1} or less to allow the rates observed, unless there was a high probability of tunneling.[16]

The indication in Figure 6 that the initial decay rates of CH_3CD_2 and C_2H_5 are similar but diverge after *ca.* 20% decay suggests the existence of two distinctly different populations of radicals, a conclusion which has also been indicated by radical growth data reported earlier.[4] These rates are about four times faster than those for CD_3CH_2 in CD_3CH_2I. This is consistent with the hypothesis that deuteration of the relatively light methyl group should have more effect on the matrix molecule motions necessary to assist geminate recombination within the cage than deuteration of the relatively heavy CH_2I group. For higher percentage decays, the difference between the effect of deuteration of the methyl and methylenic groups becomes much less again, suggesting that different mechanisms of radical decay play a role at low and high percentages of decay.

(14) P. J. Sullivan and W. S. Koski, *J. Amer. Chem. Soc.*, **85**, 384 (1963).

(15) It should be noted that the comparisons between decay rates in 3MP-d_{14} discussed in this section were made at 87°K, while those in the parent matrices were made at 77°K. It is also possible that a larger fraction of the radicals produced in the pure halide matrices is formed by processes other than dissociative capture.

(16) E. D. Sprague and F. Williams, *J. Amer. Chem. Soc.*, **93**, 787 (1971).

Free Radical Formation in Hydrocarbon Crystals by γ Irradiation. II.[1]

Relative Yields of Isomeric Alkyl by Electron Spin Resonance

by Anders Lund

The Swedish Research Councils' Laboratory, Studsvik, S-611 01 Nyköping 1, Sweden *(Received November 23, 1971)*

Publication costs assisted by the Atomic Research Council of Sweden

Single crystals of the lower *n*-paraffins containing 4–16 carbon atoms give rise to esr spectra from secondary alkyl $CH_3\dot{C}HCH_2R$ (I) and $R'CH_2\dot{C}HCH_2R''$ (II) after γ irradiation at 77 or 195 K. The conformation of radicals formed in butane differs somewhat from those trapped in the long-chain *n*-alkane crystals. The relative yields of I and II were estimated by a least-squares fit. The predominant formation of I is shown to be inconsistent with estimates based on the analysis of final products. Possible explanations are discussed in terms of reactions along the particle tracks, and ionic mechanisms. A neutralization process is suggested which would lead to the preferential formation of radicals of type I by reason of the charge distribution in the positive radical ion primarily formed.

Introduction

Radiation chemical processes in liquid hydrocarbons[2] have been extensively investigated using chemical methods. The specific considerations relating to the peculiarities of the solid state have so far received less attention.[3] Only in a few cases has the radical yield following irradiation at 77 K of *n*-alkanes been determined.[4,5] These studies were based on an analysis of the final product distribution as shown by gas chromatography. This method involves several assumptions which are implicit in the analysis.[4] For this reason, a more direct estimate of the relative yields of free alkyl in the solid by means of esr was thought to be a valuable complement to the above studies.

Esr studies of irradiated single crystals allowed an unambiguous assignment of the radicals formed in several alkanes.[1] In this study the relative importance of different alkyl radicals has been estimated for hydrocarbons in the *n*-alkane series ranging from butane to hexadecane. A comparison of the yields in samples irradiated at temperatures of 77 K and 195 K has also been carried out, in order to find out whether the rigidity of the matrix has any influence on the nature and yields of the products.

The crystal structures of the lower *n*-paraffins[6] with an even number of carbon atoms are known to consist of one molecule in a triclinic unit cell. No data on butane are known, but the results obtained here indicate a higher symmetry. Of the odd-numbered alkanes, undecane was selected for investigation in order to determine whether the differences caused by an orthorhombic crystal structure[7] might affect the nature and yields of the free radicals formed.

Experimental Section

Single crystals of the hydrocarbons butane, hexane, octane, decane, undecane, and hexadecane were prepared according to a technique which has been previously described.[8] The crystals were irradiated using a ^{60}Co γ source and a dose rate of 0.7 Mrad/hr. All the samples received equal doses of approximately 2.5 Mrads. The irradiation temperature was either 77 K or 195 K.

Esr spectra were recorded at 77 K with a Varian E-9 spectrometer operating at a frequency of 9.15 GHz and a microwave power of 1 mW. The crystalline samples were contained in Suprasil tubes and could be rotated about the tube axis, at right angles to the magnetic field direction. In some cases a small piece of the tube was cut off in the cold. This piece could be rotated about an axis perpendicular to the tube axis by means of a quartz rod which had been fused to the Suprasil ampoule. This technique was also extended to allow for rotation about three mutually perpendicular axes. Three different pieces of the tube containing the crystal were then used, one for each axis of rotation.

Spectra intended for computer analysis were recorded in digital form on paper tape by means of a C-1024 time-averaging computer supplemented with a

(1) Part I: T. Gillbro, P.-O. Kinell, and A. Lund, *J. Phys. Chem.*, **73**, 4167 (1969).

(2) T. Gäumann and J. Hoigné, Ed., "Aspects of Hydrocarbon Radiolysis," Academic Press, London, 1968.

(3) L. Kevan and W. F. Libby, "Advances in Photochemistry," Vol. II, W. A. Noyes, Jr., G. S. Hammond, and J. N. Pitts, Jr., Ed., New York, N. Y., 1964, p 183 ff.

(4) H. Widmer and T. Gäumann, *Helv. Chim. Acta*, **46**, 944 (1963).

(5) Ç. Bienfait, J. Ceulemans, and P. Claes, *Advan. Chem. Ser.*, **No. 82**, 300 (1968).

(6) (a) N. Norman and H. Mathisen, *Acta Chem. Scand.*, **15**, 1747 (1961); (b) *ibid.*, **15**, 1755 (1961); (c) *ibid.*, **18**, 353 (1964).

(7) N. Norman and H. Mathisen, Central Institute for Industrial Research, Final Technical Report, Publication No. 334, Blindern, Oslo, 1961.

(8) T. Dahlgren, T. Gillbro, G. Nilsson, and A. Lund, *J. Sci. Instrum.*, **4**, 61 (1971).

TMC Model 220 data output unit and a Tally Model 420 tape perforator connected to the spectrometer.

The analysis of spectra containing several superimposed components was attempted using a computer-assisted method. The spectrum to be analyzed was fitted to an equation of the type

$$F(x_i) = \sum_{j=1}^{m} c_j f_j(x_i)$$

by a least-squares procedure using a number of equidistant field points x_i. Here c_j represents the fraction of the component f_j present. These components are simulated in the program[9] which employs the appropriate parameters for the coupling constants a, derivative line widths ΔH_{pp}, and g factors. Either Lorentzian (L) or Gaussian (G) derivative line profiles can be used.

Results

Butane. Only one component could be identified in the spectra obtained when the crystal was rotated about the tube axis. The spectrum shown in Figure 1a was obtained for a specific angle of rotation at which the line profile became almost symmetric with respect to its center. This line shape can be reasonably well simulated using the parameters given in Figure 1b. The slight asymmetry noted in Figure 1a which becomes pronounced for other angles of rotation is probably due to a site-splitting associated with the presence of several molecules in the unit cell.

Hexane, Octane, Decane, and Undecane. The spectra obtained after irradiation at 77 K have been described previously.[1] With octane and decane a considerable improvement in spectral resolution was achieved when the sample was irradiated at 195 K. The spectrum shown in Figure 2a appeared when the field vector was adjusted for a maximum total splitting by rotating the decane crystal about the tube axis. The two components included in the fitting procedure are given in Figure 2b and Figure 2c, respectively, while the fit itself is reproduced in Figure 2d. The spectrum remaining after subtracting the component in Figure 2b from the experimental line profile is shown in Figure 2e.

Spectra from an undecane sample irradiated at 195 K were less well resolved than those obtained from the hydrocarbons with an even number of carbon atoms under similar conditions. No quantitative analysis of these spectra has been carried through.

Hexadecane. The spectra from hexadecane irradiated at 77 K showed an anisotropy comparable to that obtained for the hexane, octane, and decane samples when the crystal was rotated about the tube axis, although the spectra exhibited a lower degree of resolution. The spectrum showing the maximum overall width, Figure 3a, could be analyzed in the same manner as the corresponding spectra for hexane, octane, and decane. This does not apply to the spectra obtained after irradiation of the crystal at 195 K, Figure 3b.

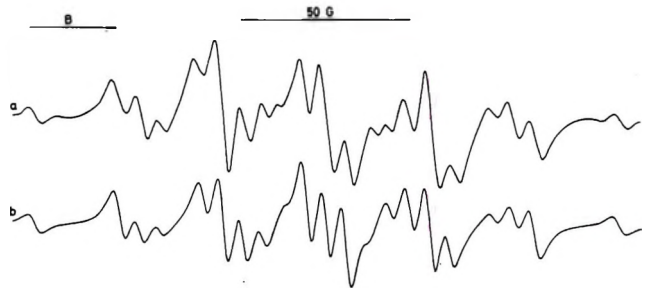

Figure 1. Esr spectrum from γ-irradiated butane at 77 K for a crystal orientation at which site-splitting caused minor asymmetry; (b) is a calculated spectrum for $CH_3\dot{C}HCH_2CH_3$ with $a_{CH_3} = 24.8$ G, $a_\alpha = 30.5$ G, $a_{\beta_1} = 36.4$ G, $a_{\beta_2} = 30.5$ G, $\Delta H_{pp} = 4$ G (L).

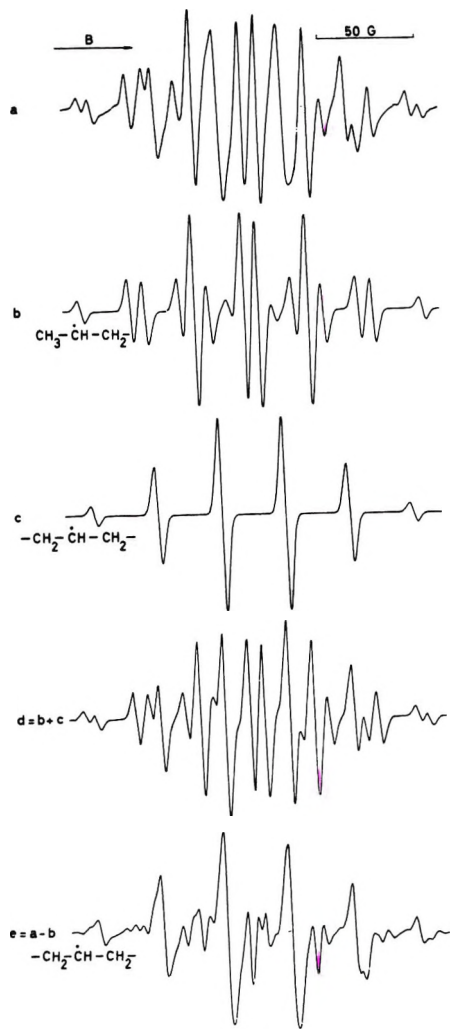

Figure 2. (a) Esr spectrum from a single crystal of decane γ-irradiated at 195 K and oriented to give a maximum overall separation; (b) simulated spectrum from $CH_3\dot{C}H(CH_2)_7CH_3$; (c) simulated spectrum from $-CH_2\dot{C}HCH_2-$; (d) spectrum synthetized from (b) + (c) through a least-squares fit to (a); parameters are given in Table I; (e) difference spectrum obtained from (a) − (b).

(9) Program ASESK written by T. Vänngård (1961); revised and extended by A. Lund and T. Shiga (1971).

Table I: Relative Amounts of Isomeric Alkyl after γ Irradiation to 2.5 Mrads at 77 and 195 K. (The Resonance Parameters Are Those Employed in the Least-Squares Fit)

Hydrocarbon	T, K	Radical	a_{CH_3}, G	a_{CH_2}, G	a_α, G	ΔH_{pp}, G	Relative amount, %
Hexane	77	$CH_3\dot{C}H(CH_2)_3CH_3$	25.9	33.6	33.2	5(L)	85 ± 5[a]
		$CH_3CH_2\dot{C}H(CH_2)_2CH_3$		33.6	33.2	5(L)	15
Octane	77	$CH_3\dot{C}H(CH_2)_5CH_3$	25.0	33.0	32.0	5.5(L)	77
		$-CH_2\dot{C}HCH_2-$		33.0	32.0	5.5(L)	23
	195	$CH_3\dot{C}H(CH_2)_5CH_3$	25.0	33.0	33.0	4(G)	88
		$-CH_2\dot{C}HCH_2-$		33.0	33.0	4(G)	12
Decane	77	$CH_3\dot{C}H(CH_2)_7CH_3$	25.0	33.0	31.5	6(L)	73
		$-CH_2\dot{C}HCH_2-$		33.0	31.5	6(L)	27
	195	$CH_3\dot{C}H(CH_2)_7CH_3$	25.9	33.6	33.2	4(G)	63
		$-CH_2\dot{C}HCH_2-$		33.6	33.2	5(G)	37
Hexadecane	77	$CH_3\dot{C}H(CH_2)_{13}CH_3$	25.9	33.6	33.2	5.0(L)	54
		$-CH_2\dot{C}HCH_2-$				6.5(L)	46
	195	$CH_3\dot{C}H(CH_2)_{13}CH_3$	25.5	32.9	32.5	3.5(G)	59
		$CH_3\dot{C}H(CH_2)_{13}CH_3$	23.1	32.7	12.5	3.5(G)	
		$-CH_2\dot{C}HCH_2-$		32.9	32.5	3.5(G)	41
		$-CH_2\dot{C}HCH_2-$		32.7	12.5	3.5(G)	

[a] The error quoted is the maximum deviation in a series of five independent determinations employing either different samples or differently oriented samples.

A site-splitting is indicated by the fact that two maxima of the overall total width were found at about right angles to each other when the crystal was rotated about the tube axis. The spectrum of Figure 3b was accordingly considered to comprise four components, two from each of two sites. Each site contributes equally to the signal strength since they represent chemically equivalent molecules within the unit cell. The resulting fit (see Figure 3c) was obtained from the input data of Table I.

Discussion

An account of the radical structure formed in the crystalline n-alkanes after γ irradiation at 77 K has previously been presented.[1] Similar species are formed after irradiation at 195 K. As a result of the improved resolution in the latter case, the assignments can be made with an increased confidence. The analysis of the spectra from decane shows that the main component (I) is characterized by the approximately isotropic couplings $a_1 = 25 \pm 1$ G (3H) and $a_2 = 33 \pm 1$ G (2H) and an anisotropic coupling a_3 (1H) which is typical of the

$$CH_3\dot{C}HCH_2R$$
I

type of radical. This species also predominates after γ irradiation at 77 K.[1]

The subtraction of the absorption due to I reveals the presence of a second component in the spectrum shown in Figure 2a. In addition to the spurious peaks attributed to the imperfection of the subtraction procedure, component II in Figure 2e comprises six lines with an approximately binominal intensity distribution. This could arise from a radical of the type

$$RCH_2\dot{C}HCH_2R'$$
II

where $a_{CH_2} \approx a_\alpha = 33$ G.

The narrower line width obtained at the higher temperature supports the hypothesis that the main broadening mechanism is the dipole–dipole interaction[5] between radicals formed in close proximity. At 195 K the matrix is softer, and this permits the recombination or diffusion of radicals formed close to the track of the ionizing particle.

In all cases except for butane, rotation about the tube axis yielded essentially similar spectra for the crystals; this indicates that there is a preferential crystal growth along this axis. Crystallographic data for pentane[6c] show that the mode of packing is quite distinct from those of the other n-paraffin structures. The chain axes of the pentane molecules in the unit cell are not parallel to each other. The site-splitting observed in butane indicates that the same phenomenon occurs here also. The nonequivalence of the methylene proton interactions (Figure 1) is attributed to the perturbing influence of the neighboring end methyl group.

With the exception of butane, there is little difference in the conclusions which can be drawn about radical structure in the other hydrocarbons. This should be particularly noted for the undecane crystal. In early studies of esr spectra of powdered hydrocarbons,[10] narrow lines were observed for the odd-numbered alkanes, but this feature could not be produced for the single crystal. Thus, the difference in crystal struc-

(10) A. V. Topchiev, Ed., "Radiolysis of Hydrocarbons," Elsevier, Amsterdam, 1964, Chapter III.

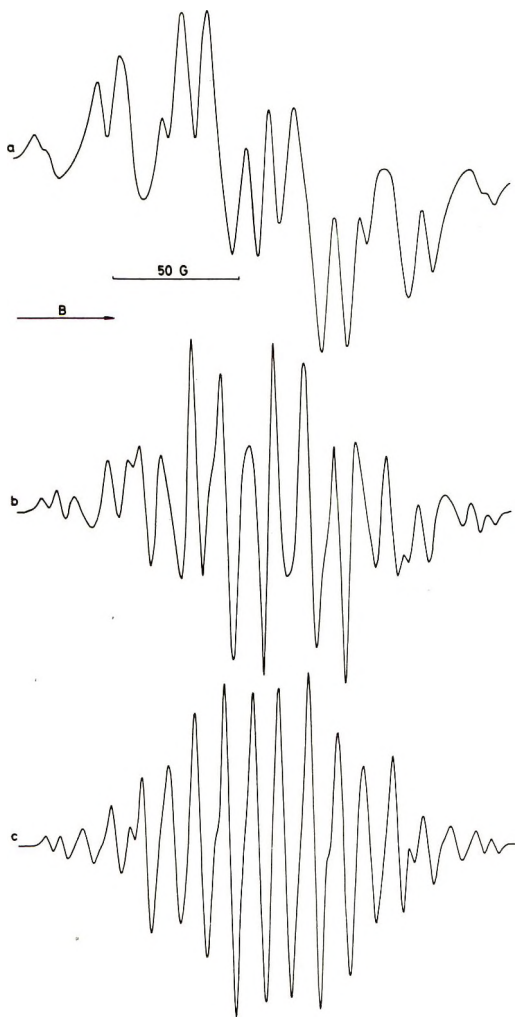

Figure 3. Esr spectra from a single crystal of hexadecane at 77 K oriented as described in Figure 2: (a) γ-irradiated at 77 K; (b) γ-irradiated at 195 K; (c) spectrum composed of the absorptions from $CH_3\dot{C}H(CH_2)_{13}CH_3$ and $-CH_2\dot{C}HCH_2-$, each radical occupying two sites. Parameters are given in Table I.

ture[7] which exists between this hydrocarbon and decane has no noticeable effect upon free radical formation.

Yields. Free radical processes in the radiation chemistry of *n*-alkanes have previously been investigated in the liquid state by the analysis of final products.[4,10] The yields of the three isomeric hexyl radicals as estimated from the product distribution after irradiation at $-78°$[4] were in the ratio 35:39:26 for 3-hexyl, 2-hexyl, and 1-hexyl, while at 50° the ratio found was 41:50:9. After irradiation of the solid at $-196°$ the following yields of C_{12} products were reported:[4] $G_{3,3}$ = 0.10 (4,5-diethyloctane), $G_{2,3}$ = 0.24 (4-ethyl-5-methylnonane), $G_{2,2}$ = 0.17 (5,6-dimethyldecane), $G_{1,3}$ = 0.16 (4-ethyldecane), $G_{1,2}$ = 0.20 (5-methylundecane) and $G_{1,1}$ = 0.08 (dodecane). The relative importance of the three radicals should then be given by the ratio $G_1:G_2:G_3 = (2G_{1,1} + G_{1,2} + G_{1,3}):(G_{1,2} + 2G_{2,2} + G_{2,3}):(G_{1,3} + G_{2,3} + 2G_{3,3}) = 27:41:32$.

The disagreement with the data obtained in this study is obviously a result of the different methods used to estimate the yields. The initial distrubution may deviate from that measured by esr unless the following conditions prevail: (1) no recombination of radicals may occur prior to the recording of the spectra; (2) the transformation of one type of radical into the other must be negligible; and (3) the validity of the least-squares data analysis must be established.

The violation of the first point would lead to erroneous conclusions if, for example, 1-hexyl radicals react with each other to form dodecane. In the crystal the distance between the terminal CH_3 groups of two adjacent molecules is only 3.62 A. Radical pairs are known to be formed in the solid,[11] probably as a consequence of the heterogenous distribution of energy by the ionizing radiation. Because of the short intermolecular distance, two 1-hexyl radicals formed in a track might be able to recombine even in the solid state. In a similar way other products might be formed at low temperatures by the reaction of radicals created in close proximity to each other.

Postirradiation reactions have been observed by esr in alkyl halide matrices[12] in which *n*-alkyl changed into *sec*-alkyl at 77 K. However, the reaction is slow because of its relatively high activation energy. This second point may therefore be of less importance.

The method of estimating the relative importance of each radical requires that the spectra of the components be known. The deliberate selection of a coupling constant which was too large by 10% for one of the components altered the estimates of the relative strength by about 5%. A rather large displacement of the center from its correct position, by one third of a line width, caused an error of 20%. It is not claimed that the resonance parameters of Table I are the optimal ones for minimizing the standard deviation of the fit. In order to achieve this condition, it would have been necessary to employ an automatic adjustment procedure for these parameters. However, five independent estimates indicated that the relative amounts of isomers in hexane could be reasonably well reproduced (Table I). Although these test runs indicate that considerable errors may arise, they would not in themselves be sufficient to account for the difference in results obtained by the analysis of final products.

The estimate of radical yields from the distribution of dimer products is an indirect method and is therefore sensitive to the reaction mechanism. The assumptions which are made here and the justification for these have been discussed by Widmer and Gäumann.[4] For reasons mentioned above, the hypothesis that radical recombination is independent of concentration,

(11) M. Iwasaki, T. Ichikawa, and T. Ohmori, *J. Chem. Phys.*, **50**, 1991 (1969).

(12) P. B. Ayscough and C. Thomson, *Trans. Faraday Soc.*, **58**, 1477 (1962).

which in particular means no track effect, may be invalid as far as solid state radiolysis is concerned. In this case where diffusion is slow, dimers should form preferably by recombination between radicals formed in close proximity to each other. Geometrical factors determined by the crystal structure would then have a selective effect upon the ability of the isomers to react. Thus the rule of statistical combination, which is valid in the liquid,[4] may be violated. Another severe restriction in this analysis is the neglect of ionic processes. The results of the radiolysis of pentane[5] have indicated that ion–molecule reactions may contribute to some extent to dimer formation in the solid state, and even more so in the case of trimers. An entirely ionic mechanism has been proposed to explain the formation of hexenes and dimers in the solid state radiolysis of hexane.[3] In this theory the formation of uncharged radicals is attributed to cases of bond disruption on neutralization of an ion radical formed primarily. The abstraction of hydrogen by the ion radical followed by neutralization and molecular hydrogen ejection creates a radical pair. About 10% of the radicals are trapped in pairs in the case of *n*-hydrocarbons.[11] The amount originally formed is difficult to estimate due to the recombination which might occur even at 77 K.

A molecular orbital calculation involving all valence electrons at the INDO level of approximation[13] yields the following charges on the carbon atoms of the hexane cation: $q_1 = 0.035$, $q_2 = 0.093$, $q_3 = 0.079$. The neutralization process should preferably occur at the carbon atom carrying the largest proportion of the positive charge. The energy gained in this reaction would be localized and could be used in C–H bond scission. The dominant formation of 2-hexyl is then qualitatively explained.

Conclusions

The relative yields of isomeric radicals determined by esr measurements do not conform with estimates from the final product distributions. Ionic mechanisms and/or reactions taking place within the track of the ionizing radiation in the solid may explain the discrepancy. Radicals of the type $CH_3\dot{C}HCH_2R$ are most easily trapped possibly as a consequence of their formation from the ion radicals. Irradiation at 195 K as opposed to 77 K gives a negligible effect upon the relative yields but influences the ability of the matrix to trap intermediates close to each other, *i.e.*, along the track of an ionizing particle.

Acknowledgments. The continued interest of Professor P.-O. Kinell has greatly stimulated this work. Discussions with Tekn. lic. T. Gillbro have helped to clarify several problems. The early experiments were made by Fil. lic. O. Edlund, and the computer programs were prepared in colaboration with Dr. T. Shiga. Financial support was obtained from the Atomic Research Council of Sweden.

(13) J. A. Pople, D. L. Beveridge, and P. A. Dobosh, *J. Amer. Chem. Soc.*, **90**, 4201 (1968).

The Bromine Atom Catalyzed Oxidation of Carbon Monoxide

by Eduardo Lissi, R. Simonaitis, and Julian Heicklen*

Department of Chemistry and Ionosphere Research Laboratory, The Pennsylvania State University, University Park, Pennsylvania 16802 *(Received October 4, 1971)*

Publication costs borne completely by The Journal of Physical Chemistry

Br_2 was photolyzed at 3660 Å and 25° in the presence of O_2 and CO. CO_2 was produced according to the rate law $\Phi\{CO_2\} = k[CO][O_2]/(I_a[M])^{1/2}$ with $k = 4.8 \times 10^{-7}$ $Torr^{-1}$ $min^{-1/2}$ for M = O_2. This law is consistent with the simple mechanism

$$Br_2 + h\nu \longrightarrow 2Br \qquad \text{rate} = I_a$$

$$Br + O_2 + CO \longrightarrow BrO + CO_2 \qquad (a)$$

$$2Br + M \longrightarrow Br_2 + M \qquad (b)$$

The constant $k = 2k_a/k_b^{1/2}$ if BrO always produces additional CO_2, is $k_a/k_b^{1/2}$ if BrO never produces additional CO_2, and is between $k_a/k_b^{1/2}$ and $2k_a/k_b^{1/2}$ otherwise. Since $k_b = 5.8 \times 10^9$ M^{-2} sec^{-1}, then $k_a = 44$–88 M^{-2} sec^{-1}. The full mechanism is outlined and the reaction steps are discussed.

Introduction

We have examined the bromine-photosensitized oxidation of CO as part of a continuing program on CO oxidation. Apparently the only previous study of this system was made over 40 years ago by Livingston,[1] who found no evidence for any reaction.

Some information does exist on the oxidation of CO sensitized by the lower halogens.[2] With fluorine, even the molecular halogen will initiate the oxidation at room temperature.[3] In fact, the oxidation proceeds beyond CO_2, and the product of the reaction is $(FCO_2)_2$.[3,4] If the milder oxidizing agent F_2O is used instead of the F_2–O_2 mixture, then CO_2 is produced.[5] The results of the F_2O study were consistent with a mechanism in which CO, in addition to reacting with F_2O, reacted with FO *via*

$$FO + CO \longrightarrow FCO + O$$

More recently the reaction has been studied in a shock tube at 800–1400°K,[6] and the rate constant for the above reaction was measured to be 7.5×10^7 M^{-1} sec^{-1} independent of temperature. However, the products of the reaction were assumed to be $CO_2 + F$, and not $FCO + O$.

With Cl_2 it is necessary to photosensitize the oxidation in order for it to proceed. The products are CCl_2O and CO_2.[7,8] The ratio $[CCl_2O]/[CO_2]$ was proportional to $[Cl_2]/[O_2]$ which indicated ClCO as the intermediate

$$ClCO + Cl_2 \longrightarrow CCl_2O + Cl$$

$$ClCO + O_2 \longrightarrow CO_2 + ClO$$

Support for this mechanism came from studies of the photooxidation of CCl_2O, both in the absence[9] and presence[10] of CO, where CO_2 was also produced. CO_2 was also found in the flash photolysis of Cl_2–O_2–CO mixtures.[11]

Experimental Section

A grease-free high-vacuum system employing Teflon stopcocks with Viton "O" rings was used. All runs were at room temperature. Pressures other than bromine were measured with an alphatron gauge. Bromine was measured by its optical absorption at 3660 Å.

Reactions were carried out in a cylindrical quartz cell 5 cm in diameter by 10 cm long. The radiation was from a Hanovia Type 30620 medium-pressure U-shaped lamp and passed through a Corning 7-60 filter before entering the reaction vessel. The effective wavelength was 3660 Å, and the transmitted intensity was monitored with an RCA 935 phototube.

Baker Analyzed reagent bromine was degassed carefully at −100°; the CO_2 impurity was reduced to <100 ppm which was undetectable in our experiments. Matheson CO and O_2 were used. The CO was passed

(1) R. Livingston, *J. Phys. Chem.*, **34**, 2121 (1930).

(2) J. Heicklen, *Advan. Photochem.*, **7**, 57 (1969).

(3) J. M. Heras, A. J. Arvía, P. J. Aymonino, and H. J. Schumacher, *Z. Phys. Chem. (Frankfurt am Main)*, **28**, 250 (1961).

(4) A. J. Arvía, P. J. Aymonino, C. H. Waldow, and H. J. Schumacher, *Angew. Chem.*, **72**, 169 (1960).

(5) A. J. Arvía, P. J. Aymonino, and H. J. Schumacher, *Z. Phys. Chem. (Frankfurt am Main)*, **51**, 170 (1966).

(6) H. Henrici, H. C. Liu, and S. H. Bauer, *J. Chem. Phys.*, **52**, 5834 (1970).

(7) M. Bodenstein, S. Lenher, and C. Wagner, *Z. Phys. Chem.*, **B3**, 459 (1929).

(8) G. K. Rollefson, *J. Amer. Chem. Soc.*, **55**, 148 (1943).

(9) G. K. Rollefson and C. W. Montgomery, *ibid.*, **55**, 142 (1933).

(10) G. K. Rollefson and C. W. Montgomery, *ibid.*, **55**, 4036 (1933).

(11) G. Porter and F. J. Wright, *Discuss. Faraday Soc.*, **14**, 23 (1953).

through a trap filled with glass wool and kept at −196° to reduce the CO_2 impurity to <10 ppm. The O_2 contained <1 ppm CO_2 and was used without purification. (A few runs in which the O_2 was passed through a trap at −196° gave identical results.)

The reactants were mixed in the reaction cell, the Br_2 being introduced first. After irradiation the reaction mixture was passed slowly through two traps, the first at −100° to retain the unreacted Br_2, and the second at −196° to retain CO_2. The fraction retained at −196° was analyzed by gas chromatography using a 0.25-in. diameter by 18-ft long Porapak Q column. Actinometry was done with matched absorbances of azomethane, where the N_2 quantum yield is one.

Results

Initially mixtures of O_2 and CO, O_2 and Br_2, and CO and Br_2 were irradiated. In none of these experiments was CO_2 produced, nor was it produced in long dark runs.

Next mixtures of all three gases were studied. First experiments were done in which only the irradiation time was altered. The CO_2 produced was proportional to the duration of irradiation; consequently, CO_2 is an initial product of the reaction. We did not look for CBr_2O, but Livingston[1] reported that it was not found in the presence of O_2. Even if it were, it would not affect our conclusions.

Then the quantum yield of CO_2 formation, $\Phi\{CO_2\}$, was obtained in several runs at various conditions.

Table I: Bromine-Photosensitized Oxidation of CO at 3660 Å and 25°

[CO], Torr	$[O_2]$, Torr	Irradiation time, min	$10^2\Phi\{CO_2\}$
	I_a = 48.5 μ/min, $[Br_2]$ = 15 Torr		
265	455	915	0.99
155	590	203	0.93
110	540	600	0.58
565	110	240	0.70
61	594	280	0.25
390	310	620	1.03
90	570	233	0.41
22	678	1006	0.103
73	237	230	0.125
44	266	823	0.082
45	270	1230	0.15
50	265	902	0.21
395	43	1128	0.28
414	31	893	0.22
215	550	1080	1.2
54	81	2600	0.055
	I_a = 8.4 μ/min, $[Br_2]$ = 15 Torr		
545	240	2340	2.3
180	575	2740	1.16
	I_a = 9.6 μ/min, $[Br_2]$ = 2 Torr		
368	430	1283	3.0

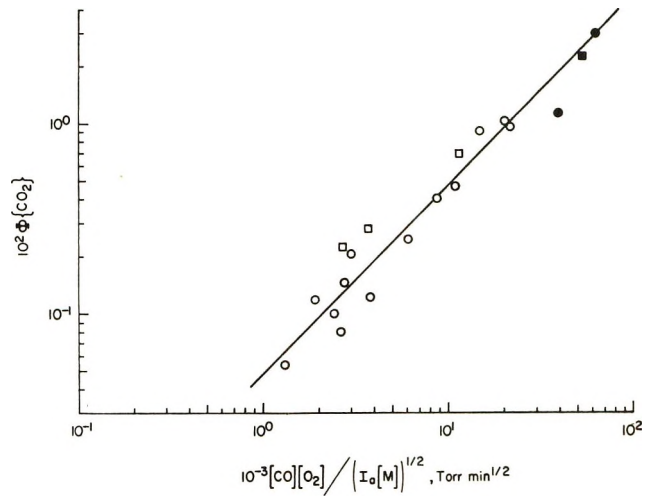

Figure 1. Plot of $\Phi\{CO_2\}$ *vs.* $[CO][O_2]/(I_a[M])^{1/2}$ in the bromine-photosensitized oxidation of CO at 3660 Å and 25°. The circles are for values of $([O_2]/[CO])\,(I_a/[M])^{1/2}$ between 0.0043 and 0.238 $min^{-1/2}$; the squares are for $([O_2]/[CO])\,(I_a/[M])^{1/2}$ between 0.8×10^{-3} and 1.7×10^{-3} $min^{-1/2}$. The filled points are those for runs at reduced intensity.

The results, corrected for the CO_2 background (always <5%), are listed in Table I in the order in which the experiments were performed. The CO pressure was varied from 44 to 565 Torr; the O_2 pressure from 31 to 678 Torr; and the absorbed intensity, I_a, from 9.6 to 48.5 μ/min. Most of the experiments were done with 15 Torr of Br_2, but one was done with 2 Torr.

A log–log plot of $\Phi\{CO_2\}$ *vs.* $[CO][O_2]/(I_a[M])^{1/2}$ is shown in Figure 1, where

$$[M] \equiv [O_2] + 0.72[CO] + 7.6[Br_2] \qquad (I)$$

Even though $\Phi\{CO_2\}$ varies by a factor of 55, all the points are reasonably well fitted by a single line of slope 1.00 and intercept 4.8×10^{-7} $Torr^{-1}$ $min^{-1/2}$. Thus the rate law is

$$\Phi\{CO_2\} = k[CO][O_2]/(I_a[M])^{1/2} \qquad (II)$$

with $k = 4.8 \times 10^{-7}$ $Torr^{-1}$ $min^{-1/2}$.

This law conforms to the simple mechanism

$$Br_2 + h\nu \longrightarrow 2Br \qquad \text{rate} = I_a$$

$$Br + O_2 + CO \longrightarrow BrO + CO_2 \qquad (a)$$

$$2Br + M \longrightarrow Br_2 + M \qquad (b)$$

Application of the steady-state hypothesis to the mechanism leads to

$$\Phi\{CO_2\} = \alpha k_a[CO][O_2]/(k_b I_a[M])^{1/2} \qquad (III)$$

where α is 1 if BrO does not produce further CO_2, is 2 if BrO always produces CO_2, and otherwise is between 1 and 2. Equating eq II and III gives $k = \alpha k_a/k_b^{1/2}$. Ip and Burns[12] give $k_b = 5.8 \times 10^9$ M^{-2} sec^{-1}, so that $k_a = 44$–88 M^{-2} sec^{-1}.

(12) J. K. K. Ip and G. Burns, *J. Chem. Phys.*, 51, 3425 (1969).

The chaperone gas, M, is of course a composite of O_2, CO, and Br_2, weighted by their respective efficiencies. The efficiencies have been studied extensively. The most reliable results are probably those of Ip and Burns[12] and DeGraff and Lang.[13] Combining their data gives relative efficiencies of 1.0, 0.72, and 7.6, respectively, for O_2, CO, and Br_2; we have adopted these values.

Some experiments were also done with visible radiation (Hg lines) both with Br_2 as well as with I_2 replacing the Br_2. With Br_2, similar results were obtained, though quantum yields were not measured. However, when I_2 replaced Br_2, at halogen pressures to match the absorbance of radiation in both systems, CO_2 production was essentially eliminated. For comparable conditions $\Phi\{CO_2\}$ in the iodine system is $<10^{-3}\Phi\{CO_2\}$ in the bromine system.

Discussion

The following reactions must surely occur and have to be considered.

$$Br_2 + h\nu \longrightarrow 2Br \qquad \text{rate} = I_a$$

$$Br + Br_2 + M \rightleftharpoons Br_3 + M \tag{1}$$

$$Br + CO + M \rightleftharpoons BrCO + M \tag{2}$$

$$Br + O_2 + M \rightleftharpoons BrO_2 + M \tag{3}$$

$$Br_3 + Br \longrightarrow 2Br_2 \tag{4}$$

$$BrCO + Br \longrightarrow Br_2 + CO \text{ (or } Br_2CO) \tag{5}$$

$$BrO_2 + Br \longrightarrow Br_2 + O_2 \tag{6}$$

The production of CO_2 would be from

$$BrCO + O_2 \longrightarrow BrO + CO_2 \tag{7}$$

$$BrO_2 + CO \longrightarrow BrO + CO_2 \tag{8}$$

The BrO radical could be removed in several ways

$$2BrO \longrightarrow BrO_2 + Br \text{ (or } 2Br + O_2) \tag{9a}$$

$$2BrO \longrightarrow Br_2 + O_2 \tag{9b}$$

$$BrO + CO \longrightarrow CO_2 + Br \tag{10}$$

$$BrO + BrCO \longrightarrow Br_2 + CO_2 \tag{11}$$

$$BrO + BrO_2 \longrightarrow Br_2 + O_3 \tag{12}$$

Reaction 9b is unimportant, but we include it for generality. Brown and Burns[14] have argued that reaction 9a produces $O_2 + 2Br$. However, since we will assume an equilibrium between Br and BrO_2, the two sets of products are kinetically equivalent.

In the above mechanism, BrO is produced only in reactions 7 and 8. Another possible source might be reaction 6 if Br_2O_2 is an intermediate. Even though the decomposition of Br_2O_2 to 2BrO is considerably endothermic, it might possibly proceed to some extent. That this is not the case was shown by Brown and Burns[14] who found that Br_2O_2 seems to decompose to $2Br + O_2$ with nearly zero activation energy. Furthermore, in the flash photolysis of Br_2 in the presence of O_2, no BrO was produced either from ground state or electronically excited Br atoms.[15]

The above mechanism leads to the observed rate law if reactions 1–3 are assumed to be in equilibrium. Furthermore, BrO is produced only when CO_2 is produced. Since $\Phi\{CO_2\} < 0.03$, then BrO can account for only $<3\%$ of the radical termination steps, which is negligible. Consequently, in terms of the above mechanism, the rate law becomes

$$\Phi\{CO_2\} = \frac{\alpha(k_7K_{2,-2} + k_8K_{3,-3})[CO][O_2]}{I_a^{1/2}(k_4K_{1,-1}[Br_2] + k_5K_{2,-2}[CO] + k_6K_{3,-3}[O_2])^{1/2}} \tag{IV}$$

where α is 1 if BrO is removed primarily by reactions 9 and 12; α is 2 if BrO is removed primarily by reactions 10 and 11; and α is between 1 and 2 otherwise.

Now $k_4K_{1,-1}$, $k_5K_{2,-2}$, and $k_6K_{3,-3}$ are the rate constants for Br atom recombination with the chaperones Br_2, CO, and O_2, respectively. Since they have the relative values 7.6, 0.72, and 1.0, eq IV can be reduced to

$$\Phi\{CO_2\} = \alpha(k_7K_{2,-2} + k_8K_{3,-3}) \times [CO][O_2]/(I_a k_5 K_{3,-3}[M])^{1/2} \tag{V}$$

It would be nice to know which of reactions 9–12 are important. Let us first assume that reaction 11 is dominant in removing BrO. Then

$$1 \gg R\{9\}/R\{11\} = \frac{k_9(k_7K_{2,-2} + k_8K_{3,-3})[O_2]}{k_{11}^2K_{2,-2}^2[CO](I_a/k_6K_{3,-3}[M])^{1/2}}$$

$$= (k_9\Phi\{CO_2\}/2k_{11}^2K_{2,-2}^2[CO]^2)(k_6K_{3,-3}[M])$$

where $R\{x\}$ is the rate of reaction x. Also $k_6K_{3,-3}[M] > k_5K_{2,-2}[CO]$, so that the above expression requires that

$$1 \gg \frac{k_9k_5^2\Phi\{CO_2\}}{2k_{11}^2k_5K_{2,-2}[CO]}$$

Furthermore DeGraff and Lang[13] give $k_5K_{2,-2} = 4.2 \times 10^9\ M^{-2}\ \text{sec}^{-1}$, and Clyne and Cruse[16] give $k_9 = 6.3 \times 10^7\ M^{-1}\ \text{sec}^{-1}$. Therefore, even for our most favorable conditions ($\Phi\{CO_2\}/[CO]$ small), it is still necessary that $k_{11} \gg k_5$. This seems extremely unlikely since reaction 5 probably has no activation energy, and reaction 11 is a four-center reaction whereas reaction 5 is not. Therefore we discard reaction 11.

By an analogous argument we can eliminate reaction 12. Assuming that it is the dominant reaction leads to the expression

(13) B. A. DeGraff and K. J. Lang, *J. Phys. Chem.*, **74**, 4181 (1970).

(14) J. Brown and G. Burns, *Can. J. Chem.*, **48**, 3487 (1970).

(15) G. Burns and R. G. W. Norrish, *Proc. Roy. Soc., Ser. A*, **271**, 289 (1963).

(16) M. A. A. Clyne and H. W. Cruse, *Trans. Faraday Soc.*, **66**, 2214 (1970).

$$1 \gg R\{9\}/R\{12\} = \frac{k_9(k_7K_{2,-2} + k_8K_{3,-3})[CO]}{k_{12}^2K_{3,-3}^2[O_2](I_a/k_6K_{3,-3}[M])^{1/2}}$$

$$= (k_9\Phi\{CO_2\}/k_{12}^2K_{3,-3}^2[O_2]^2)(k_6K_{3,-3}[M])$$

Again $[M] > [O_2]$, so that the expression reduces to

$$1 \gg \frac{k_9k_6^2\Phi\{CO_2\}}{k_{12}^2k_6K_{3,-3}[O_2]}$$

Ip and Burns[12] give $k_6K_{3,-3} = 5.8 \times 10^9\ M^{-2}\ sec^{-1}$, and again our results would require $k_{12}/k_6 \gg 1$, which is unlikely.

This leaves reactions 9 and 10 as removal steps for BrO. Reaction 9 should be dominant at sufficiently large values of $([O_2]/[CO])(I_a/[M])^{1/2}$, and reaction 10 should be dominant at sufficiently small values of the same parameter. The data are sufficiently scattered in Figure 1, so that a factor of two difference is difficult to discern. However, three of the four data points for values of $([O_2]/[CO])(I_a/[M])^{1/2} < 1.7 \times 10^{-3}\ min^{-1/2}$ lie considerably above the line in Figure 1. If this observation is meaningful, then $k_9(k_7K_{2,-2} + k_8K_{3,-3})/k_{10}^2(k_6K_{3,-3})^{1/2} \simeq 600\ min^{1/2}$.

Acknowledgment. This work was supported by the Atmospheric Sciences Section of the National Science Foundation under Grant No. GA-12385, for which we are grateful.

Photoinduced Ionic Dissociation of Tetracyanobenzene–α-Methylstyrene Complex

by Masahiro Irie,* Setsuko Tomimoto, and Koichiro Hayashi

Faculty of Engineering, Hokkaido University, Sapporo, Japan *(Received July 8, 1971)*

Publication costs borne completely by The Journal of Physical Chemistry

The formation and behavior of ions formed from excited charge-transfer states of tetracyanobenzene–α-methylstyrene complex were studied by means of optical absorption, emission, electron spin resonance, and photoconductivity measurements in 1,2-dichloroethane–cyclohexane and *n*-amyl alcohol solvents at room temperature and below. The results obtained are: (1) the charge-transfer absorption band has a maximum at $27.5 \times 10^3\ cm^{-1}$; (2) the excitation of both charge-transfer band and acceptor band results in the singlet excited electron donor–acceptor complex, giving fluorescence at $18.9 \times 10^3\ cm^{-1}$ at room temperature; (3) the triplet excited complex is also evidenced by the phosphorescence at $19.6 \times 10^3\ cm^{-1}$ at 77°K; (4) the excited complex dissociates into ions mostly from its triplet state; (5) the ions thus formed are in equilibrium between ion pairs and free ions; but (6) the equilibrium constant is so small that most ions are in pairs and recombine with the counterpart ions, by a first-order reaction.

Introduction

Excited states of electron donor acceptor (EDA) complexes have recently attracted the interest of molecular photochemists. The lowest singlet excited state of tetracyanobenzene–aromatic hydrocarbon complexes was studied by means of fluorescence measurements[1] and laser photolysis,[2] and the electronic structure in the state was found to be quite polar. The triplet excited state was also studied in detail from emission spectra[3] and electron paramagnetic resonance spectra.[4]

As expected, the EDA complexes in polar excited states may readily dissociate into ions in polar solvents and result in photochemical reactions. Potashnik, *et al.*,[5] observed the formation of ions from the triplet excited state of pyromellitic dianhydride–mesitylene complex by laser photolysis at low temperature. The ionic dissociation of the lowest singlet excited state of tetracyanobenzene–toluene complex was also suggested by Masuhara, *et al.*[6] However, it has not yet been shown unambiguously from which excited state the ionic dissociation of EDA complex occurs, singlet or tripet.

The present authors studied the photoinduced polymerization of α-methylstyrene in the presence of tetracyanobenzene and found that the polymerization pro-

(1) N. Mataga and Y. Murata, *J. Amer. Chem. Soc.*, 91, 3144 (1969).

(2) R. Potashnik and M. Ottolenghi, *Chem. Phys. Lett.*, 6, 525 (1970).

(3) S. Iwata, J. Tanaka, and S. Nagakura, *J. Chem. Phys.*, 47, 2203 (1967).

(4) H. Hayashi, S. Iwata, and S. Nagakura, *ibid.*, 50, 993 (1969).

(5) R. Potashnik, C. R. Goldschmidt, and M. Ottolenghi, *J. Phys. Chem.*, 73, 3170 (1969).

(6) H. Masuhara, M. Shimada, and N. Mataga, *Bull. Chem. Soc. Jap.*, 43, 3316 (1969).

ceeds by a cationic mechanism.[7] In this report, the studies are extended to elucidate the fundamental processes involved in the formation of ions from the excited states of the EDA complex between tetracyanobenzene and α-methylstyrene, as well as the ion decay process. The results obtained may serve to elucidate not only the initiation process of the photoinduced cationic polymerization of α-methylstyrene, but also some general features of excited states of EDA complexes between tetracyanobenzene and aromatic hydrocarbons.

Experimental Section

Tetracyanobenzene was synthesized by Lawton and McRitchie's method[8] and purified by recrystallization from ethanol and sublimation *in vacuo*. Its melting point (272°) agreed with the literature value.[9] α-Methylstyrene was washed with an aqueous solution of sodium hydroxide several times and fractionally distilled twice at 50 Torr. Acetophenone was fractionally distilled twice. 1,2-Dichloroethane was washed with dilute potassium hydroxide and water, dried over calcium chloride, and fractionally distilled twice over phosphorus pentoxide. Cyclohexane was shaken with sulfuric acid three times, washed with water, and then fractionally distilled twice. *n*-Amyl alcohol was fractionally distilled three times. Impurities remaining in these three solvents were tested by measuring their absorption and emission spectra.

Optical absorption and emission spectra were measured with a conventional recording spectrophotometer (Hitachi, Model EPS-3T) and a fluorescence spectrophotometer (Hitachi, Model MPF-2A), respectively. Electron spin reasonance measurements were carried out with an X-band spectrometer (Jeolco, Model JES-ME-2). The temperature of the samples was regulated with a constant flow of cold nitrogen gas in the resonance cavity by using a temperature control adapter (Model JES-UCT-2AX). A Ushio UXL-500D xenon lamp was used for a stationary light source. Intensity variation of light was achieved by use of neutral filters.

Photoconductivity measurement was carried out by means of an operational amplifier (Philbrick, Model P2AU) and a synchroscope (Iwasaki, Model MS-5103B). The electrodes in a Pyrex glass cell were stainless steel parallel plates of 15-mm diameter situated at a distance of 18 mm. A xenon flash lamp was used as a flash light source with a half-width of 1.3 msec. The light was filtered with cutoff or neutral filters, as necessary. Flash absorption spectra were obtained with a conventional flash photolysis instrument by an electrophotometric method.

Results and Discussion

Excited EDA Complex between Tetracyanobenzene and α-Methylstyrene. Solution of tetracyanobenzene and α-methylstyrene in 1,2-dichloroethane gives an absorption spectrum as shown in Figure 1, curve A, at room

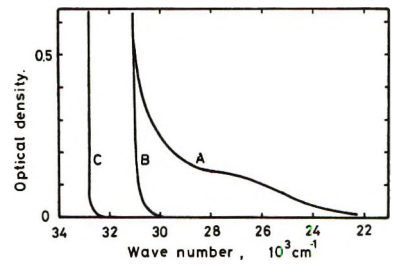

Figure 1. Electronic absorption spectra of (A) 4×10^{-4} *M* tetracyanobenzene and 1.9 *M* α-methylstyrene, (B) 5×10^{-4} *M* tetracyanobenzene, and (C) 1.9 *M* α-methylstyrene in 1,2-dichloroethane at room temperature.

temperature, which has a weak band maximum at 27.5×10^3 cm^{-1}. This is interpreted as due to an EDA complex between tetracyanobenzene and α-methylstyrene, because the former is known as a typical electron acceptor having a band with a maximum at 31.6×10^2 cm^{-1} extending down to 30.0×10^3 cm^{-1} (see Figure 1, curve B), and the latter is expected to act as an electron donor because of its low ionization potential (8.35 eV), and has the tail of its first absorption band extending to 32.0×10^3 cm^{-1} (Figure 1, curve C). According to the Benesi–Hildebrand method,[10] the molar extinction coefficient of the charge transfer band and the equilibrium constant of complex formation are determined in 1,2-dichloroethane at 27.0×10^3 cm^{-1} to be 1800 and 0.1 M^{-1} at 298°K, respectively.

Figure 2 shows fluorescence spectra of tetracyanobenzene in a mixed solvent of 1,2-dichloroethane and cyclohexane (volume ratio of 1:2) in the absence or presence of α-methylstyrene at room temperature for the excitation wave number of 31.6×10^3 cm^{-1}. Evidently, the addition of a small amount of α-methylstyrene quenches the fluorescence of tetracyanobenzene and gives a new emission band with the maximum at 18.9×10^3 cm^{-1}. The quenching by α-methylstyrene follows the Stern–Volmer relation with a quenching constant of 43 M^{-1}. These results, as well as an isosbestic point at 21.4×10^3 cm^{-1}, indicate that the new emission band is due to the fluorescence of an excited EDA complex formed by the reaction between singlet excited tetracyanobenzene and ground-state α-methylstyrene. When the composition of 1,2-dichloroethane in the solvent is increased, so that the solvent is made more polar, the emission yield decreases. It is no longer observed from the solution in pure 1,2-dichloroethane.

The formation of an excited EDA complex from a

(7) M. Irie, S. Tomimoto, and K. Hayashi, *J. Polym. Sci., Part B*, **8**, 585 (1970).

(8) E. A. Lawton and D. D. McRitchie, *J. Org. Chem.*, **24**, 26 (1959).

(9) A. S. Bailey, B. R. Henn, and J. Langdon, *Tetrahedron*, **19**, 161 (1963).

(10) H. A. Benesi and J. H. Hildebrand, *J. Amer. Chem. Soc.*, **71**, 2703 (1949).

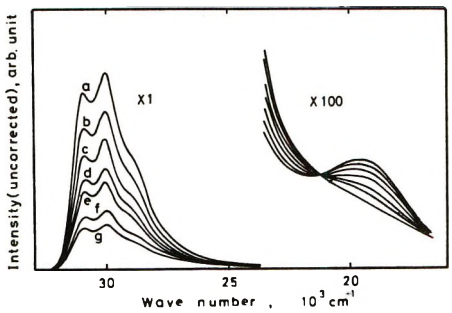

Figure 2. Fluorescence spectra of tetracyanobenzene (1.5×10^{-4} M) in the mixed solvent of 1,2-dichloroethane and cyclohexane (volume ratio 1:2) at room temperature in the absence or presence of α-methylstyrene when excited at 31.7×10^3 cm^{-1}. The concentration of α-methylstyrene is: (a) 0, (b) 0.59×10^{-2}, (c) 1.17×10^{-2}, (d) 2.34×10^{-2}, (e) 3.51×10^{-2}, (f) 5.27×10^{-2} and (g) 7.02×10^{-2} M.

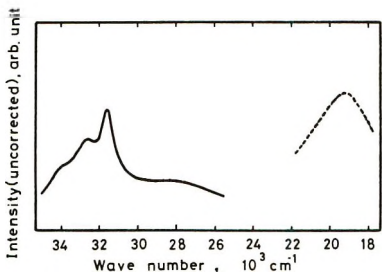

Figure 3. Excitation spectrum observed at 18.5×10^3 cm^{-1} from the solution of tetracyanobenzene (1.5×10^{-4} M) and α-methylstyrene (7.6×10^{-2} M) in the mixed solvent of 1,2-dichloroethane and cyclohexane (volume ratio of 1:2) at room temperature. The fluorescence spectrum when excited at 31.6×10^3 cm^{-1} is shown for reference (dotted line).

singlet excited electron acceptor is well known as a process of heteroexcimer formation when the complex is dissociative in its ground state.[11] In the present investigation, the small equilibrium constant of complex formation indicates the existence of abundant free acceptor and donor, which are responsible for a process similar to that for heteroexcimer formation

$$A \xrightarrow{h\nu} {}^1A^* \quad (1)$$

$${}^1A^* + D \longrightarrow {}^1(D \cdot A)^* \quad (2)$$

where A and D stand for tetracyanobenzene and α-methylstyrene, respectively.

Figure 3 shows an excitation spectrum for the emission at 18.5×10^3 cm^{-1} due to the excited EDA complex. In addition to the excitation band at 31.6×10^3 cm^{-1} responsible for process 1, the spectrum shows another broad structureless band around 28×10^3 cm^{-1}. This excitation band coincides well with the charge-transfer absorption band shown in Figure 1A, and gives support to the formation of excited singlet EDA complex from the ground-state complex

$$DA \xrightarrow{h\nu} {}^1(DA)^* \quad (3)$$

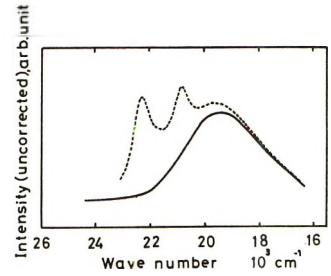

Figure 4. Phosphorescence spectra of tetracyanobenzene–α-methylstyrene complex in n-butyl chloride at 77°K when excited at 27.8×10^3 cm^{-1} (—) and 31.6×10^3 cm^{-1} (- - -). Concentration of tetracyanobenzene, 1.0×10^{-3} M; α-methylstyrene, 2.3×10^{-1} M. Phosphorescence at 22.3 and 21.0×10^3 cm^{-1} is due to triplet excited free tetracyanobenzene.

which was already studied by Iwata, *et al.*,[12] and Mataga and Murata.[1]

Direct excitation of EDA complex at the maximum of the charge-transfer band showed another weak fluorescence around 21.0×10^3 cm^{-1}. The fluorescence is probably due to excited EDA complex with another geometry, but the emission is so weak that we could not study it in detail.

Phosphorescence of the EDA complex was also observed. Figure 4 shows the phosphorescence from a glassy solution in n-butyl chloride at 77°K. The phosphorescence spectra show a band maximum at 19.6×10^3 cm^{-1} for the excitation of the charge-transfer band and that of the acceptor band as well. Neither tetracyanobenzene nor α-methylstyrene shows phosphorescence in this spectral region. The lifetime of the phosphorescence was determined to be 0.18 sec at 123°K in n-amyl alcohol.

Ionic Dissociation of Excited EDA Complex. Figure 5 shows an absorption spectrum of the degassed (prepared under vacuum of less than 10^{-5} Torr) solution of α-methylstyrene and tetracyanobenzene in n-amyl alcohol, after the photoillumination, at 113°K. It has two absorption band maxima at 21.6 and 20.2×10^3 cm^{-1}. The former band is interpreted as due to tetracyanobenzene radical anion,[13] while the latter is attributable to α-methylstyrene radical cation.[14] The simultaneous formation of both anion and cation radicals suggests the ionic dissociation of the excited EDA complex mentioned above. If the band of tetracyanobenzene radical anion is bleached by light of 21.6×10^3

(11) For example, (a) A. Weller, *Org. Photochem.*, **2**, 115 (1967); (b) N. Mataga and K. Ezumi, *Bull. Chem. Soc. Jap.*, **40**, 1355 (1967); (c) W. R. Ware and H. P. Richter, *J. Chem. Phys.*, **48**, 1595 (1968).

(12) S. Iwata, J. Tanaka, and S. Nagakura, *J. Amer. Chem. Soc.*, **89**, 2813 (1967).

(13) M. Sofue and S. Nagakura, *Bull. Chem. Soc. Jap.*, **38**, 1048 (1965).

(14) K. Tsuji, J. Lin, and Ff. Williams, *Trans. Faraday Soc.*, **64**, 2896 (1968).

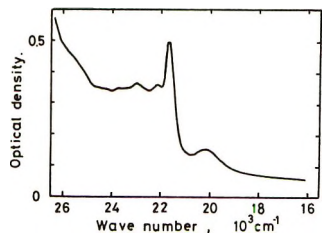

Figure 5. Absorption spectra of tetracyanobenzene (5×10^{-3} M) and α-methylstyrene (6×10^{-1} M) in n-amyl alcohol, after photoillumination with light of wave number less than 34.5×10^3 cm^{-1}, at 113°K.

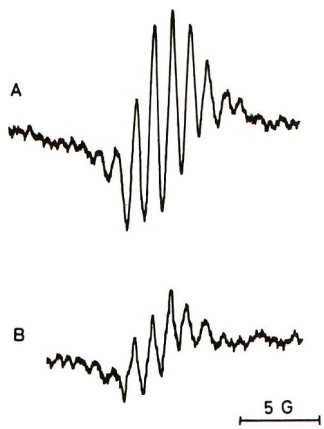

Figure 6. Electron spin resonance spectra during photolysis of the solution of tetracyanobenzene (1×10^{-2} M) and α-methylstyrene (7.6×10^{-1} M) in n-amyl alcohol at 223°K with light of wave number (A) less than 34.5×10^3 cm^{-1} and (B) less than 28.6×10^3 cm^{-1}.

cm^{-1}, the band attributable to the radical cation is found to disappear also.

Duplicate samples (7.6×10^{-1} M of α-methylstyrene and 5×10^{-3} M of tetracyanobenzene), one without and another with acetophenone, were photoilluminated at 113°K with light of wave number less than 28.6×10^3 cm^{-1}. The yield of radical anion was found to be 1.6 times larger in the presence of acetophenone than in its absence. This may be due to triplet energy transfer from acetophenone to the EDA complex, since the phosphorescent state of acetophenone was found to have an energy of 6.2×10^3 cm^{-1} higher than that of the EDA complex (19.6×10^3 cm^{-1}). The triplet photosensitization,[15] as well as the quenching by oxygen mentioned below, in the anion formation indicates that the triplet excited state of the EDA complex is responsible for its ionic dissociation, at least in part.

Figure 6 shows electron spin resonance spectra during photolysis of the viscous n-amyl alcohol solution (α-methylstyrene, 7.6×10^{-1} M; tetracyanobenzene, 1×10^{-2} M) at 223°K. The spectra are composed of nine hyperfine lines with a splitting constant of 1.04 G which are essentially identical with the spectra attributed to tetracyanobenzene radical anion.[16] The decrease in yield of the radical anion when photoillumination is limited to the charge-transfer band also indicates the two independent processes, (1) followed by (2) and (3), which result in the subsequent formation of ions. The steady-state intensity of the spectrum is linearly proportional to the light intensity. When the solution contains dissolved air, the formation of radical anion is remarkably suppressed. It is no longer observed from the solution saturated with oxygen. The reason that an electron spin resonance spectrum of α-methylstyrene radical cation was not observed is not known at the moment.

The intensity of the electron spin resonance spectrum becomes higher when measured at lower temperature, though the resolution of hyperfine lines is poorer. The transient increase of the spectrum was examined at 123°K, as shown in Figure 7. Notably, the rising curve has an S shape, suggesting that the precursor of the radical anion has a rather long life in a viscous solvent at low temperature. The radical anion disappeared by an exponential decay, when the light was turned off.

The formation of ions was also studied by observing transient photoconductivity of the degassed n-amyl alcohol solution of α-methylstyrene (7.6×10^{-1} M) and tetracyanobenzene (1×10^{-3} M) at 297°K when illuminated with a light flash. The dependence of observed photocurrent upon the wave number of light is shown in Figure 8. This indicates that charge carriers (ions) are formed through the excitation of either the acceptor band or the charge-transfer band. In addition, the excited EDA complex is necessarily involved, because the photocurrent is unobservable for wave numbers up to 34.5×10^3 cm^{-1} in the absence of the donor, α-methylstyrene. The transient rise of photocurrent does not follow the rise of the flash lamp current, but shows rather an S shape. Figure 9 shows that the initial slope of photocurrent (proportional to the ion yield) depends linearly on the intensity of the flash. It decays exponentially. These results are qualitatively consistent with those of the electron spin resonance measurements mentioned above. According to the two independent measurements, one by electron spin resonance at lower temperature under continuous light and another by photoconductivity measurements at room temperature under a flash, it is evident that the formation of ions from the excited EDA complex is a one-photon process.

In addition to the triplet photosensitization effect, the S-shaped rise observed by electron spin resonance

(15) The effect of acetophenone, benzophenone, triphenylene, fluorenone, and dibenzalacetone on the yield of tetracyanobenzene radical anion was also studied by esr measurements. An increase in the yield was found for all additives examined except for dibenzalacetone, which has a triplet energy lower than that of the EDA complex. This indicates that the effect is due to triplet energy transfer. These results will be published in detail elsewhere.

(16) A. Zewig, J. E. Lehnsen, W. G. Hodgson, and W. H. Jura, *J. Amer. Chem. Soc.*, 85, 3937 (1963).

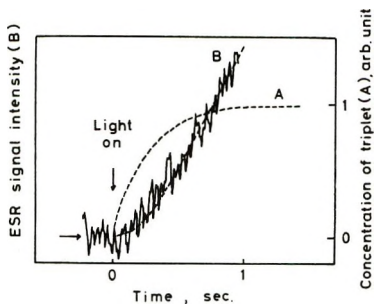

Figure 7. Transient rise of the intensity of the electron spin resonance spectrum during photolysis of the solution of tetracyanobenzene and α-methylstyrene in *n*-amyl alcohol at 123°K when the light is turned on. Curve A shows the accumulation of triplet excited EDA complex and curve B shows the change in the concentration of tetracyanobenzene radical anion expected from the lifetime of the EDA triplet state (see text).

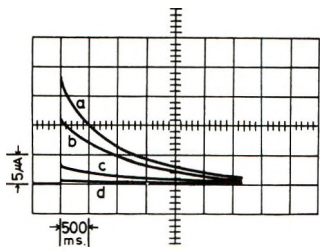

Figure 8. Observed photocurrent in the solution of tetracyanobenzene (1×10^{-3} *M*) and α-methylstyrene (7.6×10^{-1} *M*) in *n*-amyl alcohol at 297°K after a light flash of wave number less than (a) 32.3×10^3, (b) 28.6×10^3, (c) 25.6×10^3, and (d) 23.8×10^3 cm^{-1}. Applied voltage, 163 V/cm. 5 μA/div and 500 msec/div.

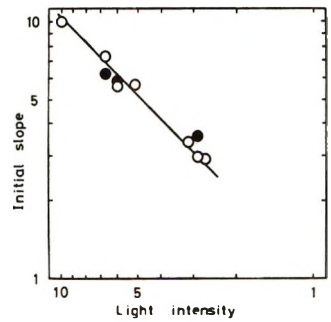

Figure 9. Dependence of the initial slope of photocurrent in the solution of tetracyanobenzene (5×10^{-3} *M*) and α-methylstyrene (7.6×10^{-1} *M*) in *n*-amyl alcohol at 297°K upon the intensity of the light flash of wave number less than 28.6×10^3 (○) and 34.5×10^3 cm^{-1} (●). Applied voltage, 163 V/cm.

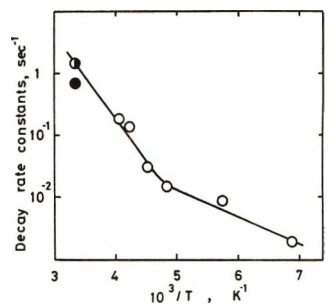

Figure 10. Dependence of the first-order decay rate constants of tetracyanobenzene radical anion formed by the photoillumination of the solution of tetracyanobenzene (5×10^{-3} *M*) and α-methylstyrene (7.6×10^{-1} *M*) in *n*-amyl alcohol, determined by electron spin resonance (○), flash absorption (◑), and photoconductivity (●) measurements, upon temperature.

agrees well with the curve expected from the observed lifetime of phosphorescence from the EDA complex (Figure 7, curve B). Therefore, the ionic dissociation of excited EDA complex is concluded to occur through its triplet state

$$^3(D\cdot A)^* \longrightarrow D\cdot^+_{solv} + A\cdot^-_{solv} \qquad (4)$$

However, it should be noted that the presence of oxygen caused a decrease in photocurrent to one sixth as much as that in its absence, but did not eliminate it completely. This fact indicates that, in addition to process (4), the direct ionic dissociation from the lowest singlet excited EDA complex

$$^1(D\cdot A)^* \longrightarrow D\cdot^+_{solv} + A\cdot^-_{solv} \qquad (5)$$

cannot be excluded, at least, at room temperature.

Decay Process of Ions. In the previous section some of the experimental results concerning the decay of ions formed from the excited EDA complex have been shown. The yield of ions is linearly proportional to the light intensity (see Figure 9), and their decay follows exponential curves (see Figure 8). These results, as well as the unreactivity of tetracyanobenzene radical anion with *n*-amyl alcohol, indicate that the decay is due to charge recombination between the anion and cation (not necessarily α-methylstyrene radical cation, but possibly some other type of cation subsequently formed) formed from an excited EDA complex. Figure 10 (open circles) shows the first-order decay constant determined by electron spin resonance at various temperatures from 245 to 145°K. It gives an activation energy of 6.2 kcal/mol above 208°K, which is close to the freezing point of *n*-amyl alcohol.

Transient optical absorption measurements at 21.6×10^3 cm^{-1} (the band maximum of tetracyanobenzene radical anion; see Figure 5) were carried out at 297°K for the *n*-amyl alcohol solution of tetracyanobenzene and α-methylstyrene. The results obtained were the same as those of the photoconductivity measurements, except that the first-order decay constant, 1.3 sec^{-1}, is twice as large as the decay constant of the photocurrent, 0.65 sec^{-1}. The former value falls on the extrapolated line for the Arrhenius plot of the decay constants determined by electron spin resonance (see the half-filled circle in Figure 10).

Let us consider what the small value of the decay constant for the transient photocurrent signifies. The

decay constant was found to be dependent upon neither the initial concentration of ions nor the applied voltage in the range examined (16–578 V/cm). Therefore, the decay exhibits the true lifetime of free ions in the solution, but not their disappearance on the electrodes. The discrepancy of the decay constants may be interpreted on the basis of a rapid equilibrium between an ion pair and free ions with a small equilibrium constant, K

$$(D\cdot^{+}_{solv}\cdots A\cdot^{-}_{solv}) \overset{K}{\rightleftharpoons} D\cdot^{+}_{solv} + A\cdot^{-}_{solv} \quad (6)$$

ion pair free ions

Both optical absorption and electron spin resonance measurements give the concentration of tetracyanobenzene radical anion, $A\cdot^{-}$, regardless of its form, paired or free, and $A\cdot^{-}$ decays by the relation

$$[A\cdot^{-}] \simeq [A\cdot^{-}_{paired}] = [A\cdot^{-}_{paired}]_0 \exp(-kt) \quad (7)$$

where k denotes the rate constant of the charge recombination process

$$(D\cdot^{+}_{solv}\cdots A\cdot^{-}_{solv}) \xrightarrow{k} D + A \quad (8)$$

On the other hand, the photocurrent depends on the concentration of free ions which decay by the following relation

$$[A\cdot^{-}_{free}] \simeq [A\cdot^{-}_{paired}]_0^{1/2} K^{1/2} \exp(-kt/2) \quad (9)$$

derived from $[A\cdot^{-}_{free}][D\cdot^{+}_{free}]/[A\cdot^{-}_{paired}] \simeq K$ and relation 7. The observed decay constant of the free ion was half as much as k for the ion pair.

The K value is presumed to be about 10^{-5} M, because it is 1.4×10^{-4} M and 3.9×10^{-6} M for (isoamyl)$_3$BuN$^+$ (tetraphenylbromide)$^-$ and Cs$^+$ (tetraphenylbromide)$^-$, respectively, in tetrahydrofuran at 203°K (dielectric constant of 11.58).[17] The association of free ions into a pair may be diffusion controlled, with a typical rate constant of 10^{10} M^{-1} sec^{-1}. These values lead to a dissociation rate constant of about 10^5 sec^{-1}. Therefore, equilibrium 6 is reasonably assumed to be maintained during the charge neutralization process 7.

Acknowledgment. The authors with to express their sincere thanks to Professor H. Baba of Hokkaido University for giving facilities to use spectrometers, to Mr. K. Hayashi of Osaka Laboratories for Radiation Chemistry, Japan Atomic Energy Research Institute, for his collaboration in photoconductivity measurements with an instrument made by himself, and to Dr. H. Yoshida of Hokkaido University for valuable discussions.

(17) C. Carvajal, K. J. Tölle, J. Smid, and M. Szwarc, *J. Amer. Chem. Soc.*, **87**, 5548 (1965).

Chemical Lasers Produced from O(¹D) Atom Reactions. IV. Competitive Eliminations of HCl and HF from the Vibrationally Excited ClFHCOH, Cl_2FCOH, and ClF_2COH Molecules

by M. C. Lin

Chemistry Division, Naval Research Laboratory, Washington, D. C. 20390 *(Received December 17, 1971)*

Publication costs assisted by the Naval Research Laboratory

Chemical HCl and HF laser emissions were observed from the competitive, four-centered unimolecular elimination reactions of chemically activated ClFHCOH, Cl_2FCOH, and ClF_2COH molecules in an optical cavity. The HF emission was found to be significantly stronger and was observed in all three reactions; the HCl emission, however, was detected only in the Cl_2FCOH system. This is attributable to a larger stimulated emission coefficient as well as a preferentially faster rate of elimination of HF than HCl. The vibrationally excited methanol molecule, which possesses at least 130 kcal/mol of internal energy, was generated by insertion of an O(¹D) atom into a C–H bond of a chlorofluoromethane molecule. The O(¹D) atom was produced from the flash-photolytic decomposition of O_3. The initial population ratios of the highest gain transitions have been estimated and compared with the values obtained from other O(¹D) atom insertion–elimination reactions reported previously.

Introduction

Recently, we have reported the observation of HF and HCl laser emissions produced from the four-centered elimination reactions of chemically activated α-fluoro-[1] and α-chloromethanols,[2] respectively. The vibrationally excited methanol molecule was generated by insertion of an O(¹D) atom into a C–H bond of a halomethane molecule

$$O(^1D) + CH_nX_{4-n} \longrightarrow H_{n-1}X_{4-n}COH^\dagger \quad (I)$$

where X = F, Cl and n = 1, 2, 3. The vibrationally excited methanol thus produced possesses at least 130 kcal/mol of internal energy, judging by the exothermicity of the analogous reaction, $O(^1D) + CH_4 \rightarrow CH_3OH$, $\Delta H^\circ = -135$ kcal/mol. On account of the large amount of excess vibrational energy ($\epsilon - \epsilon_0 \geq 100$ kcal/mol[1]) and its small molecular size, the lifetime of the excited methanol is estimated to be as short as 10^{-11} sec. Accordingly, reaction I is immediately followed by a rapid, four-centered elimination reaction (II), producing vibrationally excited hydrogen halide and carbonyl halide molecules

$$H_{n-1}X_{4-n}COH^\dagger \longrightarrow HX^\dagger + H_{n-1}X_{3-n}CO^\dagger \quad (II)$$

For n = 2, the subsequent elimination of the excited formyl halide molecule

$$HXCO^\dagger \longrightarrow HX^\dagger + CO \quad (III)$$

was also found to take place and contributed partly to the laser oscillations.[1,2] This rapid overall insertion–elimination reaction is also manifested by the comparatively short appearance times of both HF and HCl laser pulses ($t_{app} \leq 4$ μsec[1,2]).

The initial population ratios of the highest gain transitions have been estimated for HF and HCl molecules produced in a series of insertion–elimination reactions. The population ratios were found to be less than unity for all cases investigated.[1,2] In this work, we examine the relative importance of the eliminations of HCl and HF competitively from an excited α,α-chlorofluoromethanol molecule.

Experimental Section

The experimental apparatus has been described previously.[3] A Suprasil laser tube (2.5-cm i.d., 1-m length), fitted with NaCl windows at the Brewster angle, was positioned in an optical cavity formed by two 2.5-cm diameter, 3-m radius gold-coated mirrors at a separation of about 1.2 m; one of the mirrors had a 1-mm coupling hole at its center. Six 50-cm long Xe quartz flash lamps were placed coaxially around the laser tube in an alumina housing. The flash lamps were capable of delivering up to 5 kJ of energy with a pulse shape of about 3 μsec rise time and 6–8 μsec half width. Laser emissions were analyzed by passing the beams through a 50-cm Model 305 SMP03 grating monochromator and were observed by an Au–Ge detector, maintained at 77°K, in conjunction with a Tektronix Model 556 oscilloscope.

Ozone generated from an ozonizer[4] was collected in a silica gel trap maintained at −78° and was thoroughly

(1) M. C. Lin, *J. Phys. Chem.*, **75**, 3642 (1971).

(2) M. C. Lin, *ibid.*, **76**, 811 (1972).

(3) L. E. Brus and M. C. Lin, *ibid.*, **75**, 2546 (1971).

(4) H. Melville and B. G. Gowenlock, "Experimental Methods in Gas Reactions," Macmillan, London, 1964.

outgassed before use. CH_2ClF (du Pont), $CHCl_2F$ (Matheson) and $CHClF_2$ (Matheson) were subjected to repetitive degassings at $-196°$ and were stored in glass bulbs. SF_6 (Matheson), which was transferred under high pressures, was used without further purification. The reaction mixture ($P_t \leq 400$ Torr) was prepared in a 2-l. painted glass bulb; a sufficient time was always allowed for mixing before flashing. No significant drop in laser output was noticed when a 2-day-old mixture was flashed in comparison with a freshly made one. The decomposition of O_3 at room temperature under our conditions was therefore concluded to be unimportant; this is consistent with the half-life of O_3 at room temperature, $\sim 10^6$ sec (10 days).

Both flashed and unflashed samples were analyzed in the same manner with a CEC-620 mass spectrometer. A liquid N_2 trap was used to separate the condensable from the noncondensable fraction (*e.g.*, H_2CO from CO) of the sample in order to avoid complications due to the cracking patterns of the former. The results of product analyses are similar to those reported previously in the CH_nF_{4-n} and CH_nCl_{4-n} flashes.[1,2] The conversions of halomethanes were found to be about 15–20%.

Results and Discussion

The typical results obtained from flashing 30 Torr of 1:1:20 O_3–halomethane (CH_2ClF, $CHCl_2F$, and $CHClF_2$, respectively)–SF_6 mixtures are shown in Figure 1; a constant flash energy of 1.5 kJ was employed in all cases. Laser oscillations were detected in all three systems. The laser output (peak power) as a function of total sample pressure is given in Figure 2; the intensities of these three systems are comparable. The outputs reach their maxima at about 40–50 Torr total pressure. A rapid decrease in power at $P_t \geq 40$ Torr was observed in the $CHClF_2$ system, whereas only a slight drop was noticed in the $CHCl_2F$ flashes. The output of the CH_2ClF system, however, reaches its plateau value at $P_t \geq 40$ Torr and begins to fall off at pressures greater than 90 Torr. Since the partial pressures of O_3, halomethane, and SF_6 are the same in all cases, the fast decrease in power in the $CHClF_2$ system is probably attributable to a faster rate of relaxation of HX(v) by the $CHClF_2$ molecule.

The observed vibration–rotation transitions and their appearance times (in microseconds) are listed in Table I. The emissions from these three systems were found to be predominantly due to HF. The lasting sequence of the HF transitions is similar to those observed in the CH_nF_{4-n} (n = 1 and 2) systems in which the $2 \rightarrow 1$ transitions have the highest gains and, accordingly, appear first. The appearance of $3 \rightarrow 2$ transitions, which were absent in the CH_nF_{4-n} flashes, is probably attributable more to higher gains of the present systems, owing to the use of SF_6 as a diluent,[2] than to the difference in the dynamics of these unimolecular elimination reactions.

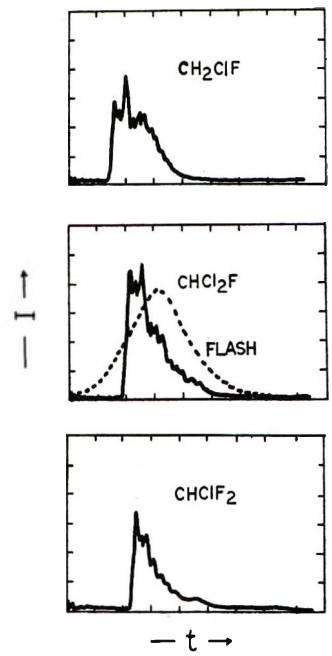

Figure 1. Total laser emission traces and the flash output at 240 nm: ordinate, emission intensity (1 V/div); abscissa, time (2 μsec/div). In all cases, flash energy = 1.5 kJ, P_t = 30 Torr (O_3:halomethane:SF_6 = 1:1:20).

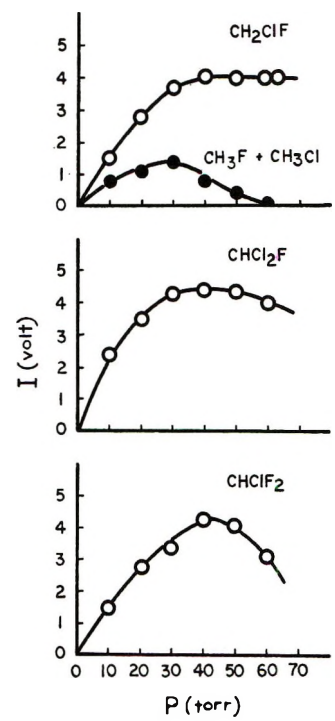

Figure 2. The effect of total pressure on the laser intensity. Flash energy = 1.5 kJ, O_3:halomethane:SF_6 = 1:1:20 for all cases except for the CH_3Cl + CH_3F mixture, in which O_3:CH_3Cl:CH_3F:SF_6 = 1:0.5:0.5:20.

HCl emissions were totally absent in both CH_2ClF and $CHClF_2$ flashes, and only one transition, $P_{10}(8)$, lasing weakly in the $CHCl_2F$ system, was detected. The strong HF emission may result from a higher

Table I: Observed HF and HCl Vibration-Rotation Transitions and Their Appearance Times in the CH_2ClF, $CHCl_2F$, and $CHClF_2$ Systems[a]

Lasing species	Transitions	ν, cm^{-1}	CH_2ClF	$CHCl_2F$	$CHClF_2$
HF	$\Delta v = 3 \rightarrow 2$				
	P(5)	3417.99[b]	4.6[d]	5.0	
	P(6)	3373.32	5.2	5.6	
	$\Delta v = 2 \rightarrow 1$				
	P(4)	3622.58	2.9	3.9	4.4
	P(5)	3577.52	3.3	4.1	4.5
	P(6)	3531.20	4.2	5.0	5.4
	P(7)	3483.71	5.0	5.5	6.7
	P(8)	3435.10	5.6	6.4	9.0
	$\Delta v = 1 \rightarrow 0$				
	P(6)	3693.64	4.3	4.6	5.1
	P(7)	3644.24	4.5	5.2	6.5
	P(8)	3593.89	5.5	7.1	9.7
HCl	$\Delta v = 1 \rightarrow 0$				
	P(8)	2703.01[c]		8.8	

[a] Flash energy = 1.5 kJ, P_{total} = 30 Torr (O_3:halomethane: SF_6 = 1:1:20). [b] Vacuum wavelengths reported by A. L. Mann, *et al.*, *J. Chem. Phys.*, **34**, 420 (1961). [c] Vacuum wavelength observed by B. O. Rank, *et al.*, *J. Mol. Spectrosc.*, **17**, 122 (1965). [d] Appearance time of the individual laser pulse, μsec.

spontaneous emission coefficient (Einstein A coefficient) and a faster elimination rate of HF than HCl. These two factors can be demonstrated by comparing the laser emission intensity of the 1:0.5:0.5:20 O_3–CH_3Cl–CH_3F–SF_6 flashes with that of the 1:1:20 O_3–CH_2ClF–SF_6 system under the same conditions as shown in Figure 2. The peak intensity of the 0.5 (CH_3Cl + CH_3F) system is about a factor of 3 lower than that of the CH_2ClF system at $P_t \leq 30$ Torr, and it decreases rapidly as pressure increases. Only HF laser emission was detected from the 0.5 (CH_3Cl + CH_3F) flashes under the present conditions. Since HCl lases in the 1:1:20 O_3–CH_3Cl–SF_6 mixtures,[2] the absence of HCl emission indicates that the gain of HCl is only slightly below the threshold in the 0.5(CH_3Cl + CH_3F) system. The rates of HCl and HF formation in this system are expected to be nearly equal, because the rate-controlling process of these insertion–elimination reactions is probably the insertion rather than the elimination step. The inversion ratios, N_1/N_0, of HF and HCl produced from O(¹D) + CH_3F and O(¹D) + CH_3Cl reactions have been estimated to be 0.5[1] and 0.6,[2] respectively; the inversion density should not, therefore, be an important factor in the present case either. Thus, the appearance of HF laser alone in the 0.5(CH_3Cl + CH_3F) flashes is attributed to the higher A coefficient of HF. The fact that the laser outputs of the three systems are significantly higher than that of the 0.5 (CH_3Cl + CH_3F) system can be concluded to be due to a preferentially faster rate of elimination of HF than HCl from the vibrationally excited methanols formed in the following reactions.

$$O(^1D) + CH_2ClF \longrightarrow ClFHCOH^\dagger \longrightarrow HF^\dagger + HClCO^\dagger \quad \Delta H^\circ_{1a} = -145 \text{ kcal/mol} \quad (1a)$$

$$O(^1D) + CH_2ClF \longrightarrow ClFHCOH^\dagger \longrightarrow HCl^\dagger + HFCO^\dagger \quad \Delta H^\circ_{1b} = -151 \text{ kcal/mol} \quad (1b)$$

$$O(^1D) + CHCl_2F \longrightarrow Cl_2FCOH^\dagger \longrightarrow HF^\dagger + Cl_2CO^\dagger \quad \Delta H^\circ_{2a} = -154 \text{ kcal/mol} \quad (2a)$$

$$O(^1D) + CHCl_2F \longrightarrow Cl_2FCOH^\dagger \longrightarrow HCl^\dagger + ClFCO^\dagger \quad \Delta H^\circ_{2b} = -160 \text{ kcal/mol} \quad (2b)$$

$$O(^1D) + CHClF_2 \longrightarrow ClF_2COH^\dagger \longrightarrow HF^\dagger + ClFCO^\dagger \quad \Delta H^\circ_{3a} = -160 \text{ kcal/mol} \quad (3a)$$

$$O(^1D) + CHClF_2 \longrightarrow ClF_2COH^\dagger \longrightarrow HCl^\dagger + F_2CO^\dagger \quad \Delta H^\circ_{3b} = -168 \text{ kcal/mol} \quad (3b)$$

The thermochemical data for these reactions are given in Table II; they were taken primarily from the JANAF tables.[5] The heats of formation of CH_2ClF, $CHCl_2F$, and formyl halides were evaluated by assuming the heats of redistribution to be small and negligible.[5] This assumption is probably valid and adequate for the present cases. For example, taking $\Delta H_\gamma^\circ \equiv 0$ for the reaction $CH_2F_2 + CCl_2F_2 \rightarrow 2CHClF_2$, then ΔH_f° ($CHClF_2$) = [ΔH_f° (CH_2F_2) + ΔH_f° (CCl_2F_2)]/2 = −113.0 ± 1.1 kcal/mol, using ΔH_f° (CH_2F_2) = −108.2 ± 0.2 and ΔH_f° (CCl_2F_2) = −117.8 ± 2 kcal/mol.[6] This is in good agreement with the experimental value, ΔH_f° ($CHClF_2$) = −112.3 kcal/mol, determined by Edwards and Small.[7] However, it is not recommended that one employ the general scheme $CX_4 + CH_2Y_2 \rightarrow 2CHX_2Y$ to calculate ΔH_f° (CHX_2Y) without correcting for the rearrangement energy.[6] For instance, the heat of redistribution for the reaction $CF_4 + CH_2Cl_2 \rightarrow 2CHClF_2$ becomes as high as +21 kcal/mol, which gives rise to an erroneous value of −123 kcal/mol for ΔH_f° ($CHClF_2$). The errors in the heats of formation of ClFCO, HClCO, and HFCO are probably as much as ±5 kcal/mol for the omission of ΔH_γ°.

The exothermicities of the laser pumping reactions 1–3 are only slightly different from those of the CH_nF_{4-n} and CH_nCl_{4-n} analogs; this is also the case for the HF laser transitions observed, as was mentioned earlier. The results given in Table I allow us to estimate the initial relative population, N_v/N_{v-1}, for the transition that has the highest gain. Assuming that HX deactivation is negligible before the first line appears and that the rotational–translational temperature is about 300°K, then the observation that the $P_{21}(4)$ HF line reaches threshold first requires $N_2/N_1 \approx 0.8 \pm 0.2$ for

(5) D. R. Stull, Ed., "JANAF Thermochemical Tables," The Dow Chemical Co., Midland, Mich., 1960.

(6) J. R. Lacher and H. A. Skinner, *J. Chem. Soc. A*, 1034 (1968).

(7) J. W. Edwards and P. A. Small, *Ind. Eng. Chem., Fundam.*, **4**, 396 (1965).

Table II: The Heats of Formation (kcal/mol at 298°K) of Various Species Involved in the Laser Pumping Reactions[a]

Species	$\Delta H_f°_{298}$	Species	$\Delta H_f°_{298}$
$O(^1D)$	104.9[b]	Cl_2CO	−52.6
CH_2ClF	−66	F_2CO	−153[d]
$CHCl_2F$	−69	ClFCO	−102
$CHClF_2$	−112.3[c]	HClCO	−41
HCl	−22.0	HFCO	−90
HF	−64.8	CO	−26.4

[a] Unless otherwise specified, all data obtained from ref 5. [b] $\Delta H_f°[O(^1D)] = \Delta H_f°[O(^3P)] + \Delta E[O(^1D) \leftarrow O(^3P)] = 59.6 + 45.3 = 104.9$ kcal/mol. [c] Reference 7. [d] J. C. Amplett, J. R. Dacey, and G. O. Pritchard, *J. Phys. Chem.*, **75**, 3024 (1971), and references cited therein.

Table III: Comparison of the Estimated Population Ratios of the Highest Gain Transitions for Various $O(^1D)$ Atom Insertion–Elimination Reactions[a]

Reactant	Lasing species	v	N_v/N_{v-1}	$-\Delta H°$	Ref
CHF_3	HF	2	0.8	155	1
CH_2F_2	HF	2	0.8	148	1
CH_3F	HF	1	0.35	143	1
$CHCl_3$	HCl	1	0.50	155	2
CH_2Cl_2	HCl	2	0.76	145	2
CH_3Cl	HCl	1	0.61	134	2
CH_2ClF	HF	2	0.8	145	This work
$CHCl_2F$	HF	2	0.8	154	This work
	HCl	1	0.5	160	This work
$CHClF_2$	HF	2	0.8	160	This work

[a] v is the vibrational quantum number of the upper laser level. The overall heat of reaction, $\Delta H°$, is in kcal/mol.

the HF molecules produced in reactions 1–3. This value is the same as that obtained for the $O(^1D)$ + CHF_3 and $O(^1D)$ + CH_2F_2 reactions. Similarly, the P_{10} (8) line of HCl lases alone, implying that the HCl molecule produced in reaction 2a has a population ratio $N_1/N_0 \approx 0.5 \pm 0.04$. These values are compiled in Table III along with, for comparison, those values estimated for other insertion–elimination reactions studied previously.[1,2]

The early appearance of laser pulse from the CH_2ClF flash (see Figure 1) is worth noting. It may result from the combination of the following two factors: (1) a faster rate of $HClFCOH^\dagger$ formation due to a higher C–H bond density, and (2) the extra contribution of $HF^\dagger$ from the elimination of vibrationally excited HFCO produced in reaction 1b.

$$HFCO^\dagger \longrightarrow HF^\dagger + CO \qquad (4)$$

The first possibility is, in fact, supported by the observation of a slightly higher conversion of CH_2ClF (~20%) in comparison with that of $CHClF_2$ or $CHCl_2F$ (~15%). Reaction 4 was concluded to be contributing a part of the laser emission from the CH_2F_2 system.[1]

The absence of HCl emission in reaction 1 is, however, puzzling, since a significant amount of CO was detected in the noncondensable fraction of a flashed CH_2ClF sample. The appearance of CO would imply that the subsequent elimination of $HClCO^\dagger$ or $HFCO^\dagger$ is important; this would, in turn, indicate that the total concentration of HCl is comparable to that of HF. A plausible explanation of its absence may be that the small population inversion created in reaction 1b is offset by a dominant amount of HCl, produced from the elimination of $HClCO^\dagger$ formed in reaction 1a, which may not have a significant inversion because of a rather widespread internal energy in the $HClCO^\dagger$ molecules. This in an interesting point which deserves further detailed investigation by employing a longer, temperature-controlled laser tube to pick up the low gain signals. Similar studies of the insertion of $NF(^1\Delta)$[3] and $NH(^1\Delta)$ into hydrocarbons are also planned.

Conclusion

The HF molecule is found to eliminate competitively with a faster rate than does HCl from the vibrationally excited chlorofluoromethanol molecules. The data compiled in Table III indicate that (1) the HF molecule produced from the elimination of an excited α-halomethanol molecule containing two or three halogen atoms has the highest gain in the $2 \rightarrow 1$ transition with a population ratio of $N_2/N_1 \approx 0.8$; (2) the HCl molecule produced from an excited methanol containing three halogen atoms, however, has the highest gain in the $1 \rightarrow 0$ transition, the inversion ratio being 0.5; and (3) the HX (X = Cl, F) molecule generated from this type of unimolecular elimination reaction, similar to few other elimination reactions studied,[8-11] always has partial inversion and possesses only a small fraction of exothermicity resulting from a random or near random distribution of reaction energy among various degrees of freedom. This conclusion, in turn, implies that the lifetime of the activated complex, $(F\cdots H\cdots R)^\ddagger$, of the exothermic bimolecular abstraction reaction $F + RH \rightarrow HF^\dagger + R$ is much shorter than 10^{-12} sec, the approximate time required for the reshuffling of vibrational energy within a molecule.[12] Complete population inversions of HF in both $2 \rightarrow 1$ and $1 \rightarrow 0$ transitions have been reported for this type of abstraction reaction.[13]

Acknowledgment. This work is partially supported by the Advanced Research Projects Agency under ARPA Order 660, which is gratefully acknowledged.

(8) P. N. Clough, J. C. Polanyi, and R. T. Taguchi, *Can. J. Chem.*, **48**, 2919 (1970).
(9) M. J. Berry and G. C. Pimentel, *J. Chem. Phys.*, **53**, 3453 (1970).
(10) T. D. Padrick and G. C. Pimentel, *ibid.*, **54**, 720 (1971).
(11) H. W. Chang, D. W. Setser, and M. J. Perona, *J. Phys. Chem.*, **75**, 2070 (1971).
(12) J. D. Rynbrandt and B. S. Rabinovitch, *ibid.*, **75**, 2164 (1971).
(13) W. H. Green and M. C. Lin, *J. Chem. Phys.*, **54**, 3222 (1971), and references quoted therein.

Chemical Lasers Produced from O(¹D) Atom Reactions. V. Carbon Monoxide Stimulated Emission from Flash-Initiated O_3 + XCN Systems

by L. E. Brus and M. C. Lin*

Chemistry Division, Naval Research Laboratory, Washington, D. C. 20390 *(Received December 17, 1971)*

Publication costs assisted by the Naval Research Laboratory

CO infrared stimulated emission has been observed from flash-initiated O_3 + XCN (X = I, Br, Cl, and CN) mixtures with SF_6 diluent. About 60 P(J) lines of vibrational transitions from 13 → 12 down to 5 → 4 are present. Dilution in SF_6 is essential for stimulated emission; rare gas diluents quench laser emission by collisionally deactivating O(¹D) to O(³P). Mass spectrometric analysis shows ~20% conversion of XCN per flash due to reaction with O(¹D). The reaction producing vibrationally excited CO† is O(¹D) + CN($X^2\Sigma$, v) → CO†($^1\Sigma^+$, v') + N(²D), where $v \leq 4$ and $v' \leq 15$. Additionally, there may be some contribution to CO† from the reaction of O(¹D) with CN($A^2\pi$).

Introduction

Pollack[1] discovered the first chemical CO laser in the flash-initiated CS_2 + O_2 system. The pumping reaction yielding vibrationally excited CO† is now thought to be[2]

$$O(^3P) + CS \longrightarrow CO^\dagger + S(^3P) + 75 \text{ kcal/mol}$$

Recently, we reported[3] a strong, kinetically simpler CO laser from flash-initiated O_3 + C_3O_2 mixtures due to the reaction

$$O(^1D) + C_3O_2 \longrightarrow 3CO^\dagger + 160 \text{ kcal/mol}$$

CO stimulated emission from a pulsed electrical discharge in C_3O_2 + O_2 mixtures had been reported earlier by Lin and Bauer.[4]

In this study we attempted to produce CO stimulated emission based on the reaction

$$O + CN \longrightarrow CO^\dagger + N$$

in flash-initiated O_3 + XCN (X = Cl, Br, I, and CN) mixtures. We find that stimulated emission does indeed occur; reported here are detailed studies of pressure effects, particular CO vibrational–rotational transitions, and mass spectrometric product analysis. The kinetic mechanism is discussed, and the pumping reaction is concluded to be principally

$$O(^1D) + CN(X^2\Sigma, v) \longrightarrow CO^\dagger(^1\Sigma, v') + N(^2D)$$

where $v \leq 4$ and $v' \leq 15$. Additionally, there may be some CO† pumping due to reaction of O(¹D) with CN($A^2\pi$).

Experimental Section

The flash-initiated laser apparatus is of conventional design and has been previously described.[5] O_3 was generated in a silent O_2 discharge and stored on silica gel at −78°. Other gases were of commercial purity: ClCN (Matheson), BrCN (Aldrich), ICN (K and K), C_2N_2 (Baker), and Xe (Linde) were repetitively degassed before use. SF_6 and Ar (both Matheson) were delivered under high pressure and used without further purification. All experiments were conducted at room temperature.

Results and Discussion

(*I*) *Pressure and Relative Proportion Dependence.* Figure 1 shows total stimulated emission pulses observed from 50 Torr of 1:1:30 O_3–C_2N_2–SF_6 and 1:2:30 O_3–BrCN–SF_6 mixtures flashed with 2.4 kJ of energy. The flash pulse has about a 6-μsec rise time and an 8-μsec half-width. The emission begins at ~5–6 μsec and continues until approximately 20 μsec; this pulse width of ~15 μsec is only 10% of that observed from the O(¹D) + C_3O_2 reaction.[3]

Figure 2 shows the dependence of peak pulse power for various mixtures upon total pressure. For both BrCN and C_2N_2, dilution with 30 parts SF_6 is slightly better than dilution with 15 parts SF_6. Maximum power was obtained near 50 Torr total mixture pressure for C_2N_2 and near 80 Torr for BrCN. In the BrCN system, 1:2:15 mixtures gave a slightly higher power than 1:1:15 mixtures; the peak power from 2:1:15 mixtures was lower by ~50%. In the case of C_2N_2, peak powers from 2:1:15 and 1:2:15 mixtures decreased by 30 and 60%, respectively, in comparison with 1:1:15 mixtures.

In the ClCN system, peak powers were only 20% of those obtained from corresponding BrCN mixtures,

(1) M. A. Pollack, *Appl. Phys. Lett.*, **8**, 237 (1966).

(2) G. Hancock and I. W. M. Smith, *Chem. Phys. Lett.*, **3**, 573 (1969).

(3) M. C. Lin and L. E. Brus, *J. Chem. Phys.*, **54**, 5423 (1971).

(4) M. C. Lin and S. H. Bauer, *Chem. Phys. Lett.*, **7**, 223 (1970).

(5) L. E. Brus and M. C. Lin, *J. Phys. Chem.*, **75**, 2546 (1971).

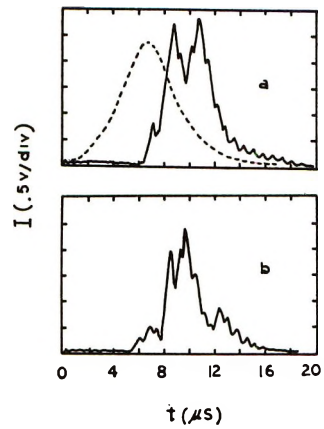

Figure 1. Total CO laser emission traces: (solid curves) laser emissions, (dotted curve) flash lamp output at 200 nm as a function of time; (a) O_3:C_2N_2:SF_6 = 1:1:30, (b) O_3:BrCN:SF_6 = 1:2:30; in both cases, P_t = 55 Torr, flash energy = 2.4 kJ.

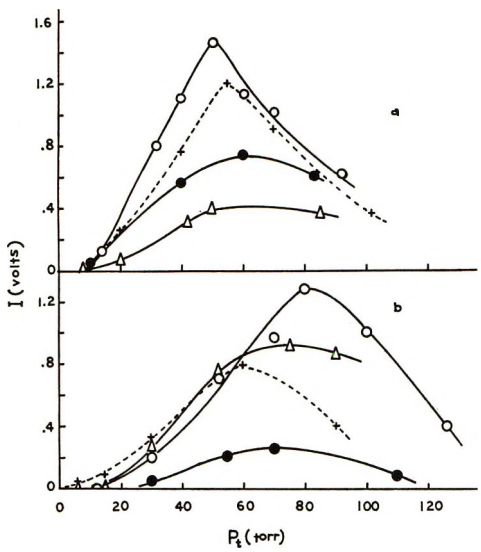

Figure 2. Relative laser peak pulse power as a function of total pressure for various mixtures, flash energy = 2.4 kJ for all cases: (a) (○) (O_3:C_2N_2:SF_6 = 1:1:30), (+) (1:1:15), (●) (2:1:15), (△) (1:2:15); (b) (○) (O_3:BrCN:SF_6 = 1:2:30), (+) (1:1:15), (△) (1:2:15), (●) (O_3:ClCN:SF_6 = 1:2:30).

and further studies were not performed. ICN has a saturation pressure at room temperature of only ~0.5 Torr and therefore could not be studied over the same pressure range as BrCN and C_2N_2. A 1:2:100 O_3–ICN–SF_6 mixture flashed at various pressures did not lase; however, 50 Torr of a 1:4:120 mixture lased very weakly. A corresponding BrCN mixture also at 50 Torr had approximately the same peak power. No further studies of ICN systems were carried out, principally owing to the low and somewhat uncertain pressures of ICN involved.

In both BrCN and C_2N_2 systems, mixtures flashed with 1.2 kJ of energy had ~30–50% of the peak pulse power obtained from mixtures flashed at 2.4 kJ.

(II) Identification of Transitions. The individual vibrational–rotational transitions were identified with a 0.5-m Minuteman 305-SMP monochromator for the 1:1:30 O_3–C_2N_2–SF_6 and 1:2:30 O_3–BrCN–SF_6 systems. These transitions appear in Table I; they are similar but not identical for the two cases. CO (v = 13) is the highest vibrational level observed in both cases; however, 11 → 10 transitions do not occur in the BrCN system, while 5 → 4 transitions are absent in the C_2N_2 system. In C_2N_2, $P_{9-8}(14)$, $P_{9-8}(15)$, $P_{8-7}(14)$, and P_{8-7} (12) are the first transitions[6] to reach threshold while in BrCN, P_{13-12} (12) and P_{13-12} (13) reach threshold first. These lines first appear 6.0–6.5 μsec after flash initiation in the C_2N_2 system and 5.0–5.3 μsec in the BrCN system.

Table I: Observed CO Vibration–Rotation Transitions from Both C_2N_2 and BrCN Systems[a]

CO transition		C_2N_2	BrCN	CO transition		C_2N_2	BrCN
13 → 12	P(15)	w[b]		8 → 7	P(22)	t	
	P(13)	s	s		P(21)	w	
	P(12)	s	s		P(20)	s	t
12 → 11	P(19)	w			P(19)	s	t
	P(18)	s			P(17)	w	w
	P(15)	s	t		P(14)	s	s
	P(14)	t	t		P(13)	t	
	P(13)	w	s		P(12)	s	s
	P(12)		t	7 → 6	P(21)	w	
	P(11)		w		P(20)	w	
	P(10)		t		P(19)	s	
	P(9)		t		P(18)	s	s
11 → 10	P(20)	t			P(17)	s	s
	P(19)	w			P(15)	w	t
	P(18)	s			P(14)	w	s
	P(17)	w			P(12)		w
	P(16)	s		6 → 5	P(21)	w	t
10 → 9	P(19)	s			P(19)	s	s
	P(17)	s	s		P(18)	t	t
	P(15)		t		P(17)	w	s
	P(14)		t		P(16)		s
	P(13)		t		P(15)		s
9 → 8	P(21)	w			P(14)		s
	P(20)	s			P(13)		t
	P(19)	s			P(12)		w
	P(18)	s		5 → 4	P(19)		w
	P(16)	s	s		P(18)		s
	P(15)	s	w		P(17)		s
	P(14)	w	w				

[a] O_3:C_2N_2:SF_6 = 1:1:30, O_3:BrCN:SF_6 = 1:2:30, P_t = 55 Torr, and flash energy = 2.4 kJ for all cases. [b] w = weak, s = strong, t = trace; no entry indicates the transition is absent.

(6) $P_{8-7}(14)$ stands for the P(14) line of the 8 → 7 CO vibrational band.

Within a given $v \rightarrow v - 1$ band, higher J lines generally reached threshold later than lower J lines. For example, P(19)–P(22) usually appeared at ~12 μsec after initiation and continued emitting until laser termination at roughly 20 μsec. During the period of stimulated emission, vibrational cascading of $CO^{\dagger}$ molecules will decrease the initial inversion on a $v \rightarrow v - 1$ band. Additionally, energy will be released into the translational and rotational degrees of freedom as the reaction proceeds, thus causing the rotational temperature to increase as a function of time. Both of these effects will cause the P line with the highest gain to shift to higher J.

In Table I a number of P(J) lines are found to be unexpectedly weak or absent. This effect is probably due to absorption of these particular frequencies by BrCN and C_2N_2, both of which have ir bands in the 2150-cm^{-1} region. Anticipating the results of section IV, we find only 20% decomposition of BrCN and C_2N_2 after a lasing pulse; during stimulated emission there is ~1.8 Torr of XCN in the laser tube.

(*III*) *Effect and Role of Diluents.* SF_6 was the only diluent in which stimulated emission occurred; attempts to use Ar or He in similar BrCN and C_2N_2 mixtures failed. Addition of 25 Torr of SF_6 to a 1:1:30 O_3–C_2N_2–SF_6 lasing mixture (55 Torr) actually *increased* the total pulse energy by a factor of 1.5, while addition of 25 Torr of Ar insteand of SF_6 *decreased* the output by a factor of 1.4. Additionally, Figure 3 shows the pronounced decrease in pulse energy observed when various Xe pressures were added to a lasing mixture at 55 Torr: for 25 Torr of added Xe, the energy is reduced by a factor of 5.1.

In chemical laser systems, the added heat capacity of inert diluents normally provides an increase in lasing power by lowering the rotational temperature. The power increases because a given population inversion on a $v \rightarrow v - 1$ band can be concentrated on fewer P(J) lines at a lower temperature. However, the anomalous He, Ar, and Xe effects we observe indicate that these rare gases directly affect the laser pumping mechanism. Similar effects have been recently observed in the HCl laser obtained from flash-initiated $O_3 + CH_nCl_{4-n}$ mixtures.[7]

In section V we will show that reaction of O(¹D) with internally excited CN is the principal $CO^{\dagger}$ pumping reaction. We believe that the anomalous effect of Xe, Ar, and He is due to collisional deactivation of O(¹D) to O(³P) by these gases. Cvetanović and coworkers[8-10] have shown that Xe deactivates O(¹D) as efficiently as CO_2 or N_2O, and at a nearly gas kinetic rate. The deactivation rate for SF_6 is zero, within experimental error, and the rates for Ar and He are small but not zero. Our observations are entirely consistent with these data.

(*IV*) *Mass Spectrometric Analysis.* Gas mixtures were analyzed with a CEC-620 mass spectrometer before and after flash photolysis; 1:2:30 O_3–ClCN (and BrCN)–SF_6 and 1:1:30 O_3–C_2N_2–SF_6 mixtures were tested. The concentrations of ClCN, BrCN, and C_2N_2 were decreased by ~20% after photolysis.

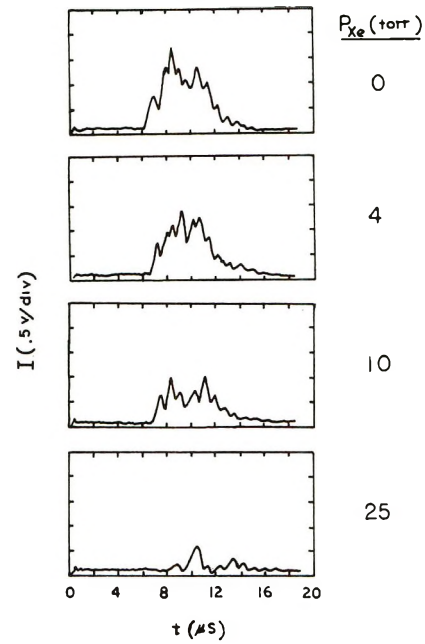

Figure 3. Effect of Xe on the CO laser intensity. Xe was added to 55 Torr of an 1:1:30 O_3–C_2N_2–SF_6 mixture; flash energy = 2.4 kJ for all flashes.

In a separate experiment we analyzed mixtures of XCN in excess O_2 (1:30 at 50 Torr) before and after flash photolysis in the laser tube. This experiment was designed to measure the extent of XCN photolysis in the laser tube, as O_2 is known to scavenge CN radicals.[11] No stimulated emission occurred during flash photolysis (X = Br and CN), and ten successive flashes were required to produce a slight (~1%) decrease in XCN concentration. Thus, we estimate that only ~0.1% of the XCN in a lasing mixture is dissociated during flash photolysis, and it follows then that the 20% XCN conversion observed is due to attack by O(¹D) atoms from O_3 photolysis.

(*V*) *Reaction Mechanism.* The general reaction mechanism of eq 1–12 is proposed

$$O_3 + h\nu \longrightarrow O(^1D) + O_2(^1\Delta) \quad (1)$$

$$XCN + h\nu \longrightarrow X + CN(X^2\Sigma) \quad (2)$$

$$CN(X^2\Sigma) + h\nu \longrightarrow CN(B^2\Sigma) \xrightarrow{M} CN(X^2\Sigma, v) \text{ or } CN(A^2\pi, v') \quad (3)$$

(7) M. C. Lin, *J. Phys. Chem.*, **76**, 811 (1972).

(8) K. F. Preston and R. J. Cvetanović, *J. Chem. Phys.*, **45**, 2888 (1966).

(9) P. M. Scott and R. J. Cvetanović, *ibid.*, **54**, 1440 (1971).

(10) G. Paraskevopoulous and R. J. Cvetanović, *J. Amer. Chem. Soc.*, **91**, 7572 (1969).

(11) N. Basco, *Proc. Roy. Soc., Ser. A*, **283**, 302 (1965).

$$CN(X^2\Sigma) + h\nu \longrightarrow CN(B^2\Sigma) \xrightarrow{-h\nu} CN(X^2\Sigma, v)$$

$$O(^1D) + XCN \longrightarrow OCN + X \quad (4)$$

$$OCN + h\nu \longrightarrow N(^2D) + CO \quad (5)$$

$$O(^1D) + CN(X^2\Sigma) \longrightarrow CO^\dagger + N(^2D)$$

$$\Delta H^\circ_{6a} = -64.1 \text{ kcal/mol} \quad (6a)$$

$$O(^1D) + CN(A^2\pi) \longrightarrow CO^\dagger + N(^2D)$$

$$\Delta H^\circ_{6b} = -90.5 \text{ kcal/mol} \quad (6b)$$

$$O(^3P) + CN \longrightarrow CO^\dagger + N(^4S)$$

$$\Delta H^\circ_{7a} = -73.8 \text{ kcal/mol} \quad (7a)$$

$$O(^3P) + CN \longrightarrow CO^\dagger + N(^2D)$$

$$\Delta H^\circ_{7b} = -18.8 \text{ kcal/mol} \quad (7b)$$

$$O + OCN \longrightarrow NO + CO \quad (8)$$

$$CN + O_2 \longrightarrow OCN + O \quad (9)$$

$$N + O_2 \longrightarrow NO + O \quad (10)$$

$$N + NO \longrightarrow N_2 + O \quad (11)$$

$$O(^1D) + O_3 \longrightarrow 2O(^3P) + O_2 \quad (12)$$

where X = I, Br, Cl, and CN; O = $O(^3P)$ or $O(^1D)$; and N = $N(^4S)$ or $N(^2D)$.

O_3 exhibits an intense uv absorption and is completely photodissociated *via* reaction 1 in our laser tube; during the early part of the flash, $O(^1D)$ can react[12] with the remaining O_3 as in reaction 12. However, as previously mentioned, only ~0.1% of the XCN is photodissociated *via* reaction 2. Norrish and coworkers[13] studied the flash photodissociation of XCN (X = I, Br, and CN) and found vibrationally excited $CN(X^2\Sigma, v)$ present *via* absorption spectroscopy. The ratio of vibrational populations $N_0:N_1:N_2:N_3:N_4$ at 5 μsec after flash initiation was 0.75:0.24:0.31:0.49:1.0 for BrCN (0.75 Torr) and 0.51:0.31:0.21:0.26:1.0 for C_2N_2 (4.6 Torr), flashed in 350 Torr of N_2 with 1.6 kJ of energy. In both cases a total population inversion exists on $v = 4 \rightarrow 3$.[14] This excitation was attributed to reaction 3, that is, repeated cycles during the photolysis flash of $CN(X^2\Sigma)$ absorption followed by emission or collisional deactivation.

Actually, collisional cross sections for deactivation of the $B^2\Sigma$ state appear to be large (~30 Å^2 for M = ICN or BrCN[15]), and in our lasing mixtures deactivation probably dominates fluorescence. Deactivation could easily produce significant amounts of $CN(A^2\pi)$, which lies 9241 cm^{-1} above $X^2\Sigma$ and is not observable in absorption spectroscopy, as well as the vibrationally excited $CN(X^2\Sigma)$ observed by Norrish and coworkers. Their results are most interesting in that $v = 4$ has the highest population of $v = 0$–4, while $v = 5$ and higher levels have much smaller populations. Actually, $v = 4$ is the highest level of the $X^2\Sigma$ state lying below $v = 0$ of the $A^2\pi$ state; their results suggest that CN radicals collisionally transferred from $A^2\pi$ levels into $v = 4$ of the $X^2\Sigma$ state. Literature data on the properties of $A^2\pi$ are sparse; however, Wentink *et al.*,[16] report that the $v = 0$ level has a lifetime of 3.5 ± 0.4 μsec independent of pressure in 0.2–2.0 Torr of CH_3CN. It is possible, then, that $CN(A^2\pi)$ could exist for several μsec in our lasing mixtures and undergo processes such as reaction 6b.

Reaction 4 is introduced to account for the high conversion (~20%) of XCN observed in the lasing mixtures. This conversion cannot be due to reaction of $O(^3P)$ with XCN, as these reactions are known[17,18] to have high activation energies. In support of this conclusion, we observed that addition of 15 Torr of Xe to a 1:1:30 O_3–C_2N_2–SF_6 mixture at 55 Torr decreased the C_2N_2 conversion from ~20 to ~5%.

Reactions 7a and 7b are spin allowed and have a combined rate constant[16] $k_7 = 6.2 \times 10^{13} e^{-2400/RT}$ cm^3/(mol sec). However, $O(^3P)$ in reaction 7 is in competition for CN with O_2 ($^3\Sigma$ and $^1\Delta$) in reaction 9. In the case of $O_2(^3\Sigma)$, $k_9 = 4.5 \times 10^{12}$ cm^3/(mol sec);[11,17] k_9 for $O_2(^1\Delta)$ is probably much larger. Thus, if we consider for the moment the situation when $O(^1D)$ has been partly deactivated to $O(^3P)$, the combined factors $k_9(^1\Delta) \gg k_7$ and $[O_2(^1\Delta)] > [O(^3P)]$ make reaction 7 unimportant in comparison with reaction 9. Reaction 7a, which is the only $O(^3P)$ reaction that could yield highly excited $CO^\dagger$, should not occur to any appreciable extent. This analysis is certainly consistent with our observation that addition of the rare gases, which do deactivate $O(^1D)$ to $O(^3P)$, quenches the stimulated emission.

Reaction 5 is the predissociated absorption of OCN radical in the 265–300-nm region. Herzberg[19] suggests that this dissociation may yield either CN + $O(^3P)$ or CO + $N(^2D)$; actually, in view of Okabe's recent value $\Delta H_f^\circ(NCO) = 37 \pm 3$ kcal/mol,[20] the dis-

(12) V. D. Baiamonte, L. G. Hartshorn, and E. J. Blair, *J. Chem. Phys.*, **55**, 3617 (1971).

(13) N. Basco, J. E. Nicholas, R. G. W. Norrish, and W. H. J. Vickers, *Proc. Roy. Soc., Ser. A*, **272**, 147 (1963).

(14) This observation led M. A. Pollack [*Appl. Phys. Lett.*, **9**, 230 (1966)] to discover a CN radical laser on $P_{13}(9)$, $P_{13}(10)$, and $P_{12}(11)$ during C_2N_2 photolysis. We have confirmed Pollack's result for C_2N_2, but find no stimulated emission during BrCN photolysis. The CN laser deserves further investigation, especially in view of possible involvement of $A^2\pi$ in the mechanism.

(15) C. K. Luk, Columbia University, private communication; see also J. A. Myer and R. W. Nicholls, *Nature (London)*, **225**, 298 (1970).

(16) T. Wentink, Jr., L. Isaacson, and J. Morreal, *J. Chem. Phys.*, **41**, 278 (1964).

(17) J. Boden and B. A. Thrush, *Proc. Roy. Soc., Ser. A*, **305**, 107 (1968).

(18) P. B. Davies and B. A. Thrush, *Trans. Faraday Soc.*, **64**, 1836 (1968).

(19) G. Herzberg, "Molecular Spectra and Molecular Structure," Vol. III, Van Nostrand, Princeton, N. J., 1967, p 499.

(20) H. Okabe, *J. Chem. Phys.*, **53**, 3507 (1970).

sociation produces CO + N(²D). However, photodissociation of OCN cannot be the $CO^\dagger$ pumping reaction, for after absorption in the 265–300-nm region, there is not enough excess energy to pump CO above $v = 1$, as D(N–CO) is known to be 104 ± 3 kcal/mol.[20]

This vibrationally "cold" CO, however, can vibrationally relax $CO^\dagger$. Reactions 5, 8, 10, and 11 together produce N_2, NO, and cold CO, all of which may relax excited $CO^\dagger$ quite efficiently. This relaxation may explain why the CO laser pulse length is only ~10% of that observed in the O(¹D) + C_3O_2 system, where similar complicating side reactions do not occur. k_8 for O(³P) is not known, but it is probably faster than k_9 for $O_2(^3\Sigma)$, as the latter is the rate-controlling step in the CN + O_2 reaction.[11,17] Reactions 10 and 11 are fast, and especially so for N(²D).[21]

Reaction 8 of O(¹D) with OCN is exothermic by 147 kcal/mol. If the majority of this energy went into CO, then this reaction could be the pumping step for the $CO^\dagger$ stimulated emission. However, the somewhat limited available data on this class of reaction suggest that the majority of the energy should go into the newly formed NO bond. Additionally, if this step were the pumping reaction, we would expect equal lasing intensities from C_2N_2, BrCN, and ClCN mixtures, as the per cent conversion in each case is approximately the same. The fact that ClCN gives only 20% the lasing intensity of the other two leads us to tentatively reject this reaction as the laser pumping step. Thus, all the above considerations suggest reactions 6a and 6b as the $CO^\dagger$ pumping sources. Reaction 6a is exothermic by 64 kcal/mol, which can yield at most $CO^\dagger$ ($v = 11$), and reaction 6b is exothermic by 90.5 kcal/mol, which yields correspondingly $CO^\dagger$ ($v = 16$). Experimentally, $v_{max} = 13$; this implies that either vibrationally excited CN, as observed by Norrish and coworkers,[13] or possibly CN($A^2\pi$) levels are reacting with O(¹D) to yield $CO^\dagger$.

Production of ground-state N(⁴S) in reaction 6 is not included, as it is spin forbidden. One would normally expect the less exothermic but spin-allowed reaction yielding N(²D) to occur. If the reaction yielding N(⁴S) were occurring, it would be possible to excite $CO^\dagger$ to considerably high v levels; the experimental absence of $v \geq 14$ molecules is consistent with the production of only N(²D).

The total concentration and internal energy distribution of CN radicals should be different in the BrCN and C_2N_2 systems, as reaction 4 provides a second source of CN radicals in the C_2N_2 case.

$$\begin{aligned} O(^1D) + C_2N_2 &\longrightarrow CN + OCN \\ O(^1D) + BrCN &\longrightarrow Br + OCN \end{aligned} \qquad (4)$$

These secondary CN radicals appear somewhat later than primary CN radicals directly from XCN photodissociation, and therefore have less chance to undergo the cyclic process 3 before reaction 4 occurs. If these secondary CN radicals are then principally vibrationally cold, they will tend to populate the lower $CO^\dagger$ levels more strongly with an upper limit of $CO^\dagger$ ($v = 11$) for CN($X^2\Sigma$, $v = 0$). We do, in fact, observe maximum gain, as previously mentioned, in the C_2N_2 system on 9 → 8 and 8 → 7 transitions, while in the BrCN system, where only primary "hotter" CN radicals exist, maximum gain is observed on 13 → 12 transitions. Note that we have neglected production of BrO + CN in reaction 4 owing to the low bond strength of XO type radicals. The reactions of O(³P) + XCN were also believed to produce X + OCN.[17,18]

Acknowledgment. We gratefully acknowledge partial support of this work under ARPA Order 660.

(21) C. L. Lin and F. Kaufman, *J. Chem. Phys.*, 55, 3760 (1971).

Identification of the A-Type Hydroxyls on Silica Surfaces

by F. H. Van Cauwelaert, P. A. Jacobs, and J. B. Uytterhoeven*

University of Leuven, Laboratorium voor Oppervlaktescheikunde, 3030 Heverlee, Belgium *(Received December 7, 1970)*

Publication costs borne completely by The Journal of Physical Chemistry

Resolved spectra of the freely vibrating hydroxyls of a silica aerosil, pretreated at 750° indicate the existence of three components. This is confirmed by deuteration experiments and the influence of the sample temperature on the relative intensity of the different components. A tentative explanation assigns the high-frequency (HF) and middle-frequency (MF) components to coupled vibrations of identical hydroxyls, and the low-frequency (LF) component to isolated hydroxyls slightly influenced by lattice oxygens. The behavior of the total band frequency on adsorption of triethylamine and benzene is discussed. The apparent stoichiometry of the adsorption reactions is correlated with the strength of interaction between the surface hydroxyls and these two adsorbates.

Introduction

When a sample of silica (Cab-O-Sil or Aerosil) is heated at temperatures above 500°, its infrared spectrum contains only a sharp band at 3750 cm^{-1}, attributed to isolated and unperturbed hydroxyls, sometimes called A-type hydroxyls.[1-3]

It was claimed by Hair and Hertl[4] that after pretreatment of an Aerosil sample at 800°, this 3750-cm^{-1} band could be resolved into three bands situated at 3751, 3747, and 3743 cm^{-1}. Hair and Hertl speculated that the central band, which accounted for about 60% of the total band intensity, could be assigned to single hydroxyls (A_1-type), while the components at 3751 and 3747 cm^{-1} were ascribed to geminal hydroxyls (A_2-type). This speculation was supported by vapor adsorption experiments.[5] Some strongly adsorbed vapors (for example, triethylamine) reacted on a 1:2 basis (one gas molecule for two hydroxyls) with the A_2-type hydroxyls, and on a 1:1 basis with the A_1-type hydroxyls. Benzene reacted on a 1:1 basis with all the hydroxyls. These conclusions were based on a comparison between the shape of adsorption isotherms determined gravimetrically or spectroscopically and the changes in intensity of the different band components. Reaction with chlorosilanes at 300° reduced the intensity of the 3751-cm^{-1} component faster than that of the 3747- and 3743-cm^{-1} components.

Hockey[6] criticized the resolution of the 3750-cm^{-1} band, stating that the splitting into three components is an artifact. He argued that water vapor in the optical path of the spectrometer can cause the appearance of small bands superimposed on the single OH band in the silica gel. The intensity of these spurious bands depends on the efficiency of the dry air flushing system.

It is true that inefficient drying of the air in the spectrograph can produce artifacts in the OH stretching region. However, these can be reduced to a negligible intensity in double-beam operations by properly handling the dry air flushing system. In agreement with Hertl and Hair, we found that the 3750-cm^{-1} band, taken under the best experimental conditions, can be decomposed into three components. However, the assignment proposed by Hair and Hertl[4] was based on the relative intensity of the different components. In this paper, an alternative assignment will be proposed, based on the behavior of the components upon deuteration, heating, and adsorption of gases.

Experimental Section

(a) *Samples and Instrumental Techniques.* The silica gel sample was an Aerosil from Degussa, with a BET area of 234 $m^2\ g^{-1}$ after calcination at 750°.

Infrared spectra were recorded on a Beckman IR-12 grating spectrometer. The scanning speed was 8 $cm^{-1}\ min^{-1}$ and the abscissa scale was expanded. Energy and slit conditions were imposed by the opacity of the silica samples, but were adjusted so that the resolution was better than 1.9 cm^{-1} at 3700 cm^{-1}.

The samples were pressed into self-supporting films containing 5 mg of silica per square centimeter. These were mounted in a vacuum infrared cell in which they could be treated *in vacuo* at any desired temperature between 10 and 500° in the spectrograph itself. Pretreatments at higher temperatures (up to 900°) were done in air: the films were then transferred from the oven to the ir cell as quickly as possible, while still hot, and evacuated at 450°. In our spectra we found no indications that traces of water vapor were adsorbed during the transfer of the film; furthermore, silica samples heated at these high temperatures have been

(1) C. G. Armistead, A. J. Tyler, F. H. Hambleton, S. A. Mitchell, and J. A. Hockey, *J. Phys. Chem.*, **73**, 3947 (1969).

(2) M. L. Hair, "Infra-red Spectroscopy in Surface Chemistry," Marcel Dekker, New York, N. Y., 1967.

(3) L. H. Little, "Infrared Spectra of Adsorbed Species," Academic Press, New York, N. Y., 1966.

(4) M. L. Hair and W. Hertl, *J. Phys. Chem.*, **73**, 2372 (1969).

(5) W. Hertl and M. L. Hair, *ibid.*, **73**, 4269 (1969).

(6) J. A. Hockey, *ibid.*, **74**, 2570 (1970).

reported to be hydrophobic.[2,7] Spectra were taken at different temperatures, which were measured with a thermocouple attached to the stainless-steel film holder. A possible influence of emission by the hot samples on the spectra taken at higher temperatures was carefully checked and found to be negligible.

Adsorption isotherms of benzene and triethylamine were determined in the spectrometer. A side arm of the cell was connected to a vacuum system with storage bulbs, to a compensating cell in the reference beam of the spectrometer, and to a mercury manometer. Appropriate slugs of gases were introduced into the cell. After equilibration, the residual gas pressure was measured and the spectrum was recorded between 3700 and 3800 cm^{-1}. In this way the decrease in intensity of the OH band upon adsorption was determined. Volumetric isotherms were also determined in a conventional BET system.

Deuteration of the sample films was carried out in the ir cell by contacting the samples with D_2O at 200° for several hours. The D_2O in the cell was replaced repeatedly.

(*b*) *Decomposition of the 3750-cm^{-1} Band.* The spectra were decomposed on a Du Pont Type 310 curve resolver. The function introduced into the channels of the curve resolver was a mixed function with 65% Lorentzian and 35% Gaussian character. The choice of this analytical function can be justified as follows. In liquid phases, the ir bands not affected by intramolecular effects are Lorentzian shaped. This has been derived both theoretically[8] and experimentally.[9,10] Hair, *et al.*,[4] also adopted a Lorentzian band shape for the A-type hydroxyls on silica gel. However, the spectroscopic determinations on powder samples require improved experimental conditions which can introduce instrumental perturbations. Rather than adopting *a priori* the theoretical band shape, we preferred to analyze the shape of experimentally obtained OH bands. This was done using the method of Abramowitz and Bauman.[11] The basic function is assumed to be a product function of the Voight type

$$A_\nu = A_0(1 + x^2)^{-1} \exp(-\alpha x^2)$$

where A_ν = the absorbance at frequency ν, A_0 = the absorbance at the center of the band, x = a measure of the frequency from the center of the band, and α = a measure of the Gaussian perturbation of the Lorentzian shape. The method can be applied to symmetrical bands, of which the half-band width and central frequency can be measured accurately. Therefore, we selected for comparison some solids in which the hydroxyls can be supposed to be unperturbed. Furthermore, the test was always applied on the high-frequency half of the peaks, since intramolecular perturbations affect mainly the low-frequency side. In hydrogen zeolite Y, the 3740- and 3650-cm^{-1} bands have 65 ± 2.5% Lorentzian shape. In kaolinite, the 3630-cm^{-1} band is 69% Lorentzian. In muscovite, 70% Lorentzian character was found for the 3685-cm^{-1} band. If the test is applied on the HF side of the 3750-cm^{-1} band in our Aerosil samples scanned at room temperature under normal resolution, a ratio of 65% Lorentzian and 35% Gaussian character was determined. This function was introduced into the curve resolver, and it was assumed that all the components had the same analytical function.

With this analytical function, the decomposition of the 3750-cm^{-1} band produces three components. The reality of these three components is substantiated by some additional experimental observations (see Results).

Results

Photographs of spectra of an Aerosil sample pretreated in an oven at 850° and subsequently evacuated at 450° are shown in Figure 1. These spectra are taken at 19, 100, 200, 300, and 400°. The peak height decreases with increasing temperature, and the half-band width increases. On the high-temperature spectra two shoulders appear, one on the low-frequency and another on the high-frequency side of the band envelope. Therefore, it was anticipated that the band could be resolved into three components. Using the appropriate peak profile as explained in the Experimental Section, an excellent fit could be obtained in the curve resolver. These components are drawn in Figure 2. They will be referred to as the HF (high frequency), MF (middle), and LF (low frequency) components.

Care was taken to avoid the influence of water vapor, quoted by Hockey[6] as a probable origin of artifacts in the OH band. This was done by a careful tuning of the double-beam balance of the spectrometer and by

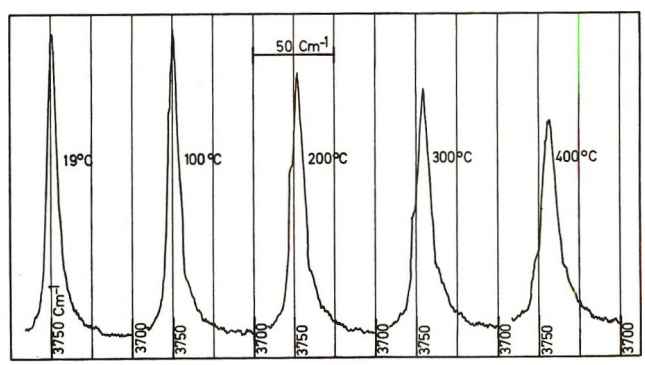

Figure 1. Photographs of the spectra of the A-type hydroxyls at different temperatures.

(7) J. A. Hockey and B. A. Pethica, *Trans. Faraday Soc.*, **57**, 2247 (1961).

(8) K. S. Seshadri and R. N. Jones, *Spectrochim. Acta*, **19**, 1013 (1963).

(9) D. A. Ramsay, *J. Amer. Chem. Soc.*, **74**, 72 (1952).

(10) J. Pitha and R. N. Jones, *Can. J. Chem.*, **44**, 3031 (1966).

(11) S. Abramowitz and R. P. Bauman, *J. Chem. Phys.*, **39**, 2757 (1963).

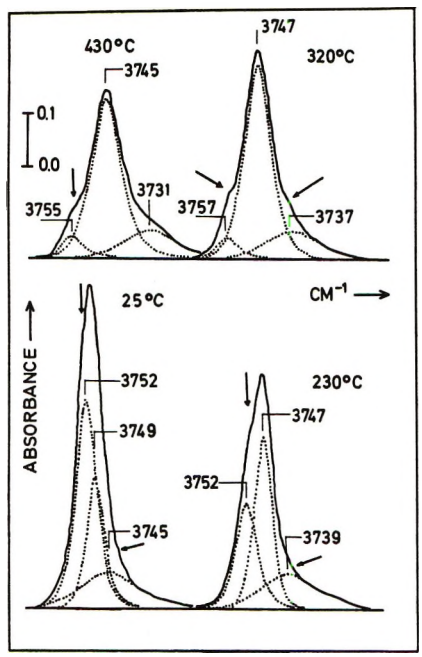

Figure 2. Resolved spectra of the A-type hydroxyls reproduced by the curve resolver. Solid lines are the experimental spectra obtained at 25, 230, 320, and 430°. The resolved components are the dashed lines.

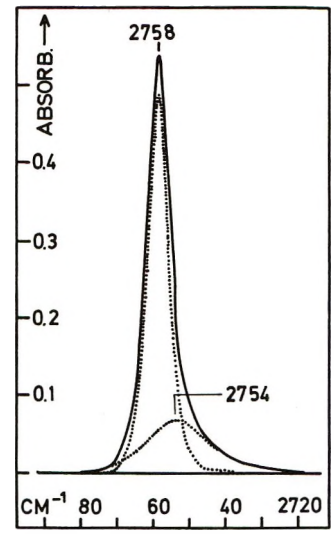

Figure 3. OD band (upper curve) resolved into two components (lower curves).

flushing the spectrometer with dry air. A perfectly straight base line was obtained when the silica film was removed from the optical beam, and absorption peaks due to gaseous water molecules could not be detected. Furthermore, it will be shown that the components quoted above shift to lower and higher frequencies as a function of the sample temperature. This would not be the case if they were due to water vapor outside the sample cell.

In Table I are collected the frequencies of the different components and the total band area as a function of the sample temperature. The band area decreases by 7.5% when the sample is heated from room temperature to 450°. This decrease is probably due to the increased thermal motion of the lattice constituents. It does not affect our observations and will not be discussed here. In agreement with Hair and Hertl,[4] we found that emission had no effect on the peak area at this temperature. It appears in Table I that the HF component has a tendency to shift upward, whereas the MF and LF components shift to lower frequencies with increasing temperatures. This is the origin of the shoulders appearing at higher temperatures.

For a fully deuterated sample, the symmetry of the OD band is higher than the symmetry of the corresponding OH band. An example of this is given in Figure 3. Decomposition of the OD band results in only two components. The isotopic ratio ν_{OH}/ν_{OD} of the LF OH band and the LF OD component is 1.356 and practically independent of the temperature. This, together with the similarity in band shape, indicates that these are corresponding bands. The HF and MF components lose their identity on deuteration and collapse into one OD band. For partially deuterated samples, the decomposition of the OH or OD band into three components was impossible: there are apparently more components in these mixed-sample spectra which are too close together to be resolved.

The changes in intensity and shape of the total OH band on adsorption of triethylamine and benzene were also followed. The integrated intensity of this band was first determined by comparing the weight loss of a sample heated at 750, 850, 900, 1000, and 1100° with the corresponding area of the OH band. The temperatures mentioned are pretreatment temperatures, but the spectra were taken at room temperature. The integrated extinction coefficient was 2.82 ± 0.07 cm μmol^{-1}. With this coefficient, adsorption isotherms were determined by measuring the decrease in band area upon adsorption of triethylamine and benzene. These isotherms are compared to the volumetrically obtained isotherms in Figure 4 for triethylamine and in Figure 5 for benzene. In order to obtain comparable units, the spectroscopic data are expressed as the num-

Table I: Frequencies (cm^{-1}), Integrated Band Areas, A (cm^{-1}), and Half-Band Widths, B (cm^{-1}), as a Function of Sample Temperature

Temp, °C	HF	MF	LF	A, cm^{-1}	B_{HF}	B_{MF}	B_{LF}
20	3753	3750	3746	6.02	8	6	21
150	3751	3747	3737	6.02	8	7	19
230	3752	3747	3739	5.97	8	7	21
320	3757	3747	3737	5.73	8	10	19
430	3755	3745	3731	5.57	8	10	20
a	3751	3747	3743		3	6	5

[a] Data estimated from Figure 7 of ref 4.

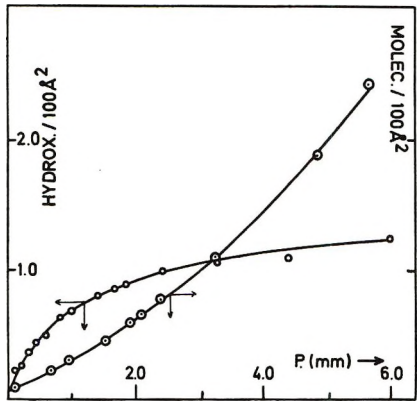

Figure 4. Comparison between spectroscopic and volumetric adsorption isotherms of $(C_2H_5)_3N$ at 137°.

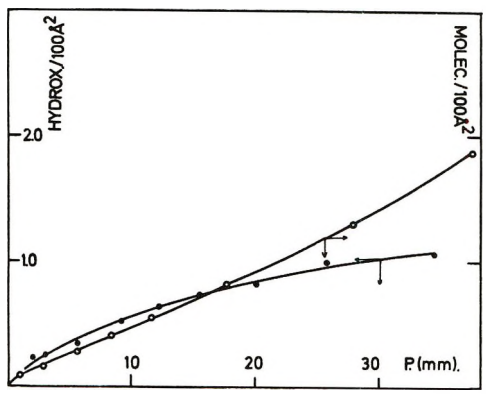

Figure 5. Comparison between spectroscopic and volumetric adsorption isotherms of benzene at 38°.

ber of disappearing hydroxyls per 100 Å², and the volumetric isotherms are calculated as the number of adsorbed molecules per 100 Å². For each molecule of benzene adsorbed, one hydroxyl group disappears. For triethylamine at low pressure, more than one hydroxyl is interacting with each adsorbed molecule, and the stoichiometry tends to 1:2 at low coverage.

The change in shape of the total OH band is not the same for adsorption of benzene and triethylamine. On adsorption of triethylamine, the overall frequency of the band decreases. At the same time, a shoulder appears on the high-frequency side of the OH band, suggesting that the high-frequency component decreases faster than the MF component at low pressures. The central frequency of the total band shifts to the frequency of the MF component. On adsorption of benzene, the overall frequency remains unchanged during the adsorption, indicating that the HF and MF components are affected in the same way.

Discussion

Correctness of the Decomposition Procedure. From these results we conclude that the 3750-cm^{-1} hydroxyl band in Aerosil or Cab-O-Sil can really be decomposed into three different components. This conclusion is in agreement with the findings of Hair and Hertl,[4] although we did not find the same pronounced details in the band that were shown by these authors. It is excluded that this decomposition is due to experimental artifacts, as claimed by Hockey.[6] The efficiency of the drying system of the spectrometer and the tuning of the double-beam balance were checked very carefully, and our spectra did not contain the details of the water vapor spectrum mentioned by Hockey.[6]

Further arguments in favor of this decomposition can be found in the systematic changes that can be produced in the spectrum by proper treatment of the sample. Upon heating, details are created in the band envelope. The data in Table I show that this is due to frequency shifts of the different components. If the components were due to water vapor outside the sample cell, these shifts would not occur.

Adsorption of triethylamine produced a shift to lower frequencies: this was due to the preferential suppression of the HF component. Adsorption of benzene resulted in a decrease of the OH band intensity, but the central frequency was unchanged since the HF and MF components decreased in identical proportions.

Deuteration changes the symmetry of the band. In partially deuterated samples, the OH and the OD band could not be decomposed. In the fully deuterated samples, only two components were needed to reconstruct the OD band. The LF component could be detected unchanged in the deuterated sample, while the HF and LF components seem to collapse into one band.

Possible Assignments for the Observed Band Components. Hair and Hertl[4] tentatively assigned the HF and LF components to geminal paired hydroxyls and the MF component to single hydroxyls. This speculation was based on the fact that the HF and LF components together accounted for 40% of the total band area, whereas the MF component accounted for 60%. These figures are considered to be the proportions of single and geminal hydroxyls by several authors.[4,5,12,13] However, we do not find support for this hypothesis in our data.

From the different behavior of the LF component on one hand and the HF and MF bands on the other, upon heating and adsorption, we conclude that the HF and MF components are due to the same or very similar hydroxyls, whereas the LF band possibly corresponds to a different species. Our observations allow the following tentative explanations, but unambiguous spectroscopic arguments are not available to make a very firm assignment.

The LF band is very insensitive toward adsorption of molecules. By deuteration it can be transformed into an OD band at corresponding frequencies and similar in shape to the OH band. Therefore, we assign it to

(12) W. Hertl and M. L. Hair, *J. Phys. Chem.*, 72, 4676 (1968).
(13) J. B. Peri and A. L. Hensley, *ibid.*, 72, 2926 (1968).

isolated hydroxyls slightly perturbed by neighboring lattice oxygens. Such a perturbation explains why it is at the lowest frequency and accounts also for the broadening of the component. Such perturbation is further in agreement with the idea of a location on sites not easily accessible to adsorbing molecules.

We believe that the HF and MF components are both due to isolated and freely vibrating hydroxyls. The splitting into two components can be due to coupling mechanisms. Hair and Hertl[4] already considered the HF and LF components to be vibrations slightly coupled through a silicon atom. However, this seems to be unlikely, since the shape of these components is completely different (see the half-band width in Table I). Instead, the HF and MF components have the same shape and may be ascribed to coupling phenomena.

Different kinds of coupling can be considered. It is conceivable that combinations with low-frequency lattice vibrations of the silica framework produce difference, summation, or combination bands near a strong fundamental vibration. We have no arguments supporting such combination.

Coupling can also exist between the vibrations of identical isolated OH groups. The coupling occurs between the electric fields associated with the vibrating protons. Farmer and Russell[14,15] applied this concept to the hydroxyl spectra in kaolinite. They could explain, at least qualitatively, the multiplicity of the bands by assuming a coupling between the vibration of three nearly equivalent hydroxyl groups. The present knowledge of the surface structure of silica does not allow a more detailed discussion of this point. Nevertheless, the behavior of the deuterated samples supports the possibility of such a coupling mechanism: owing to the different mass of the deuterium, the resulting components would be closer together than in the OH band and indistinguishable. Therefore, in the OD band, the HF and MF components merge into one peak. In the partially deuterated samples, an intermediate situation probably occurs which makes resolution impossible. Since the difference in frequency between HF and MF components is small, this hypothesis further implies that the distance between the hydroxyls is larger than it would be between geminal hydroxyls. This is in agreement with the results of recent nmr measurements on porous silica made by Freude, *et al.*[16] Unfortunately, accurate calculations cannot be made.

The apparent stoichiometry of 2:1 in the chemical and physical adsorption reactions of some organic molecules on hydroxyls is one of the arguments on which the existence of geminal paired hydroxyls was based.[5] In this work, we investigated the adsorption of triethylamine and benzene. Triethylamine reacts with an apparent stoichiometry of 2:1, and the frequency of the total band decreases during the adsorption. Benzene gives a ratio of 1:1, and the frequency of the total band remains constant. It is difficult to explain these differences only on the basis of the location of the hydroxyls: from the viewpoint of packing, the two molecules must have equal probabilities of interacting simultaneously with two hydroxyls. Probably the difference in behavior is mainly related to the strength of the interaction with the hydroxyls. This strength is reflected in the shift of the total OH band upon adsorption. Benzene adsorption shifts the OH band by 120 cm^{-1}, while triethylamine causes a shift of 930 cm^{-1} toward lower wavenumbers.

The interaction of benzene with the surface hydroxyls can be ascribed to the π electrons.[17] Geometrically the hydroxyls, in close interaction with benzene, will be in the center of the ring. If the distance between OH groups is large enough, there will only be one OH group covered, and the action of benzene is too weak to influence neighboring hydroxyls.

Triethylamine exerts a very intense force field, and the packing of the molecule is 40 $Å^2$.[18] Even if the hydroxyls are about 4 Å apart, more than one hydroxyl can be influenced by the same adsorbed molecule. Such a long-range influence of the triethylamine molecules can explain that the apparent stoichiometry of the adsorption reaction is higher than 1:1, but it cannot explain the frequency shift on adsorption.

The correlation between strength of interaction, as evidenced in the shift of the perturbed OH group, and the apparent stoichiometry can be extended to other adsorbates, such as CH_3Br and CH_3OH. Methyl bromide, causing a shift of 120 cm^{-1}, perturbs the hydroxyls following a 1:1 mechanism.[19] Methyl alcohol is more strongly adsorbed and causes a shift of about 400 cm^{-1}. According to Zecchina and coworkers,[20] it interacts on a 2:1 basis if the silica gel is pretreated up to 650°. On samples pretreated at higher temperatures, the stoichiometry changes to 1:1. This behavior of methyl alcohol emphasizes the importance of the distance between hydroxyls. Nevertheless, the correlation between the energy of interaction, as reflected in the infrared shift, with the apparent stoichiometry of unlocalized physical adsorption reactions of molecules with comparable packing indicates that a stoichiometry higher than 1:1 does not necessarily imply the existence of "geminal" paired hydroxyls.

(14) V. C. Farmer and J. D. Russell, *Spectrochim. Acta*, **20**, 1149 (1964).

(15) V. C. Farmer and J. D. Russell, *Clays Clay Min.*, **15**, 121 (1967).

(16) D. Freude, D. Müller, and H. Schmiedel, *Surface Sci.*, **25**, 289 (1971).

(17) G. A. Galkin, A. V. Kiselev, and V. I. Lygin, *Trans. Faraday Soc.*, **60**, 431 (1964).

(18) F. H. Van Cauwelaert, F. Vermoortele, and J. B. Uytterhoeven, *Discuss. Faraday Soc.*, in press.

(19) F. H. Van Cauwelaert, J. B. Van Assche, and J. B. Uytterhoeven, *J. Phys. Chem.*, **74**, 4329 (1970).

(20) E. Borello, A. Zecchina, C. Morterra, and G. Ghiotti, *ibid.*, **71**, 2945 (1967).

Acknowledgment. This work was completed with the financial help of the Katholieke Universiteit Leuven and N.F.W.O (Belgium). P. Jacobs acknowledges a grant as aspirant from N.F.W.O.

Equilibrium Studies by Electron Spin Resonance. I. The "Free" Nitrobenzene Anion Radical

by Gerald R. Stevenson,* Luis Echegoyen,

Chemistry Department, University of Puerto Rico, Rio Piedras, Puerto Rico

and Luis R. Lizardi

Department of Research and Development, Economic Development Administration, San Juan, Puerto Rico *(Received December 6, 1971)*

Publication costs assisted by the University of Puerto Rico

The anion radical of nitrobenzene ($PhNO_2$) has been observed for the first time in its most unperturbed state, *i.e.*, essentially free of solvent and counterion interactions. Utilizing the isotropic nitrogen hyperfine coupling constant, a formulation has been developed relating the solvent and counterion contributions to the nitrogen splitting for any $PhNO_2$–solvent–counterion system. The equilibrium constants for the free ion–ion pair equilibria have been determined for the $PhNO_2$–HMPA–M^+ systems. For the liquid ammonia–alkali metal (LAAM) reductions of nitrobenzene, pronounced line-width alternation phenomena have been observed. This effect has been attributed to a rapid free ion–ion pair equilibrium.

A large volume of work has been compiled which demonstrates that the nitrogen hyperfine coupling constants of nitroaromatic anion radicals vary significantly with environmental perturbations, *i.e.*, solvent and counterion interactions.[1] Solution esr spectra of nitrobenzene anion radicals have been described in terms of strong specific solvation by solvent and ion-pair complexes.[2-4]

Recently, Gross, *et al.*,[5,6] have prepared alkali metal nitrobenzenides and have recorded their esr spectra in a variety of protic and aprotic solvents. Line-width alternation was observed in acetone, acetonitrile, and dimethylformamide as a consequence of a rapid equilibrium between ion pairs and free ions. These authors correlate the nitrogen splitting constant with the size of the associated cation by plotting the nitrogen coupling constant *vs.* $(R + 0.6)$, where R is the Pauling cationic radius. By extrapolating this plot to infinite cation radius, one obtains the nitrogen splitting for the "free" anion radical.

Electrolytic reductions of *p*-dinitrobenzene anion radical show a marked nitrogen splitting dependence on concentration of supporting electrolyte in ethanol.[7] Thus, it is no longer possible to assume unperturbed conditions for anion radicals, particularly those containing polar groups, in electrolytic reductions.

The magnitude of the isotropic nitrogen coupling constant, A_n, of nitroaromatic anion radicals increases with external forces such as the solvent[8] and counterion[9] interactions. Gulick and Geske[8] observed that the radical–solvent complexes and presumably ion–ion pair formation which causes a redistribution of the unpaired spin density increases the π-spin density on the nitrogen and oxygen centers as was evident from the ^{17}O-enriched nitrobenzene anion radical. Specifically, hydrogen bonding interactions have been shown to increase the nitrogen splitting in nitrobenzene anion radical[10] to a greater degree than dipolar interactions.

(1) M. T. Jones in "Radical Ions," E. T. Kaiser and L. Kevan, Ed., Interscience Publishers, New York, N. Y., 1968, Chapter 6.

(2) J. M. Gross and M. C. R. Symons, *Trans. Faraday Soc.*, **63**, 2117 (1967).

(3) R. L. Ward, *J. Amer. Chem. Soc.*, **83**, 1272 (1961).

(4) T. Kitagawa, T. Layloff, and R. N. Adams, *Anal. Chem.*, **36**, 925 (1964).

(5) J. M. Gross, J. D. Barnes, and G. N. Pillans, *J. Chem. Soc. A*, 109 (1969).

(6) J. M. Gross and J. D. Barnes, *J. Phys. Chem.*, **74**, 2936 (1970).

(7) J. Oakes and M. C. R. Symons, *Chem. Commun.*, 294 (1968).

(8) W. M. Gulick, Jr., and D. H. Geske, *J. Amer. Chem. Soc.*, **87**, 4049 (1965).

(9) C. Y. Ling and J. Gendell, *J. Chem. Phys.*, **47**, 3475 (1967).

(10) P. Ludwig, T. Layloff, and R. N. Adams, *J. Amer. Chem. Soc.*, **86**, 4568 (1964).

Hexamethylphosphoramide (HMPA) has been found to be an excellent solvent for radical anion formation with alkali metals. A recent review by Normant[11] on the chemistry of HMPA reveals that anions are practically unsolvated due to steric hindrance around the phosphorus center, while the sterically accessibly oxygen atom results in strong cation solvation. Szwarc, *et al.*, have generated the anion radicals of nitrogen heterocyclic aromatic compounds,[12] anthracene,[13] and dianion of tetraphenylethylene[14] and describe HMPA as a powerful solvating agent for alkali metal ions[15] where many alkali salts of carbanions and radical anions are fully dissociated in this medium.

In this report, we wish to communicate the first observation of the nitrobenzene anion radical free of ion pairing and essentially free of solvent interactions. We propose a formulation using the coupling constant for the free ion as a standard from which solvent and counterion contributions to A_n may be calculated. Further, an equilibrium between this free ion and its ion pair in (HMPA) is reported.

Experimental Section

Nitrobenzene (Eastman Organic Chemicals) was vacuum distilled prior to use. Hexamethylphosphoramide was vacuum distilled from calcium hydride and stored over Molecular Sieves 4A. Tetra-*n*-butylammonium perchlorate (G. Friederick Smith Chemical Co., polarographic grade) was used without further purification.

The esr spectra were recorded on the X-band of a Varian E-3 esr spectrometer. The metal reductions in liquid ammonia were carried out as previously described.[16] HMPA was distilled from the solvated electron under high vacuum (10^{-4} mm pressure) directly into the reaction vessel. Tetra-*n*-butylammonium perchlorate was used as a counterion for all electrolytic reductions.

Results

1. $PhNO_2$–HMPA–Li. When $PhNO_2$ is reduced with lithium metal, a well resolved esr spectrum is obtained (Figure 1). The spectrum is free from metal splitting, but there are more than the theoretical 54 hyperfine lines. Upon close analysis, it is clear that the resultant esr spectrum is due to two different $PhNO_2$ anion radicals in solution, α and β, both having nearly identical g values but β having a larger nitrogen coupling constant. The outermost triplet is due to β only. The fourth line in the spectrum is the first line of α. The esr spectrum of α is more intense than that of β. The coupling constants of α and β are given in Tables I and II, the nitrogen coupling constants being 8.48 and 10.85 G for α and β, respectively.

2. $PhNO_2$–HMPA–Na. This system yields a well resolved esr signal, again due to two different radicals, α and β. The esr spectrum of β exhibits hyperfine splitting from the sodium nucleus and is the minority radical. The nitrogen coupling constants for α and β are 8.48 and 10.9 G, respectively. The entire set of coupling constants are shown in Tables I and II.

Table I: Coupling Constants for the α Species Resulting from $PhNO_2$ Reduced in HMPA[a]

Metal	A_n	A_{para}	A_{ortho}	A_{meta}
K	8.49	4.21	3.33	1.00
Na	8.48	4.20	3.33	1.01
Li	8.48	4.22	3.34	1.01

[a] All values are reported to ±0.02 G.

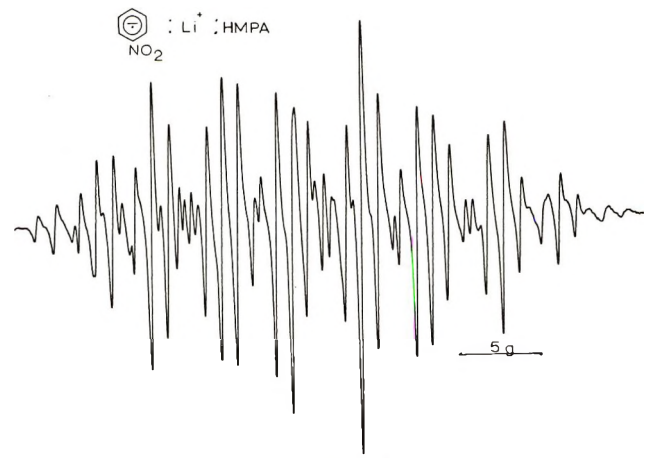

Figure 1. Esr spectrum of $PhNO_2$ reduced by Li in HMPA at room temperature. The two radicals are shown superimposed. The line width is 0.20 G.

3. $PhNO_2$–HMPA–K. The esr signal for this system is not as well resolved as for the other two systems, but the results are similar. The two radicals are recorded simultaneously as before, but the relative concentrations of the two radicals are reversed (Figure 2). The major radical now has the largest nitrogen splitting and contains metal splitting. The nitrogen coupling constant for the major radical β is 9.80 G, while that for the minor radical α is 8.49 G (Tables I and II).

4. $PhNO_2$–HMPA–Electrolytic Reduction. When a 10^{-3} M solution of $PhNO_2$–HMPA is reduced electrolytically only a single anion radical is observed. The nitrogen coupling constant varies with the concentration of the counterion. Figure 3 shows a plot of counterion concentration *vs.* the nitrogen coupling con-

(11) H. Normant, *Angew. Chem. Int. Ed. Engl.*, 6(12), 1046 (1967).

(12) J. Chaudhuri, S. Kume, J. Jagur-Grodzinski, and M. Szwarc, *J. Amer. Chem. Soc.*, 90, 6421 (1968).

(13) A. Cserhegyi, J. Chaudhuri, E. Franta, J. Jagur-Grodzinski, and M. Szwarc, *ibid.*, 89, 7129 (1967).

(14) A. Cserhegyi, J. Jagur-Grodzinski, and M. Szwarc, *ibid.*, 91, 1892 (1969).

(15) G. Levin, J. Jagur-Grodzinski, and M. Szwarc, *ibid.*, 92, 2268 (1970).

(16) F. J. Smetowski and G. R. Stevenson, *ibid.*, 90, 4661 (1968).

Table II: Coupling Constants for the β Species Resulting from $PhNO_2$ Reduced in HMPA

Metal	A_n	A_{para}	A_{ortho}	A_{meta}	A_{M^+}
K	9.80 ± 0.06	4.10 ± 0.05	3.40 ± 0.05	1.09 ± 0.02	0.25
Na	10.9 ± 0.1	4.10 ± 0.05	3.40 ± 0.05	1.00 ± 0.05	0.44
Li	10.85 ± 0.05	4.10 ± 0.05	3.40 ± 0.05	1.09 ± 0.02	<0.20

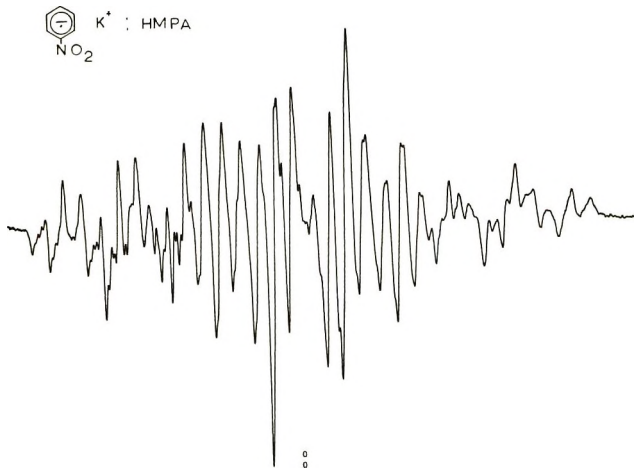

Figure 2. Esr spectrum of $PhNO_2$ reduced by K in HMPA at room temperature. The two radicals are shown superimposed. The line width is 0.20 G.

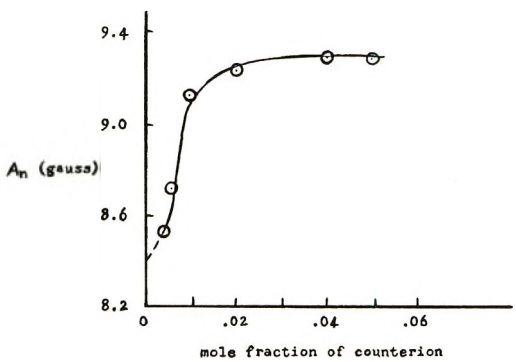

Figure 3. Variation of nitrogen-14 coupling constant with mole fraction of $(n\text{-Bu})_4NClO_4$ in HMPA for nitrobenzene radical anion at room temperature.

stant. At a 0.1 M concentration of counterion, A_n is 9.10 G. When the counterion concentration falls below 0.02 mole fraction, A_n begins to fall off rapidly. Extrapolating to zero counterion concentration, a value of about 8.4 G for the $PhNO_2$ anion radical free from counterion interaction is obtained.

5. Alkali Metal and Electrolytic Reductions of $PhNO_2$ in Liquid Ammonia. Table III shows the hyperfine coupling constants observed by Smentowski and Stevenson[16] for the liquid ammonia–alkali metal (LAAM) reduction of $PhNO_2$ at −50°. These results are in agreement with ours, except that we observe a pronounced line-width alternation effect for all three metals: Li, Na, and K. Electrolytic reduction of

Table III: Coupling Constants for the NB Anion Radical in Liquid NH_3 at −50°

Metal	A_n	A_{ortho}	A_{para}	A_{meta}	Line-width alternation
Li	10.40	3.25	3.83	1.03	Observed
Na	10.63	3.24	3.82	1.03	Observed
K	10.62	3.23	3.84	1.03	Observed
Electrolytic	10.06	3.22	3.73	1.02	None

$PhNO_2$ in liquid ammonia does not result in any line-width alternation (Table III).

Since the electrolytic reductions do not show evidence of line-width alternation, the line-width alternation in the LAAM reductions must be attributed to a rapid equilibrium process between different anion radical–cation complexes and the free ion. Unlike the HMPA reductions, only the average spectrum is observed.

Discussion

The nitrogen coupling constant of 8.48 G seen for the alkali metal reductions of $PhNO_2$ in HMPA is the lowest value reported for the $PhNO_2$ anion radidal. Such a value indicates that the anion radical in HMPA is free from any ion pairing with the counterion and that this value represents only small solvent interactions. This is substantiated by the fact that the extrapolation of the plot of counterion concentration *vs.* A_n for the HMPA electrolytic reductions to zero counterion concentration leads to a value of 8.4 G for A_n, which is approximately equal to the splitting that we observe for the alkali metal reductions in HMPA.

For the two systems $PhNO_2$–HMPA–K and $PhNO_2$–HMPA–Na, the β species (radical of larger A_n) contains metal splitting. This is proof that it is an ion pair. For the $PhNO_2$–HMPA–Li system, there is no metal splitting for either of the radicals, but the β species is the ion pair, as is evident from the larger magnitude of the nitrogen splitting. It is concluded that the following equilibrium between the free ion and the ion pair is responsible for the radicals, where the rates of the two reactions involved are slow on the esr time scale.

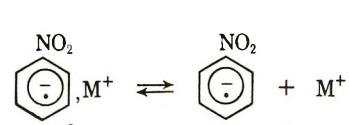

(1)

The equilibrium constant can be estimated from the relative intensities of the esr lines of the two radicals. For the Li, Na, and K reductions in HMPA, the equilibrium constants are 2.2, 1.6, and 0.6, respectively. From the equilibrium constant for the potassium reduction, the β species is the major radical and not the free ion as in the case of Li and Na. The potassium system also has the lowest A_n for the β species, 9.80 G, being approximately 1 G lower than for the other two systems.

The literature contains several examples of esr spectra resulting from two different ion pairs in solution. Chang and Johnson[17] observed two different ion pairs of the naphthalene anion radical in the fast exchange region. Two different ion pairs of the cyclooctatetraene anion radical have been observed in liquid NH_3[18] and in dimethoxyethane.[19] Further, Stevenson and Colon[20] have observed two different ion pairs of the *N*-nitrosodiethylamine anion radical in the slow exchange region.

For the $PhNO_2$–NH_3–alkali metal systems, there are also two different ion pairs in solution as evidenced by the line-width alternation effect. In this case, however, the rate processes involved in the equilibrium are rapid on the esr time scale and only the average of the two radicals is observed.

The magnitude of the nitrogen coupling constant for anion radicals derived from nitroaromatic compounds is a sensitive function of solvent, counterion, and steric[21] factors, and since in the HMPA–alkali metal reductions nitrobenzene anion radical exhibits its lowest nitrogen splitting of 8.48 G for the free ion, we can utilize this value for the free ion as a constant from which environmental effects can be measured. Equation 2 relates the nitrogen coupling constant for any $PhNO_2$–solvent–counterion interactions to this constant.

$$A_n = 8.4 + P_bA_n(\text{solvent}) + P_cA_n(M^+) \qquad (2)$$

A_n(solvent) and $A_n(M^+)$ are the maximum contributions to A_n due to the solvent and cation interactions, respectively. P_b and P_c are the fractions of these interactions found in a particular system.

Considering the ion pairs of the $PhNO_2$–HMPA–M^+ systems in terms of this equation, the solvent perturbation is neglibile; therefore, P_bA_n(solvent) = 0. Then $P_bA_n(M^+) = A_n - 8.4$. This leads to the following values for the $P_bA_n(M^+)$ term for the ion pairs of K, Na, and Li: 1.40, 2.50, and 2.40, respectively.

Gross and coworkers have reported the esr spectra for the Li, Na, and K-nitrobenzenides in water. They find no dependence of the nitrogen coupling constants upon the counterion in this polar and highly solvating solvent.

From these observations, $P_cA_n(M^+)$ is very small and can be ignored. Therefore, P_bA_n(solvent) = 14.12 − 8.4, since the nitrogen coupling constants of $PhNO_2$ in water is 14.12 G. From this, we conclude that the hydrogen bonding contribution of water to the magnitude of the nitrogen splitting is approximately 5.72 G.

In the $PhNO_2$–NH_3–M^+ systems, the nitrogen splittings are essentially invariant with the nature of the cation. However, the line-width alternation is quite prominent in these systems. Although, P_bA_n(solvent) $\gg P_cA_n(M^+)$, it is impossible to differentiate the quantitative contributions of the solvent and cation with the available data.

Presently, we are measuring thermodynamic parameters controlling the free ion–ion pair equilibria for the $PhNO_2$–HMPA and $PhNO_2$–NH_3 systems. Internal steric contributions to the total nitrogen splitting in HMPA will be included in future publications.

Acknowledgments. This research was supported in part by the University of Puerto Rico Research Fund and Research Corporation. The authors are indebted to Mrs. Luis R. Lizardi for her help in preparing this manuscript.

(17) R. Chang and C. S. Johnson, Jr., *J. Amer. Chem. Soc.*, **88**, 2338 (1966).

(18) F. J. Smentowski and G. R. Stevenson, *J. Phys. Chem.*, **73**, 340 (1969).

(19) H. L. Strauss, T. J. Katz, and G. K. Frankel, *J. Amer. Chem. Soc.*, **85**, 2360 (1963).

(20) G. R. Stevenson and C. J. Colón, *J. Phys. Chem.*, **75**, 2704 (1971).

(21) The steric contribution to the total nitrogen splitting, P_dA_n(steric), refers to the internal steric interactions of substituted nitrobenzenes. The increase in A_n due to the decoupling of the nitro group from the ring system can quantitatively be obtained from HMPA–metal systems. F. J. Smentowski and L. R. Lizardi, 158th National Meeting of the American Chemical Society, New York, N. Y., Sept 1969.

Studies of Adsorbed Species. II. An Electron Spin Resonance Study of Thianthrene and Other Sulfur Heterocyclics Adsorbed on Oxide Surfaces

by L. Petrakis* and K. S. Seshadri

Gulf Research and Development Company, Pittsburgh, Pennsylvania 15230 *(Received November 29, 1971)*

Publication costs assisted by the Gulf Research and Development Company

The radical ion of thianthrene has been generated and studied on a variety of oxide surfaces including silica–alumina and molybdena–alumina. No radical ion is formed on MgO or unmodified alumina. The spectral features of the thianthrene radical on the surfaces are identical with the spectral features of the thianthrene monopositive radical ion in frozen sulfuric and boric acids. The three components of the observed spectrum are shown to arise from g anisotropy. In the molybdena–alumina, in addition to the radical-cation signal, a resonance assigned to Mo^{5+} was observed. These two resonances have identical functional dependence on the level of molybdenum incorporated into the lattice. The role of Mo^{5+} in the electron-transfer process is considered. In addition to thianthrene, certain other sulfur heterocyclics have been studied and are discussed briefly.

Introduction

The nature of acidic sites on catalytic surfaces such as silica–alumina, alumina, and others has been the subject of many investigations. The electron spin resonance spectra of polynuclear aromatic radical ions adsorbed on these surfaces have provided tools to probe into the details of the catalytic surface.[1-3] Our previous report[4] has shown that nitrogen heterocyclics could also be profitably used. We have extended our study to certain sulfur heterocyclics which are reported here. Incorporation of transition metals in such catalytic oxides as Al_2O_3, silica, etc., can have important effects on their properties. Typical are results obtained by Richardson,[5] who generated several polyacene cations in copper-modified faujasites and has concluded that the cations are formed by electron transfer that occurs at the cation. Since many of the transition metals that are used to modify these materials are paramagnetic, esr provides a unique tool to monitor the behavior of the metal impurity and of the paramagnetic radical ions that may result from the electron-transfer reactions between adsorbate and adsorbent. In this paper, we will examine the spectroscopic aspects of the cations of the sulfur heterocyclics, and in a subsequent paper we will examine the mechanistic aspect of the adsorbate–adsorbent interaction.

Experimental Section

Electron Spin Resonance Measurements. The first-derivative spin resonance spectra were obtained with a Varian esr spectrometer operating at 9.5 GHz with 100-kHz field modulation. A solution of diphenyl picryl hydrazyl in benzene and a mechanical mixture of $MoCl_5$ in Al_2O_3 were used as standards in measuring the relative concentration of the radical ions and Mo(V), respectively. The area under the absorption spectra in all cases has been taken to be proportional to the product of the height by the square of the peak-to-peak width. The spectra of thianthrene adsorbed on SiO_2–Al_2O_3 were also obtained at -130 and at 300°. The low-temperature spectrum was obtained using the Varian variable-temperature accessory (V-4557), and the high-temperature spectrum was obtained using the high-temperature cavity constructed by Giardino and Petrakis.[6]

Materials. Aerocat AAA silica–alumina containing 25% by weight Al_2O_3 and heavy metal impurities ranging from 0.1 to 0.01%, purified by overnight heating at 500° in a current of air, was used. Davison η-Al_2O_3 without any further pretreatment was purified by a similar procedure. Modified aluminas were prepared by impregnating η-Al_2O_3 with ammonium paramolybdate, followed by drying for 2 hr at 100° with subsequent calcination at 500° overnight in a current of air. Commercial MgO was washed with boiling water, followed by drying at 100° and calcination at 500° in a current of air overnight. The catalytic samples were used in 20–40 mesh pellet form. Thiophene supplied by Eastman Kodak was purified by distillation and stored in a brown bottle. Dibenzothiophene supplied by Aldrich was purified by crystallization from hot ethanol. Thianthrene supplied by Aldrich was boiled in acetone over charcoal and further purified by crystallization from hot acetone. Purified solid com-

(1) J. J. Rooney and R. C. Pink, *Trans. Faraday Soc.*, **58**, 1032 (1962).

(2) R. P. Porter and W. K. Hall, *J. Catal.*, **5**, 366 (1966).

(3) H. M. Muha, *J. Phys. Chem.*, **71**, 640 (1967).

(4) K. S. Seshadri and L. Petrakis, *ibid.*, **74**, 1317 (1970).

(5) J. T. Richardson, *J. Catal.*, **9**, 172 (1967).

(6) D. A. Giardino and L. Petrakis, *J. Sci. Instrum.*, **38**, 1180 (1967).

pounds were checked for decomposition or other impurities by differential scanning calorimetry. The solvents used were purified by distillation.

Each catalyst was activated at 500° for 4 hr. The sulfur-containing heterocyclic compound, in benzene (10^{-2} M), was then brought into contact in the presence of air with the catalyst as it was cooling below 200°. The sample was shaken for 0.5–1 min, and the excess solvent was removed by pumping for 0.5 hr at room temperature. The catalyst was then transferred to an esr side tube (Pyrex, 4 mm o.d., 2 mm i.d.) and was sealed. The activation was done in air, in a current of air, in a current of oxygen, in flowing hydrogen, or *in vacuo*. Benzene, carbon tetrachloride, carbon disulfide, and cyclohexane were used as solvents.

We have adsorbed thiophene, benzothiophene, dibenzothiophene, and thianthrene from solution onto several oxide surfaces including MgO, Al_2O_3, silica–alumina, and molybdena–alumina. These sulfur-containing heterocyclic compounds were brought into contact with the surfaces from many solvents and under a variety of conditions. In addition, mechanical mixtures of host and adsorbate in the case of thianthrene were prepared and heated to mild temperatures (100–150°) and their spectra recorded. Finally, the spectra of sulfuric acid solutions of thianthrene were recorded, both in the liquid and frozen state, and also the spectrum of a solid solution of thianthrene in boric acid was recorded. The solid solution was prepared by dissolving thianthrene in partially dehydrated boric acid at 240°, and the solution formed was cooled to room temperature and the spectrum recorded. No attempts were made to determine the exact nature of the solid solution; in all probability it is supercooled glass.

Results

Thiophene, when adsorbed from a benzene solution on η-alumina, on silica–alumina, or on alumina containing 9% Mo, gave no resonance signal at all. Similarly, when dibenzothiophene was adsorbed on η-alumina, silica–alumina, and alumina containing from 2 to 9% Mo, a resonance signal was obtained only on silica–alumina. The observed signal had a g value of 2.0087 and a peak-to-peak line width of 11.00 G.

By far the most interesting results were obtained with thianthrene (I) and, therefore, this paper will concen-

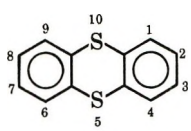

I

trate on discussing the behavior of thianthrene on the various surfaces employed. Thianthrene adsorbed from benzene solution on η-alumina or on MgO gives no resonance signal. However, when thianthrene is adsorbed from a benzene solution on silica–alumina, a

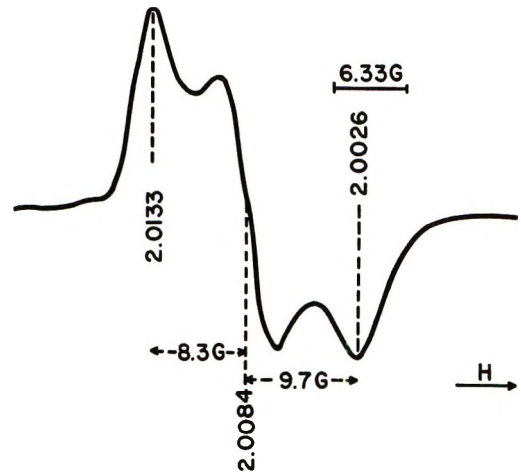

Figure 1. Esr spectrum of thianthrene radical cations on SiO_2–Al_2O_3.

pink color develops immediately and the sample exhibits a strong spin resonance signal centered at g = 2.0084 (Figure 1). The three-component spectrum is unsymmetrical, with the high-field component being both broader and further removed from the center than the low-field component. There is no evidence of any further structure superimposed on the three components. The half width of each component is about 5.0 G. Exactly the same spectrum is obtained when a mechanical mixture of thianthrene in silica–alumina is heated to 150°. The power dependence of the intensity of the observed signal is given in Figure 2. It is seen that as the microwave power is increased the amplitude of each line continues to increase. At the higher rf power levels, the amplitude of the three components remains constant despite increasing power, but at no rf power level accessible to us in our instrument did the amplitude actually decrease. The spectrum of thianthrene adsorbed on silica–alumina has also been studied as a function of temperature. Figure 3 shows the spectrum taken at two temperatures. It is seen that as the temperature is lowered the three components of the spectrum persist. At elevated temperatures, the three lines merge into one, with the distance between the slope extrema being 18.0 G, and a g value of 2.0086.

The radical ion of thianthrene in oxidizing solutions has been produced and studied in detail.[7–9] We have reproduced the sulfuric acid spectrum and in addition we have recorded it at low temperature in the frozen glassy state. Also, we have added thianthrene in molten boric acid at 240°, and we have observed that the molten sample turns pink and at room temperature yields a strong spin resonance signal. Both the frozen sulfuric acid spectrum at −73° and the room-temperature boric acid spectrum are shown in Figure 4. The

(7) H. J. Shine and L. Piette, *J. Amer. Chem. Soc.*, **84**, 4798 (1962).
(8) P. D. Sullivan, *ibid.*, **90**, 3618 (1968).
(9) H. J. Shine and P. D. Sullivan, *J. Phys. Chem.*, **72**, 1390 (1968).

Table I: Spectral Parameters of Thianthrene Radical Cation in Different Media

Medium	Distance of peaks,[a] G	g_a	g_b	g_c	g_{av}	$g_{isotropic}$
SiO_2–Al_2O_3 (room temp)	18.0	2.0133	2.0084	2.0026	2.0081	
(−80°)	17.0	2.0132	2.0088	2.0026	2.0082	
(175°)					2.0086	
H_2SO_4 solution (room temp)						2.0081[b]
H_2SO_4 (frozen)	18.0	2.0128	2.0073	2.0026	2.0076	
Boric acid	18.9	2.0140	2.0085	2.0028	2.0084	
MoO_3–Al_2O_3	16.5	2.0124	2.0077	2.0028	2.0076	

[a] Distance between high-field and low-field peaks. [b] B. Lamotte and G. Berthier, *J. Chim. Phys. Physicochim. Biol.*, **63**, 369 (1966).

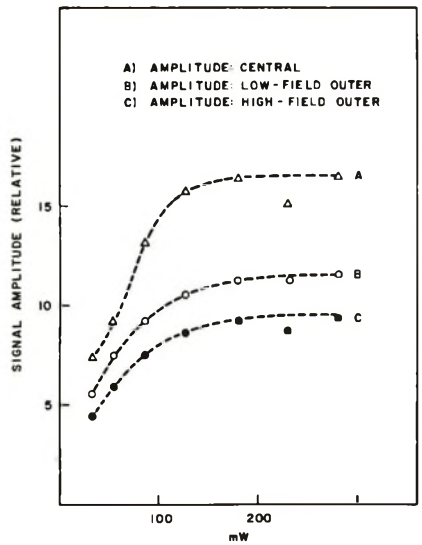

Figure 2. Variation of signal amplitude with microwave power: upper curve, central component; middle curve, low-field component; lower curve, high-field component.

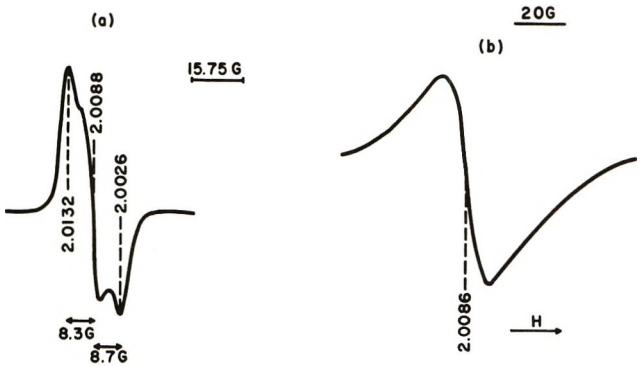

Figure 3. Temperature dependence of thianthrene radical cation on silica–alumina: (a) spectrum at −80°, (b) spectrum at 175°.

similarity of these spectra in their overall features and in their detailed spectral parameters to each other and to the spectrum from silica–alumina as well (Figure 1) is quite striking. The spectral parameters of the thianthrene radical ions in several media are summarized in Table I.

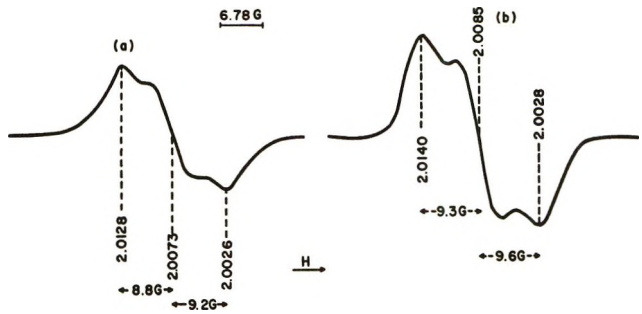

Figure 4. Thianthrene radical cation in (a) frozen sulfuric acid solution, (b) boric acid glass.

It is interesting to compare the signal intensity of thiophene, dibenzothiophene, benzothiophene, and thianthrene adsorbed on silica–alumina. No signal is observed from thiophene, while dibenzothiophene gives a signal about 2 times that of benzothiophene, and thianthrene about 15 times that of benzothiophene. The energy difference between the ground and excited states of a charge-transfer complex is given by[5,10]

$$E = I - A - W$$

where I is the ionization potential of the donor, A is the electron affinity of the acceptor, and W is the dissociation energy of the excited state. The number of cation radicals, N^+, formed from N molecules, is then

$$N^+ = N \exp(-(I - A - W)/kT)$$

The ionization potential is expected to decrease from thiophene to benzothiophene to dibenzothiophene to thianthrene (as in the case of benzene, naphthalene, and anthracene) and an exponential dependence of N^+ on the ionization potential is in agreement with the above equation. In a qualitative manner the observed intensities are as predicted. A similar variation has been observed by Richardson[5] in his study of polyacene cations on copper-doped faujasites.

The next series of experiments that we describe involves alumina modified with molybdena and treated

(10) H. McConnell, J. S. Ham, and J. R. Platt, *J. Chem. Phys.*, **21**, 66 (1953).

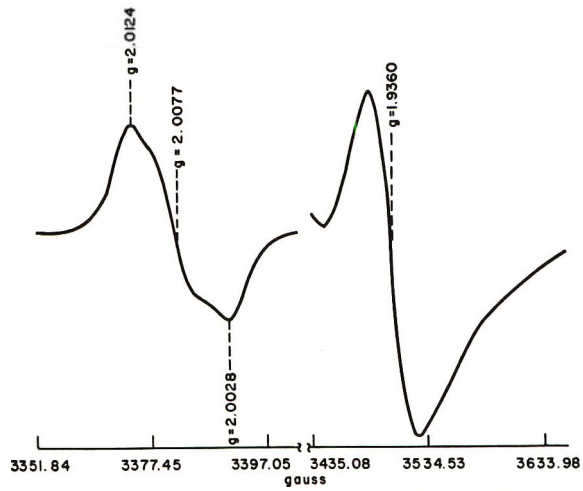

Figure 5. Thianthrene radical cation signal (g = 2.0077) and Mo^{5+} (g = 1.9360) on molybdena–modified alumina.

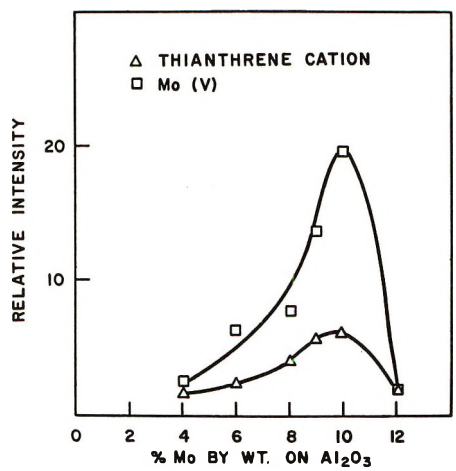

Figure 6. Relative esr intensity of thianthrene radical cation (lower curve); Mo^{5+} signal.

in the manner detailed in the Experimental Section. Mo-modified alumina with thianthrene adsorbed from a benzene, carbon tetrachloride, carbon disulfide, or cyclohexane solution readily develops a pink color and gives a spin resonance signal similar to that observed on silica–alumina (Figure 5). The g values and line widths of the three components and overall shape of the observed signal are similar to those of the spectrum observed on silica–alumina. In addition to the radical ion signal, there is a second unsymmetrical signal observed at g = 1.9360 with a peak-to-peak line width of 41.76 G. This signal is ascribed to pentavalent molybdenum.[11] The intensities of these two signals have been obtained, and the results are shown in Figure 6 for a series of samples which differ only in the amount of molybdenum incorporated into the sample.

It was observed that when MoO_3 is initially incorporated into the Al_2O_3 support and prior to any calcining there is no Mo^{5+} signal observed. However, there is an Mo^{5+} signal observed following activation of the oxides at 500° in air, O_2, or H_2 or *in vacuo*. Under all such conditions, there is Mo^{5+} production, the level of which varies with pretreatment, but it is further enhanced when thianthrene is introduced in various solvents. In addition, of course, there is radical-ion formation (Figure 5). It is of particular interest to observe that the Mo^{5+} signal intensity passes through a maximum at a concentration of about 9% Mo in Al_2O_3. This situation is quite in line with what has been observed in previous work.[11,12] But in addition to this interesting behavior of the Mo^{5+} species, it is observed that the thianthrene radical-ion signal has an identical dependence on the amount of Mo incorporated into the support, and specifically it attains its maximum at the same concentration as Mo^{5+}.

Experiments were also carried out with a sample 9% Mo by weight containing Al_2O_3 to obtain information as to the effect of activation conditions for the catalyst and the role, if any, of the solvent. The sample was heated to 500° in hydrogen, oxygen, and air and *in vacuo*, and then treated with thianthrene solution in benzene (10^{-2} M). In all cases, esr signals were observed both from the radical cation of thianthrene and from Mo^{5+}, and the relative intensities of both signals were affected by the pretreatment. In addition, a 9% Mo by weight Al_2O_3 sample was activated in a current of air and then brought into contact with thianthrene from benzene, carbon tetrachloride, carbon disulfide, and cyclohexane, all solutions being 10^{-2} M. Again, there were esr signals observed from both the Mo^{5+} and thianthrene radical ion, but unlike the case of the various activation conditions, the intensities of the two signals showed only little variation with solvent employed. The results of some of these experiments will be discussed in a subsequent paper.

Discussion

The monopositive radical ion of thianthrene in H_2SO_4 or in an aluminum chloride–nitromethane system has been studied, as we indicated, extensively.[7-9] The best resolved spectrum was obtained by Shine and Sullivan[9] in an $AlCl_3$–CH_3NO_2 solution. These authors were able to observe, in addition to the naturally abundant S-33 hyperfine splitting, splittings from all eight protons. They observed two sets of lines. One set of major splittings (a = 1.28 G) was assigned to the 2, 3, 7, and 8 protons, while the second set at minor splittings (a = 0.135 G) was attributed to the 1, 4, 6, and 9 protons. The isotropic spectrum showed altogether 25 lines centered about g = 2.0081 and spread over a total range of about 6 G. Concentrated sulfuric acid solution oxidizes thianthrene equally readily to produce the monopositive ion, but the resolution is not as good as in the $AlCl_3$–CH_3NO_2 solution, and only the major

(11) K. S. Seshadri and L. Petrakis, *J. Phys. Chem.*, **74**, 4102 (1970).
(12) V. A. Dzs'ko, E. M. Emel'yanova, Yu. I. Peherskaya, and V. B. Kazanski, *Dokl. Akad. Nauk SSSR*, **150**, 829 (1963).

proton splittings are observed. However, all of these studies have established that in the strongly oxidizing solutions of sulfuric acid or $AlCl_3$–CH_3NO_2, we are dealing with the radical cation of thianthrene. The striking similarity of the spectra of thianthrene on silica–alumina (Figure 1) to the spectra in frozen sulfuric acid and boric acid solutions (Figure 4) shows that the radical ion produced on the silica–alumina surface must be the monopositive species also. It has been shown that the highly acidic surface of silica–alumina can oxidize very effectively other polynuclear aromatics to produce the radical cations. In a more recent example, we showed that phenazine is oxidized to produce well-defined radical cations.[4] Similar results have been reported by other workers with a variety of systems.[13] An early example is the spectrum of perylene, which was shown by Hall[14] to arise both in solution and on silica–alumina surfaces from the monopositive species.

The behavior of thianthrene on MgO and Al_2O_3 surfaces is instructive. It is well known that these surfaces can readily take part in electron-transfer reactions. In an earlier study,[4] we reported that phenazine, when adsorbed on silica–alumina, forms radical cations, but on MgO forms radical anions. Flockhart and coworkers[15] have been able to produce radical cations of polynuclear aromatic hydrocarbons on alumina, provided that oxygen was present, and the reducing power of alumina surfaces has been demonstrated with the production of radical ions of such molecules as tetracyanoethylene and nitrobenzenes.[16] The behavior of thianthrene on unmodified alumina and on MgO surfaces is in sharp contrast to the behavior of aromatic hydrocarbons and of phenazine. When we attempted to produce radical ions of thianthrene on these surfaces, they developed neither any coloration nor any paramagnetic signal. Even exposure of the adsorbed thianthrene on MgO to intense light for 72 hr did not effect any electron transfer. It is conceivable that the difference in the behavior of thianthrene on one hand and hydrocarbons and phenazine on the other could be accounted for at least in part by the differences in experimental procedures. For example, Flockhart and coworkers[15] found that the pretreatment temperature played a critical role in the production of cations of aromatic hydrocarbons, the optimum oxidative ability of alumina being achieved upon calcination at 900°. The alumina we used was treated at 500° only. Other experimental differences that could contribute to this behavior are the oxygen pressure and the temperature at which the absorption was effected. However, there are probably additional and more fundamental aspects of the difference in behavior between thianthrene and the other systems. For one, it is indicated that, considering the behavior of thianthrene and phenazine on MgO, thianthrene does not have as high an electron affinity as the corresponding nitrogen heterocyclic phenazine.

There are aspects of this problem which pose additional interesting questions. For example: are we dealing with a single paramagnetic species that exhibits g and/or hfs anisotropy or are we dealing with more than one species? The accumulated evidence in this study shows that indeed we are dealing with a single species. The average g value of the cation is identical with the solution g value, indicating that there is a weak interaction with the surface and furthermore there is no distortion of the radical cation on the surface. The dependence of the three components of the spectrum on rf power also constitutes strong evidence that we are dealing with a single species. It is very unlikely that three different species would respond identically to rf power levels over as wide a range as indicated in Figure 2. Then, a three-g spectrum is not unexpected. The anisotropy itself is still rather small, but greater than with phenazine or with polynuclear hydrocarbons, and, unlike the case of these latter compounds, it is responsible for the prominent features of the spectra. The most prominent features of the phenazine spectra are due to hfs anisotropy.[4] Reduced mobility of the radical ion on the surface could very readily bring about the anisotropic condition. Apparently, the species is essentially immobile even at room temperature, for there is no difference between the room-temperature spectra and the low-temperature spectra (Figures 1 and 3). This situation is also in contrast with that which obtains with phenazine.[4] In this latter case, it was shown that lowering the temperature caused a considerable broadening of the spectra, removing most of the structure that the spectra showed at room temperature. Also, unlike thianthrene, the room-temperature spectra showed structure that was primarily due to ^{14}N nuclei, although there was associated some very small g anisotropy. In the case of thianthrene, there are no nuclei that give as strong an hfs coupling as does the ^{14}N (ignoring, of course, the small percentage of naturally abundant ^{33}S). Therefore, any hfs anisotropy due to the two sets of protons in thianthrene could not be expected to be more prevalent than the g anisotropy. In fact, each component of the three-component spectrum of thianthrene is sufficiently broad that it could very readily accommodate the hfs due to all protons. At high temperature (Figure 3), the three lines merge into a single line with a peak-to-peak width of 18.0 G and a g value of 2.0086. If the three-line spectrum is due to g anisotropy as a result of complete immobility of radical cations on the surface, elevated temperature should remove this anisotropy, resulting in a single line with a g value equal to the average of the three g values

(13) P. L. Corio and S. Shih, *J. Catal.*, **18**, 126 (1970).

(14) W. K. Hall, *J. Catal.*, **1**, 53 (1962).

(15) B. D. Flockhart, J. A. N. Scott, and R. C. Pink, *Trans. Faraday Soc.*, **62**, 730 (1966).

(16) B. D. Flockhart, I. R. Leith, and R. C. Pink, *Chem. Commun.*, 885 (1966).

in the room-temperature spectrum. This is indeed what we are observing. Recently, Bolman and coworkers[17] have studied several sulfur-containing radicals on Vycor glass by spin resonance and in all cases they have observed a three-line spectrum. The features of their spectra and of those reported here are strongly reminiscent of the spectrum of sulfur biradical in the condensed phase. Free radicals of elemental sulfur in amine solutions have been studied by spin resonance by Hodgson and coworkers,[18] and they observe a triplet structure at $-174°$, which, on increasing the temperature to $-25°$, merges into a single-line spectrum. Dudzik and Cvetanović[19] have generated sulfur biradicals on zeolites and have observed a singlet at room temperature and a triplet at 77°K. Higher mobility is possible on the surface of zeolites because of its cagelike structure. At lower temperature, the motion is restricted; consequently, the triplet structure develops. These results are in agreement with the spectral changes, observed here, with temperature. In addition, the anisotropy is larger when the lone pair is localized in an atom with large spin–orbit coupling, as is the case with sulfur.[17]

We will now consider the behavior of thianthrene on MoO_3-modified aluminas. We already indicated that thianthrene adsorbed from a variety of solvents onto Al_2O_3 produces no paramagnetic species, but when the same experiment is attempted on alumina modified by molybdena, there is a strong radical-ion signal produced in addition to the Mo^{5+} signal. Thus, the Mo plays a critical role in the production of radical cations on the surface. The implications of this are quite interesting, for potentially we may have here a tool for qualitative identification and quantitative determination of the "active sites" of the surface involved in the electron-transfer reactions. It is tempting to write down as an overall reaction $Mo^{6+} + Th \rightarrow Th\cdot^{+} + Mo^{5+}$. This would not be unreasonable, for the Mo^{6+} is a good electron trap and could be expected to hold on to the electron that the formation of the thianthrene radical cation involves. Moreover, the thianthrene radical cation might be localized on a molybdenum site. This would be in agreement with oxygen adsorption experiments to be described presently. However, there are indications that the mechanism of the electron-transfer reaction may not be a simple, direct electron transfer from thianthrene to Mo^{6+}. Accurate measurements, now underway, of the absolute concentration of $Th\cdot^{+}$ and Mo^{5+} under a variety of conditions hopefully will clarify this important point pertaining to the mechanism of electron transfer. One fact nevertheless cannot be disputed, namely, that the introduction of Mo into alumina is required to sufficiently modify the surface and thereby effect the oxidation of thianthrene.

The effect of oxygen on the signal intensities of the radical cation and Mo(V) in the thianthrene–MoO_3–Al_2O_3 catalyst system which was mentioned earlier is instructive. There is considerable decrease in the cation signal intensity, while Mo(V) is barely affected. The thianthrene signal broadens also considerably, but not the Mo^{5+} signal. The effect is completely reversible, and the initial spectrum is immediately restored when the oxygen is pumped off. The interaction is loose, and consequently the broadening of cation signal is similar to collision broadening in the gas phase. The change in the signal intensity of Mo(V) is much less compared with that of the cation. This suggests that pentavalent molybdenum could be in interstitial sites and could not be readily reacted by O_2, or that it is covered by thianthrene$\cdot^{+}$ and thus is not accessible to oxygen.

Conclusions

The observations that we have presented and discussed above lead to the following conclusions. Sulfur heterocyclics can undergo electron-transfer reactions on oxide surfaces in an analogous manner with hydrocarbons and nitrogen heterocyclics. However, they show sharp differences from the behavior of nitrogen heterocyclics and hydrocarbons. On η-alumina, unlike hydrocarbons, they are not oxidized in the presence of oxygen, and, unlike phenazine, thianthrene is not reduced on MgO. Thianthrene is oxidized on silica–alumina and molybdena–alumina, but unlike phenazine it shows spectra whose dominant features are determined by g anisotropy. Molybdenum plays a critical role in modifying the surface of alumina and thereby effecting the oxidation of sulfur heterocyclics. Qualitatively, the ionization potential of the adsorbate as well as the oxidative capability of the adsorbent determine the extent to which a given adsorbate will be involved in electron transfer reaction. The mechanistic implication of the modification of alumina by molybdenum and the role of oxygen will be discussed in a subsequent paper.

Acknowledgment. The authors wish to acknowledge the diligent technical assistance provided by Mr. Arthur V. Fareri.

(17) P. S. H. Bolman, I. Safarik, D. A. Stiles, W. J. R. Tyerman, and S. P. Strausz, *Can. J. Chem.*, **48**, 3872 (1970).

(18) W. G. Hodgson, S. A. Buckler, and G. Peters, *J. Amer. Chem. Soc.*, **85**, 543 (1963).

(19) Z. Dudzik and R. J. Cvetanović, *Proc. Int. Congr. Catal. 4th 1968*, **3**, 1082 (1969).

Nuclear Magnetic Resonance Study of the Solvation of Europium(III) Ions in Water–Acetonitrile Mixtures

by Yehuda Haas*

Department of Physical Chemistry, The Hebrew University, Jerusalem, Israel

and Gil Navon

Department of Chemistry, Tel-Aviv University, Tel Aviv, Israel *(Received August 16, 1971)*

Publication costs borne completely by The Journal of Physical Chemistry

The solvation of Eu^{3+} in acetonitrile–water solutions was investigated by nuclear magnetic resonance technique. The water proton shift was found to depend strongly on solvent composition, whereas the acetonitrile proton shift was much less sensitive to this parameter. The results show strong preferential solvation by water. A simple model is suggested for quantitative analysis, leading to fair agreement with experimental results. The water chemical shift is discussed in terms of pseudo contact interaction.

Introduction

Nuclear magnetic resonance spectroscopy has been extensively used for the study of the solvation of ions.[1-3] This method has been successfully applied to mixed solvent systems where preferential solvation, by the components with the higher affinity to the metal ions, could be observed.[4-7] Parameters which can be determined by the nmr method include[1-3] coordination numbers, rate of exchange, and equilibrium constants.

The coordination number of the rare earth ions in several crystals is known to be 9.[8-10] In solution it has been the subject of numerous investigations, employing various methods.[8] Unfortunately, no unambiguous result has emerged until now. Taking Eu^{3+} as a specific example, it seems that a coordination number of either 8 or 9 is consistent with experimental data.[8]

Recent fluorescence work[11] indicated the importance of the composition of the first solvation shell in the decay mechanisms of the excited states, in pure as well as in mixed solvents. Since the acetonitrile–water system was thoroughly dealt with in the fluorescence studies, we chose it as the subject of this research.

Solvation of rare earth ions was investigated by Reuben and Fiat[12,13] and by Lewis, *et al.*,[14] mainly in aqueous solutions, by both ^1H and ^{17}O magnetic resonance.

During the course of this work, the interest in europium compounds as shift reagents in nmr of organic compounds has increased considerably.[15,16]

The aim of this work was to obtain information on the structure of the solvated Eu^{3+} ion in water–acetonitrile mixtures. In particular, the extent to which preferential solvation by water takes place was sought.

Experimental Section

Solutions of europium perchlorate in water and in acetonitrile were prepared as previously described.[11] The starting material was Eu_2O_3 99.9%, obtained from Fluka. Water was triple distilled, and acetonitrile was Fluka spectrograde. All other chemicals were reagent grade.

The nmr spectra were taken on a HA-100 Varian spectrometer. The instrument was operated at either the HA or HR mode. The latter was necessary mainly when the shifts were over 1000 Hz from the internal

* Address correspondence to this author at the Department of Organic Chemistry, Weizmann Institute of Science, Rehovot, Israel.

(1) J. F. Hinton and E. S. Amis, *Chem. Rev.*, **67**, 367 (1967).

(2) C. Deverell, *Progr. Nucl. Magn. Resonance Spectrosc.*, **4**, 235 (1969).

(3) G. A. Webb, *Annu. Rep. NMR (Nucl. Magn. Resonance Spectrosc.)*, **3**, 211 (1970).

(4) P. Diel and T. Liepert, *Helv. Chim. Acta*, **47**, 545 (1964).

(5) A. Fratiello, R. E. Lee, D. P. Miller, and V. M. Nishida, *Mol. Phys.*, **4**, 349 (1967).

(6) N. A. Matwiyoff and H. Taube, *J. Amer. Chem. Soc.*, **90**, 2796 (1969).

(7) A. Fratiello, V. Kubo, R. E. Lee, S. Peak, and R. E. Schuster, *J. Inorg. Nucl. Chem.*, **32**, 3114 (1970).

(8) D. G. Karraker, *J. Chem. Educ.*, **47**, 424 (1970).

(9) J. A. A. Ketelaar, *Physica*, **4**, 619 (1937).

(10) R. Orbach, *Proc. Roy. Soc. Ser. A*, **264**, 458 (1961).

(11) Y. Haas and G. Stein, *J. Phys. Chem.*, **75**, 3677 (1971).

(12) J. Reuben and D. Fiat, *Chem. Commun.*, 729 (1967).

(13) J. Reuben and D. Fiat, *J. Chem. Phys.*, **51**, 4909 (1969).

(14) W. B. Lewis, J. A. Jackson, J. F. Lemons, and H. Taube, *ibid.*, **36**, 694 (1962).

(15) C. C. Hinckley, *J. Amer. Chem. Soc.*, **91**, 5160 (1969).

(16) J. K. M. Sanders and D. H. Williams, *ibid.*, **93**, 641 (1971).

standard. External lock operation using a capillary was impossible because of the high paramagnetic susceptibility of the Eu^{3+} solutions. Therefore either the water or acetonitrile signals were used for locking the field, when operating in the HA mode. All measurements were made at 31°.

The shifts were measured relative to an internal standard. We did not find any *one* internal standard appropriate for the whole range of solvent composition. Such a standard should have the following properties: sufficient solubility in both water and acetonitrile; a simple pmr spectrum, with absorption peaks well separated from water and acetonitrile; and low affinity to Eu^{3+}. We tested acetone, dioxane, *tert*-butyl alcohol, cyclopentane, and benzene. Cyclopentane proved most suitable in solutions with low water content, but solubility was too low when solutions were more than 10 *M* in H_2O. Dioxane and *tert*-butanol were appropriate for such solutions but gave erroneous results with the "dry" one. The concentration of the reference materials was always kept low (<0.1 *M*) so that its variation did not produce changes in the shifts. In Figure 1, which will be discussed later, one can see that in overlapping areas the various internal references led to consistent results.

Results

The nmr spectrum of all solutions consisted of one sharp line for each chemical species present. Except at very low water concentration or low temperatures the line widths did not exceed 1 Hz and were mostly determined by field inhomogeneities. On several occasions the integrated intensity of the spectral lines were compared to the concentration of the species as calculated from the amounts of the liquids mixed into the solutions. Agreement was always found within the experimental error of a few per cent. We can thus conclude that both water and acetonitrile molecules are exchanging very fast between the coordination sphere of the europium ion and the bulk solution. Therefore the chemical shifts of the observed signals are the weighted averaged shifts of the various sites.

The chemical shifts obtained for H_2O and CH_3CN in $Eu(ClO_4)_3$ solutions had to be compared to the salt-free shifts. It is well known that the shift of water protons of water in mixture with organic solvents depends strongly on water concentration, due to changes in hydrogen bonding. The variation of the shift in H_2O–CH_3CN mixtures using several internal standards is shown in Figure 1. It is seen that the shift changes by about 2.5 ppm and therefore the choice of the reference solution is important. Strictly, one should compare solutions (with and without salt added) with the same degree of hydrogen bonding. As an approximation, we used a salt free solution with the same water to acetonitrile ratio as the reference solution. The error introduced by this approximation is expected

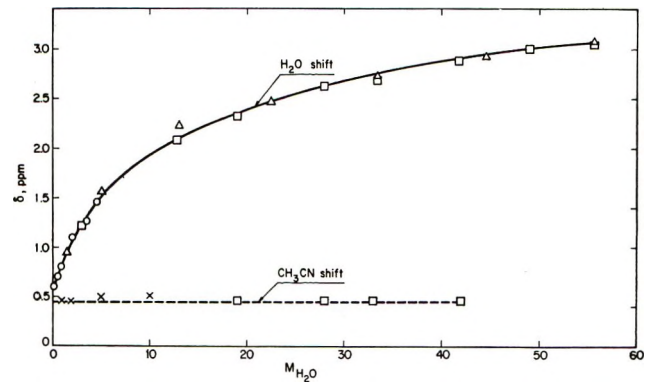

Figure 1. Pmr chemical shifts of H_2O and CH_3CN in mixtures of the two solvents, as a function of H_2O concentration. Several internal reference substances were used: ○, cyclopentane; □, dioxane; △, *tert*-butyl alcohol. The cyclopentane signal was taken as the origin.

to be significant only in low water concentrations. In this region the experimental shifts obtained for H_2O in the $Eu(ClO_4)_3$ solutions were large enough so that the error did not exceed 1–2% (10 Hz compared to 1000). This problem did not arise in the case of acetonitrile, as the shift of acetonitrile protons is not significantly dependent on solvent composition (Figure 1).

In Figure 2 the proton chemical shifts of water and acetonitrile are given as a function of europium concentration in acetonitrile solutions containing about 0.1 *M* H_2O. Acetonitrile is shifted to low field and water to high field. The acetonitrile shift is seen to be roughly proportional to the ion concentration, as is to be expected. This is clearly not the case with the water shift, which is almost independent of Eu^{3+} concentration in the range 0.5–1 *M*, and decreases only slightly at lower concentrations. This result indicates preferential solvation of the ion by water so that most of the water present in the solution is complexed. The slight decrease of the shift at lower Eu^{3+} concentrations may be due to either the increase in the proportion of free water molecules or to a change in the distribution of the water molecules in the different sites of the complex with the ion. This topic will be dealt with more extensively further on.

The proton chemical shift of water and acetonitrile as a function of solvent composition at different Eu^{3+} concentrations is given in Figures 3 and 4, respectively. It is apparent that while the acetonitrile shift approaches zero monotonously as water concentration is increased, the water shift changes from a large positive value to a negative one. Focusing our attention to the 1 *M* $Eu(ClO_4)_3$ solutions, we find that at low water concentrations (up to about 0.5 *M*) the shift is to a high field, and its magnitude does not change much with water concentration. Further increase in water concentration causes a very sharp decrease in the chemical shift. The shift changes sign and finally

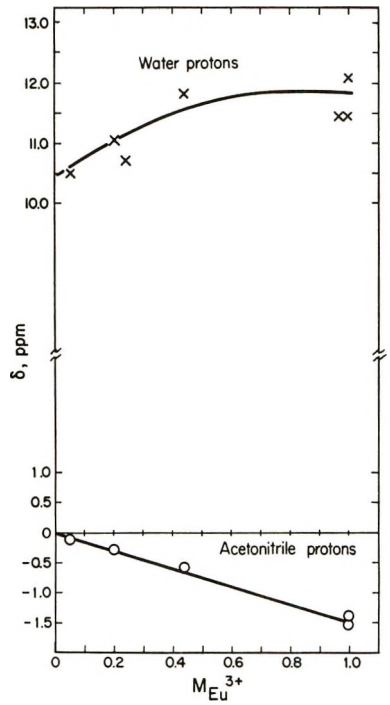

Figure 2. Pmr chemical shifts of water and acetonitrile in solutions of $Eu(ClO_4)_3$ in CH_3CN, as a function of Eu^{3+} concentration. Water concentration ~0.1 *M*.

reaches a minimum at about 10 *M* H_2O. The third region is similar to the acetonitrile shift as the shift monotonously approaches the value for pure aqueous solution. This value is −0.25 ppm for 1 *M* solution, in fair agreement with previous work.[12]

A quantitative attempt to account for this unusual behavior will be given further on. Qualitatively, the three regions can be explained as follows. At low water concentrations, the shift is essentially due to the water molecules bound to the ion in an energetically favorable site. As water concentration is increased, more and more unbound water molecules are present in the solution, causing a decrease in the shift. Increase of the fraction of free water molecules cannot be the only reason for the observed decrease, as it is evident that the shift actually changes its sign. This leads us to postulate the existence of another site in the solvation shell of the ion, into which water molecules can enter. This site should give rise to a shift with the opposite sign to the first one. Such a change in sign is expected if pseudo contact interaction contributes to the shift, as will be discussed later. Finally, when hydration is practically complete, the shift rises slowly to the value in pure water due to dilution.

In order to check the effect of the perchlorate anion on the chemical shifts, a series of measurements was performed on 0.24 *M* $Eu(ClO_4)_3$ solutions, with and without addition of 2.25 *M* $NaClO_4$. The results are given in Figure 5. The water shift in the presence of excess perchlorate is seen to be displaced to higher fields in all water concentrations. Nevertheless, the

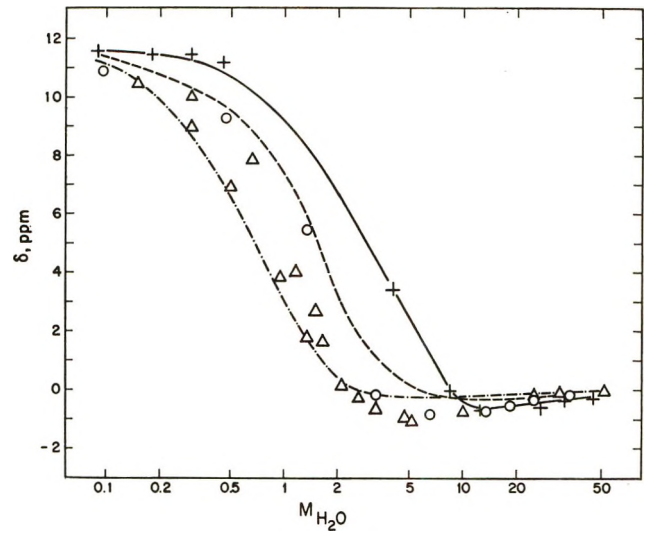

Figure 3. Experimental pmr chemical shifts of H_2O in solutions of $Eu(ClO_4)_3$ in H_2O–CH_3CN mixtures, as a function of water content. +, 1 *M* $Eu(ClO_4)_3$; ○, 0.5 *M* $Eu(ClO_4)_3$; △, 0.25 *M* $Eu(ClO_4)_3$. Theoretical curves with $K_a = 120$, $K_e = 720$ are also shown; for explanation, see text: —, 1 *M* $Eu(ClO_4)_3$; – – –, 0.5 *M* $Eu(ClO_4)_3$; — · —, 0.25 *M* $Eu(ClO_4)_3$.

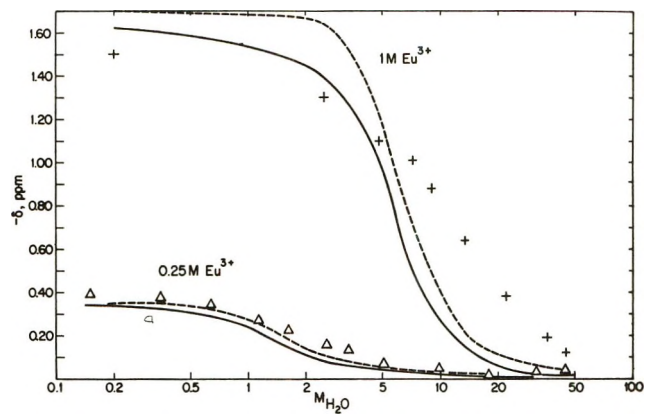

Figure 4. Experimental pmr chemical shifts of CH_3CN in solutions of $Eu(ClO_4)_3$ in H_2O–CH_3CN mixtures, as a function of water content: +, 1 *M* $Eu(ClO_4)_3$; △, 0.25 *M* $Eu(ClO_4)_3$. Two sets of theoretical curves are given, calculated with the same equilibrium constants as those used for the curves in Figure 3: ——, $\delta_a^A = 420$ Hz, $\delta_e^A = 60$ Hz; – – – –, $\delta_a^A = 600$ Hz, $\delta_e^A = -300$ Hz.

general behavior including sign change is preserved. Solution with lower water content than 1.5 *M* could not be studied because of limited solubility of $NaClO_4$.

Interpretation of the Results. In this section we wish to present a quantitative elaboration of the conclusions drawn above. Specifically, we try to compare the experimental results with the results of a computation based on a simple model for the solvation of the Eu^{3+} ion in mixtures of water and acetonitrile.

A solution of an ion in a mixture of two solvents contains, in general, every possible combination of the solvent molecules in the coordination sphere of the ion. In the following we shall neglect effects of com-

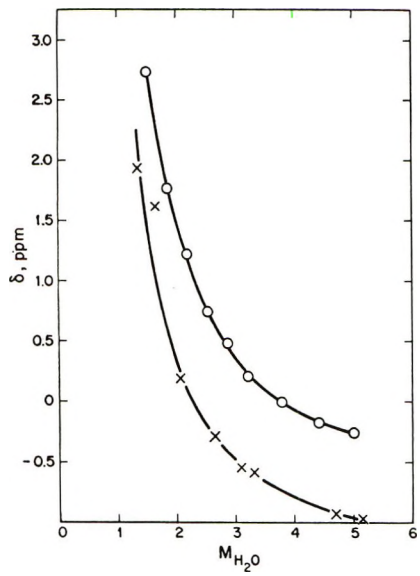

Figure 5. Effects of perchlorate anion on the pmr shift of water in solutions of $Eu(ClO_4)_3$ in H_2O–CH_3CN mixtures as a function of water content; $Eu(ClO_4)_3$ concentration is 0.24 *M*; ×, without $NaClO_4$ added; ○, with 2.25 *M* $NaClO_4$ added.

plexation or ion-pairing by anions and assume a constant coordination number (*i.e.*, not dependent on solvent composition). In equilibrium, the concentration of these complexes will be a unique fraction of the solvent composition. These concentrations will be governed by equilibrium constants K_i. If these are known, the concentration of each species can be calculated.

As has been pointed out above, experimental data show that the system is in the fast exchange limit. In this limit, the chemical shift of the protons of a given solvent is given by the weighted average of the shifts of the different species present. In our case these correspond to the different complexes described above, and the free solvent. Knowing the concentration of each such species, and its particular chemical shift, one can calculate the shift at any given composition.

In what follows we give such a calculation, based on the following assumptions.

(1) The coordination number of Eu^{3+} is 9, independent of solvent composition.

(2) Following Ketelaar,[9,10] the nine coordination sites can be divided into two distinct ligand groups. One group of three equivalent sites shall be denoted equatorial and the second group of six equivalent sites we denote axial.

(3) Only two equilibrium constants govern the system: K_a, which is a measure for the affinity of water molecules to the axial sites, and K_e, determining water affinity to the equatorial sites. The concentration of each species will be determined by these equilibrium constants, weighted by a proper statistical factor, which is proportional to the number of sites unoccupied by H_2O molecules.

(4) Finally, only two different specific chemical shifts will be considered: all axial molecules are assumed to be magnetically equivalent with a specific shift δ_a and all equatorial molecules are equivalent with a specific shift δ_e. Generally $\delta_a \neq \delta_e$. This assumption is based on the fact that the shift of a ligand proton is determined mainly by the symmetry of the complex and the distance from the central ion. Within our model, all axial (or equatorial) ligands are geometrically equivalent, regardless of the composition of the complex, and therefore also magnetically equivalent.

The main features of our treatment are the use of only two distinct magnetic species and two equilibrium constants. Preliminary calculations indicated that the use of either 8 or 9 as the coordination number leads to approximately the same agreement with experimental results and to about the same stability constants.

Rather than devising an arbitrary model for coordination 8, we preferred to use the known symmetry for the 9 coordination existing in hydrated crystals as the basis for the detailed computation.

A further justification of this choice is the similarity between the geometric parameters found in crystals and those obtained by us (see Discussion).

In what follows, we denote the different complexes by indicating the number of their axial and equatorial water molecules. Thus E_l^k denotes a complex with k axial water molecules and l equatorial water molecules.

The concentration of the E_l^k species is thus given by

$$[E_l^k] = \frac{[(6-k)K_a]^k[(3-l)K_e]^l[W_f/A_f]^{k+l}}{\sum_{k=0}^{6}\sum_{l=0}^{3}[(6-k)K_a]^k[(3-l)K_e]^l(W_f/A_f)^{k+l}} E_{tot} \quad (1)$$

where W_f is the free (uncomplexed) water concentration, A_f is the free acetonitrile concentration, and E_{tot} is the total Eu^{3+} concentration.

Calculation of $[E_l^k]$ requires knowledge of W_f and A_f, which are not experimentally available. Actually, only one of them is an independent variable and could be calculated by an iterative method. The procedure was to calculate for given values of W_f, K_a, K_e, and E_{tot} concentrations of the various E_l^k's according to eq 1. W_f was iterated until self-consistency was obtained using the criterion

$$W_f + \sum_{k=0}^{6}\sum_{l=0}^{3}(k+l)[E_l^k] = W_{tot}$$

W_{tot} is the experimental total water concentration.

The chemical shift for a given composition of the solvent could now be obtained from the formula

$$\delta_{calcd} = [W_{tot}]^{-1}\left\{\sum_{k=0}^{6}\sum_{l=0}^{3}(k\delta_a + l\delta_e)[E_l^k]\right\} \quad (2)$$

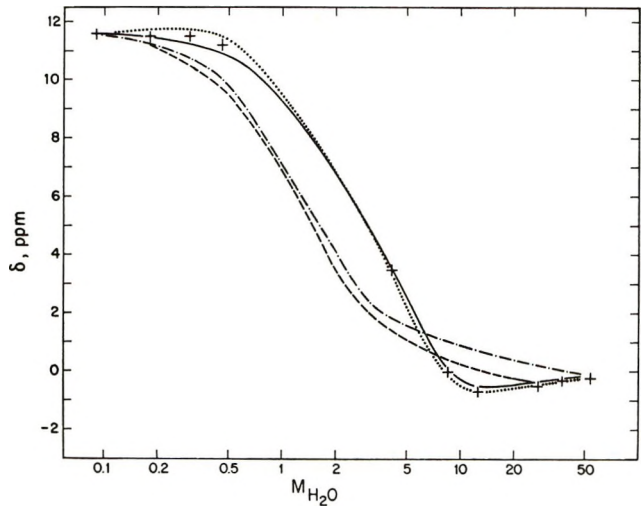

Figure 6. Theoretical curves for the pmr chemical shift of water in 1 *M* solutions of $Eu(ClO_4)_3$ in H_2O–CH_3CN mixtures, as a function of water content: +, experimental points; — · —, $K_a = 4$, $K_e = 8$, $\delta_a^W = -3200$, $\delta_e^W = 5980$; – – – –, $K_a = 128$, $K_e = 256$, $\delta_a^W = -2800$, $\delta_e^W = 5190$; ·····, $K_a = 128$, $K_e = 1150$, $\delta_a^W = -1020$, $\delta_e^W = 1625$; ——, $K_a = 120$, $K_e = 720$, $\delta_a^W = -1180$, $\delta_e^W = 1950$ (best fit).

Here δ_a and δ_e are the appropriate values for *water*. A similar equation holds, of course, for acetonitrile. δ_a and δ_e were determined as follows. In pure aqueous solution, the chemical shift is given by

$$\delta_{aq} = (3\delta_e + 6\delta_a)E_{tot}/W_{tot} \quad (3)$$

This equation gives one relation between the two constants. Their absolute values were determined by an iterative method, using the experimental value of the shift with the lowest water concentration as the criterion for good fit. The values for δ_a and δ_e obtained were used to calculate the chemical shifts of water in all the different compositions, and the agreement with experimental results was tested by a least-mean-squares procedure, for each pair of K_a and K_e.

Calculations were carried out for the water shifts obtained with 3 different Eu^{3+} concentrations measured experimentally. It was found that the fit with the experimental water shift was good only with high values (>100) of K_a and K_e. The agreement was not as sensitive for higher *absolute* values of the K's as it was to their *ratio*. This is physically understandable, as such high values indicate a strong preferential solvation by water, and the main difference between various calculations arises because of changes in the occupation of the sites within the complex. A plot of the results with several pairs of equilibrium constants is given in Figure 6. The curves giving the best fit and the parameters leading to them are given in Figure 3.

It is seen from Figure 6 that at a ratio of $K_e/K_a = 2$ the agreement with experimental results becomes very poor. Calculations with $K_a > K_e$, *i.e.*, a stronger affinity for water in the axial sites, failed completely to reproduce the experimental results.

It should be mentioned also that attempts to use equilibrium constants without statistical factors led to less satisfactory results. As seen from Figure 3 the shifts of acetonitrile protons were of the same sign over the whole concentration range. This did not allow unambiguous evaluation of the two specific chemical shifts and the two equilibrium constants simultaneously. Therefore we used the equilibrium constants obtained from the analysis of the water shift and tried to obtain agreement with experimental results by varying only the specific chemical shifts. Results of several calculations are given in Figure 4. A good agreement with experimental results could be obtained for the 0.25 *M* $Eu(ClO_4)_3$ solutions, whereas the calculations for the 1 *M* solutions lead to less satisfactory results. It is seen that the computed results are insensitive to the value of the specific chemical shift of the equatorial acetonitrile molecules δ_e^A. This is understandable as the equatorial sites are preferentially occupied by water molecules.

Discussion

The results clearly demonstrate the preferential solvation of Eu^{3+} by water in acetonitrile–water mixtures. The direct observation of signals due to molecules in the solvation shell was hampered by the fast exchange with bulk molecules. Still, due to the high affinity of water to Eu^{3+}, it was possible to assign the signal of water protons in solutions with very low water content essentially to bound molecules. Analysis of the results with different water concentrations showed that even in this case the signal was not due to a single magnetic species. A complete interpretation would require knowledge of the number of these species and their specific chemical shifts. Furthermore, one should know the equilibrium constants governing the occupation of the sites corresponding to these magnetic species.

Clearly, the many parameters involved cannot be deduced from the results without ambiguity. We thus preferred the use of an admittedly oversimplified model, in which only two equilibrium constants were used. This model is based on the structure suggested for hydrated rare earth ions in crystals by Ketelaar. According to the model six ligand molecules are at the corners of a triangular prism, and three molecules, forming a plane in which the ion is placed, protrude from the rectangular sides of the prism.

Our results show that the three equatorial sites have a much higher affinity to water than the six axial sites. This may indicate that water molecules are somewhat closer to the ion when in an equatorial site. In crystals of the rare earth ethyl sulfates the distance between the central ion and an equatorial molecule was found to be almost equal to the distance to an axial molecule.[9,10]

The results for the water chemical shift are also consistent with the structure of the complex outlined

above. We note that the two shifts obtained differ in sign and magnitude. Such differences cannot be accounted for by a contact interaction, especially as the distances to the central ion are not widely different. We are thus led to the conclusion that the dominant term contributing to the chemical shift is the pseudo-contact interaction. This can easily account for the change in sign, as the pseudo-contact term depends explicitly on the angular coordination of the ligand[17]

$$\frac{\Delta\nu}{\nu_0} = \frac{C}{R^3}(3\cos^2\theta - 1)\mathrm{F}(g) \qquad (4)$$

where $\mathrm{F}(g)$ is a function of the g tensor components. θ is the angle between the principal axis of the g tensor and the radius vector of length R connecting the metal ion with the observed nucleus.

In the original expression,[17] the constant C depended only on the spin quantum number S. In the case of Eu^{3+} one should take into account spin–orbit coupling and population of low-lying electronic levels. The angular dependence is unlikely to be affected by such changes. We can therefore calculate the angles giving rise to the observed shifts.

Identifying the principal symmetry axis of the complex with the principal axis of the g tensor, let θ_a and θ_e denote the angles between the principal axis and the axial and equatorial ligand, respectively.

Equation 4 leads to the following ratio between δ_a and δ_e (neglecting the small difference in R)

$$\frac{\delta_a}{\delta_e} = \frac{3\cos^2\theta_a - 1}{3\cos^2\theta_e - 1} = \frac{-1180}{1950}$$

As $\theta_e = 90°$ we find $\theta_a = 43°$.

This result is in good agreement with $\theta_a = 39°$ obtained for the hydrated crystal.[10] Thus the symmetry suggested by Ketelaar is consistent also with the hydrated ion in solution.

Attempts to calculate the relative importance of the contributions of the contact and pseudo-contact terms to the proton shifts of water in solutions of the rare earth ions have been made before.[18] No calculation was given for Eu^{3+}. It seems that the method used in this work, *i.e.*, use of a solution containing essentially only bound water molecules, might be of some help in such calculations.

As noted in the preceding section, agreement of calculated with experimental results is much poorer when we consider the acetonitrile shift. The absolute values of the shifts are smaller than those of water in agreement with the R^{-3} term in the expression for the chemical shift derived from a pseudo-contact interaction. Agreement with experimental results was found to be relatively insensitive to the magnitude, and even to the sign of the ratio δ_a^A/δ_e^A. This ambiguity does not allow us to discuss further the binding of acetonitrile to Eu^{3+}.

It was assumed that ion pairing does not take place. This assumption is doubtful, especially in solutions with low water content. Thus in a study of the optical absorption and fluorescence of Eu^{3+} in acetonitrile the existence of ion pairing was indicated.[11]

The presence of ion pairing does not necessarily affect the nmr spectrum. An attempt to estimate the extent of this effect was done by varying the perchlorate concentration. The results show that anion concentration has an effect on the shift although it does not change its general behavior as a function of water content. This effect might be due to ion pairing, but may also be assigned to other phenomena such as effective reduction of free water concentration by coordination to the ClO_4^- and Na^+ ions or a change in equilibrium constants due to change in ionic strength. Evidently the assumption of a single pair of equilibrium constants, even with a given ionic strength, is an oversimplification. Usually there are distinct constants for each equilibrium. The constants obtained in this work should be looked upon as weighted averages. Introduction of more constants could of course lead to better agreement with experiment, but this advantage should have been counteracted by the introduction of much more ambiguity into the results.

The high values obtained for K_a and K_e show clearly the preferential solvation of Eu^{3+} by water. A study of the solvation of Co^{2+} [5] in mixed solvents has shown that acetonitrile has a very low affinity to this ion also as compared to water. On the other hand, a similar study of the solvation of Ag^+ [19] has shown that this ion is preferentially solvated by acetonitrile. The nmr results presented here are in line with data obtained from the quenching of Eu^{3+} fluorescence by water in acetonitrile solutions.[11]

Finally, we note that the line width of the water proton signal allows us to set a lower limit to the exchange rate between bound and bulk molecules. The line widths at room temperature were lower than 1 Hz. Using the values obtained for the chemical shifts of the bound water molecules we obtain $k_{exchange} > 3 \times 10^6$ sec^{-1}. This value is in line with previous results estimated from T-jump and p-jump measurements[20,21] yielding $k_{exchange}$ 8×10^7 sec^{-1}. Cooling the solutions to $-50°$ (slightly above the freezing point) leads to broadening of the line, but not to separa-

(17) H. M. McConnel and R. E. Robertson, *J. Chem. Phys.*, **29**, 136 (1958).

(18) J. Reuben, Ph.D. Thesis, The Weizmann Institute, Rehovot, 1968.

(19) H. Schneider and H. Strehlow, *Z. Phys. Chem. (Frankfurt am Main)*, **49**, 44 (1966).

(20) A. J. Graffeo and J. L. Bear, *J. Inorg. Nucl. Chem.*, **30**, 1577 (1968).

(21) G. Geier, *Ber. Bunsenges. Phys. Chem.*, **69**, 617 (1965).

tion into two distinct lines. This broadening may be due to a slower rate of exchange but also to broadening of the resonance line due to bound molecules.[22]

Acknowledgment. We are grateful to Professor Gabriel Stein for helpful discussions.

(22) Y. Haas and G. Navon, to be published.

The Nuclear Magnetic Resonance Chemical Shift of the Water Proton in Aqueous Tetraalkylammonium Halide Solutions at Various Temperatures

by Marie-Madeleine Marciacq-Rousselot,

Laboratoire de Physique Experimentale Moléculaire, Faculté des Sciences, 9, Quai Saint-Bernard, 75 Paris 5ème, Tour 32, 2ème étage, France

Anne de Trobriand, and Michel Lucas*

Department de Génie Radioactif, CENFAR, B.P.N°6, 92-Fontenay-aux-Roses, France *(Received August 20, 1971)*

Publication costs assisted by Commissariat a l'Energie Atomique

In the present article we report the results of nmr measurements of the chemical shift of the water proton in solutions of tetrabutyl-, tetrapropyl- and tetramethylammonium bromides, chlorides, and fluorides at various temperatures and concentrations. Changes in the molal heat capacity of chloroform and of solid tetrabutylammonium bromide in aqueous solutions of tetrabutylammonium fluoride, chloride, and bromide are included as well. At low temperatures the downfield shift of the water proton increases in the order $Br^- < Cl^- < F^-$ and $Me_4N^+ < Pr_4N^+ < Bu_4N^+$. This is consistent with an increase in water structure promotion when the alkyl chains of the quaternary ammonium salts are lengthened. At higher temperatures the order is the same for the anions but is reversed for the cations. Heat capacity changes have been measured at 20 and 25°. According to the currently accepted interpretations of such measurements, Bu_4NF should be a strong structure promoter (which is also consistent with the nmr measurements). The structure of water apparently collapses or changes abruptly when the molality of Bu_4NBr is 1.2 *m*. There are thus conflicting conclusions regarding the effect of dissolved Bu_4NBr on the structure of water. The change in heat capacity and the nmr spectra indicate that it may be a structure breaker, whereas a number of other measurements suggest that it is a structure maker.

I. Introduction

Since Frank and Wen[1] introduced the concept of water structure promotion by the salt tetrabutylammonium bromide, aqueous solutions of this salt have been extensively studied, and evidence has accumulated which suggests that this salt is a strong water structure former. Among the properties of the solution which are taken as showing the effect, we may include the high heat capacity,[1] the near-infrared spectra of H_2O–D_2O solutions,[2] and the increase of the reorientation time of water molecules upon the addition of the quaternary ammonium bromide.[3]

However not all properties of solutions of this compound in water lead directly to the conclusion that it is a structure former at various temperatures and concentrations. Thus the lowering of the temperature of maximum density of the solution (TMD) by the addition of structure-breaking salts would require that, if tetra-*n*-butylammonium bromide were a structure former, the TMD would be raised. One would expect this from the behavior of *tert*-butyl alcohol which does raise the TMD of its aqueous solutions,[4] and which in other respects appears to be a water structure former.[5] However the bromide lowers the TMD of its aqueous solution comparatively to pure water.[6]

In the same vein, nmr measurements of the chemical shift of the water proton in solutions of the bromide are also puzzling.[7] The shift is in the same direction as that caused by such structure breakers as CsI, or by higher temperatures. The decision is a difficult one be-

(1) H. S. Frank and W.-Y. Wen, *Discuss. Faraday Soc.*, **24**, 133 (1957).

(2) J. D. Worley and I. M. Klotz, *J. Chem. Phys.*, **45**, 2868 (1964).

(3) H. G. Hertz and M. D. Zeidler, *Ber. Bunsenges. Phys. Chem.*, **68**, 821 (1964).

(4) F. Franks and D. J. G. Ives, *Quart. Rev.*, **20**, 1 (1966).

(5) R. G. Anderson and M. C. R. Symons, *Trans. Faraday Soc.*, **65**, 2550 (1969).

(6) A. J. Darnell and J. Greyson, *J. Phys. Chem.*, **72**, 3021 (1968).

(7) H. G. Hertz and W. Spalthoff, *J. Elektrochem.*, **63**, 1096 (1959).

cause of the questions which have been raised regarding the nature of the hydrogen bond. If one assumes that the H bond has some covalent character, then the direction of the shift (upfield with increasing salt concentration) can be explained by an increase in the covalent character in the presence of the organic salt with an accompanying increase in the proportion of organized water in the solution.[8]

On the other hand, if an electrostatic model of the H bond is assumed, the direction of the shift caused by this salt must be interpreted as a decrease in the H bonding in the water, that is, the salt is a structure breaker.

In addition, recent measurements of the change in heat capacity (ΔC_p) of chloroform in the solutions of the bromide showed that at a salt molality of 1.2 ΔC_p decreased abruptly.[9] This result can be interpreted as a sign of the collapse of the water structure in solutions more concentrated than 1.2 *m* at room temperature. Finally an additional complication in the interpretation of the nmr spectra of water in aqueous solutions of quaternary ammonium chlorides is found in the recent communication by Davies, *et al.*[10] They reported that they had confirmed the results of Hertz and Spalthoff at 25°; increasing the length of the alkyl chains of quaternary ammonium salts causes the water proton resonance to shift upfield (in the structure-breaking direction). However lowering the temperature to 0° reverses the trend. That is at the lower temperature the larger the cation, the more it acts as a structure promoter.

In an attempt to make clear the effect of the tetraalkylammonium salts on the water structure, we report here the results of nmr measurements of the chemical shift of the water proton in solutions of tetrabutyl-, tetrapropyl-, and tetramethylammonium bromides, chlorides, and fluorides when the temperature and salt concentration are varied. In addition some molal heat capacity changes for chloroform and tetrabutylammonium bromide in aqueous solutions of tetrabutylammonium fluoride, chloride, and bromide are also reported.

II. Experimental Section

Chemicals. Bu_4NBr, Pr_4NBr, Me_4NBr, Pr_4NCl, and Me_4NCl (Eastman Kodak), were purified according ref 11. Bu_4NCl, Bu_4NF, Pr_4NF, and Me_4NF were prepared by titration of the corresponding hydroxides (Fluka). The Bu_4NCl and Bu_4NF solutions were in addition purified by several recrystallizations of the hydrates. The solutions of the tetraalkylammonium fluorides were analyzed for the cation and anion content by gravimetric analysis with $Na(C_6H_5)_4B$ and $CaCl_2$. The analyses agreed with each other to within 1%.

Nmr Measurements. Nmr spectra were obtained with a Varian A 60 spectrometer operating at 60 MHz and equipped with the V 6040 temperature controller.

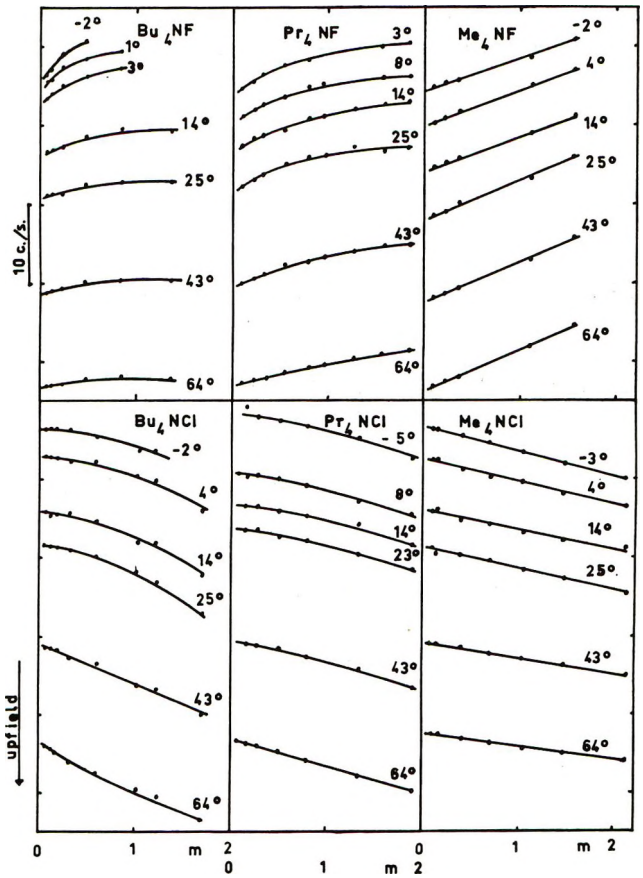

Figure 1. Plots of the chemical shift between the peak due to the water proton and a peak due to protons in the CH_3 groups against the salt molality for tetraalkylammonium fluoride and chloride solutions.

The chemical shift between the peak due to the water protons and a peak due to protons in the CH_3 groups of the tetraalkylammonium ions was measured. The CH_3 protons were used as an internal standard. This eliminates the need for corrections due to differences in the bulk diamagnetic susceptibilities of the various solutions. It was shown[5] that similar results are obtained from an external standard like chloroform or an internal standard like tetramethylammonium chloride.

Heat Capacity Measurements. The calorimeter and the procedure have already been described in detail.[12] The heat of solution ΔH of small quantities of liquid chloroform or solid tetrabutylammonium bromide in the various salt solutions investigated was measured at two temperatures: 15 and 25° for chloroform and 20 and 30° for tetrabutylammonium bromide. The heat capacity change for the solution process from the pure liquid or pure solid state is $\Delta C_p = \Delta(\Delta H)/\Delta T$.

(8) J. Clifford and B. A. Pethica, *Trans. Faraday Soc.*, 60, 1483 (1964).

(9) M. Lucas and A. Feillolay, *J. Phys. Chem.*, 75, 2330 (1971).

(10) J. Davies, S. Ormondroyd, and M. C. R. Symons, *Chem. Commun.*, 1426 (1970).

(11) B. E. Conway, R. E. Verrall, and J. E. Desnoyers, *Trans. Faraday Soc.*, 62, 2738 (1966).

(12) M. Lucas, *Bull. Soc. Chim. France*, 2902 (1970).

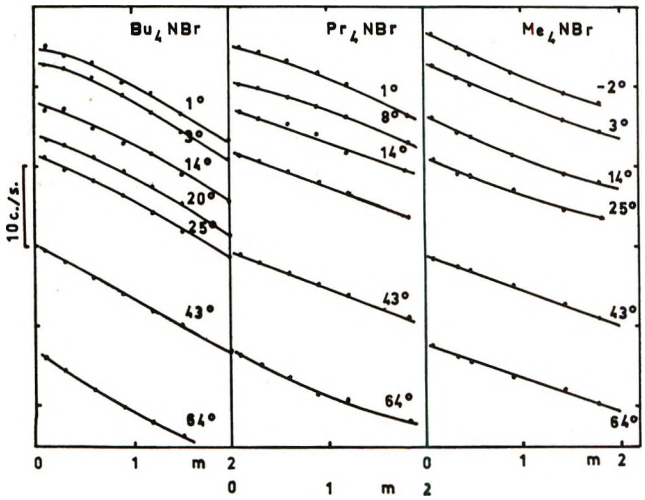

Figure 2. Plots of the chemical shift between the peak due to the water proton and a peak due to protons in the CH_3 groups against the salt molality for tetraalkylammonium bromide solutions.

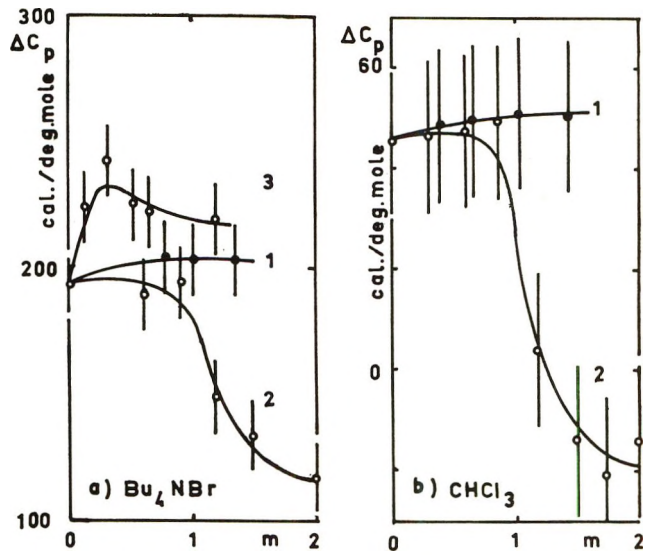

Figure 3. (a) Heat capacity change at 25° for the process of solution of pure solid Bu_4NBr in aqueous tetrabutylammonium halide solutions: 1, Bu_4NCl solutions; 2, Bu_4NBr solutions; 3, Bu_4NF solutions. (b) Heat capacity change at 20° for pure liquid $CHCl_3$ in aqueous tetrabutylammonium halide solutions: 1, Bu_4NCl solutions; 2, Bu_4NBr solutions. Abscissa: salt molality.

Results

In Figures 1 and 2 the chemical shift (as ordinate) is plotted against salt molality (as abscissa) for different salts and different temperatures. The temperature in general was controlled within ±2°.

Figure 3a shows the plots of the heat capacity change at 25° against salt molality for the process of dissolving solid Bu_4NBr in various aqueous salt solutions. Figure 3b shows similar plots for the heat capacity change at 20° for liquid chloroform in the same salt solutions. Each measurement of the enthalpy of solution represents the mean of four determinations. The range of the salt concentration investigated was limited by the crystallization of the clathrate. The estimated errors are shown by vertical bars in the figures.

III. Discussion

1. ΔC_p *Measurements.* Figures 3a and 3b show some interesting features. The first is that the heat capacity change in tetrabutylammonium bromide solution is almost constant until a concentration of 1.2 *m* is reached. At this point it decreases abruptly. In tetrabutylammonium chloride or fluoride solutions this abrupt decrease does not appear. In addition the ΔC_p in dilute fluoride solutions at first increases with fluoride molality and then falls slightly, but is always higher than in bromide solutions. According to currently accepted interpretations of heat capacity measurements,[13] this should indicate a breaking of the water structure in the Bu_4NBr aqueous solutions when the salt molality is higher than 1.2 *m*. At lower molalities the ΔC_p is rather constant, and one cannot decide the effect of the changing salt concentration on the structure of the water. In aqueous Bu_4NCl solutions the sudden decrease in ΔC_p is not evident, and in Bu_4NF solutions the measurements appear to show an increase in the extent of hydrogen bonding by the salt. A similar conclusion was reached by Narten and Lindenbaum[14] from their X-ray studies. They showed that the near-neighbor distance between water molecules at 25° decreased from 2.85 Å in pure water to 2.80 Å in aqueous 1.4 *m* Bu_4NF solution, indicating stronger H bonding. The Bu_4NF salt thus appears to be a structure promoter. Bu_4NBr may be a structure breaker in its effects on the structure of pure water, because the structure-breaking effect of Br^- competes with the structure-forming effect of Bu_4N^+, as postulated by Lindenbaum, *et al.*,[15] to explain the variation of the osmotic coefficients of tetraalkylammonium fluorides and iodides with temperature. From the picture of the aqueous Bu_4NF solution given by Narten and Lindenbaum,[14] an explanation for the sudden break at 1.2 *m* in Bu_4NBr aqueous solutions may be proposed. In Bu_4NF solutions the water is pictured as an extended ice-I lattice in which all water molecules, F^- ions, and N atoms are found to occupy network positions. The butyl chains of the cations are visualized to be located in the cavities. There is one-half cavity for one network position, and a butyl chain occupies two cavities. A crude calculation shows that at a salt molality of about 3, all cavities should be occupied so that at higher molalities this structure would no longer be

(13) R. K. Mohanty, T. S. Sarma, S. Subramanian, and J. C. Ahluwalia, *Trans. Faraday Soc.*, 67, 305 (1971).

(14) A. H. Narten and S. Lindenbaum, *J. Chem. Phys.*, 51, 1108 (1969).

(15) S. Lindenbaum, I. Leifer, G. E. Boyd, and J. W. Chase, *J. Phys. Chem.*, 74, 761 (1970).

stable. If in the solution the F^- ions are replaced by the structure-breaking Br^-, then it may be supposed that the collapse of the water structure should appear at a lower molality.

Now if the quaternary ammonium bromide is indeed a water structure breaker, there is an apparent contradiction between this property and the high heat capacity of its aqueous solution.

The proposal has been made by Millero,[16] from apparent molal volumes of $NaB(C_6H_5)_4$, by Kalfoglou,[17] from osmotic measurements on tetraphenylphosphonium halide solutions, and by Jolicoeur, *et al.*,[18] from near-infrared measurements, that ions like $B(C_6H_5)_4^-$ or $(C_6H_5)_4P^+$ should be water structure breakers. The reason for this effect is not clear at present but is evidently related to the interactions of phenyl groups with liquid water. The ΔC_p for solid $NaB(C_6H_5)_4$ in water at 25° is, however, rather large and very similar to that of solid Bu_4NBr (170 and 180 cal/deg mol, respectively[19]). Thus a high heat capacity could be associated with a structure-breaking character.

In addition the partial molal heat capacities $\overline{C_p°}_2$ of KF, KCl, KBr, and KI at infinite dilution in water at 25° are, respectively, −28, −29, −29.5, and −30.2 cal/deg mol.[1,20] That is they are very similar although the water structure forming character of the anions is very different. The structure-breaking character certainly increases much from Cl^- to I^- and the $\overline{C_p°}_2$ should have been much more negative for the largest anion. Clearly there is some other effect than the structure-modifying ability of the ion which must be taken into account to explain the experimental value. It would be associated with a positive contribution increasing with the size of the anion, and the absolute value should depend on the balance between the size effect and the structure-breaking character of the anion. Thus a large heat capacity of a solution would not in itself be sufficient to conclude that the water is more strongly organized. Rather one should take the increase or decrease of the heat capacity change associated with the solution of a given molecule or salt on the addition of another compound as an indication of the water structure modifying ability of this compound.

2. Nmr Measurements. The results given in Figures 1 and 2 are summarized in Figure 4, which shows plots of the chemical shift against salt molality at 2, 25, and 43°. It is apparent that the effect of the salt depends on the nature of the salt, the concentration of the solution, and its temperature. The effect of the salts at low molalities (<0.5) at 2° will be discussed according to the classical theory,[20] excluding the alternative interpretation based on the hypothetical partial covalent character of the H bond.[8] It is found that with fluorides, the water proton resonance is shifted downfield, and with bromides, the resonance is shifted upfield. Chlorides are intermediate. This would normally be interpreted in terms of structure making by the fluorides and structure breaking by the bromides, that is strenghtening the H bond by the first and weakening it by the last. In addition the overall effect of the salts may be explained by assuming that the larger the cation the more it behaves as a structure former, as hypothesized by Frank and Wen,[1] and the larger the anion the more it behaves as a structure breaker, so that there is a competing effect between the larger cation and anion as postulated previously.[15]

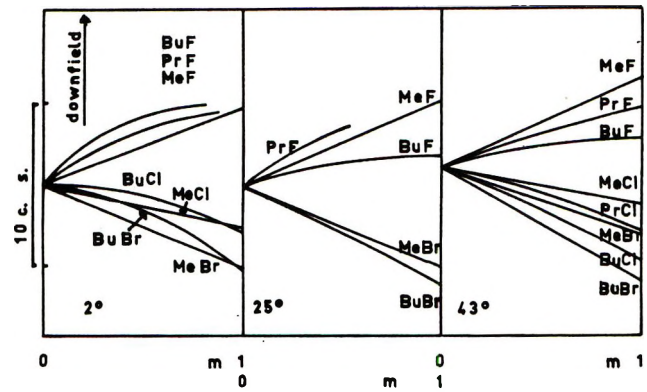

Figure 4. Plots of the chemical shift for the different quaternary ammonium salts solution at some fixed temperatures. Abscissa: salt molality.

At 43° the picture is different. The tetraalkylammonium fluorides still appear to strenghten the H bond of water, and chlorides and bromides seem to weaken it. However, the overall effect on the proton chemical shift is in the order $Me_4NF > Pr_4NF > Bu_4NF \gg Me_4NBr\ Pr_4NBr > Bu_4NBr$. This order is what would be expected if one assumed that larger ions, regardless of charge, act as structure breakers. Insofar as the tetraalkylammonium ions are concerned, there is a reversal in the effect of increasing the length of the alkyl chains when the temperature is raised from 2 to 43°.

At 25° the situation is not clear, since this is an intermediate temperature. In every case the fluorides are stronger structurants than the bromides (which is consistent with our measurements of ΔC_p). The salt Bu_4NF behaves as a water structure former as is also deduced from X-ray diffraction studies.[14] If the covalent H-bond interpretation[8] is rejected, as the results of the present nmr measurements at low temperature together with the measurements of ΔC_p apparently suggest, then at 25° Bu_4NBr appears to be a structure breaker. This is also partially consistent with ΔC_p

(16) F. J. Millero, *J. Chem. Eng. Data*, **16**, 229 (1971).

(17) G. Kalfoglou and H. L. Bowen, *J. Phys. Chem.*, **73**, 2728 (1969).

(18) C. Jolicoeur, N. Dinh The and A. Cabana, *Can. J. Chem.*, **49**, 2009 (1971).

(19) T. S. Sarma and J. C. Ahluwalia, *J. Phys. Chem.*, **74**, 3547 (1970).

(20) E. Wicke, *Angew. Chem., Int. Ed. Engl.*, **5**, 106 (1966).

measurements. This picture is consistent with the variation with concentration of the activity coefficients of the tetraalkylammonium halides as reported in the literature.[21,22] In fluoride solutions it is found that at 25° the activity coefficients are very high. This can be explained through the overall structure-making character of the salt,[21] the structuration of the solution decreasing the activity of water and therefore increasing the activity of the salt. If the bromides are assumed to be structure breakers, then the activity of water is not much decreased by the addition of these salts and the activity coefficients of the bromides should be low as is the case. In addition it should be noticed that from nmr measurements, as the temperature is raised, then the structure-promoting effect of Bu_4NF strongly decreases. This effect is consistent with that observed with the activity coefficients, which are much lower at high temperature than at low temperature, that is the increase of the activity coefficient with the salt concentration in the solution is high at low temperature and low at high temperature. On the other hand, the structure-breaking character of Me_4NBr does not appear to change as much with temperature as does the fluoride. Correspondingly an increase of temperature should not modify but slightly the variation of the activity coefficient of Me_4NBr with its concentration. This is what can be deduced from the data in ref 15.

However the question of the effect of Bu_4NBr on water structure at 25° arises. From nmr measurements it should be a structure breaker at all concentrations. From ΔC_p data it appears to be so at a concentration about 1.2 *m*. From near-infrared measurements,[2,18] it should be a structure former at molalities less than 3.8 and a structure breaker at higher molalities. The increase of the time of reorientation of water in the vicinity of the butyl chains of the salt[3] is given two different explanations. It may be due to either structure making[3] or the action of dispersion forces between water molecules and the protons of the methylene groups.[8] Then the answer to the question should depend on the relative confidence which is given to each experimental method. In addition the salt may be a structure breaker of the initial structure of pure water, but it may produce a structure of a different type in which it may play a prominent role through cation–cation interactions[23] (which have been neglected in the discussion), and stabilization of water molecules through dispersion forces.

It may be concluded that Frank's concept of structure making by large organic ions is consistent with our results at low temperature, but that the effect of tetrabutylammonium bromide on water is still an open question.[24]

(21) S. Lindenbaum and G. F. Boyd, *J. Phys. Chem.*, **68**, 911 (1964).

(22) W.-Y. Wen, S. Saito, and C. M. Lee, *ibid.*, **70**, 1244 (1966).

(23) F. Franks and H. T. Smith, *Trans. Faraday Soc.*, **63**, 2586 (1967).

(24) NOTE ADDED IN PROOF. An interpretation of high ΔC_p is given by M. Lucas and A. de Trobriand, *C. R. Acad. Sci.*, in press.

Proton Magnetic Resonance Investigation of the Environment of Aromatic Compounds in Aqueous Zwitterionic Micellar Solutions[1]

by E. J. Fendler,[2] C. L. Day, and J. H. Fendler*

Department of Chemistry, Texas A&M University, College Station, Texas 77843 *(Received October 26, 1971)*

Publication costs assisted by the U. S. Atomic Energy Commission

Interactions of benzene, nitrobenzene, 2,4-dinitrophenyl sulfate, its *in situ* hydrolysis products, and 2,4-dinitrophenoxide ion with micellar 3-(dimethyldodecylammonio)propane-1-sulfonate, DDAPS, have been investigated in aqueous solutions by pmr spectroscopy. Proton magnetic resonance frequencies of benzene and nitrobenzene protons as well as those of the terminal CH_3, the dodecyl CH_2, the $N-(CH_3)_2$, and the CH_2SO_3 shift linearly upfield as a function of solubilizate concentration. The dependence of the resonance frequencies on the solubilizate concentration and the limiting values are discussed critically and compared to previously obtained values for other micellar systems. It is proposed that both benzene and nitrobenzene interact primarily with the charged surface of DDAPS but that the dynamic solubilization site of the latter is somewhat closer to the micelle interior than that for benzene. Chemical shift determinations for the benzene–sodium dodecyl sulfate, NaLS, system, and those available for the CTAB–benzene system suggest that benzene is mainly in the interior of the NaLS micelle but is located near the surface of CTAB and DDAPS. A reactive substrate, 2,4-dinitrophenyl sulfate, is located primarily in the micelle interior, whereas its *in situ* hydrolysis product and 2,4-dinitrophenoxide ion interact to a greater extent with the polar head groups.

Introduction

Catalysis of organic reactions by micelles has been discussed in terms of substrate solubilization and rate differences in the micellar and bulk phases.[3,4] The environment of solubilized substrates in the micellar phase and the nature of the substrate–micelle interactions are, therefore, of great importance. Proton magnetic resonance spectroscopy has been utilized to obtain information on the environment of benzene,[5-7] nitrobenzene,[6] phenol,[8] *N,N*-dimethylaniline,[6] and cyclohexane[6] in aqueous cationic micellar hexadecyltrimethylammonium bromide, CTAB, and anionic micellar sodium dodecyl sulfate, NaLS. Although of great potential interest, no previous pmr investigations have been carried out either on the interaction of reactive substrates and their products with micelles or on that of any organic compounds with a zwitterionic micellar surfactant. We have investigated, therefore, the pmr spectra of micellar 3-(dimethyldodecylammonio)propane-1-sulfonate, DDAPS, as a function of increasing solubilizate concentration as well as the spectra of the organic solubilizates, and substrates, themselves in a micellar environment. Our choice of benzene and nitrobenzene as solubilizates allows comparisons of the solubilization by cationic, anionic, and zwitterionic surfactants. We have used benzene, nitrobenzene, potassium 2,4-dinitrophenyl sulfate, its *in situ* hydrolysis products, and 2,4-dinitrophenoxide ion as substrates. Examination of a reactive system, such as the hydrolysis of 2,4-dinitrophenyl sulfate, affords direct correlations between micelle–substrate interactions and micellar catalysis of the rate of hydrolysis.

Experimental Section

Reagent grade benzene (Baker and Adamson), nitrobenzene (Fisher), and *p*-nitrophenol (Fisher) were checked for purity (spectra and melting point) and were used without further purification. Potassium 2,4-dinitrophenyl sulfate was prepared and purified as previously described.[9]

3-(Dimethyldodecylammonio)propane-1-sulfonate, DDAPS, was prepared by the addition of 85.36 g (0.40 mol) of *N,N*-dimethyldodecylamine (Pfaltz and Bauer) to a stirred solution of 48.86 g (0.40 mol) of 1,3-propane sultone (Aldrich) in 400 ml of reagent grade acetone. The reaction mixture was stirred for *ca.* 2 hr, cooled, and filtered. After two recrystallizations from methanol–acetone (10/90, v/v) and drying *in vacuo* over phosphorus pentoxide, the shiny white crystals of DDAPS decomposed at *ca.* 250–255°. The purity of DDAPS was established by the absence of a minimum in its surface tension as a function of concentration determined at 25.0° using a du Noüy ten-

(1) Supported, in part, by the U. S. Atomic Energy Commission.

(2) National Institutes of Health Research Career Development Awardee.

(3) E. H. Cordes and R. B. Dunlap, *Accounts Chem. Res.*, 2, 329 (1969).

(4) E. J. Fendler and J. H. Fendler, *Advan. Phys. Org. Chem.*, 8, 271 (1970).

(5) J. C. Eriksson and G. Gillberg, *Surface Chem.*, 148 (1965).

(6) J. C. Eriksson and G. Gillberg, *Acta Chem. Scand.*, 20, 2019 (1966).

(7) T. Nakagawa and K. Tori, *Kolloid Z.*, 194, 143 (1964).

(8) J. J. Jacobs, R. A. Anderson, and T. R. Watson, *J. Pharm. Pharmacol.*, 23, 148 (1971).

(9) E. J. Fendler and J. H. Fendler, *J. Org. Chem.*, 33, 3852 (1968).

siometer. The critical micelle concentration at 25.0° in doubly distilled water was found to be 1.2×10^{-3} *M*.

Pmr spectra (60 MHz) were obtained with a modified Varian Associates A-60 spectrometer at ambient probe temperature (41 ± 0.5°) or at 26 ± 0.5° (probe temperature maintained with a V-6040 variable temperature controller). The probe temperature was monitored with methanol before and after each scan and was found to remain constant within the limits of detection. All spectra were determined on solutions of DDAPS in water using a capillary containing a 10% solution of tetramethylsilane (TMS) in chloroform as an external standard; chemical shifts are given on the δ scale in parts per million relative to TMS (δ 0 ppm) or in ν values in hertz at 60 MHz (TMS 0 Hz) and are accurate to at least ±0.02 ppm. In all cases, the resonance frequency of the solvent water relative to the standard at a given temperature exhibited a negligible shift over the surfactant concentration range employed, and consequently bulk susceptibility corrections were not applied. The samples were prepared immediately prior to determination of their spectra. The chemical shift data are the average of at least three spectra obtained after temperature equilibrium at sweep widths of 250 and 500 Hz. At sweep widths of 250 Hz, the chemical shifts of the downfield protons were measured from the external chloroform (ν 435.5 Hz) and those of the upfield protons from the external TMS. The calibration of the spectrometer remained constant in all determinations. The spectra of 2,4-dinitrophenyl sulfate were obtained on samples at pH 9.00 (0.05 *M* DDAPS adjusted with 5.00 *M* potassium hydroxide). The spectra of "hydrolyzed" 2,4-dinitrophenyl sulfate were obtained on samples of the substrate after complete hydrolysis (determined spectrophotometrically at the λ_{max} of the phenoxide ion, 358 nm, using linear Beer–Lambert plots).

The pH measurements of the solutions of 2,4-dinitrophenyl sulfate and 2,4-dinitrophenoxide ion were carried out using a Radiometer PHM-26 expanded scale pH meter.

Results and Discussion

Pmr Spectra of Aqueous Micellar DDAPS. The pmr resonance frequencies (δ) for micellar 5.0×10^{-1} *M* and nonmicellar DDAPS in D_2O and H_2O are given in Table I. At 60 MHz the spectrum of micellar DDAPS consists of a resonance at 52.5 Hz for the terminal CH_3 protons, a broad resonance centered at 78.0 Hz for the CH_2 protons in the hydrocarbon chain, an apparent doublet centered at 173.0 Hz for the methylene protons adjacent to the sulfonate group, a broad resonance for the *N*-methyl protons centered at 186.0 Hz, and a multiplet (an apparent doublet) centered at 203.0 Hz for the $N-CH_2$ protons.

Comparison of these spectra and data for analogous cationic and anionic micelles suggests that the ammonium and sulfonate ions are in close proximity on the micellar surface and are highly hydrated.[4] Ionic micelles in the concentration region just above their critical micelle concentration are considered to be oblate or prolate spheroids.[10] A spherical structure for zwitterionic DDAPS micelles can be visualized in which the 12 carbon atom chains are randomly coiled in the micelle interior and the ammonium and sulfonate groups are located at the micelle–water interface. The structure, however, is not rigid. Micellar surfactants are in a dynamic equilibrium with their monomers (and possibly small *n*mers),[10] and the functional groups may have considerable mobility. Indeed, the absence of appreciable broadening of the resonance lines of the surfactant and solubilizate protons as well as the observation of only one set of resonances for each of the chemically different protons of micellar DDAPS and the solubilizates distinctly indicate that the equilibrium constant between monomers and micelles is greater than the limit for pmr detection at 26–41°, that rotation about the $N-CH_3$ and CH_2-SO_3 bonds is relatively rapid, and that exchange of the solubilizate between the micellar and bulk aqueous phase is rapid on the pmr time scale.

It is also quite probable that the intermediate interior of DDAPS micelles, as well as the Stern layer, contains a significant amount of water. Data for other spherical ionic micellar systems amply support this postulate.[11,12] Pmr investigations of the spin-

Table I: Chemical Shifts of DDAPS in Water and Deuterium Oxide[a]

	[DDAPS], *M*				
	0.50		1.0×10^{-1}	1.0×10^{-2}	1.0×10^{-3}
δ	H_2O	D_2O	D_2O	D_2O[b]	D_2O[b]
CH_2CH_3	0.875 0.866[c]	0.866	0.870	0.834	
CH_2CH_3	1.300 1.283[c]	1.292	1.298	1.254	1.233
$N(CH_3)_2$	3.100 3.100[c]	3.102	3.108	3.070	3.029
CH_2SO_3[d]	2.883 2.867[c]	2.872	2.878	2.820	
NCH_2	3.383 3.367[c]	3.372	3.473	3.360	

[a] In parts per million relative to TMS at 41° and 60 MHz unless specified otherwise. [b] At 31° and 100 MHz (Varian Associates HA-100 with a Hewlett-Packard 200 ABR audio-oscillator and frequency counter). [c] At 26°. [d] Chemical shifts of the more intense lower field resonance line of the apparent doublet are 2.941 (41°) and 2.925 ppm (26°) in H_2O and 2.930 ppm (41°) in D_2O.

(10) J. L. Kavanau, "Structure and Function in Biological Membranes," Vol. 1, Holden-Day, San Francisco, Calif., 1965.

(11) W. L. Courchene, *J. Phys. Chem.*, **68**, 1870 (1964).

(12) A. S. Waggoner, O. H. Griffith, and C. R. Christensen, *Proc. Nat. Acad. Sci. U. S.*, **57**, 1198 (1967).

lattice relaxation times of the water protons in aqueous micellar sodium alkyl sulfate solutions[13] have demonstrated that the mobility of water is decreased in micellar solutions and suggest that water molecules near the micellar surface may be in close proximity to the hydrophobic hydrocarbon chain and conceivably are in simultaneous contact with more than one chain. Additionally, ionic micelles generally have a "rough" or "loose" surface, in which the head groups interact with water molecules and some of the hydrocarbon chains protrude into the outer layer or the aqueous phase.[14] Investigations of the ^{19}F magnetic resonance shifts of surfactants of the type $CF_3(CH_2)_n$-COO^-Na^+ also have indicated that the terminal CF_3 groups remain, at least partially, exposed to water molecules even though they are well removed from the micellar surface.[15] Precise pmr data for the solubilization of benzene in sodium dodecanoate, polyoxyethylene(23) lauryl ether, and other media[16] also indicate water penetration into the micelle interior. These results contradict the "classical" spherical micelle model, in which water is located only at the micellar surface and the interior consists of an essentially nonaqueous or "hydrocarbonlike" environment.

Solubilization of Benzene and Nitrobenzene. The pmr resonance frequencies for 0.50 *M* DDAPS and those for benzene and nitrobenzene as a function of the concentration of the latter are given in Tables II and III. It is apparent that both benzene and nitrobenzene are solubilized by DDAPS, since their solubilities in water are 2.4×10^{-2} [17] and 7.3×10^{-3} *M*,[18] respectively. Increasing concentrations of benzene and nitrobenzene result in upfield shifts of the DDAPS protons. The difference in chemical shift ($\Delta\delta$) for the DDAPS protons from 0 to 0.18 *M* benzene is in the order $N(CH_3)_2$ (0.070 ppm) > $CH_2SO_3 \sim CH_2CH_3$ (0.052 ppm) > CH_3CH_2 (0.027 ppm), whereas that for nitrobenzene over the same concentration range is CH_3CH_2 (0.100 ppm) $\gg CH_3CH_2$ (0.400 ppm) $\gtrsim CH_2SO_3 \sim N(CH_3)_2$ (0.035 ppm). Plots of the chemical shifts of DDAPS as a function of the solubilizate concentration exhibit a minor discontinuity in the region of 0.02–0.06 *M* (Figure 1), whereas those for benzene and nitrobenzene are linear over the same concentration range (Figure 2). Similar discontinuities have been observed in the CTAB–benzene and CTAB–nitrobenzene systems.[5,6] The breaks in plots of the observed chemical shifts as a function of benzene and nitrobenzene concentration were interpreted in terms of a change in the solubilization site of the aromatic solubilizate in CTAB micelles.[5] At a concentration of less than 1.0 mol of benzene per mole of CTAB, benzene was proposed to be solubilized by absorption at the micelle–water interface. At higher benzene concentrations, which correspond to the discontinuities in the plots of the observed resonance frequencies for the N–CH_3, –CH_2–, and α-CH_2 protons as a function of solubilizate concentration, absorption saturation occurs and benzene and nitrobenzene are suggested to be located in the interior.[5] Although this interpretation is attractive, one should also consider that at high concentrations of added hydrocarbons, or organic substrate, the micelle structure is most probably perturbed, in terms of size and shape, by the ad-

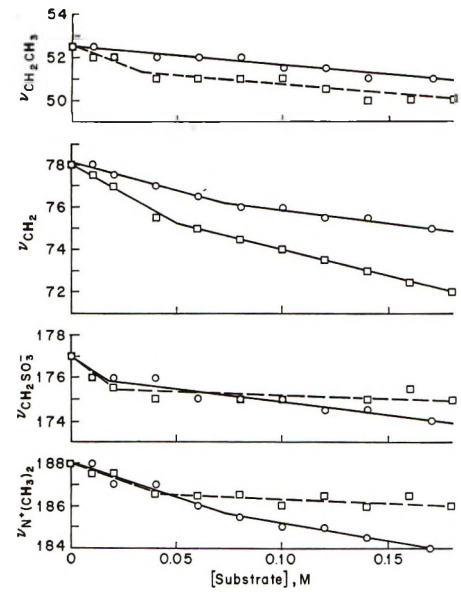

Figure 1. Plots of the observed chemical shifts (ν, Hz) of 0.50 *M* DDAPS at 60 MHz and 41° as a function of benzene (○) and nitrobenzene (□) concentration.

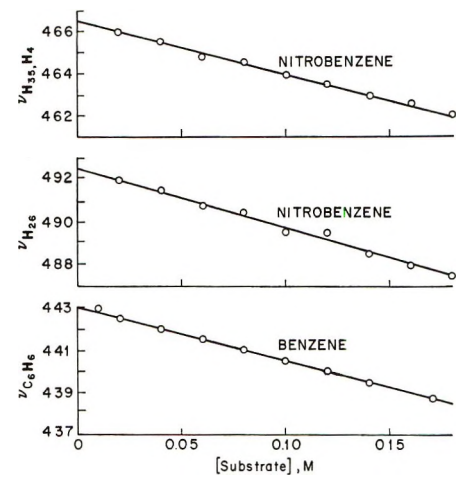

Figure 2. Plots of the observed chemical shifts (ν, Hz) of benzene and nitrobenzene in 0.50 *M* DDAPS at 60 MHz and 41° as a function of benzene and nitrobenzene concentration.

(13) J. Clifford and B. A. Pethica, *Trans. Faraday Soc.*, **61**, 182 (1965).

(14) J. Clifford, *ibid.*, **61**, 1276 (1965).

(15) N. Muller and R. H. Birkhahn, *J. Phys. Chem.*, **71**, 957 (1967).

(16) J. E. Gordon, J. C. Robertson, and R. L. Thorne, *ibid.*, **74**, 957 (1970).

(17) S. J. Rehfeld, *ibid.*, **74**, 117 (1970).

(18) J. H. Fendler and G. L. Gasowski, *J. Org. Chem.*, **33**, 1865 (1968).

ditive. It is possible that the observed discontinuities in the plots of ν for the DDAPS protons as a function of increasing benzene and nitrobenzene concentration (Figure 1) are a consequence of an alteration in the micelle structure, *i.e.*, size, shape, and/or water content, which results in the same average environment for the aromatic solubilizate protons.

Table II: Chemical Shifts of Benzene and of 0.50 *M* DDAPS as a Function of Benzene Concentration[a]

$[C_6H_6]$, *M*	δ				
	CH_3CH_2	CH_2CH_3	$N(CH_3)_2$	CH_2SO_3[b]	C_6H_6
0.01	0.873	1.296	3.112	2.938	7.383
0.02	0.872	1.293	3.107	2.930	7.375
0.04	0.868	1.283	3.095	2.925	7.367
0.06	0.867	1.275	3.085	2.922	7.358
0.08	0.863	1.268	3.077	2.918	7.350
0.10	0.860	1.265	3.070	2.913	7.342
0.12	0.857	1.260	3.065	2.910	7.333
0.14	0.855	1.257	3.058	2.907	7.325
0.16	0.852	1.252	3.053	2.902	7.316
0.17	0.850	1.250	3.050	2.900	7.312
0.18	0.848	1.248	3.047	2.898	7.308

[a] In parts per million relative to external TMS at 41°. [b] Chemical shift of the more intense downfield resonance line of the apparent doublet.

Table III: Chemical Shifts of Nitrobenzene and of 0.50 *M* DDAPS as a Function of Nitrobenzene Concentration[a]

$[C_6H_5NO_2]$, *M*	δ					
					$C_6H_5NO_2$	
	CH_3CH_2	CH_3CH_2	$N(CH_3)_2$	CH_2SO_3[b]	H_{345}[c]	H_{26}[d]
0.01	0.870	1.290	3.112	2.938	...	...
0.02	0.863	1.282	3.105	2.925	7.767	8.200
0.04	0.853	1.263	3.093	2.922	7.758	8.192
0.06	0.850	1.250	3.092	2.922	7.746	8.179
0.08	0.848	1.242	3.090	2.920	7.742	8.175
0.10	0.845	1.233	3.088	2.918	7.733	8.158
0.12	0.843	1.225	3.087	2.918	7.725	8.158
0.14	0.840	1.217	3.087	2.917	7.717	8.142
0.16	0.837	1.208	3.085	2.917	7.708	8.133
0.18	0.835	1.200	3.083	2.915	7.700	8.125

[a] In parts per million relative to external TMS at 41°. [b] Chemical shift of the more intense downfield resonance line of the apparent doublet. [c] Chemical shift of most intense peak of the H_{345} multiplet. [d] Chemical shift of the second downfield resonance line of the H_{26} "quartet."

The observed resonance frequencies of benzene and nitrobenzene in aqueous micellar DDAPS (0.50 *M*) are linear functions of their concentration over the range of 0.01–0.18 *M* (Figure 2). At concentrations greater than *ca.* 0.30 *M* for benzene and *ca.* 0.25 *M* for nitrobenzene, two distinct phases became apparent. In the concentration range of complete homogeneity, the observed chemical shifts were fitted to eq 1, where

$$\nu = \nu_0 + a[X] \quad (1)$$

ν and ν_0 are the observed and limiting chemical shifts and X is the solubilizate, or substrate. Similar relationships have been observed for other surfactants and salts.[15,16] The values of ν_0 and a for benzene and nitrobenzene in DDAPS and in other media are given in Table IV. It is apparent that ν_0 approaches the chemical shift of benzene in water. Such results can be interpreted to imply that benzene and nitrobenzene are solubilized in an aqueous environment of the DDAPS micelle. However, water is not restricted to the surface of the micelle (*vide supra*) and, therefore, resemblence of the extrapolated chemical shifts of benzene to zero surfactant concentration (ν_0) cannot be considered as evidence that the solubilization site is the surface of the micelle. Indeed, ν_0 values in a wide variety of surfactants and short chain tetraalkylammonium bromides approach those for *benzene in water* and in no instance have been found to approach those in cyclohexane (see ν_0 values in Table IV).

A somewhat more meaningful interpretation can be given to the slopes of plots of the observed chemical shifts for the surfactant or solubilizate protons *vs.* the concentration of the added solubilizate, *i.e.*, the a values defined by eq 1 (Table IV, and those for the surfactant protons given below). The upfield shifts of the resonance frequencies and resulting negative a values are indicative of mutual shielding of the surfactant and aromatic protons, *i.e.*, a negative contribution to the local magnetic field by the aromatic ring.

Considering the solubilization of benzene and nitrobenzene in DDAPS it is apparent that the respective a values, obtained from initial slopes, for the aromatic protons (−25 and −34, respectively) and for the terminal CH_3 protons (−9, −37) and the CH_2 protons (−30, −56) of micellar DDAPS are considerably more negative for nitrobenzene than for benzene. It is more significant, however, that initial a values for the protons of the head groups, CH_2SO_3 (−60 for C_6H_6, −76 for $C_6H_5NO_2$) and $N(CH_3)_2$ (−33 for C_6H_6 and −38 for $C_6H_5NO_2$), are more negative in the case of benzene than those for the terminal CH_3 and for the CH_2 groups. The negative a values for the head group protons suggest that both benzene and nitrobenzene are solubilized predominantly in the region of the charged surface of the DDAPS micelle, although the latter compound is "buried" somewhat more deeply, as manifested by the larger negative a values for the terminal CH_3 and the CH_2 protons. A similar situation has been found for the solubilization of these compounds by cationic CTAB.[5,6]

It is instructive to compare the solubilization of benzene in cationic micellar CTAB, zwitterionic DDAPS, and anionic NaLS. In order to allow comparisons of the a values for surfactants of each charge type, we investigated the pmr parameters for the ben-

Table IV: Pmr Parameters for Benzene and Nitrobenzene in Solvents and Aqueous Micellar Surfactants[a,b]

Medium	Benzene		Nitrobenzene			
			$H_{2,6}$		$H_{3,4,5}$	
	ν_0	a	ν_0	a	ν_0	a
Water	441.4[c]		494 ± 2[c]		464 ± 2[c]	
	444.18 ± 0.25[d]	14 ± 17[d]				
	443.82 ± 0.23[d]	13 ± 15[d]				
Cyclohexane	424.3[c]		477.8[c]		442.4[c]	
	425.99 ± 0.21[d]	−2.23 ± 0.18[d]				
	425.62 ± 0.15[d]	−2.16 ± 0.13[d]				
CTAB (0.1729 M)[e]	438.9	∼−39.9	490.9	∼−73	464.5	∼−71
NaLS (0.100 M)	442.0	−66.6				
DDAPS (0.500 M)	442.0	−25.1	492.55	−33.9	466.4	−25.0
Sodium decanoate (0.400 M)[d]	439.13 ± 0.14	−30.8 ± 1.4				
	438.69 ± 0.16	−34.1 ± 1.6				
Polyoxyethylene(23) lauryl ether (2.08×10^{-3} M)[d]	443.80 ± 0.04	+24.0 ± 4.1				
	443.38 ± 0.07	+29.4 ± 5.1				
Tetramethylammonium bromide (1.00 M)[d]	444.33 ± 0.10	−2.1 ± 6.3				
	444.26 ± 0.11	+0.4 ± 6.5				
Tetra-*n*-butylammonium bromide (1.00 M)[d]	442.70 ± 0.04	−5.9 ± 0.54				
	444.01 ± 0.04	−9.1 ± 0.52				

[a] ν_0 is the chemical shift in hertz at 60 MHz in the solvent or that extrapolated to zero surfactant or salt concentration and a is the slope of the line defined by eq 1. [b] See the Experimental Section or the cited reference for experimental conditions. [c] Calculated from data in ref 5 and 6; ν_0 values were calculated using $\nu_{H_2O} - \nu_{CHCl_3}$ (external standard) = 158.8 Hz and $\nu_{TMS} - \nu_{H_2O}$ = 267.7 Hz. [d] Taken from data in ref 16; ν_0 values were calculated using our experimentally determined values at 60 MHz and 41° for ν_{CH_3CN} (122.0 Hz) and ν_{DMSO} (160.5 Hz) in H_2O relative to an external TMS standard (10% TMS in $CHCl_3$).

zene–NaLS system (Table V). The order of the change in chemical shift as a function of benzene concentration for surfactants is NaLS (a = −67) > CTAB (a = −40) > DDAPS (a = −25). The order for the surfactant protons, however, is more informative—for the terminal CH_3 protons the order is NaLS (a = −31) > DDAPS (a = −9) > CTAB (a = −6) and for the CH_2 protons the order is NaLS (a = −54) > CTAB (a = −36) > DDAPS (a = −30). It is evident that the dynamic solubilization site of benzene, *i.e.*, the average environment in the micellar phase, differs in these micellar systems and that benzene is conceivably solubilized near the surface of CTAB and DDAPS micelles whereas it is closer to the interior in NaLS micelles. This conclusion contrasts with a recent suggestion, based on absorption spectrophotometry, that the solubilization site of benzene is the micellar interior for both CTAB and NaLS,[19-21] but it is in agreement with the interpretation of the observed enhanced and decreased reactivity of e_{aq}^- with benzene in micellar CTAB and NaLS, respectively.[22,23]

Solubilization of 2,4-Dinitrophenyl Sulfate, Its Hydrolysis Products, and 2,4-Dinitrophenoxide Ion. The resonance frequencies of 0.50 M DDAPS as a function of the concentration of 2,4-dinitrophenyl sulfate (**1**), its hydrolysis products (2,4-dinitrophenoxide ion and sulfate ion (**2**)), and 2,4-dinitrophenoxide ion (**3**) in the absence of sulfate ion are given in Table VI. Owing to the low intensities of the aromatic protons of **1**, **2**, and **3**, under our experimental conditions, their chemical shifts were not measured.

Table V: Chemical Shifts of Benzene and of 0.10 M NaLS as a Function of Benzene Concentration[a]

$[C_6H_6]$, M	δ		
	CH_3CH_2	CH_3CH_2	C_6H_6
0	0.867	1.300	
0.01	0.867	1.283	7.358
0.02	0.867	1.283	7.342
0.03	0.850	1.267	7.333
0.06	0.842	1.242	7.292
0.08	0.833	1.233	7.283
0.10	0.817	1.217	7.258
0.12	0.800	1.192	7.233

[a] In parts per million relative to external TMS at 40°.

The mechanism for the hydrolysis of 2,4-dinitrophenyl sulfate in water as well as in aqueous micellar systems most probably involves rate-determining sulfur–oxygen bond fission with the elimination of 2,4-dinitrophenoxide ion[9]

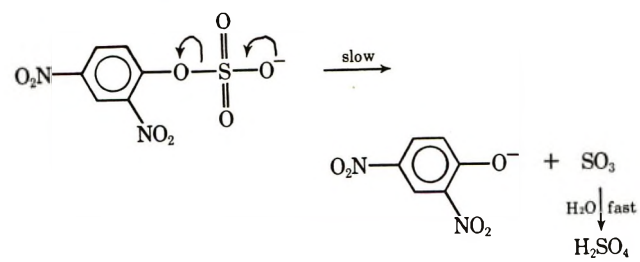

(19) S. J. Rehfeld, *J. Phys. Chem.*, **75**, 3905 (1971).
(20) For a comment on ref 19, see, however, ref 21.

Table VI: Chemical Shifts of 0.50 *M* DDAPS in the Presence of 2,4-Dinitrophenyl Sulfate Anion (Prior (**1**) and Subsequent (**2**) to Hydrolysis) and 2,4-Dinitrophenoxide Ion (**3**)[a]

[Substrate]	δ CH_3CH_2			CH_3CH_2			$N(CH_3)_2$			CH_2SO_3[b]		
	1	**2**	**3**	**1**	**2**	**3**	**1**	**2**	**3**	**1**	**2**	**3**
0.01	0.842	0.865	0.860	1.260	1.285	1.282	3.093	3.108	3.120	2.912	2.933	2.958
0.02	0.837	0.863	0.858	1.253	1.280	1.275	3.092	3.105	3.117	2.910	2.933	2.953
0.04	0.830	0.860	0.855	1.238	1.268	1.262	3.088	3.100	3.110	2.907	2.930	2.943
0.06	0.822	0.858	0.853	1.225	1.256	1.248	3.085	3.095	3.102	2.903	2.927	2.933
0.08	0.815	0.855	0.850	1.212	1.247	1.237	3.082	3.090	3.095	2.900	2.923	2.923
0.10	0.807	0.853	0.848	1.197	1.235	1.223	3.078	3.085	3.088	2.897	2.920	2.913
0.12	0.800	0.850	0.845	1.183	1.223	1.210	3.075	3.080	3.082	2.893	2.917	2.903

[a] In parts per million relative to external TMS at pH 9 and 26°. [b] Chemical shift of the more intense downfield resonance line of the apparent doublet.

This hydrolytic reaction is dependent on the concentration of dipolar aprotic solvents and is relatively weakly catalyzed by micellar surfactants.[24] The magnitude of the micellar catalysis is greatest for zwitterionic DDAPS, less for cationic CTAB, still less for nonionic polyoxyethylene(24) dinonylphenyl ether, and is unaffected by anionic NaLS.[24,25] These micellar rate effects can result from differential solvation of the initial and transition states and from different rates in the micellar and aqueous pseudo phases.[4]

It is apparent from Figure 3 that the chemical shifts of the DDAPS protons as a function of the concentrations of **1**, **2**, and **3** differ markedly. The extrapolated ν_0 values for **1** are identical, within experimental error, with those in water. The relative magnitude of the a values in the presence of **1** is greater for the terminal CH_3 (−23) and for the CH_2 (−42) protons than for the $N(CH_3)_2$ (−9.8) and CH_2SO_3 (−10.4) head group protons, indicating that 2,4-dinitrophenyl sulfate is located primarily in the interior of the DDAPS micelle. This result is not unexpected, since the presence of two nitro groups in the substrate is known to enhance micelle–substrate binding presumably *via* interaction with the hydrophobic parts of micellar surfactants.[4] The observed feeble micellar catalysis of the neutral hydrolysis of **1** in the presence of cationic and zwitterionic micelles[24,25] is not the consequence, therefore, of a lack of favorable binding, but rather of the similarity in the modes of hydrolysis in the micellar and bulk phases. It is significant that the a values for DDAPS in the presence of **2** and **3** are different than those in the presence of **1**. More particularly, the slopes are smaller for the terminal CH_3 protons (a = −8 for **2** and **3**) and for the CH_2 protons (a = −34 for **2** and a = −39 for **3**) than those in the presence of **1**. Conversely, a values for the $N(CH_3)_2$ head group protons (a = −15 for **2** and a = −21 for **3**) are greater for **2** and **3** than for **1**, whereas they are slightly smaller for the CH_2SO_3 head group protons in the presence of **2** (a = −9) and are markedly greater (a = −30) in the presence of **3** than those values in the presence of **1**.

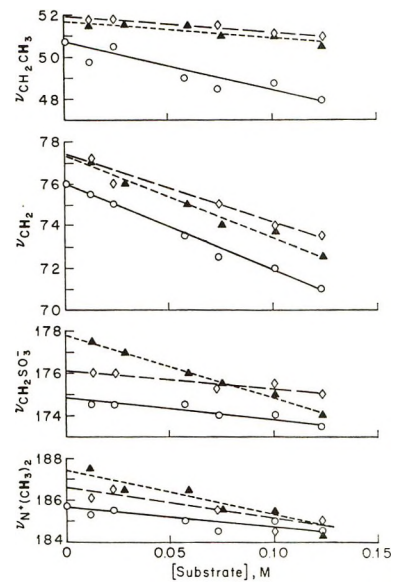

Figure 3. Plots of the observed chemical shifts (ν, Hz) of 0.50 *M* DDAPS at 60 MHz and 26° as a function of the concentration of 2,4-dinitrophenylsulfate (○), its *in situ* hydrolysis products (△), and 2,4-dinitrophenoxide ion (▲).

These results imply that both the *in situ* hydrolysis product (**2**) of **1**, and 2,4-dinitrophenoxide ion (**3**) are apparently in a more polar environment than 2,4-dinitrophenyl sulfate. It is probable that the transition state for the hydrolysis of 2,4-dinitrophenyl sulfate involves an appreciable degree of charge separation and hence resembles the products more than the reactant. One might speculate that the lack of a more

(21) J. H. Fendler and L. K. Patterson, *J. Phys. Chem.*, **75**, 3907 (1971).

(22) J. H. Fendler and L. K. Patterson, *ibid.*, **74**, 4608 (1971).

(23) K. M. Bansal, L. K. Patterson, E. J. Fendler, and J. H. Fendler, *Int. J. Radiat. Phys. Chem.*, **3**, 321 (1971).

(24) E. J. Fendler, R. R. Liechti, and J. H. Fendler, *J. Org. Chem.*, **35**, 1658 (1970).

(25) L. W. Smith, M.S. Thesis, Texas A&M University, 1973.

pronounced micellar catalysis may be the consequence, in part, of an energy loss in transferring the initial state of the substrate to a more polar environment in the transition state. It also should be noted that **3** interacts more strongly than **2** with the protons adjacent to the sulfonate head group (*i.e.*, CH_2SO_3).

Our general conclusion is that considerable care is required in interpreting solubilization sites in micellar systems, since not only is the structure of micelles incompletely understood but also the reactants, transition states, and products may have different environments in the micellar phase.

Additivity in the Carbon-13 Chemical Shifts of 1,2-Disubstituted Ethanes[1]

by G. E. Maciel,*[2] L. Simeral, R. L. Elliott, B. Kaufman, and K. Cribley

Department of Chemistry, Colorado State University, Fort Collins, Colorado 80521, and Department of Chemistry, University of California, Davis, California 95616 *(Received December 1, 1971)*

Publication costs assisted by Colorado State University

^{13}C chemical shifts were obtained on 54 compounds of the type XCH_2CH_2Y, with X and Y varying over the groups H, CH_3, $CH{=}CH_2$, $C{\equiv}CH$, $C{\equiv}N$, C_6H_5, $COCH_3$, OH, OCH_3, Cl, Br, I, and NO_2. The observed range of shifts was 80 ppm. The data were analyzed in terms of an additivity model, with a characteristic α- and β-substituted effect assigned to each group X and Y according to a linear regression analysis. The standard deviation of this analysis was 2.5 ppm, and the groups showing generally poorest additivity behavior were I and H.

Introduction

The use of the ^{13}C nmr (cmr) chemical shift parameter for studying substituent effects emerged early in the history of cmr research. Much of the cmr work of the 1960's was concerned with exploring and cataloging the gross patterns of substituent effects on ^{13}C shieldings, and many of these gross patterns are now fairly well characterized at an empirical level.

One aspect of substituent effects to receive early attention is the extent to which they are additive. A general type of defining relationship for additivity effects in ^{13}C chemical shifts can be summarized in eq 1.

$$^{i}\delta_{P}^{A,B,\cdots} = {}^{i}\delta_{P}^{A} + {}^{i}\delta_{P}^{B} + \cdots \quad (1)$$

In this equation, $^{i}\delta_{P}^{A,B,\cdots}$ represents the chemical shifts of the ith specific carbon of a "polysubstituted" species related to a parent compound P by substitution of the groups A, B, ... at precisely defined positions on P, measured with respect to the ith carbon of P as the chemical shift reference. The symbol $^{i}\delta_{P}^{A}$ represents the chemical shift of the ith carbon of a species related to P by the introduction of a specific substituent A at a specific position. An alternative and equivalent representation of the additivity relationship is embodied in eq 2, where $^{i}\delta_{P,R}$ represents the chemical shift of the ith specific position in P with respect to some chemical shift reference line R.

$$^{i}\delta_{R}^{A,B,\cdots} = {}^{i}\delta_{P}^{A} + {}^{i}\delta_{P}^{B} + \cdots + {}^{i}\delta_{P,R} \quad (2)$$

Previous studies of additivity relationships in ^{13}C chemical shifts,[3-12] based upon relationships like those of eq 1 or 2, or upon specialized variations of them, have been concerned largely with exploring the kinds of systems for which the relationships are applicable within certain arbitrary limits, and to search for specific cases in which the failures of additivity relationships are most dramatic. Such cases of large deviation have been

(1) Supported by National Science Foundation Grants No. GP-8119 and GP-27577.

(2) Address correspondence to this author at the Department of Chemistry, Colorado State University.

(3) P. C. Lauterbur, *J. Amer. Chem. Soc.*, **83**, 1838, 1846 (1961).

(4) G. B. Savitsky and K. Namikawa, *J. Phys. Chem.*, **67**, 2430 (1963).

(5) G. B. Savitsky, *ibid.*, **67**, 2723 (1963).

(6) D. M. Grant and E. G. Paul, *J. Amer. Chem. Soc.*, **86**, 2984 (1964).

(7) G. B. Savitsky and K. Namikawa, *J. Phys. Chem.*, **68**, 1956 (1964).

(8) G. B. Savitsky, R. M. Pearson, and K. Namikawa, *ibid.*, **69**, 1425 (1965).

(9) G. E. Maciel and J. J. Natterstad, *J. Chem. Phys.*, **42**, 2427 (1965).

(10) G. B. Savitsky, P. D. Ellis, K. Namikawa, and G. E. Maciel, *ibid.*, **49**, 2395 (1968).

(11) G. Miyajima and K. Takahaski, *J. Phys. Chem.*, **75**, 331 (1971).

(12) D. E. Dorman, M. Jautelat, and J. D. Roberts, *J. Org. Chem.*, **36**, 2757 (1971).

Table I: ^{13}C Chemical Shifts and Additivity Relationships for $X-C^xH_2-C^yH_2-Y$ Compounds[a]

X	Y	δ^x	δ^y	δ^x_{calcd}[b]	δ^y_{calcd}[b]	Method[c]	Source[d]	δ^i[e]	δ^j
OH	OH	−36.47	−36.47	−37.89	−37.89	1	Ea		
Br	Br	−3.23	−3.23	−6.20	−6.20	1	Ea		
Cl	Cl	−16.93	−16.93	−19.03	−19.03	1	Ea		
$C^iH=C^jH_2$	$CH=CH_2$	−6.31	−6.31	−6.66	−6.66	1; C	Al		
OC^iH_3	OCH_3	−45.02	−45.02	−44.84	−44.84	1; A, B	Al	−31.14	
H	H	+20.25	+20.25	+19.19	+19.19	2	M		
C^iH_3	CH_3	+1.84	+1.84	+2.48	+2.48	2; B, C, E[g]	M	+13.57	
C^iN	CN	+12.58	+12.58	+12.96	+12.96	2; C	Ea	−91.57	
C_6H_5	C_6H_5	−10.72	−10.72	−9.53	−9.53	2; C	Ea		
I	I	−1.67	−1.67	+9.55	+9.55	2	Al		
$C^iOC^jH_3$	$COCH_3$	−9.83	−9.83	−10.08	−10.08	2; C, B	Ea	−179.61	
I	C_6H_5	+20.99	−13.20	+17.01	−16.99	1; C	Ea		
I	C^iH_3	+18.26	0.00	+15.43	−3.40	1; A, B	Ea	+11.63	
I	OH	+13.50	−40.02	+14.68	−43.02	1; C, F	Ba		
I	H	+28.27	+6.19	+23.59	+5.15	1; C, E[f]	Ea		
Br	OC^iH_3	−3.18	−45.47	−4.17	−47.87	1; C	Fr	−31.16	
Br	C_6H_5	−5.76	−12.29	−4.81	−10.92	1; A	Ba		
Br	$CH=CH_2$	−4.45	−10.10	−2.21	−10.65	1; A	Ba		
Br	Cl	−3.81	−16.41	−6.32	−18.91	1; C	Ba		
Br	CN	+0.76	+4.88	+0.04	+6.72	1; A	Ba		
Br	OH	−7.69	−35.73	−7.14	−36.95	1; C	Ba		
Br	C^iH_3	−8.06	+0.64	−6.39	+2.67	1; A, B	Al	+14.29	
Br	H	+0.11	+7.86	+1.77	+11.22	1; C	Ea		
Cl	CN	−12.22	+5.21	−12.67	+6.60	1; C, F	Ea		
Cl	H	−13.03	+8.35	−10.94	+11.10	2; C, E[f]	M		
Cl	C_6H_5	−17.07	−12.08	−17.52	−11.04	1; A	Ea		
Cl	COC^iH_3	−18.80	−11.76	−16.15	−12.96	1; C	Fr	−2.51	
Cl	C^iH_3	−20.04	+0.83	−19.10	+2.55	1; A, B	Ba	+15.07	
Cl	OH	−19.16	−35.87	−19.85	−37.07	1; C	Ea		
CN	C_6H_5	+8.26	−4.23	+8.11	−4.68	1; C	Ea		
CN	OC^iH_3	+8.61	−40.27	+8.75	−40.63	1; A	CS	−31.28	
CN	C^iH_3	+8.40	+7.72	+6.53	+8.91	1; A, B	Ea	+14.19	
CN	H	+16.49	+16.72	+14.69	+17.46	1; B	Ea		
C^iN	OH	+5.72	−30.52	+5.78	−30.71	2; C	Al	−92.89	
OH	H	−30.15	+9.30	−28.98	+10.28	1; A, B	Al		
OH	C^iH_3	−36.65	+1.25	−37.14	+1.73	1; A, B	Al	+17.10	
OH	$CH=CH_2$	−34.57	−10.23	−32.96	−11.59	1; A	Ba		
OH	OC^iH_3	−34.15	−47.26	−34.92	−47.81	1; C	CS	−31.24	
OH	C_6H_5	−36.16	−12.24	−35.56	−11.86	2; C	Ea		
OH	$C\equiv CH$	−43.39	+4.52	−37.37	+5.70	1; C, F	Al		
OC^iH_3	H	−40.67	+12.37	−38.90	+13.25	1; C	P	−30.40	
OC^iH_3	C^jH_3	−47.37	+4.17	−47.06	+4.70	1; C	P	−30.66	+17.05
COC^iH_3	H	−9.17	+19.60	−4.87	+13.98	1; B, C	Ea	−1.50	
COC^iH_3	C^jH_3	−18.10	+9.76	−13.03	+5.82	1; A, B, C	Ea	−1.96	+13.69
COC^iH_3	$CH=CH_2$	−0.91	−15.41	−8.85	−7.89	1; A	Al	−2.22	
C_6H_5	H	−1.91	+11.64	−2.95	+12.61	2; A, C	Ea		
C_6H_5	C^iH_3	−11.12	+2.50	−11.11	+4.06	1; A, B	CS	+13.49	
C_6H_5	$CH=CH_2$	−8.59[i]	−8.44[i]	−6.93	−9.26	1; C	Al		
NO_2	C^iH_3	−50.19	+6.04	−51.00	+6.41	1; B, D	Ea	+16.83	
NO_2	H	−43.65	+15.33	−42.84	+14.96	1; D	Al		
$C^i\equiv C^jH$	C^hH_3	+6.69	+4.96	+6.44	+2.25	1; A, B	KK	−56.51	−41.01
$C^iH=C^jH_2$	H	0.00	+14.28	−2.68	+15.21	2; B, C	Ph	−128.06	−100.89
$CH=CH_2$	C^iH_3	−8.98	+4.83	−10.84	+6.66	1; C	KK	+14.00	
$C^i\equiv C^jH$	H	+15.09	+13.57	+14.60	+10.80	2; C	Fa	−58.55	−40.92
CH_3	H	+10.55	+10.83	+10.64	+11.03	2; C, E[g]	M		

[a] Chemical shifts in parts per million with respect to C_6H_{12}. Positive numbers refer to higher shielding. [b] Values calculated according to eq 3. [c] The numbers 1 and 2 refer to the frequency sweep and Fourier transform modes, respectively. The designations A, B, C, D, and E refer to the methods of peak assignment employed, as indicated in the text. The designation F refers to use of internal dioxane as the reference rather than C_6H_{12}, for reasons of solubility, using the relationship $\delta^s_{C_6H_{12}} = \delta^s_{C_4H_8O_2} - 40.10$ ppm in order to convert the shift of species s with respect to dioxane to the shift of species s with respect to cyclohexane. [d] The source of the compound, according to the key: Ea, Eastman; Al, Aldrich; KK, K and K; Ba, J. T. Baker; M, Matheson; Fr, Frinton; CS, Chemical Samples; Fa, Farchan; Ph, Phillips; P, prepared as indicated in the Experimental Section. [e] Chemical shift of the C^i substituent carbon, as indicated in column X or Y. [f] H. Spiesecke and W. G. Schneider, *J. Chem. Phys.*, **35**, 722 (1961). [g] Reference 6. [h] Chemical shift of the methyl carbon is +14.14 ppm. [i] Assignments of δ^x and δ^y may be reversed.

viewed as betraying a special kind of pairwise interaction that is either absent or largely additive in the cases for which the equation holds within the specified limits. These patterns of additivity and deviations from additivity can be important in providing guidelines and tests for emerging theories of chemical shifts. From a more practical point of view, to the extent that additivity relationships are reasonably valid, they provide a valuable means of making peak assignments and in making optimum choices of experimental systems; these advantages are especially apparent if there is a reliable basis for predicting for what cases one is likely to encounter large deviations from the additivity relationship.

Most of the previously reported results on additivity relationships in ^{13}C chemical shifts were based upon data in which uncertainties of ± 1 ppm are not uncommon. Such uncertainties are appreciable fractions of the magnitude of effects or relationships that may be of interest. As currently available methods of both the continuous wave and Fourier transform types are capable of providing data routinely with precision limits smaller than the above by nearly a factor of 100, a more detailed and precise appraisal seems in order. The present report is concerned with exploring additivity relationships in high-precision chemical shifts in 54 compounds of the type XCH_2CH_2Y, 1,2-disubstituted ethanes, including ethyl compounds (X = H).

Experimental Section

Materials. All compounds except methyl ethyl ether and methyl propyl ether were obtained from commercial suppliers and were used as obtained unless gc or pmr analysis showed purity of less than 98%. In those cases, the materials were distilled. The commercial source of each substance is indicated in Table I. The methyl ethyl ether and methyl propyl ether were prepared by standard Williamson synthesis procedures.[13]

Measurements. The cmr spectra were obtained on natural-abundance samples in one of two modes: (1) center band, frequency sweep at 25.1 MHz on a ^{19}F-locked, synthesizer-based spectrometer system using time averaging, based on modifications of a Varian HA-100 spectrometer described previously;[14] (2) pulse-Fourier-transform mode at 22.6 MHz using a Digilab pulse and FTS/NMR-3 data system interfaced to a Bruker HFX-90 spectrometer. In each mode, both coherent and incoherent proton decoupling were employed. Unless sample volatility required probe cooling, the sample temperature was typically 44 ± 1° in method 1 and typically 38° in method 2. Data precision of about ±0.02 ppm was typical in both modes. Samples were neat liquids containing 10% cyclohexane as an internal standard; this concentration was chosen because of sensitivity limits of method 1, with which the project was initiated.

Results and Discussion

Table I contains the ^{13}C chemical shifts of 54 compounds of the type XCH_2CH_2Y, with X and/or Y spanning the following range of groups: H, CH_3, $CH{=}CH_2$, $C{\equiv}CH$, $C{\equiv}N$, C_6H_5, $COCH_3$, OH, OCH_3, Cl, Br, I, NO_2. Assignments of the carbon resonances were based on the following five approaches: (A) the use of coherent proton decoupling in conjunction with previously assigned proton resonances; (B) off-resonance proton decoupling, for distinguishing between ^{13}C resonances of the two methylene groups of interest and resonances of the carbons in a substituent; (C) comparison with similar compounds with assigned ^{13}C resonances, including the *gross* application of additivity relationships, where such large shift differences are predicted that deviations of a few parts per million would not introduce uncertainties; (D) broadening due to an adjacent ^{14}N nucleus; and (E) resonances for the species have been assigned previously. The specific method(s) of assignment used for each compound is also shown in Table I. Also included in Table I are ^{13}C chemical shifts of some substituent carbons.

In analyzing the data in terms of exploring the extent of validity of additivity relationships, we start with a model that assumes that each substituent X exerts a distinct substituent effect at both the α and β positions. Thus, for a compound $X\text{-}C^zH_2C^yH_2\text{-}Y$

$$^z\delta = \Delta_\alpha{}^z + \Delta_\beta{}^y + \delta_{cx}{}^E \quad (3)$$

$$^y\delta = \Delta_\alpha{}^y + \Delta_\beta{}^z + \delta_{cx}{}^E \quad (4)$$

where δ^z is the chemical shift of the C^z carbon with respect to cyclohexane, $\Delta_\alpha{}^z$ is the substituent effect exerted by X at the α position, and $\delta_{cx}{}^E$ is the chemical shift of ethane with respect to cyclohexane. The data in Table I were subjected to a linear regression analysis[15] based upon eq 3 and 4, and the resulting computed chemical shifts are included in Table I. The substituent effects $\Delta_\alpha{}^z$ and $\Delta_\beta{}^z$ found in this way are collected in Table II. This set of substituent parameters, which accounts for chemical shifts covering a range of 80 ppm, leads to a standard deviation of 2.48 ppm. This is a measure of reliability of this additivity model, with two parameters per substituent and only one basic "structural" parameter. The value of this last parameter was given as 19.19 ppm by the linear regression. This value compares to 20.25 ppm, which was obtained by direct measurement. These results lead to the conclusion that for most X, Y combinations, the chemical shifts can be predicted within useful limits without explicit recognition of the pairwise combinations; only

(13) A. I. Vogel, "A Textbook of Practical Organic Chemistry," Wiley, New York, N. Y., 1952, p 309.

(14) V. J. Bartuska, T. T. Nakashima, and G. E. Maciel, *Rev. Sci. Instrum.*, **41**, 1458 (1970).

(15) Program No. BMDO2R, Biomedical Computer Programs, University of California Publications in Automatic Computation, University of California Press, Berkeley, Calif., 1970.

parameters that specifically recognize each separate substituent are necessary. While there is considerable precedent for such relationships in the cmr literature, these results are still noteworthy in the light of the high concentrations employed and the attendant medium effects that are expected.

Table II: Additivity Constants for Substituent Effects on ^{13}C Shielding

X	$\Delta_\alpha{}^{X\,a}$	$\Delta_\beta{}^{X}$
I	+4.40	−14.04
CN	−4.50	−1.73
C≡CH	−4.59	−8.39
CH_3	−8.55	−8.16
Br	−17.42	−7.97
$CH{=}CH_2$	−21.87	−3.98
$COCH_3$	−24.06	−5.21
C_6H_5	−22.14	−6.58
Cl	−30.13	−8.09
OH	−48.17	−8.91
OCH_3	−58.09	−5.94
NO_2	−62.03	−4.23

$\delta_{cx}{}^{E}$ = 19.19

[a] Values in parts per million, as defined in eq 3 and 4.

Of the 99 shifts of the 54 compounds which were characterized in the analysis, only 15 shifts (corresponding to 11 compounds) showed deviations from additivity, *i.e.*, difference between shift calculated according to eq 3 and experimental shift, greater than or equal to 3 ppm. Within the framework of the working model, such deviations could be due to any of the following effects, some of which are interrelated: (i) conformational effects, (ii) specific intermolecular or intramolecular interactions between X and Y, (iii) variation in C–C–H and/or C–C–X bond angles, and (iv) medium effects. While it is not likely that one could determine the importance of each of these contributions at the present time, two points are worth noting. First, all of the five iodine-containing compounds fall into the list of ten compounds that give large deviations. Iodine, as a substituent, is well known to introduce large and poorly characterized influences into ^{13}C chemical shifts;[16−20] the influences have been attributed from time to time to intramolecular and intermolecular neighbor anisotropy effects, intramolecular and intermolecular dispersion effects, and steric interactions. The second point is that three of the eleven compounds on this list of large deviations have X = H. This may indicate that such compounds have an uncommonly low level of X–Y interaction or related geometry perturbations, considerably lower than the average, so they appear to be the deviant compounds.

It is reasonable that to a considerable extent the factors responsible for the substantial deviations between predicted and experimental chemical shifts that occur in some cases tend to mutually compensate for each other in the linear regression analysis. In this sense, the substituent parameters given in Table II can be considered reasonable estimates of the intrinsic substituent effects that operate at the carbon attached to the substituent and at the carbon atom separated from the substituent by one CH_2 group. The substituent parameters given in Table II are not susceptible to fundamental interpretation by any theories currently available. However, they should provide meaningful guidelines for emerging theories of substituent effects on ^{13}C chemical shifts, as well as for the empirical prediction of experimental chemical shifts.

Acknowledgment. The authors gratefully acknowledge the financial assistance of the National Science Foundation in the purchase of the Bruker spectrometer and the Digilab data system.

(16) H. Spiesecke and W. G. Schneider, *J. Chem. Phys.*, **35**, 722 (1961).

(17) G. B. Savitsky and K. Namikawa, *J. Phys. Chem.*, **67**, 2754 (1963).

(18) G. E. Maciel, P. D. Ellis, J. J. Natterstad, and G. B. Savitsky, *J. Magn. Resonance*, **1**, 589 (1969).

(19) M. R. Bacon and G. E. Maciel, *J. Amer. Chem. Soc.*, submitted for publication.

(20) T. Schaefer, W. F. Reynolds, and T. Yonemoto, *Can. J. Chem.*, **41**, 2969 (1963).

Transport Properties of Polar Gases. Collision Integrals for the Kihara Spherical Core Plus Dipole–Dipole Potential

by A. Das Gupta and T. S. Storvick*

Chemical Engineering Department, University of Missouri—Columbia, Columbia, Missouri 65201
(Received August 18, 1971)

Publication costs assisted by the Engineering Experiment Station, University of Missouri—Columbia

The transport collision integrals for the Kihara spherical core plus dipole–dipole terms are reported. The calculations were performed at fixed orientation during an encounter, and the average collision integral for all orientations was calculated assuming all orientations are equally probable. The potential function parameters are evaluated using the viscosity data for ten polar gases. The experimental data are reproduced within experimental error for all of these gases. The value of the spherical core diameter was used as a fitting parameter. The size of this core was found to be smaller than expected from physical argument.

Introduction

The low-density properties of gases provide a primary source of information about the intermolecular potential functions of simple molecules. The transport collision integrals that come from the Chapman–Enskog solution of the Boltzmann equation have been used extensively to evaluate parameters in the empirical potential functions that are used in these studies. Tabulated values of these collision integrals are available for the 12-6,[1] 9-6,[2,3] 28-7,[3] exp-6,[4] Morse,[5] Kihara,[6] and the sperical-shell potentials.[7] The more elaborate models have been used to describe the properties of quasispherical, polyatomic molecules with some encouraging success.

All real polyatomic molecules have dipole or higher multipole moments, and it is important to compute the effect that these forces have on the transport properties. Monchick and Mason[8] used the Stockmayer 12–6–3 potential model to compute the collision integrals for dipolar gases. The properties of these gases are significantly altered by including the dipole forces. The agreement with the experimental data for polar gases was as good as the previous work for nonpolar gases.

Smith, Munn, and Mason[9] have used the 12–6–5 potential model to represent the transport properties of quadrupolar gases. The effect of the quadrupole moment is much less than the dipole moment, but these corrections should not be neglected when accurate representation is necessary.

The Kihara potential has been extensively used to model the properties of polyatomic gases. It is the purpose of this paper to report the transport collision integrals for the Kihara spherical-core potential with point dipoles located at the center of the core. The collision integrals are computed assuming a fixed orientation[8,9] during an encounter, and the average collision integral is obtained by averaging over all orientations assuming each configuration is equally probable. Potential function parameters obtained from the viscosity data for ten polar gases are reported.

Calculations

The Kihara sperical-core potential has been described in detail elsewhere.[6,10] The extension of this model to include a point dipole at the center of the core has been used by O'Connell and Prausnitz[6] with others[11] to compute the second virial coefficients of polar gases. The form of this potential with the dipole–dipole term added is

$$U = 4\epsilon\left[\left(\frac{\sigma - 2a}{r - 2a}\right)^{12} - \left(\frac{\sigma - 2a}{r - 2a}\right)^{6}\right] - \frac{\mu_1\mu_2}{r^3}G(\theta_1, \theta_2, \phi) \quad (1)$$

where ϵ is the minimum potential energy and σ is the separation when $U = 0$ that would be obtained when

(1) J. O. Hirschfelder, C. F. Curtiss, and R. B. Bird, "Molecular Theory of Gases and Liquids," Wiley, New York, N. Y., 1954, pp 1126–1127.

(2) G. M. Roe, L. F. Epstein, and M. D. Powers, *J. Chem. Phys.*, **20**, 1665 (1952); L. F. Epstein, *ibid.*, **20**, 1670 (1952).

(3) F. J. Smith, E. A. Mason, and R. J. Munn, *ibid.*, **42**, 1334 (1965).

(4) E. A. Mason, *ibid.*, **23**, 49 (1955).

(5) F. J. Smith and R. J. Munn, *ibid.*, **41**, 3560 (1964).

(6) J. P. O'Connell and J. M. Prausnitz, "Advances in Thermophysical Properties at Extreme Temperatures and Pressures," ASME, United Engineering Center, New York, N. Y., 1965, pp 19–31. Tabulated collision integrals available as Document No. 8432, ADI Auxiliary Publications Project.

(7) A. G. DeRocco, T. S. Storvick, and T. H. Spurling, *J. Chem. Phys.*, **48**, 997 (1968).

(8) L. Monchick and E. A. Mason, *ibid.*, **35**, 1676 (1961).

(9) F. J. Smith, R. J. Munn, and E. A. Mason, *ibid.*, **46**, 317 (1967).

(10) A. E. Sherwood and J. M. Prausnitz, *ibid.*, **41**, 429 (1964).

(11) C. S. Lee, J. P. O'Connell, C. D. Myrat, and J. M. Prausnitz, *Can. J. Chem.*, **48**, 2993 (1970).

the dipole moments, μ_1 and μ_2, are zero; $2a$ is the Kihara sperical core diameter; r is the separation of the core centers; and $G(\theta_1, \theta_2, \phi)$ is the dipole orientation function[12]

$$G(\theta_1, \theta_2, \phi) = 2 \cos \theta_1 \cos \theta_2 - \sin \theta_1 \sin \theta_2 \cos \phi \quad (2)$$

In eq 2, θ_1 and θ_2 are the angles of inclination of the dipole vectors with the line connecting the centers of the Kihara cores and ϕ is the azimuthal angle between the two dipole vectors. The value of G is in the range $-2.0 \leqslant G \leqslant 2.0$ for all orientations.

Since we are considering only like molecule interactions, eq 1 can be rewritten as

$$U = 4\epsilon\left[\left(\frac{1 - \gamma^*}{r^* - \gamma^*}\right)^{12} - \left(\frac{1 - \gamma^*}{r^* - \gamma^*}\right)^{6} - \frac{\delta^*}{r^{*3}}\right] \quad (3)$$

where

$$\delta^* = (\delta/2)G(\theta_1, \theta_2, \theta_3) \quad (4)$$

and

$$\delta = \mu^2/2\epsilon\sigma^3 \quad (5)$$

The range of values of δ^* will be $-\delta \leq \delta^* \leq \delta$ when the range of G is substituted into eq 4.

The numerical calculations of the collision integrals can now be made if we assume that a pair of molecules will have a fixed relative orientation during a collision. Monchick and Mason[8] first used this approximation. The physical argument for this assumption is that most of the interaction in any collision occurs in the region of closest approach. One relative orientation approximately describes this collision in the short interval the pair of molecules are close together. Therefore, the collision integrals are calculated for a fixed value of δ^*, and these collision integrals are averaged over all possible orientations to obtain the collision integral that represents the average contribution of a collision to the gas property.

The collision integrals for fixed δ^* and for $\gamma^* = 0.0$, 0.2, 0.4, and 0.6 were computed using the numerical integration scheme described in detail in an earlier paper.[7] These tables were prepared for values of $\delta^* = \pm 2.0, \pm 1.5, \pm 1.0, \pm 0.5$, and 0.0. We estimate that these values of δ^* (or δ) will cover the range of interest for real molecules. The collision integrals $\Omega^{(l,s)^*}$ are defined in the usual way[13] and have a value of unity for a rigid sphere with a diameter σ. The unaveraged collision integrals for viscosity, $\Omega^{(2,2)^*}$, are shown in Figure 1 as functions of the reduced temperature $T^* = kT/\epsilon$ for several values of δ^*. The values of $\Omega^{(l,s)^*}$ at constant T^* are not symmetric about $\delta^* = 0.0$. This dependence on δ^* is nearly parabolic, but at low T^* it has a very sharp minimum at $\delta^* \approx 0.5$.

There is no experimental evidence to support the assignment of weighting factors to particular molecular orientations when the average collision integrals are

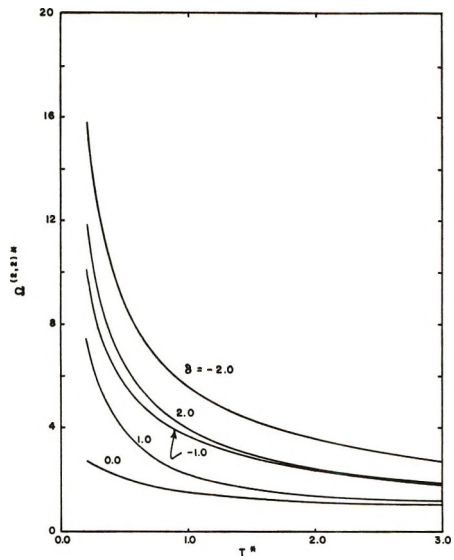

Figure 1. The unaveraged collision integral for viscosity $\Omega^{(2,2)^*}$ as a function of T^* at different values of δ.

calculated. Therefore, we assumed equal weights for each orientation and obtained the averages from

$$\langle\Omega^{(l,s)^*}\rangle = \frac{\int_{-1}^{1} d(\cos\theta_1) \int_{-1}^{1} d(\cos\theta_2) \int_{0}^{2\pi} d\phi \Omega^{(l,s)^*}}{8\pi} \quad (6)$$

The integrations in eq 6 were done numerically using a five-point Gaussian quadrature. A nine-point Lagrangian interpolation was used to obtain $\Omega^{(l,s)^*}$ from the $\Omega^{(l,s)^*}$ *vs.* δ^* tables for values of δ^* in the range $-0.5 < \delta^* < 0.5$ and a four-point Aitken interpolation for all other values of δ^*. The accuracy of the numerical integration methods and the interpolations used to obtain $\langle\Omega^{(l,s)^*}\rangle$ should give an overall accuracy of better than 0.3%. The values at the lowest temperature are subject to the greatest error, because the collision integrals are most difficult to evaluate there.

The average collision integrals are too extensive to be included here, and they can be obtained elsewhere.[13] These tables include $\langle\Omega^{(l,s)^*}\rangle$, for $l = 1, 2, 3$ and $s \geq l$, A^*, B^*, C^*, E^*, F^*, the Kihara approximations to the Chapman–Enskog second-order approximation for viscosity, heat conductivity, and diffusion, and the isotopic thermal diffusion factor. All of these quantities have been defined in an earlier paper.[7]

Comparison with Experimental Data

The usual procedure used to test a potential model is to adjust the potential parameters until the calculated

(12) Reference 1, p 27.

(13) Tables of the collision integrals and auxillary functions in the Chapman–Enskog theory will appear immediately following these pages in the microfilm edition of this volume of the journal. Single copies may be obtained from the Books and Journals Division, American Chemical Society, 1155 Sixteenth Street, N.W., Washington, D. C. 20036, by referring to code number JPC-72-1470. Remit check or money order for $5.00 for photocopy or $2.00 for microfiche.

Table I: Potential Parameters Determined for Several Substances on the Basis of Different Models

Substances	Kihara spherical core plus dipole–dipole ϵ/K, °K	σ, Å	$2a$, Å	δ_{max}	Kihara spherical core ϵ/K, °K	σ, Å	$2a$, Å	Stockmayer ϵ/K, °K	σ, Å	δ_{max}	Lennard-Jones ϵ/K, °K	σ, Å
Ammonia[a-c,e]	424.70	2.99	0.03	0.69	456.76	3.04	0.02	434.52	2.97	0.69	437.89	3.07
Acetone[e]	459.69	5.00	0.36	0.49	466.53	5.09	0.42	388.50	5.15	0.54	409.32	5.20
Chloroform[e]	434.72	5.33	0.84	0.06	441.75	5.30	0.76	382.22	5.38	0.06	382.26	5.38
Ethanol[e]	469.72	4.48	0.44	0.25	478.14	4.49	0.46	333.39	4.80	0.28	358.08	4.75
Hydrogen sulfide[b,e]	354.32	3.51	0.11	0.20	353.81	3.52	0.05	344.91	3.52	0.20	335.42	3.56
Methanol[e]	435.50	3.79	0.19	0.42	463.51	3.79	0.20	395.68	3.85	0.44	387.87	3.93
Methylamine[c]	356.69	3.96	0.28	0.25	367.00	3.97	0.35	303.05	4.09	0.27	305.63	4.10
Sulfur dioxide[a,b,d,e]	322.55	4.05	0.29	0.44	329.70	4.09	0.20	300.48	4.10	0.45	292.59	4.18
Sulfuryl fluoride[f]	237.50	4.71	0.85	0.18	246.80	4.70	1.01	185.19	4.90	0.21	184.25	4.91
Water vapor[g-i]	771.03	2.48	0.01	1.04	732.41	2.74	0.01	775.95	2.47	1.04	705.59	2.76

[a] P. K. Chakraborti and P. Gray, *Trans. Faraday Soc.*, **61**, 2422 (1965). [b] A. K. Pal and A. K. Barua, *ibid.*, **63**, 341 (1967). [c] L. G. Burch and C. J. G. Raw, *J. Chem. Phys.*, **47**, 2798 (1967). [d] P. Gray and A. O. S. Maczek, "Proceedings of the Fourth Symposium on Thermophysical Properties," J. R. Moszynski, Ed., ASME, United Engineering Center, New York, N. Y., 1968, pp 380–391. [e] A. K. Pal and A. K. Barua, *Brit. J. Appl. Phys.*, **1**, 71 (1968). [f] K. C. Chang, R. J. Hesse, and C. J. G. Raw, *Trans. Faraday Soc.*, **66**, 590 (1970). [g] B. Latto, *Int. J. Heat Mass Transfer*, **8**, 689 (1965). [h] C. F. Bonilla, S. J. Wang, and H. Weiner, *Trans. ASME*, **78**, 1287 (1956). [i] J. Kestin and H. E. Wang, *Physica*, **26**, 575 (1960).

transport properties agree with the experimental values. The heat conductivity and the thermal diffusion properties are known to be affected by inelastic collisions between the pairs of molecules. The procedure used to obtain the average collision integrals did not treat the internal degrees of freedom, so these properties were not selected for analysis in this work.

The viscosity coefficient is not as sensitive to the inelastic encounters, and accurate experimental measurements are available for several pure gases. According to the classical Chapman–Enskog theory the viscosity coefficient is given by[14]

$$\eta = \frac{266.93 \times 10^{-7}\sqrt{MT}f_\eta}{\sigma^2\langle\Omega^{(2,2)*}\rangle} \qquad (7)$$

where M is the molecular weight and f_η is a slowly varying function of the temperature that corrects for the higher Chapman–Enskog approximations. The value of f_η differs from unity by less than 0.8% over the full range of the potential parameters used in this work.

The potential parameters ϵ/k, σ, and $2a$ were determined by interpolating the average collision integrals $\langle\Omega^{(2,2)*}\rangle$ on T^*, δ, and γ^* using the experimental values of the dipole moments. The "best" set of potential parameters is obtained by minimizing the function

$$\bar{V} = \frac{1}{N-1}\sum_{i=1}^{N}(\eta_i(\text{exptl}) - \eta_i(\text{calcd}))^2 \qquad (8)$$

where N is the number of data points. The potential function parameters obtained by this analysis for ten polar gases are given in Table I. These parameters used with eq 7 represent all of the experimental data within 2% with the exception of steam where larger deviations occur at the lower temperatures.

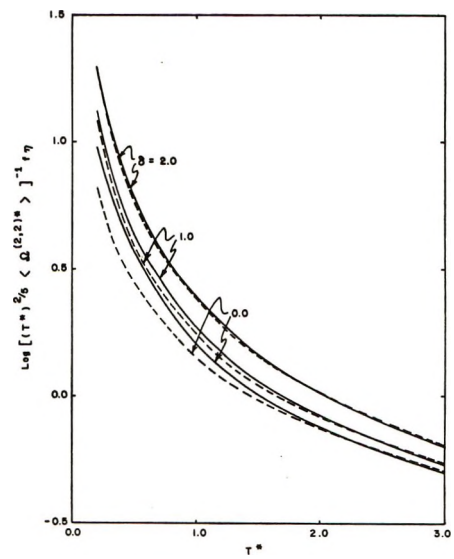

Figure 2. The dimensionless viscosity function *vs.* temperature for $\gamma^* = 0.0$ (- - - -) and $\gamma^* = 0.4$ (——).

Discussion

The influence of the dipole moment on the calculated viscosity values can be studied by rearranging eq 7. The average collision integrals go to infinity as $(T^*)^{-2/5}$ as T^* gets small and they go to zero as $(T^*)^{-1/6}$ as T^* gets large. A plot of the experimental quantity log $[\eta/(M^{1/2}T^{9/10})]$ *vs.* T is equivalent to a plot of log $[(T^*)^{2/5}\langle\Omega^{(2,2)*}\rangle]^{-1}f_\eta$ *vs.* T^* except for numerical scale factors.[9] This plot depends only upon the computed collision integrals, and it is shown in Figure 2 for different values of δ and γ^*. When $\delta = 2.0$, the calculated viscosities for $\gamma^* = 0.0$ and 0.4 are nearly the same for

(14) Reference 1, p 526.

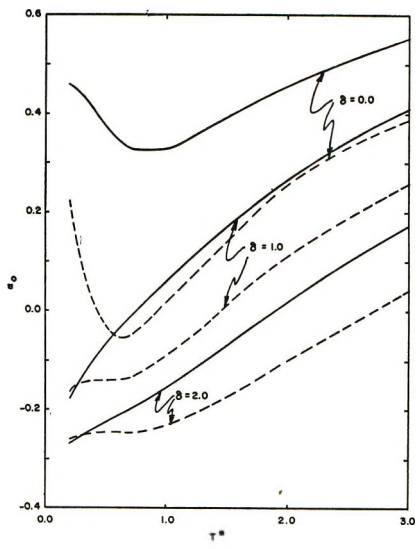

Figure 3. The isotopic thermal diffusion factor α_0 *vs.* temperature for $\gamma^* = 0.0$ (- - - -) and $\gamma^* = 0.4$ (—).

each value of T^*. When $\delta = 0.0$, the viscosity increases as the spherical core size γ^* increases. From this we conclude that the viscosity of a gas increases with the core size but decreases with an increasing dipole moment. This agrees with the fact that an increase in the core sizes increases the back-scattering, which increases $\langle\Omega^{(2,2)*}\rangle$ and decreases η, while an increase in polarity increases the small-angle scattering, which increases $\langle\Omega^{(2,2)*}\rangle$ and decreases the value of η. Consequently, a simultaneous increase in the core size and the dipole moment results in a cancellation of the two effects.

The isotopic thermal diffusion factor α_0 is sensitive to both the core size and the dipole–dipole interaction. In Figure 3, we have plotted α_0 *vs.* T^* for $\gamma^* = 0.0$ and 0.4 and $\delta = 0.0$, 1.0, and 2.0. For nonpolar gases ($\delta = 0.0$), the addition of a very small core removes the temperature inversion of α_0. The inversion temperature for dipolar gases ($\delta \neq 0.0$) increases with increasing δ. The separation of all of the curves with increasing γ^* suggests that α_0 data would be useful for assigning the core size in this model. Experimental difficulties obtaining α_0 produce such large experimental errors in these measurements that this cannot be done with available experimental procedures.

The Kihara spherical core potential parameters were obtained from the viscosity data for ten polar gases, and the results are listed in Table I. The data were fitted assuming the dipole moment was zero ($\delta = 0$) and with the dipole–dipole term added. The spherical core diameters ($2a$) for these substances are smaller than expected from physical considerations, *e.g.*, the bond lengths in the molecule. Furthermore, the energy-scaling factors ϵ/k for only four of the gases (ammonia, methyl alcohol, sulfuryl chloride, and water) are different for these two fitting procedures by more than 3%. The value 3% is about the maximum accuracy we expect to determine ϵ/k from viscosity measurements. Although the values of σ and $2a$ for these two models differ by more than 3%, the value of $\sigma + 2a$ is significantly different for only methyl alcohol and water. This indicates that adjustments in γ^* and δ can be made so that a "good" fit of the viscosity data can be obtained with or without the dipole–dipole term as we observed in Figure 2. Spurling and DeRocco[15] also concluded that the Kihara spherical-core potential with or without the dipole–dipole terms contains enough flexibility to represent the second virial coefficients of polar gases.

The value of $2a$ for the Kihara spherical core with or without the dipole–dipole term must be used as a fitting parameter. There appears to be no systematic way to assign a value to this parameter before fitting the viscosity data to obtain ϵ/k and σ. This is a disadvantage of this model that appears to be overcome by the spherical-shell potential with the dipole–dipole term added.[16]

Table I also contains the potential function parameters obtained from the Stockmayer potential ($\gamma^* = 0.0$) and the Lennard-Jones 12–6 potential ($\gamma^* = 0.0$, $\delta = 0.0$) using the same ten sets of viscosity data. There is a significant difference in the energy and distance scaling parameters for these models and the Kihara spherical core models. The Kihara models generally represent the data more accurately, but we expect this when we have an extra parameter ($2a$) to use in our fitting procedure. We note also that the parameters for the Stockmayer and the Lennard-Jones potentials are in good agreement with those previously reported for these gases.[17]

It would be most useful to compare the Kihara spherical core plus dipole–dipole potential parameters in Table I with the values obtained from second virial coefficient data. The numerical difficulties encountered in summing the series required to obtain the second virial coefficients have been solved, and this work is currently under way.

Acknowledgments. Financial assistance for this work was received from the Department of Defense under Contract No. DAAA 13-68-C-0033 and from the National Science Foundation. Computational services were provided by the Computer Engineering Development Center and the Computational Services Center at the University of Missouri—Columbia.

(15) T. H. Spurling and A. G. DeRocco, *Phys. Fluids*, **10**, 231 (1967).

(16) A Das Gupta and T. S. Storvick, "Proceedings of the Fifth Symposium on Thermophysical Properties," C. F. Bonilla, Ed., ASME, United Engineering Center, New York, N. Y., 1970, pp 160–167.

(17) Reference 1, p 1112.

Comparison of Dynamic with Isothermal Techniques for the Study of Solid State Decomposition Kinetics

by D. W. Johnson, Jr.,* and P. K. Gallagher

Bell Telephone Laboratories, Inc., Murray Hill, New Jersey 07974 *(Received October 4, 1971)*

Publication costs assisted by Bell Telephone Laboratories, Inc.

Three dynamic methods for deriving kinetic parameters from TG data have been used for the sulfate decomposition in the systems beryllium sulfate tetrahydrate, freeze-dried beryllium sulfate, freeze-dried aluminum sulfate, and freeze-dried iron(II) sulfate. The three methods include a difference–differential method, an integral method, and a differential method. The results from the dynamic methods are compared with those from isothermal decomposition studies performed on the same set of samples. It was found that the differential method was the most satisfactory dynamic technique for these systems. Its advantages included the derivation of kinetic parameters which closely reproduced those obtained by isothermal studies and its versatility of use.

Introduction

Dynamic thermogravimetry (TG) methods for deriving kinetic parameters from solid state decompositions have become popular for several reasons. Among these are the following. (1) In the last 15 years several theoretical approaches to the derivation of kinetic parameters from dynamic data have appeared. These techniques were reviewed and categorized quite completely by Flynn and Wall.[1] (2) Dynamic techniques demand less time-consuming experiments than do the isothermal techniques. (3) They allow one to easily follow the reaction over its entire range. (4) They remove the problem of selecting several identical samples as in isothermal analyses.

Dynamic techniques do, however, in some cases give less accurate results than do carefully performed isothermal experiments. The purpose of this work was to perform kinetic analyses on dynamic TG data and compare the results with those obtained by conventional isothermal techniques. The same sample lots were used in these dynamic studies as were used to obtain the published isothermal results for the decompositions in the systems beryllium sulfate,[2] aluminum sulfate,[3] and iron(II) sulfate.[4] The beryllium sulfate system was chosen for a detailed study on the effect of sample sizes and heating rates.

Three popular dynamic techniques were used for the comparative study. These have been outlined by Sharp and Wentworth,[5] and this paper will largely follow their nomenclature. In principle, each of the methods combines the rate equation or equations in question with the Arrhenius equation to eliminate the rate constant. For the reaction order equations this involves the elimination of the rate constant k from the equations

$$\frac{d\alpha}{dt} = k(1 - \alpha)^n$$

and

$$k = A \exp(-E/RT)$$

where α = fraction reacted, t = time, k = rate constant, n = reaction order, A = preexponential term, E = activation energy, R = gas constant, and T = temperature. Also used is the relationship $dT/dt = \beta$ where β is the heating rate.

A special case arises here in order to keep the preexponential term consistent with those previously derived by isothermal techniques.[2-4] For the isothermal studies the fractional order cases ($n = {}^1/_2$ or ${}^2/_3$) were written as the contracting area or volume equations

$$1 - (1 - \alpha)^{1/2} = kt$$

and

$$1 - (1 - \alpha)^{1/3} = kt$$

Upon differentiation these follow the rate

$$\frac{d\alpha}{dt} = k\frac{(1 - \alpha)^n}{1 - n}$$

Therefore, in this study the above rate equation was used for any cases in which $n < 1$. A brief description of each method as applied to this study follows.

(1) J. H. Flynn and L. A. Wall, *J. Res. Nat. Bur. Stand., Sect. A*, **70**, 487 (1966).

(2) D. W. Johnson and P. K. Gallagher, *J. Amer. Ceram. Soc.*, to be published.

(3) D. W. Johnson and P. K. Gallagher, *ibid.*, **54**, 461 (1971).

(4) D. W. Johnson and P. K. Gallagher, *J. Phys. Chem.*, **75**, 1179 (1971).

(5) J. H. Sharp and S. A. Wentworth, *Anal. Chem.*, **41**, 2060 (1969).

Method I

The method by Freeman and Carroll[6] is termed a difference–differential method. For this work adaption of Freeman and Carroll's[6] eq 20 might better be labeled a differential–differential method since two numerical differentiations are used. Also, to be consistent with other terminology the fraction reacted, α, is used. Equation 20[6] then appears as

$$\frac{\mathrm{d}[\log(\mathrm{d}\alpha/\mathrm{d}T)]}{\mathrm{d}[\log(1-\alpha)]} = n - \frac{E}{2.3R}\frac{\mathrm{d}(1/T)}{\mathrm{d}[\log(1-\alpha)]}$$

By plotting $\mathrm{d}[\log(\mathrm{d}\alpha/\mathrm{d}T)]/\mathrm{d}[\log(1-\alpha)]$ *vs.* $\mathrm{d}(1/T)/\mathrm{d}[\log(1-\alpha)]$ the slope is $-E/2.3R$ and the intercept is the order of the reaction. The preexponential term can be derived from the relationship

$$\frac{\mathrm{d}\alpha}{\mathrm{d}T} = \frac{A}{m\beta}(1-\alpha)^n \exp(-E/RT)$$

where $m = 1$ for $n \geq 1$ and $m = 1 - n$ for $n < 1$.

Method II

This is an integral method (no differentiation of experimental curve) developed by Coats and Redfern.[7] For this, one assumes various orders of reaction and compares the linearity of each case to ascertain the correct order. The orders zero, one-half, two-thirds, and first have been used since each of these correspond to a simple model for solid state decompositions. Using this the Coats and Redfern equations[7] become

$$\log\left[\frac{1-(1-\alpha)^{1-n}}{T^2}\right] = \log\left[\frac{AR}{\beta E}\left(1-\frac{2RT}{E}\right)\right] - \frac{E}{2.3RT} \quad \text{for } n \neq 1$$

and

$$\log\left[\frac{-\ln(1-\alpha)}{T^2}\right] = \log\left[\frac{AR}{\beta E}\left(1-\frac{2RT}{E}\right)\right] = \frac{E}{2.3RT} \quad \text{for } n = 1$$

This approach uses the fact that

$$\log\left[\frac{AR}{\beta E}\left(1-\frac{2RT}{E}\right)\right]$$

is nearly constant. By plotting the appropriate left side of the above equations *vs.* $1/T$, the slope equals $-E/2.3R$ and the intercept equals

$$\log\left[\frac{AR}{\beta E}\left(1-\frac{2RT}{E}\right)\right]$$

thus allowing calculation of the activation energy E and preexponential term A. In this study the average temperature for the reaction range was used for the calculation of the preexponential term A.

Method III

The general differential technique was originated by Achar, Brindley, and Sharp[8] and was rederived by Sharp and Wentworth.[5] It offers the advantage of not being restricted to reaction order type models as with methods I and II but can be adapted to any kinetic model in which the rate can be expressed as a faction of α. Again, one plots the data for each of the selected models and compares the linearity to define the appropriate model. The defining equation is

$$\log\left[\frac{\mathrm{d}\alpha/\mathrm{d}T}{\mathrm{f}(\alpha)}\right] = \log\frac{A}{\beta} - \frac{E}{2.3RT}$$

The function $\mathrm{f}(\alpha)$ is derived from the form $\mathrm{d}\alpha/\mathrm{d}t = k\mathrm{f}(\alpha)$. Thus for order-type reactions

$$\frac{\mathrm{d}\alpha}{\mathrm{d}T} = k\frac{(1-\alpha)^n}{m}$$

and

$$\mathrm{f}(\alpha) = \frac{(1-\alpha)^n}{m}$$

where $m = 1$ for $n = 1$ and $m = 1 - n$ for $n < 1$. Another example used in this study is the Erofeev equation

$$[-\ln(1-\alpha)]^{1/n} = kt$$

$$\frac{\mathrm{d}\alpha}{\mathrm{d}t} = kn(1-\alpha)[-\ln(1-\alpha)]^{1-1/n}$$

$$\mathrm{f}(\alpha) = n(1-\alpha)[-\ln(1-\alpha)]^{1-1/n}$$

Again by plotting $\log[(\mathrm{d}\alpha/\mathrm{d}T)/\mathrm{f}(\alpha)]$ *vs.* $1/T$ one can calculate the activation energy and pre-exponential term from the slope and intercept.

Experimental Section

Previously prepared and characterized samples of beryllium sulfate tetrahydrate,[2] freeze-dried beryllium sulfate,[2] freeze-dried aluminum sulfate,[3] and freeze-dried iron(II) sulfate[4] were used. Samples (0.6–12 mg) were loaded onto a platinum pan at room temperature and heated in oxygen at a constant rate in a digital recording thermobalance described by Gallagher and Schrey.[9] This device generates a set of weight and temperature points (about 500–1000 over the temperature range 25–1000°).

These data are then processed in several steps using a GE-Honeywell 635 computer. First, the weight data are converted into α, fraction reacted. For methods I and III the value of $\mathrm{d}\alpha/\mathrm{d}T$ is calculated for each datum point by least-squares fitting a quadratic poly-

(6) E. S. Freeman and B. Carroll, *J. Phys. Chem.*, **62**, 394 (1958).
(7) A. W. Coats and J. P. Redfern, *Nature*, **201**, 68 (1964).
(8) B. N. N. Achar, G. W. Brindley, and J. H. Sharp, *Proc. Int. Clay Conf., Jerusalem*, **1**, 67 (1966).
(9) P. K. Gallagher and F. Schrey, *Thermochim. Acta*, **1**, 465 (1970).

nomial to the nine α *vs.* T data points centered around the point in question. The slope is then derived for the point using this analytical expression. The slopes $d[\log (d\alpha/dT)]/d[\log (1 - \alpha)]$ and $d[1/T]/d[\log (1 - \alpha)]$ in method I are calculated in an exactly analogous fashion.[10] The appropriate functions described earlier for each method are then plotted using a special Xerox graphical terminal unit. Finally, a straight line through the points is calculated using the method of least squares, and the activation energy and preexponential terms are calculated from this line.

For method I only one plot need be made, and the order of the reaction is described by the intercept provided that the parameters of the reaction do not change during the course of the reaction. For methods II and III, however, a separate calculation needs to be made for each hypothesized kinetic model. This is not tedious using a computer. It is necessary, however, to select parameters which allow the choice of the model which best represents the experimental data. To do this for method II a hypothetical value of α was calculated at each experimental temperature point such that this ideal α would reproduce the least-squares straight line value of the function at that temperature. The standard deviation of these ideal values of α with respect to the experimental α points was used as the degree of fit parameter, and the model which minimized this standard deviation was chosen to represent the data.

For method III it was impossible to calculate the ideal values of α since this treatment contained $d\alpha/dT$. Therefore, the ideal values of $d\alpha/dT$ were similarly calculated and compared with the experimental values to give a standard deviation. It was this parameter which was used to select the appropriate models with method III.

Results

The most complete dynamic study was done on the sufate decomposition of the reagent grade beryllium sulfate tetrahydrate. Therefore, examples of the plots used will be drawn from the data of this study. Figures 1, 2, and 3 are representative plots of the same weight *vs.* temperature data for methods I, II, and III, respectively. The vertical axis is necessarily undefined in Figures 2 and 3 since several forms of the equations are plotted on each figure to illustrate the fit of different orders or different models. The mathematical standard deviation parameters for these data are shown in Table I.

Table II summarizes the results of a study using different sample weights of reagent grade beryllium sulfate, at a heating rate of 2.5°/min. The order of the reaction in these and subsequent tables is the exact intercept value for method I and is one of the four simply modeled values 0, $^1/_2$, $^2/_3$, or 1 for methods II and III depending on the model giving the smallest

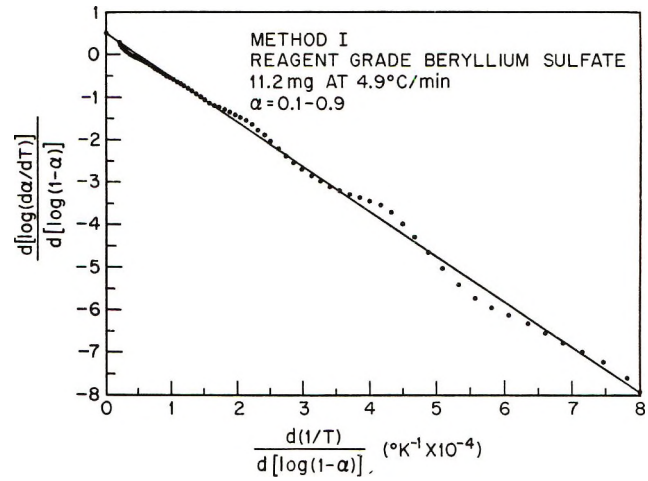

Figure 1. Example of data points with least-squares straight line using method I.

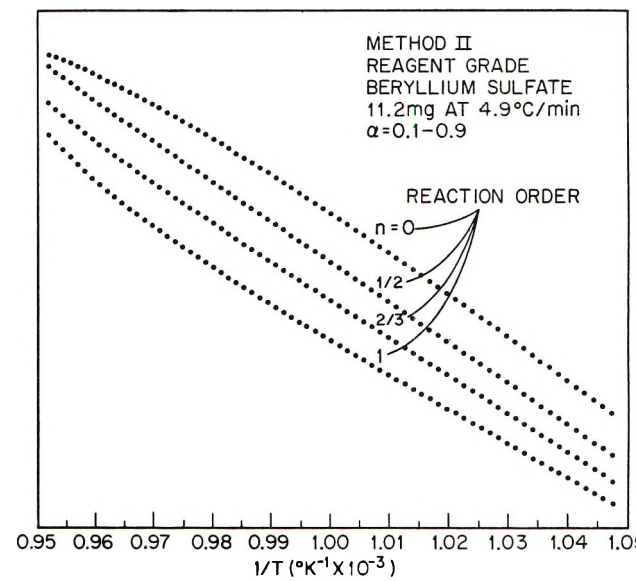

Figure 2. Examples of data sets using various models with method II.

standard deviation. Figures 4 and 5 (methods II and III, respectively) show the graphical data points used to obtain the results in Table II. Table III similarly illustrates the effect of different heating rates for reagent grade beryllium sulfate.

Comparison of the three dynamic methods with the results from the previous isothermal studies are shown in Table IV for freeze-dried beryllium sulfate, in Table V for freeze-dried aluminum sulfate, and in Table VI for freeze-dried iron(II) sulfate. For each system identical ranges of α were used for both the dynamic

(10) Calculation of $d\alpha/dT$ by simple point differences produced no significant changes compared with the above procedure. Calculation of the more complex second derivatives for method I by simple differences caused considerable scatter of points in the plots compared with the smoothed data, but the kinetic parameters were again not changed significantly.

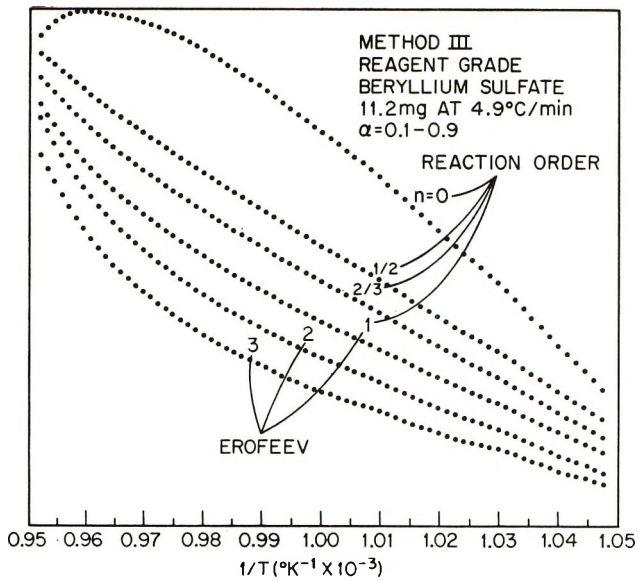

Figure 3. Examples of data sets using various models with method III.

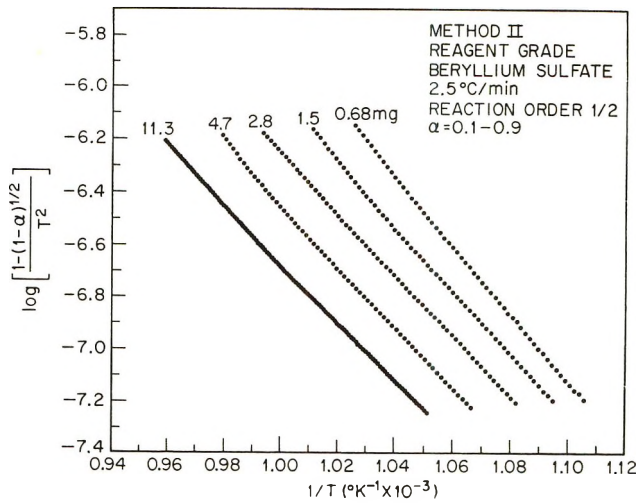

Figure 4. Effect of sample weights using method II.

Table I: Comparison of Standard Deviation for Several Kinetic Models for 11.2 mg of Reagent Beryllium Sulfate Heated at 4.9°/min; α = 0.1–0.9

Method	Kinetic model		Stand dev	Activation energy, kcal/mol	Preexp term, sec^{-1}
I	Order	$n = 0.50$		48	1.3×10^{7}
	Order	$n = 0$	0.022	41	6.5×10^{5}
II		$n = 1/2$	0.002	48	1.3×10^{7}
		$n = 2/3$	0.006	51	3.5×10^{7}
		$n = 1$	0.014	56	2.0×10^{9}
III	Order	$n = 0$	0.0010	31	3.9×10^{3}
		$n = 1/2$	0.0002	49	1.6×10^{7}
		$n = 2/3$	0.0006	54	2.1×10^{8}
	Order or Erofeev	$n = 1$	0.0012	66	2.5×10^{11}
	Erofeev	$n = 2$	0.0010	36	5.1×10^{4}
		$n = 3$	0.0030	26	2.5×10^{2}
Isothermal order		$n = 1/2$		52	4.0×10^{8}

Table II: Effect of Sample Weight for Reagent Beryllium Sulfate Heated at 2.5°/min; α = 0.1–0.9

Method	Sample size, mg	Kinetic model	Activation energy, kcal/mol	Preexp term, sec^{-1}
I	0.68	Order $n = 0.94$	77	2.3×10^{13}
	1.5	$n = 0.48$	56	2.5×10^{9}
	2.8	$n = 0.57$	55	5.8×10^{8}
	4.7	$n = 0.60$	58	1.7×10^{9}
	11.3	$n = 0.33$	47	7.2×10^{6}
II	0.68	Order $n = 1/2$	60	2.1×10^{10}
	1.5	$n = 1.2$	56	1.7×10^{9}
	2.8	$n = 1/2$	53	2.5×10^{8}
	4.7	$n = 1/2$	53	1.9×10^{8}
	11.3	$n = 1/2$	51	3.7×10^{7}
III	0.68	Order $n = 1/2$	63	1.2×10^{11}
	1.5	$n = 1/2$	59	9.3×10^{9}
	2.8	$n = 1/2$	54	3.2×10^{8}
	4.7	$n = 1/2$	58	1.6×10^{9}
	11.3	$n = 1/2$	54	1.3×10^{8}
Isothermal	15–21	Order $n = 1/2$	52	4.0×10^{8}

and isothermal studies. These ranges are beryllium sulfate, α = 0.1–0.9; aluminum sulfate, α = 0.15–0.9; iron(II) sulfate; α = 0.25–0.9.

Discussion

The standard deviation parameters in Table I verify the visual deduction from Figures 2 and 3 that the order $1/2$ model gives the best straight line. It is generally possible to visually choose the best straight line, but the standard deviation parameter gives a quantitative value and is more economical to derive than the plots on a computing machine. Note that the plots for method III generally show a greater degree of nonlinearity for a poor fitting model than do those of equations of method II. It was found that this sensitivity of curvature to degree of fit was quite useful for rapidly rejecting poor fitting models. Also, Figure 3 illustrates the use of method II for models other than order equations even though none of these other models was appropriate for these data.

An attempt was made to adapt other kinetic models (Erofeev and power law) to the method II type of analysis. It became evident, however, that this method was completely insensitive to these models. For instance, a set of data would fit equally poorly to all of the Erofeev equations regardless of the value of the parameter n.

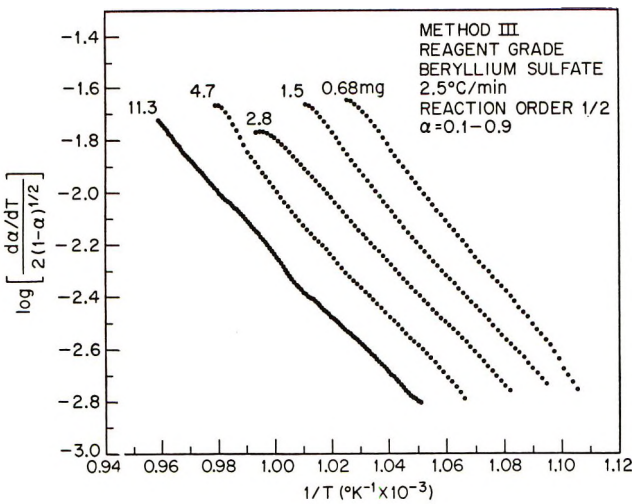

Figure 5. Effect of sample weights using method III.

Table III: Effect of Heating Rate for about 11-mg Samples of Reagent Beryllium Sulfate; α = 0.1–0.9

Method	Heating rate, °C/min	Kinetic model	Activation energy, kcal/mol	Preexp term, sec^{-1}
I	1.2	Order n = 0.56	55	4.8×10^{8}
	2.5	n = 0.33	47	7.2×10^{6}
	4.6	n = 0.50	48	1.3×10^{7}
II	1.2	Order n = 1/2	53	1.8×10^{8}
	2.5	n = 1/2	51	3.7×10^{7}
	4.9	n = 1/2	48	1.3×10^{7}
III	1.2	Order n = 1/2	54	2.7×10^{8}
	2.5	n = 1/2	54	1.3×10^{8}
	4.9	n = 1/2	49	1.6×10^{7}
Isothermal	...	Order n = 1/2	52	4.0×10^{8}

Table IV: Kinetic Results for Freeze-Dried Beryllium Sulfate (0.74 mg at 2.5°/min); α = 0.1–0.9

Method	Kinetic model	Activation energy, kcal/mol	Preexp term, sec^{-1}
I	Order n = 1.14	87	5.2×10^{17}
II	Order n = 1/2	63	3.2×10^{11}
III	Order n = 1/2	64	5.7×10^{11}
Isothermal	Order n = 1/2	54	2.7×10^{9}

The effect of sample size on the kinetic parameters (Table II, Figures 4 and 5) shows reasonably constant activation energies (which correlate well with isothermal results) regardless of sample size with the exception of the smallest sample, 0.68 mg. It is believed that the balance weighings for such small samples are of the lesser accuracy, and a lesser significance is attached to

Table V: Kinetic Results for Freeze-Dried Aluminum Sulfate (2.5–2.7 mg); α = 0.15–0.9

Method	Heating rate, °C/min	Kinetic model	Activation energy, kcal/mol	Preexp term, sec^{-1}
I	2.5	Order n = 0.54	75	2.0×10^{12}
	10	n = 0.06	41	3.3×10^{5}
II	2.5	Order n = 0	47	3.7×10^{6}
	10	n = 0	44	1.3×10^{6}
III	2.5	Order n = 1/2	75	1.7×10^{12}
	10	n = 1/2	59	1.4×10^{9}
Isothermal	...	Order n = 1/2	69	1.9×10^{10}

Table VI: Kinetic Results for Freeze-Dried Iron(II) Sulfate (3.9–4.3 mg); α = 0.1–0.95

Method	Heating rate, °C/min	Kinetic model	Activation energy, kcal/mol	Preexp term, sec^{-1}
I	2.5	Order n = −0.46	19	5.1×10^{1}
	10	n = 0.37	29	2.2×10^{4}
II	2.5	Order n = 2/3	30	1.5×10^{4}
	10	n = 0	29	2.1×10^{4}
III	2.5	Order n = 1/2	32	4.3×10^{4}
	10	n = 1/2	36	1.2×10^{6}
Isothermal	...	Order n = 1/2	49	1.0×10^{9}

these data. The apparent preexponential terms show a general downward trend with increasing sample size. This effect is pronounced in Figures 4 and 5, and it is expected since at any temperature the rate of reaction will be slower for a large sample than for a small one due to lower thermal transfer in the large sample. The data in Table III showing the effect of heating rate again illustrate relatively constant activation energies from all three dynamic methods and again correlate well with the isothermal results. One would expect to see the apparent preexponential terms decrease with high heating rates due to a temperature lag in the samples. This effect is generally seen in Table III. The preexponential terms derived by dynamic methods should extrapolate to the isothermal value for zero heating rates if the sample sizes are similar. This trend is evident in Table III, particularly for methods II and III.

The agreement between methods is not particularly convincing for the data on freeze-dried beryllium sulfate, freeze-dried aluminum sulfate, and freeze-dried iron(II) sulfate in Tables IV, V, and VI. For the freeze-dried beryllium sulfate case an exceptionally small sample weight (0.74 mg) puts in doubt the relia-

bility of the dynamic data. In the case of the aluminum sulfate the agreement with the isothermal results is apparently best using the method III. For the freeze-dried iron(II) sulfate case the reaction is complicated by an intermediate oxidation[11] during the dehydration and decomposition. This complexity could account for the poor correlation. Again, as in general, method III provided results most nearly matching those from isothermal studies.

Summary

The three outlined dynamic methods for deriving kinetic information from TG data have been successfully used for the sulfate decomposition of reagent grade beryllium sulfate tetrahydrate. The apparent activation energies for each of these dynamic methods and from previously described isothermal results were in the range 47–59 cal/mol and were relatively independent of analysis method, heating rate, or sample size. The apparent preexponential terms decreased for increasing sample size or heating rate as expected from a limited rate of thermal transfer.

Use of the dynamic techniques on freeze-dried beryllium sulfate, aluminum sulfate, or iron(II) sulfate produced less consistent results due to excessively small samples or complicated decomposition reactions.

With this outlined experience, these authors have found method III to be the most useful dynamic technique. The results from this method most consistently match the isothermal results in terms of kinetic model, activation energy, and preexponential term. The method is a sensitive one in that the plots are nearly linear for the proper model but are generally highly skewed for other models. Finally, the method has the powerful advantage of accepting kinetic models other than the reaction order type.

Acknowledgments. The authors wish to thank D. J. Nitti and F. Schrey for their assistance in gathering and processing these data.

(11) P. K. Gallagher, D. W. Johnson, and F. Schrey, *J. Amer. Ceram. Soc.*, **53**, 440 (1970).

An Approximate Equation of State. II. A Simplified Form for the Barker–Henderson Theory

by R. M. Gibbons

The Gas Council, London Research Station, London, S.W. 6, England *(Received June 11, 1971)*

Publication costs assisted by The Gas Council

The Barker–Henderson theory (BH) with the Lennard-Jones potential is the best approximate theory for dense fluids based on a pairwise potential. The integrals involved in the BH theory can be most easily evaluated in the form proposed by Mansoori, Provine, and Canfield. In this paper it is shown that two of these integrals may be accurately expressed without any numerical integration, as explicit functions of the reduced temperature and volume for the entire fluid density range and that in the range $0.65 < kT/\epsilon < 100.0$ the remaining integrals may be obtained accurately by five-point Simpson's rule integrations. In this form the evaluation of the integrals is quick enough to allow the BH theory to be used conveniently in iterative calculations. The interpretation and determination of the Lennard-Jones force constants for use with the BH theory are discussed. It is shown that the best force constants for B, obtained by Gosman, do not lead to the best agreement for C or give good agreement when used with the BH theory. The basis of the use of the force constants of Michels is reviewed and it is found, in agreement with other authors, that they are good effective force constants but that force constants can be obtained which give better agreement with the experimental vapor pressure and equally good agreement elsewhere. However, the best constants which were found did not eliminate the serious errors in the critical region.

I. Introduction

The perturbation theory of Barker and Henderson (BH)[1–4] for dense fluids is the most accurate theory that has been developed so far for systems of particles interacting with a pair-wise potential. Calculations have been carried out for a number of pair potentials including the Barker and Pompe[3] and Lennard-Jones

(1) J. A. Barker and D. Henderson, *J. Chem. Phys.*, **47**, 2856 (1967).
(2) J. A. Barker and D. Henderson, *ibid.*, **47**, 4714 (1967).

potentials;[2,4] the discussion in this paper is mainly confined to calculations with the Lennard-Jones potential since this appears to be the best "effective" potential. The evaluation of the integrals which occur in the theory, involving the pair potential and radial distribution functions, $u(R)$ and $g(R)$, is somewhat lengthy even with the aid of modern computers. In their original work, Barker and Henderson evaluated these integrals by numerical integration using the tabulations of Bearman and Throop[5] for the Percus–Yevick (PY) $g(R)$ as an approximation for the true $g(R)$ for hard spheres. In later work they obtained $g(R)$ for the PY equation analytically[6] for the region $1 < R < 5.0$. Mansoori, Provine, and Canfield (MPC)[7] reformulated the integrals so that they could be evaluated numerically from the Laplace transforms of the PY $g(R)$ and $u(R)$, and $g(R)$ for $1.0 < R < 2.0$ only since this led to considerably simpler forms for the integrals. All these forms of the BH theory and also the variational form proposed by Mansoori and Canfield[8,9] give very similar results and show good agreement with one another and the Monte Carlo calculations.[10-12]

The calculated values obtained from the BH theory and the Monte Carlo calculations[10-12] have also been compared with experimental data for argon. In order to make this comparison it is necessary to specify the force constants for the Lennard-Jones potential and in all the work done previously these values have been taken as $\epsilon/k = 119.8$ K and $\sigma = 34.05$ nm. With these values for the force constants good agreement is obtained between the calculated values and the experimental data except along the vapor liquid boundary. It is now known[13] that three-body forces form a significant part of the interactions in a real fluid and calculations have been made for the BH theory including a three-body interaction term, but this led to worse agreement with the experimental data than that obtained from the pair interaction alone. These results have been interpreted to mean that the Lennard-Jones potential is not a true pair potential but an "effective" potential which already includes the effect of three-body forces.

It is the purpose of this paper to show that the integrals which occur in the BH theory can be evaluated almost exactly without extensive numerical integration and that the force constants for the Lennard-Jones potential greatly affect the agreement between the values calculated from the BH theory and experimental data for argon. It is shown in section II how the integrals in the BH theory, as reformulated by MPC, can be evaluated with negligible error for the entire fluid phase by a seven-term Taylor series for two of the integrals and five-point Simpson's rule integrations for the remaining integrals.

In the BH theory as formulated in ref 1 and 2 the Lennard-Jones potential is being used as an effective potential which includes the effects of three-body forces. In applying this theory to a real system, such as argon, errors will arise from both the approximations made in deducing the expressions for the BH theory and assumption of pairwise additivity for the molecular interactions and the form chosen for the effective potential. The failure of the effective potential to describe accurately the true pair potential is implicit in the assumption that it can simultaneously describe the effect of both pairwise and three-body forces It is shown in section III that the agreement with experimental data for argon of values calculated from the BH theory with the Lennard-Jones potential depends strongly on the choice of the force constants. Agreement of the BH theory with Monte Carlo values for the same potential is, of course, unaffected by changes in the force constants.

For the virial coefficients B and C this effect is shown by comparisons of experimental data for argon with values calculated from the exact classical expressions for B and C for the Lennard-Jones potential with the Michels[14] and Gosman[15] sets of force constants. Both these sets of constants were obtained from data for B, the Michels values being determined from data in the range 273–473 K and the Gosman values from data in the range 90–300 K and were therefore determined as force constants for the pair potential. The exact classical values for B and C calculated with both these sets of constants do not agree with experimental error with the experimental data, which is a consequence of the inadequacy of the Lennard-Jones potential as a pair potential as noted by other authors.[13,16] For the BH theory this effect is demonstrated by comparing experimental data for argon with values calculated from the BH theory for these two sets of constants and a set obtained by adjusting the BH theory to give best agreement with experimental data for the vapor pressure and orthobaric densities. Since these

(3) J. A. Barker, D. Henderson, and W. R. Smith, *Phys. Rev. Lett.*, **21**, 134 (1968).

(4) J. A. Barker, D. Henderson, and W. R. Smith, *J. Chem. Phys.*, **53**, 508 (1970).

(5) G. J. Bearman and R. J. Throop, *ibid.*, **42**, 2408 (1963).

(6) W. R. Smith and D. Henderson, *Mol. Phys.*, **19**, 411 (1970).

(7) G. A. Mansoori, J. A. Provine, and F. B. Canfield, *J. Chem. Phys.*, **52**, 5295 (1970).

(8) G. A. Mansoori and F. Canfield, *ibid.*, **51**, 4958 (1969).

(9) G. A. Mansoori and F. Canfield, *ibid.*, **51**, 4947 (1969).

(10) W. W. Wood, "Physics of Simple Fluids," H. N. V. Temperley, J. S. Rowlinson, and G. S. Rushbrooke, Ed., North-Holland Publishing Co., Amsterdam, 1968.

(11) I. R. McDonald and K. Singer, *J. Chem. Phys.*, **50**, 2308 (1969).

(12) I. R. McDonald and K. Singer, *Quart. Rev. Chem. Soc.*, **24**, 238 (1970).

(13) J. S. Rowlinson, *Chem. Brit.*, **6**, 525 (1970).

(14) A. Michels, H. Wijkers, and H. Wijkers, *Physica*, **15**, 627 (1949).

(15) A. L. Gosman, R. D. McCarty, and J. G. Hust, NSRDS-NBS 27, (1969).

(16) R. D. Weir, I. Wynne-Jones, J. S. Rowlinson, and G. Saville, *Trans. Faraday Soc.*, **63**, 1320 (1967).

values reflect the errors in the BH theory as well as the assumption of pairwise additivity, it is not possible to separate the errors in these results caused by the assumption of pairwise additivity from those due to the effect of the approximations in the BH theory. It would be possible to separate these effects if the best effective force constants for Monte Carlo calculations were available, and it was because such force constants are not available that the influence of the force constant was examined by using force constants based on the BH theory.

II. Expressions for the BH Theory

Barker and Henderson[1,2] have shown that the change in the free energy of a system of hard spheres caused by perturbing it with a pairwise and additive energy of interaction, $u(R)$, may be approximated, using the "macroscopic" approximation, by the expression

$$\frac{F - F_0}{RT} = \frac{\Delta F}{RT} = \frac{2\pi N}{RT}\rho I_1 - \frac{\pi N}{RT}\rho\left(\frac{\partial\rho}{\partial p}\right)_0 I_2 \quad (1)$$

where

$$I_1 = \int_\sigma^\infty g(d,R)u(R)R^2\mathrm{d}R \quad (2)$$

$$I_2 = \int_\sigma^\infty g(d,R)u^2(R)R^2\mathrm{d}R \quad (3)$$

and $g(d,R)$ is the radial distribution function for a system of hard spheres of diameter d, defined as

$$d = -\int_0^\sigma (e^{-\beta U(R)} - 1)\mathrm{d}R \quad (4)$$

The subscript 0 indicates that F_0 and $(\partial\rho/\partial p)_0$ are properties of the reference hard-sphere system for which Barker and Henderson used the Padé approximant of Ree and Hoover.[17] In this work the hard-sphere system properties are represented by the combination of the solutions of the PY equation proposed by Carnahan and Starling[18] since this equation is in better agreement with the Monte Carlo results for hard spheres and also is easier to extend to mixtures.

To evaluate the integrals in eq 2 and 3 Barker and Henderson approximated $g_0(d,R)$ by the values for the PY radial distribution function. For the Lennard-Jones potential the integrals have been most simply evaluated by MPC, who showed that using the definition of Frisch, *et al.*,[19] for a truncated Lennard-Jones potential, the integrals may be written as

$$I_1 = \int_\sigma^\infty g(d,R)u(R)R^2\mathrm{d}R = \int_0^\infty G(S,d)U_1(C,S)\mathrm{d}S - \int_\alpha^\sigma g(d,R)u(R)R^2\mathrm{d}R \quad (5)$$

$$I_2 = \int_\sigma^\infty g(d,R)u^2(R)R^2\mathrm{d}R = \int_0^\infty G(S,d)U_2(C,S)\mathrm{d}S - \int_\alpha^\sigma g(d,R)u^2(R)R^2\mathrm{d}R \quad (6)$$

where $G(S,d)$ is the Laplace transform of $Rg(d,R)$ and the truncated Lennard-Jones potential is defined as the Laplace transform of $U(C,S)$ where

$$U_1(C,S) = \epsilon/k\ 4/C^6(S^{10}/C^6 10! - S^4/4!) \quad (7)$$

$$U_2(C,S) = 16\epsilon^2/(k^2C^{12})(S^{22}/(22!C^{12}) - 2S^{16}/(16!C^6) + S^{10}/10!) \quad (8)$$

and $C = d/\sigma$. It is readily established that

$$RU(R) = LU_1(S) = 4\epsilon/k\ ((d/R)^{12} - (d/R)^6)R \quad (R > d) \quad (9)$$
$$= 0 \quad (R < d)$$

$$RU(R)^2 = LU_2(S) = 16\epsilon^2/k^2((d/R)^{12} - (d/R)^6)^2R \quad (R > d) \quad (10)$$
$$= 0 \quad (R < d)$$

It is obviously desirable to obtain these integrals as explicit functions of y and T^* since the resulting expressions would be quick and easy to evaluate. This is not possible for all values of y and T^* but for the fluid state y and T^* are restricted to the range $0 < y < 0.45$ and $0.65 < T^*$ since at lower temperatures and higher densities the solid is the stable phase. In practice there is also an upper limit to T^* which is governed by the temperature at which the molecule dissociates or the electronic energy levels start to contribute appreciably to the thermodynamic properties; for most molecules this restricts T^* to values of less than 100.0.

The integrals from 0 to ∞ on the right-hand side of eq 3 and 4 can easily be obtained as explicit functions of y and T^* for the conditions of the fluid phase. $U_1(S,C)$ and $U_2(S,C)$ depend on the reduced temperature solely through the parameter C so it is convenient to write these integrals in the form

$$\int_0^\infty G(S,d)U_1(S,C)\mathrm{d}s = \frac{4\epsilon}{k}\{-A_0/C^6 + A_1/C^{12}\} \quad (11)$$

$$\int_0^\infty G(S,d)U_2(S,C)\mathrm{d}s = \frac{16\epsilon^2}{k^2}\{4A_1/C^{12} - 2A_2/C^{18} + A_3/C^{24}\} \quad (12)$$

where

$$A_n = \int_0^\infty \frac{G(S,d)S^{(4+6n)}}{(4+6n)!}\mathrm{d}S \quad (n = 0, 1, 2, 3) \quad (13)$$

The integrals A_n can be obtained as explicit functions of y by expanding $G(S,d)$ as a Taylor series in y.

(17) F. H. Ree and W. G. Hoover, *J. Chem. Phys.*, **40**, 939 (1964).
(18) N. F. Carnahan and K. E. Starling, *ibid.*, **51**, 635 (1969).
(19) H. L. Frisch, J. L. Katz, E. Praestgaard, and J. L. Lebowitz, *J. Phys. Chem.*, **70**, 2016 (1966).

Table I: The Constants A_{nm} for the Taylor Series Expansions of the Integrals I_1 and I_2[a]

m	$-A_{1m}$	A_{2m}	$-A_{3m}$	A_{4m}
1	0.17098051 01	0.66965421 00	0.33799722 01	0.12350979 01
2	0.20611843 01	0.14137944 01	0.81905065 01	0.31744174 01
3	0.19587719 01	0.34726062 01	0.24643505 02	0.10383922 02
4	0.27089067 01	0.10572803 02	0.93863732 02	0.43420411 02
5	0.31273086 01	0.38498141 02	0.43421295 03	0.22214783 03
6	0.15560788 01	0.16173614 03	0.23583851 04	0.13436417 04
7	0.67851940 02	0.72080959 03	0.14391655 05	0.92671196 04

[a] $A_{nm} = \int_0^\infty S^{(-2+6n)} \frac{\partial^m G}{\partial y^m}(y,d)\mathrm{d}S$

$$A_n = \int_0^\infty S^{(4+6n)} G(S,d)\mathrm{d}S = \sum_{m=0}^{\infty} (y - y_0)^m/m!\, A_{nm} \tag{14}$$

where

$$A_{nm} = \int_0^\infty S^{(4+6n)} \frac{\partial^m G}{\partial y^m}(S,d)\mathrm{d}S$$

Expressions for $\partial^m G/\partial y^m$ can be obtained analytically from the expression for $G(S)$ in (7), and the integrals in eq 14 may be obtained numerically using Simpson's rule. If y_0 is taken as zero, the coefficients of the series correspond to part of the virial series. This choice of y_0 would require the Taylor series to represent the function for the range of arguments $0 < y < 0.45$. To minimize the number of terms in the series, y_0 was taken as 0.2 so the range of arguments of the series lies between $-0.2 < y - y_0 < 0.25$. With this choice for y_0 a seven-term series represents the integrals in I_1 to better than $1:10^5$ and the integral in I_2 to better than $1:10^4$; the constants for these expressions are listed in Table I. Replacement of the exact integrals by the Taylor series will therefore introduce no significant error into the calculated properties of the fluid. Furthermore, these errors occur for the maximum value of the argument of the Taylor series. For other values of the argument it can be shown from the theory of Taylor series[20] that the error must be smaller.

The integrals from d to σ in eq 5 and 6 are much smaller than the other integrals since the integrations are over such a short range of R, varying from 1.0 to $\sim$1.03 at $T^* = 1.0$ to 1.0 to $\sim$1.3 at $T^* = 100.0$. It is sufficient to evaluate them by a five-point Simpsons rule using the form for the PY $g(R)$ given in terms of real variables by MPC. The first and second derivatives of these integrals with respect to y are also required and can be obtained in like manner from the analytical derivatives of the expressions for $g(R)$. It is possible to obtain a Taylor series expansion of these integrals but the limits depend on the temperature, so it is necessary to retain the answer as a function of R as well as y. As a result, there is little advantage in evaluating these integrals analytically instead of by a five-point numerical integration.

The pressure, energy, and entropy for the system can be obtained directly from the free energy by use of standard thermodynamic relationships which, for convenience, are rewritten in terms of reduced quantities as

$$PV/RT = y\partial(F/RT)/\partial y \tag{15}$$

$$U/RT = -T^*\partial(F/RT)/\partial T^* \tag{16}$$

$$S/R = F/RT - U/RT \tag{17}$$

Using these relationships, the explicit expression of the compressibility is

$$PV/RT = (PV/RT)_0 + 6y/T^*\Big[2(I_1 + yI_1') - 1.0/T^* \times \left\{\left(\frac{\partial y}{\partial p}\right)_0 (y\,I_2' + I_2) + \left(\frac{\partial^2 y}{\partial p^2}\right)_0 \left(\frac{\partial p}{\partial y}\right)_0 yI_2\right\}\Big] \tag{18}$$

where I_1 and I_2 are as defined in eq 2 and 3 and a prime indicates a derivative with respect to y. The energy is obtained from numerical differentiation of F with respect to T^* and S from U and F in conjunction with eq 17. In making comparisons with experimental data for U and S it is convenient to compare the deviation from the corresponding ideal property, and for argon the ideal energy and entropy may be expressed as

$$U/RT = U_0(T_0)/RT + {}^3/_2(T - T_0)/T \tag{19}$$

$$S/R = S_0(T_0)/R - \ln(RTV) + {}^5/_2 \ln(T/T_0) \tag{20}$$

where $U_0(T_0)$ and $S_0(T_0)$ are values assigned to the ideal energy and entropy at temperature T_0 and 1 atm.

III. Results

Using the results in eq 1 and 15–18 the reduced properties of argon can be calculated from the BH theory. Some values of Z calculated in this way, us-

(20) W. Kaplan, "Advanced Calculus," Addison-Wesley, Reading, Mass., 1959.

ing the Ree–Hoover–Pade approximant for the hard-sphere functions, are shown in Table II together with values of Z at the same reduced conditions calculated by MPC.[7] The values in columns 2 and 3, respectively, calculated by using the Taylor series expansion for $G(S)$ and by evaluating all the integrals numerically, show there is excellent agreement between the values obtained by these two methods. There are minor differences between the results in column 3 and those of MPC, listed in column 4, which the author was unable to account for, but the values in column 3 agreed within 1 part in 10^4 with values of Z obtained by numerical differentiation of F. The last column of the table shows values of Z obtained using the Starling–Carnahan[18] equation for the hard-sphere functions which agree well with the other values for Z. In the calculations discussed in the rest of this paper the Starling–Carnahan equation is used for the hard-sphere functions since it is simpler, more accurate, and is easily extended to mixtures.

These comparisons of calculated values of Z can be made at the same reduced conditions and so are *independent* of the choice of force constants. However to compare experimental data with calculated values from either the BH theory or Monte Carlo calculations it is necessary to specify the force constants so that the experimental properties corresponding to reduced conditions may be determined. In all previous work with the BH theory the values of 119.8 K and 34.05 nm, obtained by Michels, *et al.*,[14] from data for B in the range 273 K to 473 K, have been used. However, the Lennard-Jones potential is an approximate potential and Gosman[15] has shown that the values 112.4 K and 35.76 nm give best agreement with data for B in the range 90–300 K. Neither of these sets of values gives agreement within the experimental error for B, as can be seen from the plot in Figure 1[21,22] of the errors of the values for B, calculated from the tables in ref 21 for both of these sets of constants. These errors in the calculated values of B are much smaller than the errors in the values for C, calculated from the tables in ref 21, which are shown in Figure 4. This is not surprising as C depends on three-body forces and B does not. Better overall agreement for B and C can be obtained by treating the Lennard-Jones potential as an "effective" potential which includes the effect of three-body forces and by choosing force constants which minimize the combined errors in the calculated values of B and C. Clearly, this will involve *increasing* the errors in the calculated values of B and so, in principle, it will not be possible to obtain "effective" force constants from data for B alone. As

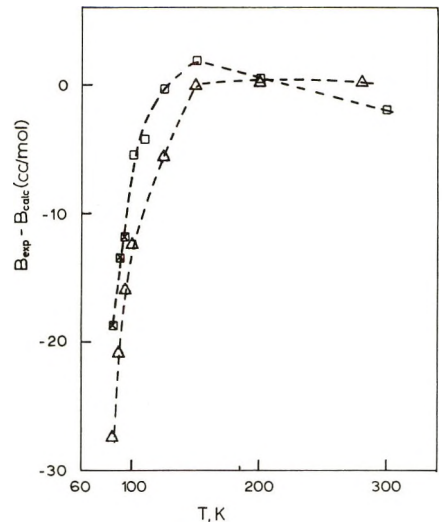

Figure 1. The difference between the experimental values of B taken from ref 22 and values calculated from the exact classical expression for B for the Lennard-Jones potential.[21] The points marked with △ are for Michel's set of constants, and the □ are for Gosman's set of constants.

Table II: Compressibility Factors for the BH Theory with the Lennard-Jones Potential along Selected Isotherms for ϵ/k = 119.8 K and σ = 34.05 nm

y	Z^a	Z^b	Z^c	Z^d
		T^* = 2.74		
0.10472	0.98731	0.98731	0.9878	0.98703
0.20944	1.20916	1.20916	1.21056	1.20699
0.31416	1.93976	1.93976	1.94310	1.93390
0.41888	3.72662	3.72683	3.73292	3.72212
		T^* = 1.35		
0.10472	0.51403	0.51403	0.51489	0.51359
0.20944	0.27326	0.27326	0.27685	0.27060
0.31416	0.65414	0.65415	0.66083	0.64815
0.41888	2.54619	2.54680	2.55523	2.54701
		T^* = 0.722		
0.10472	−0.37122	−0.37123	−0.36905	−0.37203
0.20944	−1.45477	−1.45477	−1.44368	−1.45797
0.31416	−1.85598	−1.85595	−1.83845	−1.86034
0.41888	−0.22475	−0.22338	−0.20825	−0.21517

[a] This work using the Ree–Hoover equation for hard spheres. All derivatives were obtained analytically. The integrals were obtained by Simpson's rule integration using 601 points and a step length of 0.1 for the integrals of $G(S,c)$ and a five-point integration for the integrals of $g(R)$. All computations were done on a UNIVAC 1108 computer; the integrals of $G(S,c)$ were done using 18-digit precision variables. [b] This work using the Ree–Hoover equation for hard spheres and a seven-term Taylor series for the integrals of $G(S,c)$. The coefficients of the Taylor series were obtained by a 601-point Simpson's rule integration using double precision variables and are listed in Table I. [c] Calculated by MPC.[7] [d] This work using the Carnahan–Starling equation for hard spheres and a seven-term Taylor series for the integrals of $G(S,c)$.

(21) J. O. Hirschfelder, C. F. Curtiss, and R. B. Bird, "Molecular Theory of Gases and Liquids," Wiley, New York, N. Y., 1951, pp 1114–1120.

(22) E. B. Smith and J. Dymond, "The Virial Coefficients of Gases," Clarendon Press, Oxford, 1969.

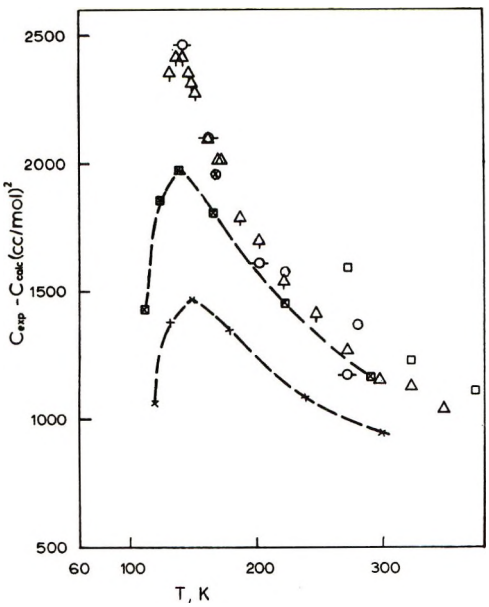

Figure 2. Experimental and calculated values for C. The experimental values represented by △, ▲,-○- and □ were taken from ref 14, 23, 24, and 25, respectively. The other values were calculated from the exact classical expression for C for the Lennard-Jones potential.[21] The points marked with × are for Michel's set of constants, and the ⊠ are for Gosman's set of constants.

can be seen from Figures 1 and 2[23-25] the Michels constants are inferior to the Gosman constants both as force constants for a pair potential and as an "effective" potential for B and C. *A priori* therefore, there are no grounds for using the Michels values as effective force constants for the range 90–300 K. *A posteriori* there is ample justification for their use since they give good agreement with experimental data for both the BH theory and Monte Carlo calculations, though this does not show whether they are the "best" effective constants for this potential. In contrast, as is shown below, the results obtained using Gosman's force constants with the BH theory are in very poor agreement with experimental data despite the fact that the Gosman force constants are better for both B and C.

Clearly, the best "effective" force constants for a particular potential will be based on agreement of some exact (*e.g.*, Monte Carlo) values for that potential with experimental data that depend on three-body forces as well as the pair potential, just as the best force constants for a pair potential are obtained from data for B, which only depends on the pair potential. Since the assumption of pairwise additivity precludes an exact description of a real system, the force constants and the overall agreement with all of the data for the system will depend on the experimental property chosen to determine the best force constants. The accuracy with which an "effective" potential can approximate the behavior of a real system can only be examined by comparing exact calculated values with experimental values using the "best" "effective" force constants.

However, force constants based on agreement of Monte Carlo values with experimental data have not been determined. McDonald and Singer[11] have sought the best force constants for argon based on Monte Carlo values but the values they obtained showed substantial scatter. The effect of varying the force constants was therefore examined by using the results calculated for the BH theory. This has the inevitable disadvantage that the approximations in the BH theory affect the results as well as the errors which arise from the assumption of pairwise additivity. It should be noted, however, that these changes in the force constants do not affect the agreement between the BH theory and Monte Carlo values since it is only the experimental values corresponding to given reduced conditions which are altered.

It remains to specify the property which depends on both pairwise and three-body interactions which is to be used to determine the best effective force constants. Preliminary calculations with the Michels values showed the vapor pressure and orthobaric densities to be the properties most sensitive to small changes in the force constants. The values 117.5 K and 0.3396 nm (hereafter called the "C" set) were obtained by adjusting the force constants so that the values calculated at the conditions of phase equilibria, which are given by

$$p_l = p_g$$

$$F_l + PV_l = Fg + PVg$$

gave best agreement with the experimental data.

The effect of the choice of force constants on the agreement with experimental data of the vapor pressure calculated from the BH theory can be seen in Figure 3. The vapor pressure calculated for the "C" set of constants agrees well with the experimental data but the vapor pressure calculated with the Michels set differs by ~10% even though there are only small differences (~2%) between the two sets of force constants. The vapor pressure calculated for the Gosman constants in Figure 3 show surprisingly good agreement with the experimental data, but as can be seen from Figure 4, the values calculated for the orthobaric densities for this set of constants are grossly in error while both the "C" and Michels sets of constants lead to good agreement with the data.

The calculated single phase properties are much less sensitive to small changes in the force constants as can be seen from the plots of the compressibility

(23) A. Michels, J. M. Levelt, and W. de Graaf, *Physica*, 24, 659 (1958).

(24) R. W. Crain, Jr., and R. E. Sonntag, *Advan. Cryog. Eng.*, 11, 379 (1966).

(25) E. Whalley, Y. Lubien, and W. G. Schneider, *Can. J. Chem.*, 31, 722 (1953).

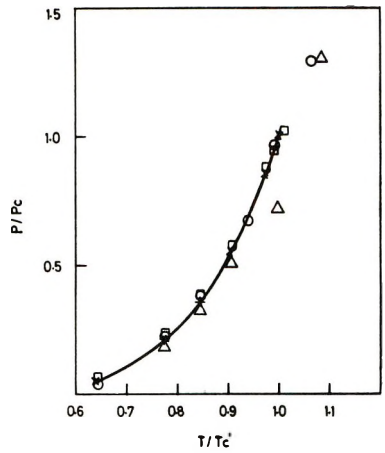

Figure 3. The calculated and experimental vapor pressure curve. The line is drawn through the experimental data taken from ref 15. The points marked with △ are for values calculated with Michel's set of constants, the □ are the values calculated with Gosman's set of constants, and the ○ are for the "C" set of constants.

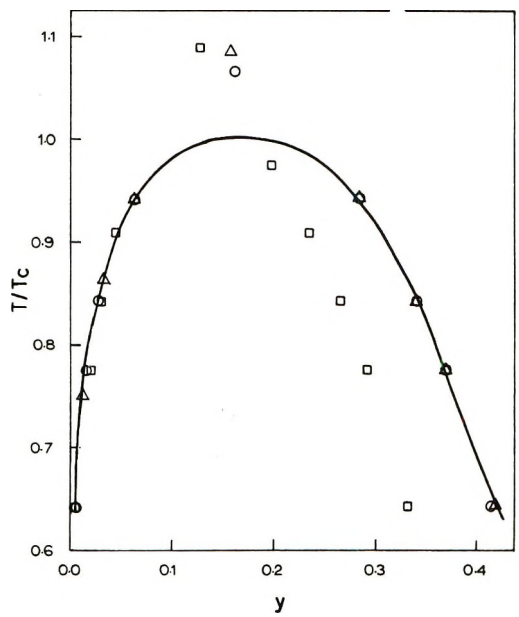

Figure 4. The calculated and experimental densities along the vapor–liquid boundary. The line is drawn through the experimental data from ref 15. The points marked with △, □, and ○ indicate the values calculated from the BH theory with Gosman, Michel's, and "C" sets of constants, respectively.

and energy in Figures 5 and 6. For these properties the calculated values obtained with the "C" and Michels sets of constants show good agreement with one another and the experimental data while the values calculated from the Gosman force constants are greatly in error. Similar results were obtained for a number of properties, including the entropy and latent energy, but lack of space precludes showing these results here. The calculated critical properties have the same reduced values for all three sets of constants but

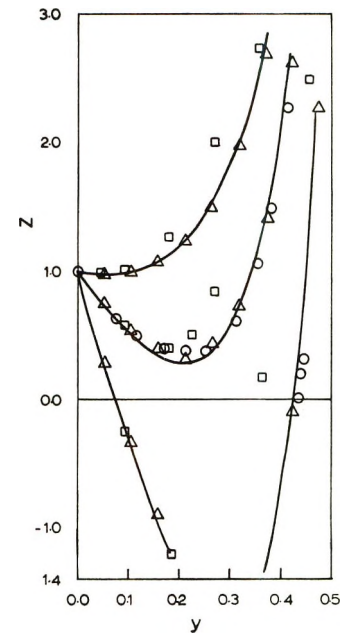

Figure 5. The compressibility factor as a function of reduced density for selected isotherms. The reduced density $y = 12.45/V$ (cm³/mol). The lines are drawn through the values calculated with Michel's set of constants. The △ and □ show values calculated from Gosman and the "C" set of constants, respectively, and the circles show the experimental data taken from ref 15.

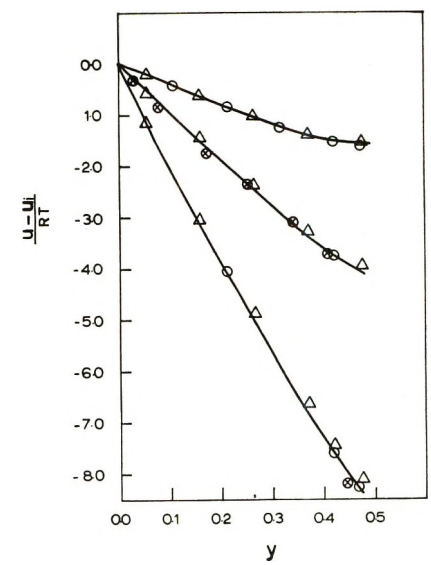

Figure 6. The excess energy as a function of y for selected temperatures. The line is drawn through the values calculated with Michel's set of constants. The points marked by △ and ○ show the values calculated with the "C" set of constants and experimental data taken from ref 15, respectively.

the values calculated from the "C" set of constants are slightly closer to the experimental values than those calculated from the Michel constants. Surprisingly, the values calculated for the Gosman constant are near quantitative for T_c and p_c, 152.63 K and 49.31 atm, respectively, but are substantially in error for V_c.

It is perhaps appropriate to mention the connection of this work with other recent work on the theory of liquids. The method outlined in paper I[26] of this series provides a derivation of the Mayer series in a form equivalent to the Zwanzig series, using the nomenclature of Moffat and Kozak.[27] The method in part I also closely resembles the method Weeks, Chandler, and Anderson[28,29] use in obtaining their estimate for the hard-sphere radius to be used in their perturbation theory. In fact, the first term of the expression for $g(R)$ arising from the method in part I is identical in form with the expression for the equation of their reference fluid, except that they are considering a Lennard-Jones potential truncated at the point of minimum energy rather than the total potential. Their reference fluid therefore corresponds to a fluid in which an arbitrary particle interacts with all other particles *via* a truncated Lennard-Jones potential while all other particles interact with one another *via* hard-sphere potentials. The equation for the choice of their equivalent hard-sphere diameter can be written in a form analogous to that of the BH theory

$$R(\mathrm{WCA}): \quad \int_0^{R(\mathrm{WCA})} R^2 e^{\beta u_{\mathrm{HS}}(R)} g_{\mathrm{HS}}(R)\mathrm{d}R = \int_0^{Rm} R^2 e^{\beta u_{\mathrm{HS}}(R)} g_{\mathrm{HS}}(R)(1 - e^{-\beta U(R)})\mathrm{d}R$$

$$R(\mathrm{BH}): \quad \int_0^{R(\mathrm{BH})} (1)\mathrm{d}R = \int_0^{\sigma} (1 - e^{-\beta U(R)})\mathrm{d}R$$

and $R_m = 2^{1/6}\sigma$.

The WCA choice of diameter involves approximating the actual integrals by equivalent hard-sphere integrals for a bigger range of R and a wider range of arguments of the exponential function than does the BH diameter but some mutual cancellation of errors can be expected in that the integral is made up of approximately equal positive and negative contributions for that part of the integral which is not accurately represented by a hard sphere. It has been shown in part I that the BH theory diameter leads to good approximations for some of the integrals in $g(r)$. It was not apparent why this should be so for all orders of integrals, and hence density, and it is possible that the WCA equation leads to better estimates for the equivalent hard diameter for the higher order integrals.

IV. Conclusion

It has been shown how the amount of computation required to evaluate the integrals in the BH theory with the Lennard-Jones potential as presented in ref 1 and 2 can be greatly reduced by expanding the PY expression for the Laplace transform of $g(R)$ in a Taylor series about a nonzero value of the density. This technique can be applied to the BH theory for any intermolecular potential which can be conveniently expressed in terms of an inverse Laplace transform for $R > d$. In this form of the BH theory the Lennard-Jones potential is being used as an effective potential which includes the effect of three-body forces.

It is shown that the agreement of experimental data with values calculated from the BH theory depends strongly on the choice of the effective force constants while comparisons of the BH theory with Monte Carlo values calculated for the same potential are independent of the force constants. With a suitable choice of force constants the agreement with experimental data can be much improved on that obtained with the Michels force constants which hitherto have been the only force constants to be used.

The simplification of the evaluation of the integrals in the BH theory is not of great importance for the direct calculation of properties of pure substances but it does allow iterative calculations to be carried out rapidly and economically. The extension of the method to mixtures will greatly increase the utility of the BH theory for mixtures, as the computation requirements of the BH theory are very large for mixtures.

(26) R. M. Gibbons, *J. Phys. Chem.*, **75**, 3568 (1971).
(27) M. J. Moffat and J. J. Kozak, *J. Chem. Phys.*, **55**, 3794 (1971).
(28) J. D. Weeks and D. Chandler, *Phys. Rev. Lett.*, **25**, 149 (1971).
(29) J. D. Weeks, D. Chandler, and H. D. Anderson, *J. Chem. Phys.*, **55**, 5422 (1971).

Pulse Radiolysis and Polarography. II. Use of an On-Line Computer in the Determination of the Half-Wave Potentials of Short-Lived Inorganic Radicals[1,2]

by Jochen Lilie

Radiation Research Laboratories, Mellon Institute of Science, Carnegie-Mellon University, Pittsburgh, Pennsylvania 15213
(Received September 23, 1971)

Publication costs assisted by Carnegie-Mellon University and the U. S. Atomic Energy Commission

An on-line computer has been used in the polarographic determination of the half-wave potentials of a number of short-lived inorganic radicals. The radicals are formed by 2-μsec pulses of 3-MeV electrons in the environment of a dropping mercury electrode. The current changes resulting from the reduction or oxidation of the radicals are measured at different times after the beam as a function of the applied voltage and the information obtained is accumulated in the computer memory for averaging and data processing purposes. The half-wave potentials of radicals formed by the reaction of the hydroxyl radical with halogenides and pseudohalogenides have been measured. These radicals were reduced at the dropping mercury electrode, with reduction of Br_2^- ($E_{1/2}$ = −0.57 V (sce)) the easiest. Observations on certain other inorganic radicals (*e.g.*, HPO_2^-) are also reported. It has been demonstrated, by comparison with charge-transfer reactions known from esr measurements, that the half-wave potentials of the radicals can be used to decide whether a reduction of the radicals by a solute is energetically possible or not. All examined radicals with half-wave potentials more positive than −0.8 V are reduced by nitromethane in its alkaline form and all radicals with values more negative than −0.9 V are not reduced.

Introduction

In previous work[2] a system for the polarographic determination of pulse radiolytically produced radicals was reported. The radicals were produced by a pulse of 12-MeV electrons in the vicinity of a dropping mercury electrode. The polarogram was obtained by displaying the current *vs.* time curve for each potential on an oscilloscope, taking Polaroid pictures, and then plotting one point of each picture against the applied voltage. This method is time consuming and not very accurate. In the present studies the polarographic experiment has been improved by interfacing it with a PDP-8 computer. A program has been set up for controlling the pulse radiolysis and polarography, for data acquisition and processing. By this method one gets in short time accurate polarograms of the radicals and the products formed from them. The method is described here along with measurements on the radicals produced from a number of halogenides and pseudohalogenides (*e.g.*, Br_2^-, $(SCN)_2^-$). It was found, from esr measurements,[3] that certain radicals are reduced by the nitromethane according to

$$CH_2NO_2^- + X\cdot \longrightarrow \cdot CH_2NO_2 + X^- \qquad (1)$$

and that others add to the nitromethane anion according to

$$CH_2NO_2^- + Y\cdot \longrightarrow YCH_2\text{–}NO_2^- \qquad (2)$$

In the previous examination[2] of alcohol radicals, it was possible to decide from the polarographic half-wave potentials whether a charge-transfer reaction to different organic substances such as carbonyl and nitro compounds is possible or not. It should be possible to decide from polarographic measurements whether or not reaction 1 is energetically possible. In general, the extension of the reduction potential scale known from normal polarography for the various radicals should give much information on the equilibria of redox reactions of radicals with stable compounds or radicals with other radicals.

Experimental Section

The experimental arrangement of the polarographic cell for pulse irradiation with 3-MeV van de Graaff electrons is in principle the same as that described previously,[2] where 12-MeV LINAC electrons were used. Figure 1 shows the cell with the dropping mercury electrode, the mercury pool, and the platinum sheet as auxiliary electrodes and the saturated calomel reference electrode. By this arrangement in combination with a good conducting solution, one gets an overall resistance of the current-measuring circuit of less than 200 ohms, so that with the maximum current of a few microamperes the voltage change by the iR drop is less than 1

(1) Supported in part by the U. S. Atomic Energy Commission.

(2) Part I: J. Lilie, A. Henglein, and G. Beck, *Ber. Bunsenges. Phys. Chem.*, **75**, 458 (1971).

(3) D. Behar and R. W. Fessenden, *J. Phys. Chem.*, in press.

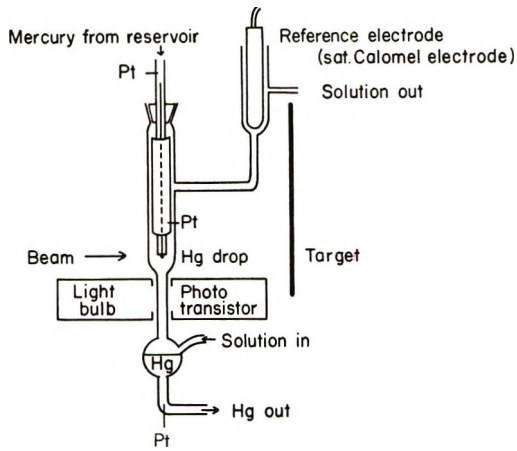

Figure 1. The polarographic cell.

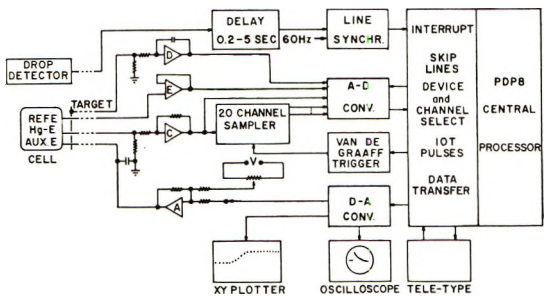

Figure 2. The computer interface for the polarographic pulse radiolysis.

mV. In contrast to the previous study, the mercury was free dropping and a light beam together with a phototransistor served to detect the fall of the drop. The various polarographic events are synchronized to the signal from the falling drop and sequenced under program control by a PDP-8 computer.

The Hardware System. The polarographic system consists of a pulsed 3-MeV van de Graaff and the various hardware items schematically illustrated in Figure 2. The van de Graaff is capable of being triggered on demand with square pulses of 0.5 μsec or longer and currents up to several hundred milliamperes. The sequence of events is triggered by the falling drop. After a variable delay of 0.5–5 sec, a gate is opened which lets through two interrupt pulses of length 10 μsec separated by 16.667 msec and synchronized to the line (60 cycles). These pulses are connected to the interrupt bus of the computer. If the program allows an interrupt to occur, these pulses immediately initiate the running program and the computer triggers the electron beam and starts the measuring programs. In Figure 2 the measuring circuit is shown. The current from the mercury drop electrode runs over a 50-ohm resistor R to ground. This time-dependent voltage drop is amplified and goes to the sampler, which stores the analog signal in 20 consecutive channels. The 20-channel sampler used here was developed by Fessenden and used in his esr and microwave conductivity experiments.[4] A quartz clock switches after a variable time the incoming voltage from one channel to the next, and this voltage is then held at the output of the channel. The signal is then digitized under program control by the relatively slow A–D converter. In most cases in the polarographic work a time of 25 μsec between the channels was used, so that the time dependence over 500 μsec was measured and displayed. For plotting the polarogram only one channel n ($1 \leq n \leq 20$) was used. There is also a direct connection from the amplifier to one A–D input for reading the current before and at long times after the beam pulse. The variable voltage is applied to the cell over an operational amplifier to the auxiliary electrodes of the cell. The voltage is normally scanned by the D–A output of the computer but can also be manually changed with a potentiometer. The potential of the measuring electrode is determined relative to the reference electrode, a saturated calomel electrode, that is connected over a voltage follower to one A–D input of the computer. The dose of the beam is measured by integrating the electrons absorbed from the target with an operational amplifier (D in Figure 2). The operational amplifiers used for A, D, and E are of the Fairchild ADO 84/10 FET input type; the amplifier C is a Philbrick P45A model. Outputs from the computer are the trigger signals to the van de Graaff generator and to the sampling unit, two D–A converters that are connected to an X–Y plotter used for plotting the polarograms, an oscilloscope with two D–A converters (for X and Y) that is used for displaying the time dependence of the measured current after the beam pulse, and a teletype.

The Program System. Figure 3 shows the simplified flow chart of the program. The computer normally stays in a waiting loop, displaying on the oscilloscope the last observed time dependence of the polarographic current after the beam. If a program interrupt is detected, the computer examines whether it is the teletype or the drop-synchronization mode. The teletype mode is used to signal the computer that a parameter has to be changed and is activated when the user presses a special key (see Table I). The computer then asks for the corresponding parameter, reads in the new value, and returns to the waiting loop for an interrupt. If a drop synchronization interrupt occurs, the sampler is triggered and the base line is measured. Upon the second interrupt that occurs 16.67 msec later, the van de Graaff and the sampler are triggered, the time dependence of the current is determined, and the base line is subtracted. The dose is measured by integrating the current picked up by the target. If averaging is required, the computer waits for the next drop interrupt and this procedure is repeated N_{rep} times (see Table I). If the averaging is done and no smoothing is required, the current of the chosen sampler channel (i_n) and the

(4) R. W. Fessenden, to be published.

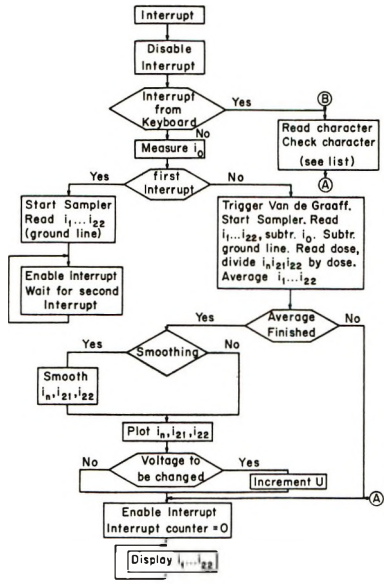

Figure 3. Flow diagram of the program system for polarographic pulse radiolysis.

currents 1 and 3 msec after the beam are divided by the dose and plotted on the X–Y plotter. If smoothing is desired, this is signalized to the computer by the appropriate switch register. When this is done the current values measured for the last nine voltage settings are used to calculate the middle ones ($n_{last} - 4$) by the method of Savitsky and Golay,[5] using a quartic fit. These points then are plotted.

Table I

Command key	Reaction
Linefeed	Read U_0, U_{end}, number of voltages between U_0 and U_{end}. Set $U = U_0$
Rubout	Read number of averages $N_{rep} \geq 1$
Control P	Read N, indicating which sampler channel (i_n) has to be plotted $1 \leq N \leq 20$
Control Z	Plot time dependence $i_1 \ldots i_{22}$ on X–Y plotter
Control C	End of program
Return	Return to main program
Other characters	Print character as comment. Read and check next character

After finishing the plotting of the three points, the polarographic voltage is changed if the corresponding switch in the switch register is set. If not, the voltage remains constant. This also happens if the polarogram is finished by reaching the end voltage or if the ground current is too high. Restart of the voltage scan is affected by pressing a push button or the appropriate command on the teletype.

The Solutions. For the polarographic measurements it is necessary that the conductivity of the solution be as high as possible. Therefore, 1 M solution of an inert electrolyte was always used. For neutral and alkaline solution, Na_2SO_4 was used and in acid solutions $NaClO_4$–$HClO_4$ was used as the electrolyte. The water was triply distilled, with the second stage containing alkaline $KMnO_4$ solution. The solutions were deaerated with ultrapure nitrogen. If the reaction with OH radicals was to be studied, the solution was saturated with N_2O that was washed with acid $CrCl_2$ solution for removal of the oxygen. The N_2O served to convert the electrons formed by the beam into OH radicals according to

$$N_2O + e_{aq}^- \xrightarrow{H_2O} N_2 + OH\cdot + OH^-$$

as is conventional in many radiation chemical experiments. The other chemicals used were Baker Analyzed reagents.

Results and Discussion

In N_2O-saturated solution, the main highly reactive species present after the pulse is the OH radical. If, for example, the solution contains 10^{-4} M KSCN, the solute reacts very fast with OH, forming $(SCN)_2^-$.[6] These radicals then disappear by reaction with each other, and the concentration follows second-order kinetics. Figure 4 illustrates the measured polarographic current for different applied voltages after the pulse irradiation of KSCN solutions. In (c), the current decreases immediately after the beam, and after passing a minimum it returns to positive values. Since a negative current results from an oxidation of the species (electrons are abstracted from the compound and are flowing through the electrode to the voltage source), this means that the radicals $(SCN)_2^-$ formed after the pulse are oxidized at this voltage, the electrode serving as anode. The positive current at the end shows the reduction of the $(SCN)_2^-$ and the products formed by disproportionation of $2(SCN)_2^-$ to $(SCN)_2$ and $2SCN^-$.[7] (Here the electrons are flowing from the mercury drop to the compound, and the electrode works mainly as cathode.) Since the reduction half-wave potential of the $(SCN)_2^-$ is at a more negative voltage (see below), the reduction of $(SCN)_2^-$ is very slow at 0 V; the main observed current is due to the reduction of the $(SCN)_2$. At more negative voltage (curve b), the current starts near zero, rises to a maximum at 200 μsec, and then decreases slowly. This means that there is no oxidation of the radicals observed, but one sees a reduction. This reduction, however, is relatively slow and therefore it takes 200 μsec to reach the maximum current. This type of electrode kinetics has also been observed for the reduction of alcohol radicals and will be de-

(5) A. Savitsky and M. J. E. Golay, *Anal. Chem.*, **36**, 1627 (1964).

(6) J. H. Baxendale, P. L. T. Bevan, and D. A. Scott, *Trans. Faraday Soc.*, **64**, 2389 (1968).

(7) M. Schöneshöfer, G. Beck, and A. Henglein, *Ber. Bunsenges. Phys. Chem.*, **74**, 1011 (1970).

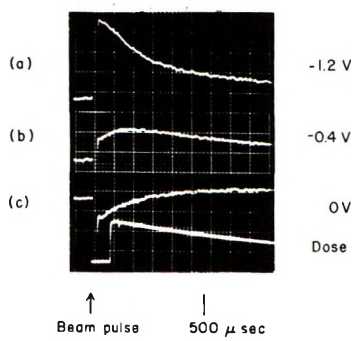

Figure 4. Time dependence of the current after the beam pulse, solution N_2O saturated with 10^{-3} *M* KSCN, 1 *M* Na_2SO_4 (the display of the dose is shifted 1 cm to the right). Voltage *vs.* sce.

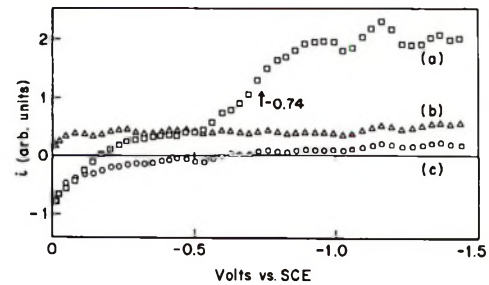

Figure 5. Polarogram of the products present in the solution at (a) 25 μsec after beam, (b) 1 msec after beam, (c) 3 msec after beam. Solution N_2O saturated, 10^{-3} *M* KSCN, 1 *M* Na_2SO_4.

scribed in more detail in part III of this series, along with the pH dependencies of polarographic curves.[8] The relatively slow decay following the maximum of the current results from a superposition of the disproportionation of the $(SCN)_2^-$ forming $(SCN)_2$ that is also reduced and the decay of the concentration due to the diffusion of the particles to the electrode.[2] At −1.2 V (a), the current maximum is immediately after the pulse, showing that at this voltage the $(SCN)_2^-$ radicals are reduced fast. For the decay, the same explanation holds as for curve b.

Figure 5 shows the polarograms obtained at 25 μsec, 1 msec, and 3 msec after the pulse. There are two steps for the curve at 25 μsec. The first one, which occurs above −0.3 V, shows that the oxidation of the radical starts at the most positive voltage. Therefore, one cannot accurately measure the half-wave potential for that step. The second step at −0.74 V is assigned to the reduction of the $(SCN)_2^-$. This type of polarogram is only found if there is enough SCN^- in the solution to push the equilibrium $SCN + SCN^- \rightleftharpoons (SCN)_2^-$ to the right. At low SCN^- concentration ($<10^{-4}$ *M*) only a broad rise in the polarogram is found, resulting from the presence of two different electroactive species (SCN and $(SCN)_2^-$) that are in equilibrium. The product existing 1 msec after the pulse (curve b) is reduced at all potentials one can measure. This is the $(SCN)_2$, formed by disproportionation of two $(SCN)_2^-$ radicals.[7] At 3 msec after the beam (curve c) there is nearly no reduction seen. Therefore, it can be concluded that this compound is unstable and disappears in the millisecond time scale. (For a stable electroactive species, the current decreases owing to the diffusion of the particles to the electrode by $t^{-1/2}$. Therefore, from 1 msec to 3 msec the current would drop only by 42%.) Table II shows a list of the half-wave potentials similarly measured for radicals formed by the reaction of OH radicals with different inorganic compounds. The only other short-lived radicals for which half-wave potentials have been measured are the α and β alcohol radicals.[2]

Table II: Half-Wave Potentials for the Reduction of Inorganic Radicals (*vs.* Sce)[a]

Reaction	Radical	$E_{1/2}$	pH
Br^-–OH	Br_2^-	−0.57	7
Cl^-–OH	Cl_2^-	−0.64	2
SCN^-–OH	$(SCN)_2^-$	−0.74	7
I^-–OH	I_2^-	−0.79	7
CN^-–OH	?	−0.93	10
HPO_3^{2-}–OH	PO_3^{2-}	−1.09	7–10
$H_2PO_2^-$–OH	HPO_2^-	−1.10	9–10
HCOOH–OH	COOH	−1.25	3
$HCOO^-$–OH	COO^-	−1.54	7

[a] No reduction step on Hg electrode, broad rise of *i*–*V* curve: CO_3^{2-}–OH, CNO^-–OH, CNO^-–e, N_3^-–OH.

Looking on Table II one sees that the radicals Br_2^-, $(SCN)_2^-$, and I_2^-, which are capable of being reduced by nitromethane anion (according to eq 1), have the smallest negative values of the half-wave potential for the reduction (above the dotted line). (Cl_2^- is only found in acid solution where the nitromethane is not dissociated and no charge transfer occurs.) The radicals that are not reduced by $CH_2NO_2^-$ have potentials more negative than −0.9 V or are not reduced at the dropping mercury electrode in the alkaline solution. From this one can assign to the nitromethane in its alkaline form a reducing power corresponding to a half-wave potential for one-electron transfer of −0.8 to −0.9 V. (This potential cannot be measured directly, since there is no oxidation observed of the nitromethane at the mercury electrode. It is only reduced with $E_{1/2} = -0.90$ V[9] at pH 8–12.) All radicals with a potential for reduction more positive than −0.8 V can be reduced by the nitromethane; all radicals with a potential more negative than −0.9 V cannot be reduced, and for them the only possible reaction with the nitromethane is the addition (reaction 2). Addition may also take place for radicals that are reduced, but since the simpler electron

(8) M. Grätzel, A. Henglein, J. Lilie, and M. Scheffler, *Ber. Bunsenges. Phys. Chem.*, in press.

(9) L. Meites, "Polarographic Techniques," Interscience, New York, N. Y., 1965, p 5698.

transfer can occur more easily, the reduction is usually faster than the addition and as a result redox products are the main products. Of the organic radicals, only the reaction of α-alcohol radicals with nitromethane anion has been examined by esr,[10] and it was found that these radicals add according to reaction 2. For these radicals no reduction at the dropping mercury electrode has been found.[2] This agrees with the above conclusions, but some other groups of organic compounds should also be examined by esr.

Figure 6a shows the polarogram of an N_2O-saturated solution containing Na_2HPO_3. In this solution the main radical is PO_3^{2-}, formed by H abstraction from HPO_3^{2-}. One sees an oxidation of this radical at small negative voltages with a low current. The most probable reaction is the oxidation from the P^{4+} to the P^{5+} state, forming the phosphate ion. At negative voltages the radical is reduced. Here the current change is much higher, so that one can assume a reduction that goes further than one step, but with the experimental technique used here there is no direct way to determine how many electrons are transferred. This is only possible by comparison with other reactions (see below). In Figure 6b the polarogram of the radicals formed from hypophosphite (NaH_2PO_2) by H abstraction by OH is shown. One sees that this HPO_2^- radical is also oxidized at small negative voltages, forming the phosphite, but at a bit more negative voltages ($E < -0.5$ V) the main reaction is the reduction. There is no sharp step in the polarogram. That means there are some relatively slow chemical steps in the reduction and one cannot say which reactions occur during this reduction. At more negative voltages the reduction current rises in a relative sharp step. The half-wave potential for this step is within experimental error the same as for the reduction of the radicals formed from HPO_3^{2-} (see above). The radical that has been formed by the OH (HPO_2^-) has the oxidation number 2+. At voltages between −0.6 and −1 V this is reduced to 1+ or 0. The reduction to the phosphorus itself is much more likely than to 1+, since the oxidation number 1+ is the starting substance itself (that is not reduced at the electrode!), and the slow rising reduction current between −0.5 and −0.8 V indicates a reduction that is not simply a one-electron addition (see below). The measured half-wave potential of −1.10 V is identical with the standard reduction potential of the reaction $P + 3H_2O + 3e^- \rightleftarrows PH_3 + 3OH^-$ of $E = -0.87$ V against the standard hydrogen electrode.[11] This means −1.11 V against sce. Since the same potential has been found for the reduction of the PO_3^{2-} (curve 6a), this can indicate that this is the step that determines the reduction of the PO_3^{2-}. As long as the reduction cannot go to the final product, there is only a slow reduction indicated by the light rise of the curve between −0.2 and −0.8 V. The main reaction observed is the oxidation, but when the reduction can go on, the radicals are reduced and one gets the high reduction current.

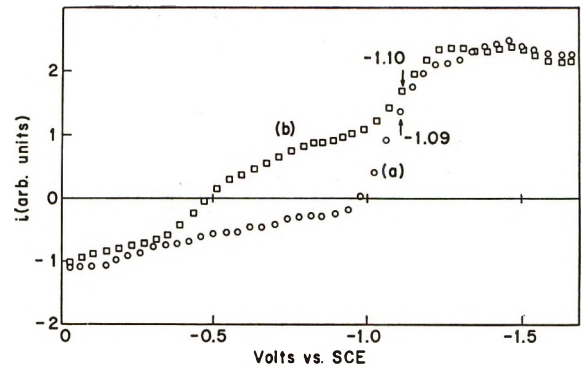

Figure 6. Polarogram of the radicals (a) PO_3^{2-} and (b) HPO_2^- 25 μsec after the beam at pH 9.

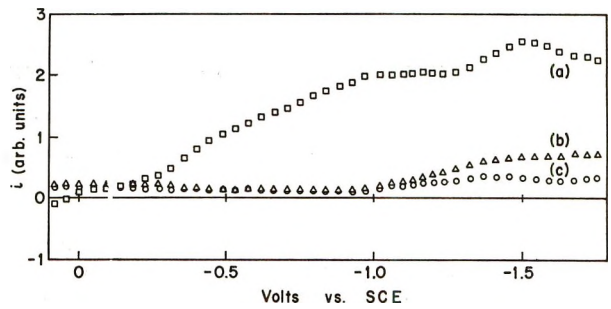

Figure 7. Polarogram of the product present in the solution at (a) 25 μsec after beam, (b) 1 msec after beam, (c) 3 msec after beam. Solution N_2O saturated with 1 M Na_2SO_4.

Figure 7 shows the polarogram of a solution containing only Na_2SO_4 and N_2O. In this solution the only reactive species after the beam are OH radicals which disappear from the solution by reaction with each other, mainly forming H_2O_2. One sees that near 0 V the current is very small, rising continuously with more negative voltage and staying nearly constant after −1 V. From normal polarography one knows that such a slow rise is characteristic of an irreversible electrode reaction that involves chemical reactions following or preceding electron transfer or a slow heterogeneous charge transfer (reversible reactions involving one-electron transfer have steps with $E_{3/4} - E_{1/4} = 59$ mV). The reduction of H_2O_2, for example, is known as an irreversible case with a broad step, and one can assume similar conditions for the reaction of the OH radical at the electrode. The measured $E_{1/2}$ does not bear any thermodynamic significance and cannot be correlated with chemical reducing or oxidizing power. Similar polarograms were found for the radicals formed

(10) K. Eiben and R. W. Fessenden, *J. Phys. Chem.*, 72, 3387 (1968).

(11) R. C. Weast, Ed., "Handbook of Chemistry and Physics," The Chemical Rubber Co., Cleveland, Ohio, 1969, p D 109.

from the reaction of OH with N_3^-, CNO^-, HCO_3^-, SO_3^{2-}, and HSO_4^-. In all of these cases (including OH) it was found in the esr measurements that no reduction of the radicals occurred, but rather that the radicals added to the nitromethane (eq 2).

From these and the previous[2] results, one sees that the polarographic determination of half-wave potentials gives good values for the reducing and oxidizing power of radicals. From the $E_{1/2}$ values it can then be decided whether a charge-transfer reaction is energetically possible or not. Since the radical reactions considered are very fast, a reaction that has been found to be possible from these energy values normally takes place.

Polymer-Solvent Interactions from Gas-Liquid Partition Chromatography

by R. D. Newman and J. M. Prausnitz*

Department of Chemical Engineering, University of California, Berkeley, California 94720 *(Received February 16, 1971)*

Publication costs assisted by the Paint Research Institute

A chromatographic technique for measuring activity coefficients at infinite dilution is applied to polymer–solvent systems. The solid support is coated with polymer above its glass transition temperature; a small amount of solvent is introduced into the carrier; its retention time is measured and used to calculate the activity coefficient. Consideration is given to the effect of gas flow rate, solvent sample size, solid loading, and chemical nature of the solid support. Special care must be taken with polar solvents. Experimental results are given for 13 solvents with polystyrene ($\bar{M}_n = 9.7 \times 10^4$) at 150, 175, and 200°. Experimental results for benzene, cyclohexane, and *n*-pentane with polyisobutylene ($\bar{M}_v = 6.6 \times 10^4$) at 25° compare favorably with results obtained from static (vapor pressure) measurements.

Few polymer solution studies have been made in the highly concentrated region. This region, however, is of interest in biomedical applications as well as in the polymer industry, particularly in the manufacture of polymer films which, often for health requirements, must be free of (toxic) volatile matter. We discuss here a convenient experimental method for obtaining fundamental thermodynamic data on polymer–solvent systems at conditions where the low-molecular-weight component is at infinite dilution.

It has been pointed out by numerous authors[1-4] that gas–liquid partition chromatography may be used for measuring activity coefficients in liquid mixtures. Such measurements are particularly useful for obtaining the activity coefficient of a volatile component when infinitely dilute in a (relatively) nonvolatile component. Extensive measurements of this kind have been reported by Cruickshank and coworkers[5-7] Application of a chromatographic technique to polymer–solvent systems was discussed by Smidsrød and Guillet,[8] by Schreiber, *et al.*,[9] and by Hammers and De Ligny.[10]

Experimental Section

Apparatus. The gas chromatograph used was a Varian Aerograph 1520 equipped with a thermal-conductivity detector; a schematic diagram is shown in Figure 1. Column-oven temperature control was improved to ±0.1° by the use of a Hallikainen Instrument Co. thermotrol. Low-temperature results were obtained by using a water bath for the column; temperature control for the water bath was ±0.02°. Flow of the helium carrier gas was controlled by a Negretti and Zambra precision regulator valve. Carrier gas flow rate was measured at the outlet by a soap-bubble flowmeter. Pressure at the inlet and outlet was measured to within 0.1 mm with a mercury manometer. Liquid

(1) P. E. Porter, C. H. Deal, and F. H. Stross, *J. Amer. Chem. Soc.*, **78**, 2999 (1956).

(2) A. Kwantes and G. W. A. Rijnders, "Gas Chromatography," Butterworths, London, 1958.

(3) A. J. B. Cruickshank, M. L. Windsor, and C. L. Young, *Proc. Roy. Soc., Ser. A*, **295**, 259 (1966).

(4) A. J. B. Cruickshank, M. L. Windsor, and C. L. Young, *ibid.*, **295**, 271 (1966).

(5) B. W. Gainey and C. L. Young, *Trans. Faraday Soc.*, **64**, 349 (1968).

(6) C. L. Young, *ibid.*, **64**, 1537 (1968).

(7) C. P. Hicks and C. L. Young, *ibid.*, **64**, 2675 (1968).

(8) O. Smidsrød and J. E. Guillet, *Macromolecules*, **2**, 272 (1969).

(9) D. Patterson, Y. B. Tewari, H. P. Schreiber, and J. E. Guillet, *ibid.*, **4**, 376 (1971); W. R. Summers, Y. B. Tewari, and H. P. Schreiber, *ibid.*, **5**, 12 (1972).

(10) W. E. Hammers and C. L. De Ligny, *Recl. Trav. Chim. Pays-Bas*, **90**, 912 (1971).

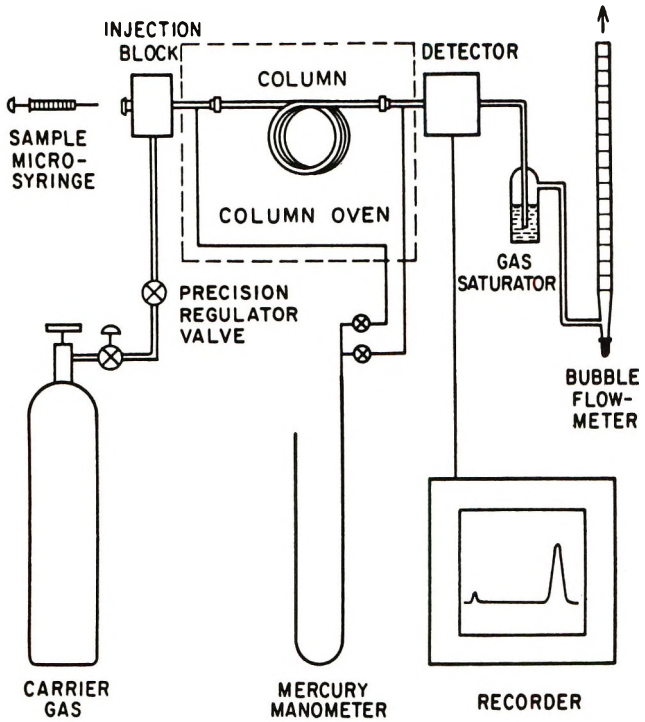

Figure 1. Gas chromatographic apparatus.

solutes were injected through a silicone rubber septum using a 1-μl. Hamilton syringe.

Preparation of Columns. The stationary phases were coated onto Fluoropak-80, 60–80 mesh or onto Chromosorb P, AW-DMCS by dissolution in chloroform or ether, mixing, and slow evaporation. When constant weight was attained, the coated support was packed into 5 ft of 0.25-in. stainless-steel tubing. The tubing was then coiled to fit the chromatograph oven.

Stationary Phases and Solutes. *n*-Hexadecane was obtained from Aldrich Chemical Co. and squalane was obtained from Varian Associates. These compounds were of 99% minimum purity and were used without further purification. The polystyrene used was obtained from Pressure Chemical Co., Pittsburgh, Pa. Two molecular weights were used: $\bar{M}_n$ = 37,000 (batch 7b), $\bar{M}_n$ = 97,600 (batch 4a). This polystyrene has a very narrow molecular weight distribution ($\bar{M}_w/\bar{M}_n$ = 1.06 for both samples), and it was used without further treatment. Polyisobutylene was obtained by fractional precipitation of Enjay Vistanex LMMS from benzene using methanol as precipitant. The initial fraction was discarded, and a large second fraction was retained for experimental use. The viscosity-average molecular weight of this fraction was 66,000.

Solute sample size was kept as small as possible consistent with obtaining a measurable peak; usually it was less than 0.1 μl of solvent. The solutes used were reagent grade materials obtained from standard supply sources. Since solute purity is not of major importance in these measurements, the solvents were used without further purification. The peak maximum retention time was independent of sample size over the range of sample sizes 0.001 to 0.1 μl.

Solid Supports. The customary solid support for glpc measurements is firebrick or one of the Chromosorb materials. These are all diatomaceous earths in origin; for polar solvents these give badly asymmetric peaks and a dependence of retention time on sample size. Conder, Locke, and Purnell[11] have developed a method of obtaining activity coefficients from these asymmetric peaks which assumes that part of the retention is due to adsorption on the various exposed surfaces. However, in our work with polystyrene a low surface energy support, Fluoropak 80 (powdered polytetrafluoroethylene), was tried and found to give symmetric peaks with polar as well as nonpolar solutes.

Data Reduction

Conder[12] points out that symmetric peaks on Fluoropak do not necessarily prove absence of adsorption. He suggests that the retention volume consists of two contributions, one due to bulk sorption, the other due to surface adsorption

$$V_N = K_L V_L + K_s A_s \tag{1}$$

where V_N = observed retention volume, V_L = volume of liquid phase, K_L = distribution coefficient for bulk solution, K_s = distribution coefficient for surface adsorption, and A_s = surface area. Rearrangement of eq 1 gives

$$\frac{V_N}{V_L} = K_L + \frac{K_s A_s}{V_L} \tag{1a}$$

Retention volume data, taken on a series of columns having different loadings, and extrapolated to zero flow rate, are plotted according to eq 1a. The intercept gives the desired quantity, K_L.

Guillet and Smidsrød[8] have shown that activity coefficients can be measured for a polymer–solvent system only when the polymer is above its glass transition temperature. Since the polymer is viscous even at elevated temperatures, there is a slight resistance to mass transfer. To ensure that the retention volumes are those at equilibrium, retention–volume data were extrapolated to zero flow rate as illustrated in Figure 2. The value of V_N obtained from this extrapolation was plotted according to eq 1a to give K_L, as illustrated in Figure 3. The retention volume per gram of stationary phase is designated by V_g; it is related to K_L by

$$V_g = \frac{K_L}{\rho_2} \tag{2}$$

where ρ_2 is the density of the stationary phase.

Patterson, Tewari, Schreiber, and Guillet[9] have dis-

(11) J. R. Conder, D. C. Locke, and J. H. Purnell, *J. Phys. Chem.*, **73**, 700 (1969).

(12) J. R. Conder, *Anal. Chem.*, **43**, 367 (1971).

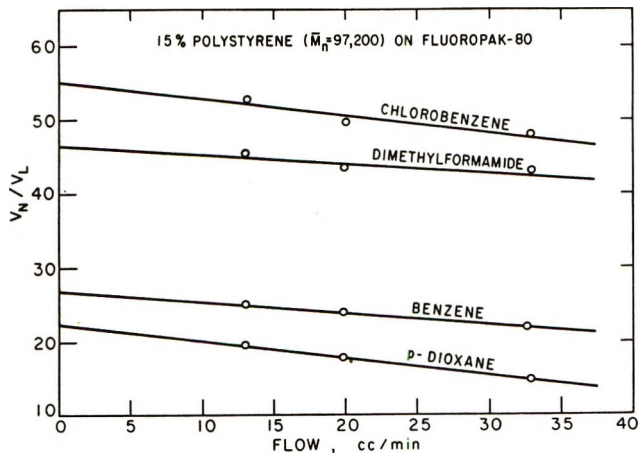

Figure 2. Data reduction at 150° to obtain V_N/V_L at zero flow rate.

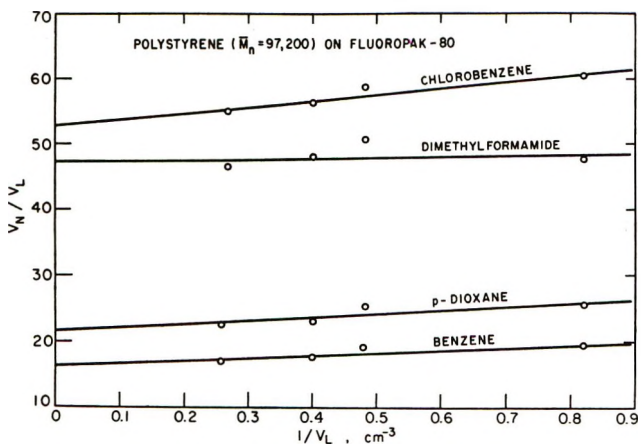

Figure 3. Data reduction to obtain K_L at 150°.

cussed how activity coefficients may be obtained from quantities measured by glpc. Their equation is

$$\ln \gamma_1^{\infty} = \ln\left[\frac{273.2R}{P_1^s V_g^{\circ} M_2}\right] - \frac{P_1^s(B_{11} - v_1)}{RT} \qquad (3)$$

where subscript 1 refers to the volatile component and subscript 2 refers to the polymer; γ^{∞} is the infinite dilution activity coefficient; M is the molecular weight; R is the gas constant; P^s is the saturation vapor pressure at temperature T; v is the liquid molar volume at T; V_g° is the specific retention volume corrected to 0°, and B_{11} is the second virial coefficient of pure 1 at T. The quantity V_g° is given by

$$V_g^{\circ} = Q(t_g - t_r)\frac{273.2}{T}\cdot\frac{1}{W_2}\cdot f_p \qquad (4)$$

where

$$f_p = \frac{3}{2}\frac{\left[\left(\frac{P_i}{P_o}\right)^2 - 1\right]}{\left[\left(\frac{P_i}{P_o}\right)^3 - 1\right]} \qquad (5)$$

where Q is the flow rate at the column outlet; T is the temperature in degrees Kelvin; t_g is retention time from injection to peak maximum for the solvent; t_r is the retention time of an air sample; W_2 is the weight of polymer in the column; P_i is inlet pressure; and P_o is outlet pressure.

Patterson, *et al.*, point out that the activity coefficient given by eq 3 is not convenient for polymer–solvent systems since the polymer molecular weight must be accurately known and the activity coefficient tends to $-\infty$ as $M_2 \to \infty$. They propose the following equation based on weight fraction w

$$\ln \Omega_1^{\infty} = \ln\left(\frac{a_1}{w_1}\right)^{\infty} = \ln\left[\frac{273.2R}{P_1^s V_g^{\circ} M_1}\right] - \frac{P_1^s}{RT}(B_{11} - v_1) \qquad (6)$$

where $(a_1/w_1)^{\infty}$ is the activity coefficient at infinite dilution. The Flory–Huggins theory (using segment fractions) gives the activity of the solvent

$$\ln a_1 = \ln \phi_1 + \left(1 - \frac{1}{r}\right)\phi_2 + \chi^*\phi_2^2 \qquad (7)$$

where ϕ is the segment fraction.[13]

Noting that $r = (M_2\rho_1^*/M_1\rho_2^*)$, it can be shown that for $\phi_1 \to 0$

$$\chi^* = \ln\left[\frac{273.2R}{P_1^s V_g^{\circ} v_1^* \rho_2^*}\right] - \left(1 - \frac{v_1^*\rho_2^*}{M_2}\right) - \frac{P_1^s}{RT}(B_{11} - v_1) \qquad (8)$$

where the parameter v^* (core specific volume) is similar to the excluded volume in the van der Waals equation (see Eichinger and Flory[13]). The core density is denoted by ρ^*.

Results

Equation 6 was used to calculate Ω_1^{∞} from chromatographic retention data. The steps are as follows. A series of four columns was prepared, each one having different loading of stationary phase but the same amount of support. At a given temperature, peak maximum retention volumes were measured at various flow rates for a variety of solvents. V_N/V_L values were calculated and extrapolated to zero flow rate (Figure 2). These V_N/V_L values were then plotted according to eq 1 to give K_L as indicated in Figure 3. V_L gives V_g, the retention volume per gram of stationary phase. This value was corrected to 0° to give V_g°. Virial coefficients were obtained from the correlation of O'Connell and Prausnitz.[14] Polystyrene densities were obtained from McGowan.[15]

(13) B. E. Eichinger and P. J. Flory, *Trans. Faraday Soc.*, **64**, 2035, 2053, 2061, 2066 (1968).

(14) J. P. O'Connell and J. M. Prausnitz, *Ind. Eng. Chem., Process Des. Develop.*, **6**, 245 (1967).

(15) J. C. McGowan, *Polymer*, **10**, 841 (1969).

K_L values are shown in Table I; activity coefficients are given in Table II.

Table I: Experimental K_L Values for Polystyrene ($\bar{M}_n$ = 97,000) Systems

	150°	175°	200°
Cyclohexane	7.0	5.6	4.7
Benzene	16.1	10.5	7.2
Toluene	27.8	17.3	11.4
Ethylbenzene	47.0	25.2	15.3
Styrene	72.0	37.0	21.9
Dioxane	21.4	13.1	8.5
1,2-Dichloroethane	16.2	10.3	6.8
Chlorobenzene	52.8	30.7	18.8
Nitroethane	19.0	10.9	6.5
Methyl ethyl ketone	9.3	6.3	4.5
Cyclohexanone	71.3	38.6	23.4
Dimethylformamide	47.2	25.2	14.5
Acetonitrile	8.0	5.3	3.7

Table II: Activity Coefficients (Weight Fraction) Ω_1^∞ for Solvents at Infinite Dilution in Polystyrene ($\bar{M}_n$ = 97,000)

	150°	175°	200°
Cyclohexane	12.2	10.5	8.92
Benzene	5.44	5.67	5.81
Toluene	5.22	5.29	5.34
Ethylbenzene	4.96	5.47	5.67
Styrene	4.11	4.57	4.69
Dioxane	5.17	5.41	5.71
1,2-Dichloroethane	4.55	4.83	5.10
Chlorobenzene	3.72	3.85	4.04
Nitroethane	11.0	11.6	12.6
Methyl ethyl ketone	9.44	9.30	9.12
Cyclohexanone	5.81	6.14	6.26
Dimethylformamide	10.6	10.8	11.0
Acetonitrile	19.8	19.8	19.7

The results shown are those for polystyrene $\bar{M}_n$ = 97,000. Experimental data for polystyrene $\bar{M}_n$ = 37,000 are essentially the same as those reported for polystyrene $\bar{M}_n$ = 97,000.

The activity coefficients for the strongly polar solutes tend to be larger than those for the nonpolar solutes. As temperature rises, the activity coefficients of the nonpolar solutes increase, except for cyclohexane. The activity coefficients of the polar solutes are not significantly affected as the temperature increases from 150 to 200°.

To test the validity of the chromatographic method a comparison was made with activity coefficients determined by other methods. Table III[16,17] gives activity coefficients for several solvents in squalane and *n*-hexadecane. The static results were obtained from vapor pressure measurements. Infinite dilution values for the static results were obtained by extrapolation. In addition to chromatographic results obtained in this work, those of Cruickshank and coworkers are also shown. There is good agreement between static and chromatographic measurements. The support for our chromatographic work was Chromosorb P AW-DMCS. Activity coefficients were found to be independent of coverage for coverage ratios above 20%. Changing the carrier gas flow rate by a factor of three did not affect the measured activity coefficients.

Table III: Comparison of Limiting Activity Coefficients from Glpc and Static Measurements

Solvent	Stationary phase	Temp, °C	γ_1^∞ Glpc		γ_1^∞ Static
n-Pentane	Squalane	30	0.617		0.631[a]
		25		0.655[b]	
Cyclohexane	Squalane	30	0.515	0.535[b]	0.525
n-Hexane	Squalane	30	0.641	0.687[b]	0.650
	n-Hexadecane	20	0.904	0.905[b]	0.907[c]
		30	0.903	0.905[b]	0.900[c]
		60	0.893	0.895[b]	0.895[c]

[a] Ashworth and Everett.[16] [b] Cruickshank, Windsor, and Young.[4] [c] McGlashan and Williamson.[17]

To determine whether the solid support influences the results, experimental data were obtained for squalane with benzene and with *n*-hexane first, using Fuoropak and second, using Chromosorb. Figure 4 shows data plotted according to the method of Purnell and Conder (eq 1a). At infinite coverage the two supports give the same value of V_N/V_L. The agreement between the results on the two supports was taken as evidence that the Fluoropak may be used for

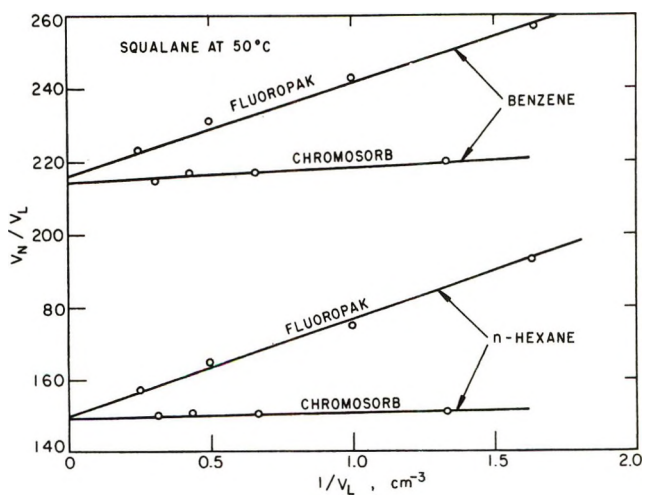

Figure 4. Data reduction to obtain K_L. Comparison of two supports.

(16) A. J. Ashworth and D. H. Everett, *Trans. Faraday Soc.*, **56**, 1609 (1960).

(17) M. L. McGlashan and A. G. Williamson, *ibid.*, **57**, 588 (1961).

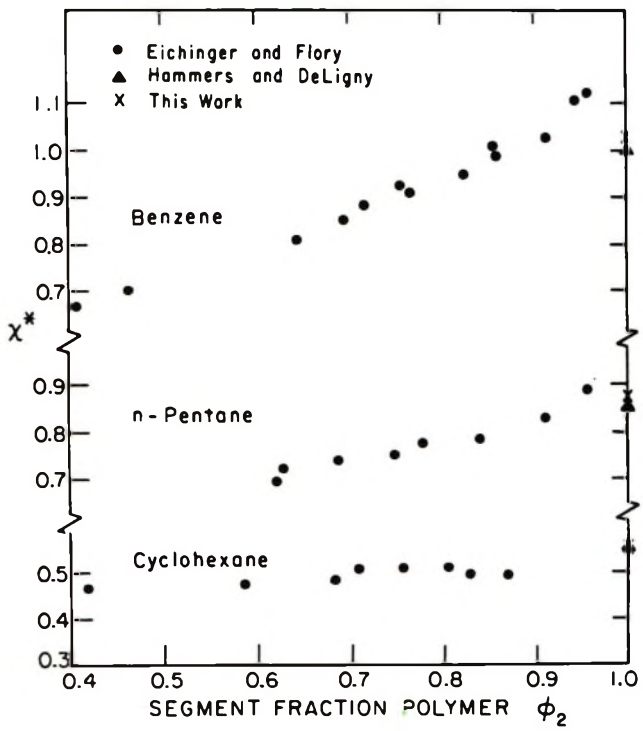

Figure 5. χ^* parameters for polyisobutylene with benzene, *n*-pentane, and cyclohexane at 25°.

chromatographic measurements if the data are reduced properly. The Fluoropak support is desirable since it produces nearly symmetric peaks with polar solvents. Polar solvents gave highly asymmetric peaks on Chromosorb and therefore Chromosorb was not used in our polystyrene studies.

For polymer systems it is difficult to compare chromatographic results with those obtained by static methods because experimental data using a static method rarely extend to highly concentrated solutions. However, static data up to about $\phi_2 = 0.95$ have been reported by Eichinger and Flory[13] for some polyisobutylene systems. Table IV shows Flory χ^* values for several solvents with polyisobutylene, and Figure 5 gives Flory χ^* parameters as a function of polymer segment fraction. The circles correspond to results obtained by Eichinger and Flory, the crosses represent our chromatographic results, and the triangles show the chromatographic data of Hammers and De Ligny.[10] While agreement is good, it appears that our chromatographic results, as well as those reported by the Dutch workers, are somewhat lower than those obtained by extrapolation of the static data. To understand this discrepancy we are currently obtaining additional chromatographic data as well as static data in the region very close to $\phi_2 = 1$.

Table IV: Flory χ^* Values[a] for Polyisobutylene Systems from Chromatographic Measurements

Solvent	25°	40°	50°
Benzene	1.03	0.96	0.92
Cyclohexane	0.55	0.54	0.53
n-Pentane	0.87	0.801	0.797

[a] Based on segment fraction.

Acknowledgment. We are grateful to the Paint Research Institute, to Esso Research and Engineering Company, and to the donors of the Petroleum Research Fund for financial support and to H. H. Kuo for assistance in performing the experiments.

Heats of Immersion in the Zirconium Oxide–Water System[1]

by H. F. Holmes,* E. L. Fuller, Jr., and R. B. Gammage

Reactor Chemistry Division, Oak Ridge National Laboratory, Oak Ridge, Tennessee *(Received November 18, 1971)*

Publication costs assisted by the Oak Ridge National Laboratory and the U. S. Atomic Energy Commission

Calorimetric measurements of the heat of immersion of zirconium oxide in water have been made using samples outgassed at temperatures ranging from 25 to 500°. Samples having a common chemical history and specific surface areas of 3.7 to 87.4 m^2/g (calcining temperatures of 600 to 1000°) were used in the present study. The magnitude of the heat of immersion (values ranging up to -1100 $ergs/cm^2$) clearly indicates that the initial interaction of water with an outgassed zirconium oxide surface is chemical in nature. A significant fraction (varying from 8 to 36%) of the heat of immersion was observed as a slow evolution of heat. This slow component could be separated into two concurrent first-order processes having half-lives of 4 to 30 min. The sample having the largest specific surface area exhibited a pronounced maximum in the heat of immersion as a function of the outgassing temperature. There is experimental evidence that the slow heat release and the maximum are phenomena related to porosity and an increase in hydrophobicity at the higher outgassing temperatures. Relating the results to the crystal modification present in the various samples strongly suggests that the metastable tetragonal form has a much lower surface energy than the stable monoclinic form. With the exception of the just-mentioned phenomenon the heat of immersion (on a unit area basis) decreased with decreasing specific surface area.

Introduction

Zirconium oxide is an important ceramic material, has certain desirable catalytic properties, and is a corrosion product of structural alloys containing zirconium. In view of this, it is surprising that very little has been done to investigate the surface chemistry of zirconium oxide. One isolated value for the heat of immersion of zirconium oxide in water has been reported.[2] In addition, the porous structure of zirconium oxide samples prepared by hydrolysis, precipitation, and calcination has been studied by means of nitrogen adsorption isotherms.[3]

The utility of heat of immersion measurements as an investigative technique in surface chemistry has been well established.[4] Our previous efforts in this field have been confined to thorium oxide.[5–8] Unlike thorium oxide, which exists only in a face-centered cubic structure, zirconium oxide has two crystalline habits, a monoclinic form which is stable below about 1100° and a tetragonal structure which is stable above this temperature.[9] The tetragonal form cannot be retained by quenching from high temperatures but can exist at room temperature if the zirconium oxide is prepared by precipitation or calcination of a salt at reasonably low temperatures.[10] The opportunity to compare the heat of immersion of zirconium oxide, with its unusual phase behavior, with available data for other oxides lends added incentive to the present investigation.

Experimental Section

The calorimeter and its associated instrumentation and techniques have been described in detail.[5] All of the immersion experiments were performed at 25.0°. Sample bulbs and the heat of bulb breaking correction were identical with those used previously.[5] Accuracy of the calorimetric data is estimated to be about 2%, with the limiting factor being the extended reaction period. Total heat evolution during an immersion experiment varied from about 5 to 85 J, depending on sample weight and specific surface area. The calorimeter was calibrated electrically several times during each loading of five samples. For purposes of comparison, the results were reduced to a unit area basis by means of the specific surface areas measured by nitrogen adsorption.

Samples used in the present study were prepared from the same lot of zirconium hydroxide by calcination at selected temperatures in the range of 600–1000°.[11] Pertinent properties of these samples are

(1) Research sponsored by the U. S. Atomic Energy Commission under contract with Union Carbide Corp.

(2) W. D. Harkins and G. E. Boyd, *J. Amer. Chem. Soc.*, 64, 1195 (1942).

(3) H. Th. Rijnten in "Physical and Chemical Aspects of Adsorbents and Catalysts," B. G. Linsen, Ed., Academic Press, New York, N. Y., 1970, Chapter 7.

(4) *E.g.*, A. C. Zettlemoyer and K. S. Narayan in "The Solid-Gas Interface," E. A. Flood, Ed., Marcel Dekker, New York, N. Y., 1967, Chapter 6.

(5) H. F. Holmes and C. H. Secoy, *J. Phys. Chem.*, 69, 151 (1965).

(6) H. F. Holmes, E. L. Fuller, Jr., and C. H. Secoy, *ibid.*, 70, 436 (1966).

(7) E. L. Fuller, Jr., H. F. Holmes, C. H. Secoy, and J. E. Stuckey, *ibid.*, 72, 573 (1968).

(8) H. F. Holmes, E. L. Fuller, Jr., and C. H. Secoy, *ibid.*, 72, 2095 (1968).

(9) *E.g.*, F. A. Mumpton and R. Roy, *J. Amer. Ceram. Soc.*, 43, 234 (1960).

(10) C. T. Lynch, F. W. Vahldiek, and L. B. Robinson, *ibid.*, 44, 147 (1961).

given in Table I.[12] It should be emphasized that the monoclinic phase is the stable low-temperature (below about 1100°) form of zirconium oxide. Sample pretreatment consisted of outgassing for 24 hr at a selected temperature in the range of 25 to 500°. This was selected as the standard outgassing period since outgassing for longer periods had no effect on the results. Final pressures were in the range of 10^{-5} to 10^{-6} Torr and were obtained with a conventional vacuum system (oil diffusion pump and liquid nitrogen trap). As a check on chemical reduction of the surface by organic contaminants,[13] several samples outgassed at 500° were given the oxygen treatment described previously.[5] This treatment had no detectable effect on the results, thus indicating that surface reduction is not a complicating factor in the case of zirconium oxide.

Table I: Properties of ZrO_2 Samples[a]

Sample	Calcining temp, °C	Phase[a]	Specific surface[b] area, m^2/g	Crystallite[a] size, Å
A	600	T[c]	87.4	84
B	700	T	70.8	122
C	800	T	52.7	129
D	900	T + M (tr)	24.5	215
E	1000	M	3.68	264

[a] From X-ray analysis. [b] From nitrogen adsorption at 77°K after outgassing at 300°. [c] T = tetragonal, M = monoclinic, (tr) = trace. [d] Detectable (spectrochemically) impurities (in wt %): Al, 0.01; Ca, 0.04; Cr, 0.004; Cu, 0.001; Fe, 0.3; Mg, 0.002; Mn, 0.005; Si, 0.04; Ti, 0.001.

Results and Discussion

Figure 1 displays the heat of immersion of these five samples of zirconium oxide as a function of the temperature at which the samples were outgassed prior to the immersion experiments. Some indication of the type of interaction involved in the adsorption process can be drawn from the magnitude of the heats of immersion. A physically adsorbed water molecule, occupying an area of 10.6 Å^2 and having a net heat of adsorption of 3 kcal/mol, is equivalent to a heat of immersion of only 315 ergs/cm^2 (including the surface enthalpy of water). The vast majority of the data in Figure 1 is considerably more energetic than this. This clearly indicates that a substantial fraction of the interaction of water with an outgassed zirconium oxide surface is a chemical process. This is not surprising in view of the general occurrence of surface hydroxyl groups on oxide surfaces. Such groups have been shown to exist on zirconium oxide surfaces.[14] Variation of the heat of immersion with outgassing temperature is due to the removal of variable amounts of adsorbed water during the outgassing periods. On

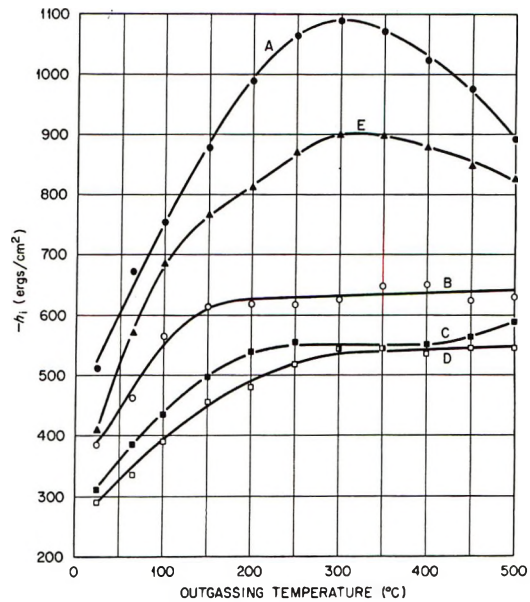

Figure 1. Total heat of immersion of ZrO_2 in water at 25°.

subsequent exposure to liquid water during the immersion process this adsorbed water is replaced with a correspondingly large net heat of adsorption.

Considering only samples A, B, C, and D in Figure 1, the heat of immersion (on a unit area basis) decreases with decreasing specific surface area, with samples C and D having very near the same heat of immersion. This is precisely the behavior observed with two series of thorium oxide samples whose specific surface areas were also varied by calcination at progressively higher temperatures.[5,7] The present trend is opposite to the behavior observed for the heat of immersion of silica,[15-17] titanium oxide,[18] and alumina[19] in water, where the heat of immersion generally decreased with increasing specific surface area. However, in those studies the specific area of the samples was not varied by thermally sintering a common starting material. We explain the present trend by postulating that as the calcination temperature is increased a less heterogeneous and less energetic surface is produced. Such a postulate is consistent with the results obtained for

(11) J. H. Shaffer, W. P. Teichert, W. K. R. Finnell, F. F. Blankenship, and W. R. Grimes, Reactor Chemistry Division Annual Progress Report, ORNL-4076, Dec 31, 1966, p 38.

(12) The data in Table I were obtained by the Analytical Chemistry Division of the Oak Ridge National Laboratory.

(13) C. M. Hollabaugh and J. J. Chessick, *J. Phys. Chem.*, **65**, 109 (1961).

(14) E. L. Fuller, Jr., and H. F. Holmes, unpublished results.

(15) A. C. Makrides and N. Hackerman, *J. Phys. Chem.*, **63**, 594 (1959).

(16) W. H. Wade, R. L. Every, and N. Hackerman, *ibid.*, **64**, 355 (1960).

(17) J. W. Whalen, *Advan. Chem. Ser.*, **No. 33**, 281 (1961).

(18) W. H. Wade and N. Hackerman, *J. Phys. Chem.*, **65**, 1681 (1961).

(19) W. H. Wade and N. Hackerman, *ibid.*, **64**, 1196 (1960).

thorium oxide where samples calcined at 1200° or above had homogeneous surfaces[6,8] and the heat of immersion was independent of specific surface area.[7]

The discussion in the preceding paragraph obviously does not apply to sample E which shows a large increase in the heat of immersion (on a unit area basis) as compared to sample D, which has a much larger specific surface area. From Table I, sample E is the only one of this series which consists entirely of the monoclinic form, which is the stable low-temperature phase from bulk thermodynamics. The results obtained with sample E strongly support the suggestion that the stabilizing factor for the occurrence of the tetragonal form in small crystallite, high area zirconium oxide is the much lower surface energy of the tetragonal form as compared to the monoclinic form. This suggestion originated in a paper by Garvie.[20] This idea has received further support from work by other investigators.[21–23] Garvie[20] suggested a crystallite size of about 300 Å as the dividing line between tetragonal and monoclinic zirconium oxide. This size agrees fairly well with the data shown in Table I. Using thermodynamic arguments and the enthalpy difference between the monoclinic and tetragonal forms,[24] Garvie estimated that, if the surface free energy increased by 360 ergs/cm^2 on changing from the tetragonal to the monoclinic structure, then this could account for the stabilization of the tetragonal structure in small crystallites.[20] This is approximately the increase in the heat of immersion on going from sample D to sample E. This observation lends credence to Garvie's hypothesis.

In marked contrast to our results for thorium oxide,[5,7] sample A exhibits a pronounced maximum in the heat of immersion as a function of outgassing temperature. There are essentially two possible explanations for such a maximum. One is the loss of surface area by sintering at the higher outgassing temperatures. However, surface area measurements before and after such an outgassing period showed no significant change in specific surface area. The second and more likely explanation involves the acquisition of a partial hydrophobic character at the higher outgassing temperatures. In other words, not all of the water removed during outgassing is replaced during the immersion process. This hypothesis has been invoked to explain the maximum observed for the heat of immersion of Al_2O_3,[25] SiO_2,[15–17,26] TiO_2,[18,27] Fe_2O_3,[28] and ZnO.[29] However, other samples of Al_2O_3,[19] TiO_2,[30] and Fe_2O_3[28] have been observed not to have a maximum in the heat of immersion as a function of outgassing temperature. We will present data concerning this hypothesis in a later section.

The vast majority of reported heat of immersion measurements are rapid processes, *i.e.*, they are considered to be instantaneous within the capabilities of the calorimeters used. Such was not the case for the zirconium oxide samples used in the present study. typical behavior observed on immersing a sample is illustrated by some data for sample A (Figure 2). The unaccomplished temperature rise is that portion of the total corrected temperature rise which has not yet occurred at a given time. This quantity is quite analogous to the unreacted fraction in chemical kinetics and, as a matter of fact, this semilog plot is what one would obtain for a first-order process. As shown in Figure 2 this very slow process has a half-life of 27 min.

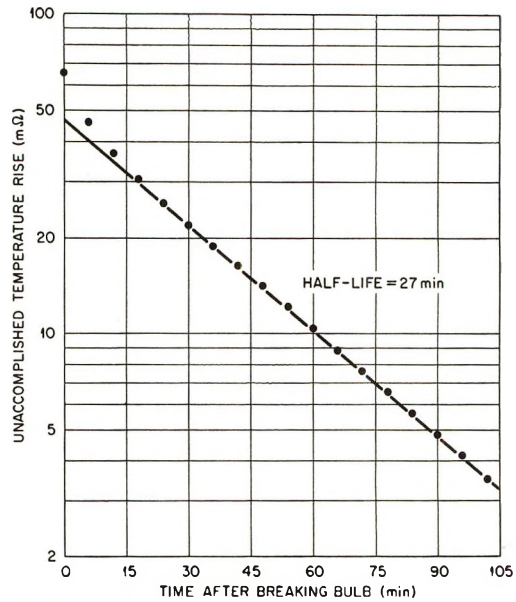

Figure 2. Very slow heat of immersion of ZrO_2 in water at 25°. Sample A outgassed at 300°.

As can be seen in Figure 2, the data at short time intervals deviate markedly from the straight line. If one again plots this deviation as a first-order process, he obtains the result shown in Figure 3. A very nice straight line results but, this time, with a half-life of 3.7 min. Figures 2 and 3 are typical of the behavior which we have observed with all five zirconium oxide samples. Apparently, we are observing two simul-

(20) R. C. Garvie, *J. Phys. Chem.*, **69**, 1238 (1965).

(21) A. Krauth and H. Meyer, *Ber. Deut. Keram. Ges.*, **42**, 61 (1965).

(22) Yu M. Polezhaev, *Zh. Fiz. Khim.*, **41**, 2958 (1967); *Russ. J. Phys. Chem.*, **41**, 1590 (1967).

(23) K. S. Mazdiyasni in "Reactivity of Solids," J. W. Mitchell, R. C. DeVries, R. W. Roberts, and P. Cannon, Ed., Wiley, New York, N. Y., 1969, p 115.

(24) J. P. Coughlin and E. G. King, *J. Amer. Chem. Soc.*, **72**, 2262 (1950).

(25) T. Morimoto, K. Shiomi, and H. Tanaka, *Bull. Chem. Soc. Jap.*, **37**, 392 (1964).

(26) G. J. Young and T. P. Bursh, *J. Colloid Sci.*, **15**, 361 (1960).

(27) T. Morimoto, M. Nagao, and T. Omori, *Bull. Chem. Soc. Jap.*, **42**, 943 (1969).

(28) T. Morimoto, H. Naono, N. Katayama, and M. Nagao, *ibid.*, **42**, 1490 (1969).

(29) T. Morimoto, M. Nagao, and M. Hirata, *Kolloid-Z. Z. Polym.*, **225**, 29 (1968).

(30) T. Omori, J. Imai, M. Nagao, and T. Morimoto, *Bull. Chem. Soc. Jap.*, **42**, 2198 (1969).

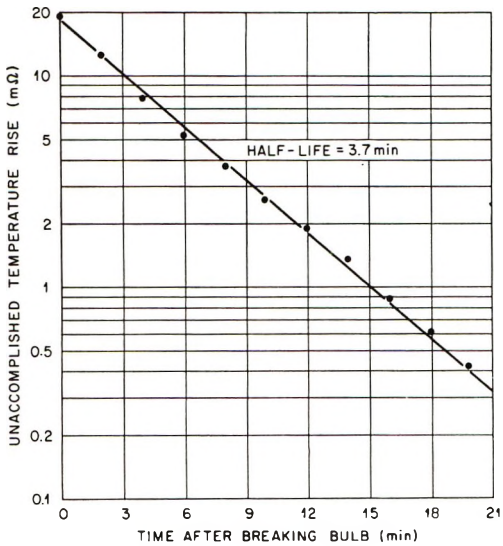

Figure 3. Slow heat of immersion of ZrO_2 in water at 25°. Sample A outgassed at 300°.

taneous first-order processes with half-lives of about 4 ± 1.5 and 30 ± 5 min for the slow and very slow processes, respectively. Within the experimental error, the kinetics of these slow processes was the same for all samples and was also independent of outgassing temperature. In contrast to the kinetics, the quantity of energy involved in the slow processes was dependent on the sample of the outgassing temperature. This point is illustrated by the data (on a unit area basis) for the very slow (30-min half-life) process which are shown in Figure 4. Although the data are not as reproducible as the total heats of immersion, sample B appears to have a maximum value at an outgassing temperature of about 150°. The maximum value for sample A occurs at about the same outgassing temperature as observed for the total heat of immersion. With the exception of sample A there is a general increase in the very slow heat of immersion for outgassing temperature above 350°. Sample C appears to have a slight peak at an outgassing temperature of 250°. Results for the slow heat (4-min half-life) followed the general trends shown in Figure 4 but with a smaller quantity of heat involved. The slow heat of immersion of sample A varied from about 40 to 150 ergs/cm² with the maximum value occurring at an outgassing temperature of about 350°. Results for the other four samples were generally less than 50 ergs/cm².

Total (slow plus very slow processes) slow heats of immersion of these samples of zirconium oxide are shown in Figure 5. Trends with outgassing temperature are generally the same as observed with the very slow heats of immersion (Figure 4). The data shown in Figure 5 represent a significant fraction of the total heat of immersion of zirconium oxide (Figure 1). This fraction varies from about 8 to 36% of the total heat, is largest for sample A, and is dependent on outgassing

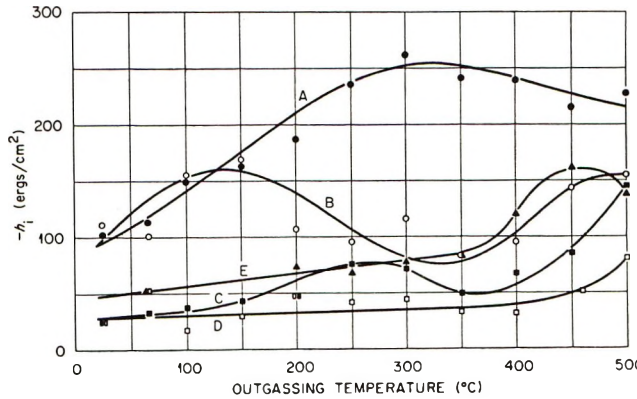

Figure 4. Very slow heat of immersion of ZrO_2 in water at 25°.

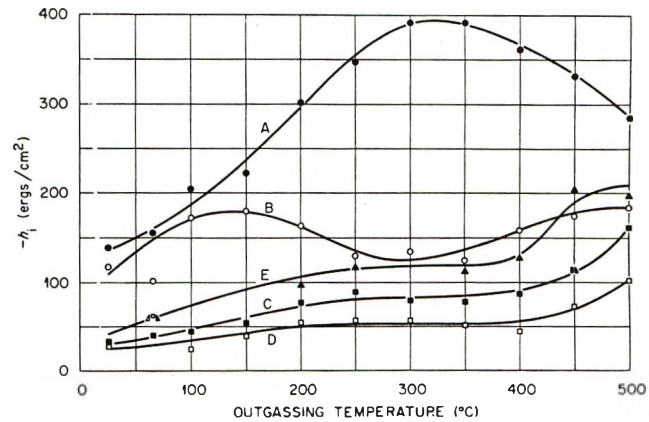

Figure 5. Total slow heat of immersion of ZrO_2 in water at 25°.

temperature. Slow heats of immersion have previously been reported for the immersion of alumina,[31] silica,[17,31] and thoria[5,7] in water. For the alumina–water system the quantity of slow heat and its half-life increased with outgassing temperature.[31] Corresponding data were not given for the silica–water system. For both systems the slow heat phenomena were attributed to a slow rehydroxylation of surface oxide group resulting from the outgassing procedure. If the slow step in the immersion process were rehydroxylation of surface oxide groups, one would expect the half-life of the slow heat to vary with outgassing temperature. However, half-lives for the slow processes in the thoria–water system,[5,7] as well as the present system, are essentially independent of outgassing temperature. Because slow heat was *always* observed with porous samples but *never* with nonporous samples, the slow step in the thoria–water system was postulated to be the diffusion of water into the porous structure of the particles.[5,7] A detailed porosity analysis has not been done on the present zirconium oxide samples, but samples prepared in a similar manner are known to be porous.[3] This does not imply that rehydroxylation is not oc-

(31) C. A. Gunderjahn, D. A. Paynter, P. E. Berghausen, and R. J. Good, *J. Phys. Chem.*, **63**, 2066 (1959).

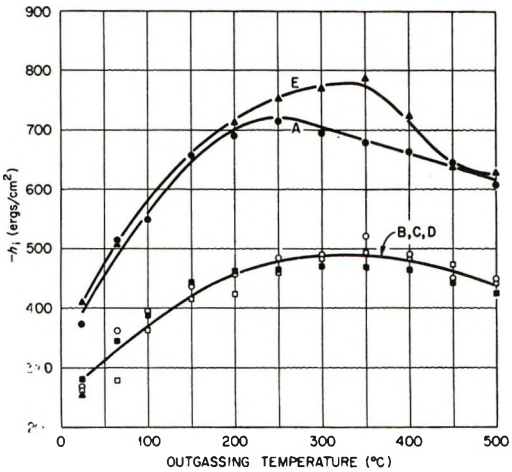

Figure 6. Immediate heat of immersion of ZrO_2 in water at 25°.

curring during the slow processes, but only that any such surface oxide groups are located in the interior of pores.

By a simple subtraction one can obtain the heat which is released immediately on immersion of the samples. These data, again on a unit area basis, are shown in Figure 6. Within experimental error, the immediate heat of immersion is the same for samples B, C, and D at all outgassing temperatures. This fact indicates that the initial, rapid interaction of water with the surfaces of these three samples is identical and independent of specific surface area. Sample E, which is the only sample in the stable monoclinic modification, is now the most energetic on this basis. The magnitude of the immediate heats of immersion leads one to conclude that a substantial fraction, if not the majority, of the rehydroxylation of surface oxide groups is a rapid reaction. However, all of the samples now exhibit a maximum in the heat of immersion as a function of outgassing temperature. This observation leads one to suspect that a not inconsequential portion of the surface oxide groups, even on the open surface, rehydroxylate at a slow rate.

As expected, weight loss data from the preparation of calorimetric samples were found to be very dependent on the ambient atmosphere at the time of sample preparation. However, the data were quite reproducible if the samples were prepared in the same time period. Such data for samples A and D are shown in Figure 7. Just as was seen in the data for the total heats of immersion, these two samples, having a common chemical history but different calcining temperatures, have quite different surface characteristics. Sample D has the more usual type of weight loss curve. The inflection in the weight loss curve for sample A comes at just the point where the maximum occurs in the heat of immersion data. This would indicate that, in some manner, the removal of water between 300 and 500° is reducing the ability of the surface to interact with water. The data shown in Figure 7 reflect a further

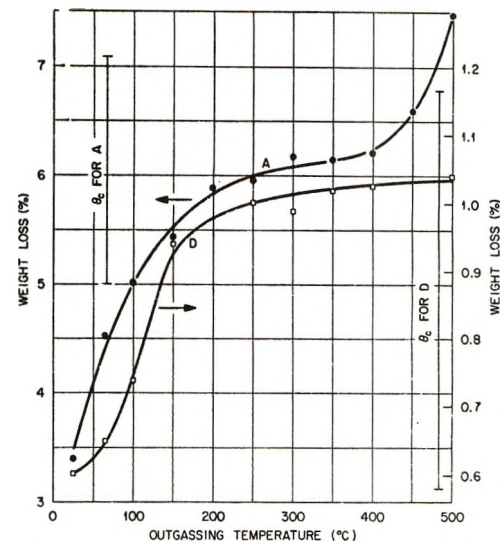

Figure 7. Weight loss on outgassing ZrO_2.

interesting difference in samples A and D. There are two vertical scales in this figure labeled θ_0 for A and θ_0 for D. These are the calculated water chemisorption capacities for these two samples using an average value for the area occupied by a surface hydroxyl group.[32] While the total weight loss between 25 and 500° is equivalent to about 0.7 monolayer of chemisorbed water for sample D, it is equivalent to about two monolayers in the case of sample A. If one assumes that all of the material which is lost on outgassing is water, then one can, by using the heat of immersion data, calculate the average net heat of adsorption for the water which is lost between outgassing at 25 and 300°. These values turn out to be 8.8 and 6.6 kcal/mol of water for samples A and D, respectively. Not only is there more water per unit area on sample A, but the adsorption process is more energetic than on sample D.

Finally, the results of some simple experiments are pertinent to the discussion of this system. Aliquots of samples A and C were outgassed at 300 and 500°, and then liquid water was placed on the samples. Subsequently the samples were dried in a stream of dry air (P/P_0 less than 0.01) to a constant weight, with the amount of irreversibly adsorbed water calculated from the increase in weight due to the water treatment. The results are given in Table II. Monolayers were calculated using an average value for the area occupied by a surface hydroxyl group.[32] The time intervals given in the first column refer to the time lapse between placing liquid water on the sample and starting the flow of dry air. About 8 hr was required to produce a visibly dry sample, but an additional 1 to 2 weeks of dry air flow was necessary to produce a constant weight. On this basis the data in the first row are roughly analogous in duration to a calorimetric experiment. The data for sample C are, within experimental error, inde-

(32) D. R. Vissers, *J. Phys. Chem.*, **72**, 3236 (1968).

pendent of outgassing temperature and length of time in liquid water. This can explain the relative constancy of the heat of immersion of sample C over this range of outgassing temperatures and indicates that the calorimeter is detecting all of the adsorption process. Sample A is, again, quite a different matter. The data certainly indicate that the calorimeter is *not* sensing all of the reaction. Furthermore, the maximum in the heat of immersion curve for sample A (Figure 1) may be an artifact because, after outgassing at 300° a larger fraction of the total adsorption process is complete in the time interval of a calorimetric experiment. The extremely slow rehydration process which requires more than 1 week for completion (and is, therefore, not measured by the calorimeter) in the case of sample A points to the production of a surface with considerable hydrophobicity in the kinetic sense. However, it should be emphasized that the data in Table II do not rule out porosity as a factor in the slow processes observed with the calorimeter. The experimental data in this paper point to both porosity and hydrophobicity as complicating factors in the zirconium oxide–water system. At the same time, the data do not permit one to decide which of these factors is dominant in specific cases. It should be emphasized that we have applied the term hydrophobicity to this system only in the kinetic sense. From the magnitude of the heats of immersion in Figure 1 it would not make sense to use hydrophobicity as indicating that these surfaces have no affinity for water.

Table II: Monolayers of Irreversibly Adsorbed Water on ZrO_2 at 25°

Days in H_2O (L)	A outgassed at 300°	A outgassed at 500°	C outgassed at 300°	C outgassed at 500°
0	1.45	1.13	0.60	0.59
1		1.41	0.62	
3	1.79	1.52		
7		1.70	0.57	
35				0.64
80	2.04	2.03		

Our tentative conclusions are that the characteristics of the zirconium oxide–water interface are intermediate between those of the thoria–water interface and the silica–water interface. Of the systems reported in the literature, the alumina–water system more closely resembles the zirconium oxide–water system in behavior. Our own work has shown that there is a great deal of complexity in the chemistry of the thorium oxide–water interface. The zirconium oxide–water interface gives indications of being at least equally, if not more, complex.

A Comparison of Measured Optical Anisotropy Values with Those Calculated by Means of Two δ-Function-Potential Models

by W. H. Nelson

Department of Chemistry, University of Rhode Island, Kingston, Rhode Island 02881 *(Received January 3, 1972)*

Publication costs assisted by the University of Rhode Island

Molecular optical anisotropies of 16 model compounds of known structure have been calculated by two methods based upon a δ-function-potential model. Calculated values have been compared with those measured by means of Rayleigh light scattering from gases at 6328 Å. The usefulness of the models for the calculation of optical anisotropies of candidate molecules has been discussed.

Two methods, both of which are based upon a δ-function-potential model, have been applied extensively for the calculation of bond polarizability components. The method published by Lippincott and Stutman[1] has been used quite effectively to predict molecular refractions. The second method, that of Long and Plane,[2] involves slightly different assumptions, and has been applied successfully to predict absolute Raman intensities of A_1 vibrational modes for a variety of simple molecules.[2,3]

(1) E. R. Lippincott and J. M. Stutman, *J. Phys. Chem.*, **68**, 2926 (1964).

(2) T. V. Long and R. A. Plane, *J. Chem. Phys.*, **43**, 457 (1965).

(3) B. Fontal and T. G. Spiro, *Inorg. Chem.*, **10**, 9 (1971).

Table I: A Comparison of Calculated and Measured Optical Anisotropy Values for 16 Molecules

Molecule	Lippincott–Stutman 10^{24} cm^{-3} $\alpha_{\|\|}$[a]	Long–Plane 10^{24} cm^{-3} $\alpha_{\|\|}$	Lippincott–Stutman 10^{24} cm^{-3} $\alpha_{\perp}$[b]	Long–Plane 10^{48} cm^{-6} γ^2	Lippincott–Stutman 10^{48} cm^{-6} γ^2	Obsd 10^{48} cm^{-6} γ^2
H_2	0.326	0.94	1.1	0.044	0.735	0.099
N_2	2.6	2.1	1.49	0.36	1.28	0.48
O_2	3.0	2.4	1.18	0.83	3.30	1.19
Cl_2	8.20	6.8	2.78	10.8	29.3	6.75
CO	2.4	2.0	1.45	0.33	0.95	0.28
NO	2.7	2.1	1.32	0.56	1.91	0.71
HCl	2.3	2.5	2.09	0.19	0.05	0.097
SO_2	3.3	2.6	1.04	4.34	7.56	4.18
NH_3	0.62	0.80	0.48	0.084	0.0001	0.083
C_2H_6				0.27	3.9	0.60
C_2H_4				7.17	2.59	3.60
C_2H_2				4.89	1.04	3.46
CH_3OH				0.00	3.16	0.63
CH_3Cl				3.88	1.61	2.40
CH_2Cl_2				5.44	2.17	7.91
$CHCl_3$				4.25	1.88	7.19

[a] $\alpha_{\|\|}$ is the longitudinal bond polarizability. [b] $\alpha_{\perp}$ is the transverse bond polarizability

Recently, it has been shown[4] that it is possible to determine the structures of relatively large, highly labile molecules in solution by means of depolarized Rayleigh scattering intensity measurements if bond polarizability component values are available. For each candidate molecular structure a diagonalized polarizability tensor with nonzero elements, α_{xx}, α_{yy}, and α_{zz}, can be obtained by the addition of diagonalized bond polarizability tensors transformed to the molecular coordinate system.[5] Consequently, the molecular optical anisotropy, $\gamma^2 = {}^1/_2[(\alpha_{xx} - \alpha_{yy})^2 + (\alpha_{xx} - \alpha_{zz})^2 + (\alpha_{yy} - \alpha_{zz})^2]$, can be calculated and the intensity of depolarized Rayleigh scattered light predicted for a candidate molecule either as a gas[6] or as a solute species[7-9] dissolved in a weakly interacting solvent such as cyclohexane or carbon tetrachloride.

A comparison of calculated and measured depolarized scattered light intensities allows an assignment of the correct molecular structure to be made if the different candidate structures are characterized by substantially different optical anisotropies. Naturally, if the light scattering method is to be applied successfully it is critically important that bond polarizability components be measured or calculated precisely since differences in optical anisotropy associated with candidate structures may be small. If differences in the calculated anisotropy values for candidate structures are small, or if uncertainties in the calculated or measured molecular anisotropy values are large, the Rayleigh scattering depolarization method is handicapped as a means of determining molecular structure. Because only a handful of bond polarizability components have been determined experimentally, it is essential that the precision of the most promising methods of bond polarizability component calculation be examined to determine whether or not they can be applied reliably for the purpose of calculating molecular optical anisotropies.

Calculations

Molecular optical anisotropies for 16 representative model compounds of known structure have been calculated by the methods of Lippincott and Stutman and Long and Plane, respectively. In order to determine and compare the suitability of each method of calculation for the purpose of predicting anisotropy values, the calculated values have been compared with those experimentally determined by means of dipolarized laser scattering[10] from gases. Results appear in Table I.

Discussion

It is remarkable that the Long–Plane Model allows the calculation of anisotropy values for all 16 molecules with an average error of only 36%. Quite notably, all calculated values except that of ethanol are within at least an order of magnitude of the correct ones. Hence, it appears that optical anisotropies of candidate structures can be calculated with considerable confidence. It might be pointed out that the models really are even better than the anisotropy data indicate since errors in the polarizability components appear nearly as the square in anisotropy values. Of course

(4) W. R. Russo and W. H. Nelson, *J. Amer. Chem. Soc.*, **92**, 1521 (1970).

(5) R. S. Smith and E. Mortensen, *J. Chem. Phys.*, **32**, 503 (1960).

(6) R. Gans, *Ann. Phys.*, **37**, 881 (1912); **65**, 97 (1921).

(7) A. Unanue and P. Bothorel, *Bull. Soc. Chim. Fr.*, 573 (1964).

(8) D. J. Coumou, J. Hijmans, and E. L. Mackor, *Trans. Faraday Soc.*, **60**, 2244 (1964).

(9) D. J. Coumou, *ibid.*, **65**, 2654 (1969).

(10) N. J. Bridge and A. D. Buckingham, *Proc. Roy. Soc., Ser. A*, **295**, 334 (1966).

it is the larger errors in the calculated anisotropy values which are of concern to light scattering work. Fortunately, candidate structures often do have optical anisotropies which differ by many orders of magnitude and have corresponding vastly different predicted depolarized Rayleigh light scattering intensity values.[4] Conjugated systems and other molecules such as CH_2Cl_2 and $CHCl_3$ which do not obey the bond additivity principle for molecular refraction[10] are not expected to be treated successfully using these simple models.

COMMUNICATIONS TO THE EDITOR

Electron Spin Resonance Studies of Cation Radicals in Trifluoromethanesulfonic Acid

Publication costs assisted by the Food and Drug Administration

Sir: Concentrated sulfuric acid was been widely used as a solvent for the generation of positive ion free radicals for esr studies.[1] However, the conventional use of sulfuric acid suffers from many limitations, *i.e.*, large microwave dielectric losses, high viscosity, high freezing point, and low radical yield coupled with short radical lifetime partially due to the low solubility of the organic compounds under study.

In the study of the color transformation of dibenzo-*p*-dioxins (I) in acid solution[2] which are characteristic for

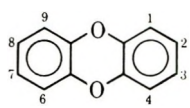

I

compounds containing the dibenzo-*p*-dioxin ring system, most of the highly chlorinated species were extremely insoluble in concentrated sulfuric acid. In all instances, an oxidizing agent was required for the generation of cation radicals, and the radical lifetimes were short even with well degassed and sealed samples. The purpose of this communication is to report the use of trifluoromethanesulfonic acid (TFMS acid) as a convenient solvent for the generation of cation radicals in esr studies.

The esr spectrum of I in concentrated sulfuric acid has been reported with hydrogen peroxide and potassium nitrate as oxidizing agents.[3,4] The spectrum consists of five lines with intensity ratios of 1:4:6:4:1, arising from the interaction of the delocalized, unpaired electron with the four equivalent protons in the 2, 3, 7, and 8 positions.

Two additional ^{13}C splittings were also observed and reported.[3] An identical spectrum (Figure 1) was obtained in TFMS acid without the addition of an oxidizing agent other than the small quantity of oxygen present in the acid. The measured g factor, proton, and ^{13}C coupling constants were tabulated and are shown in Table I for both sulfuric and TFMS acids as solvents. The line width was found to be less than 40 mOe. No decrease in radical concentration was detected in 6 months in a well degassed, sealed sample.

Table I: Comparison of Measured Esr Parameters of Dibenzo-*p*-dioxin in TFMS and Sulfuric Acids

	TFMS	H_2SO_4[3]
g Factor	2.0038	2.0034; 2.0038[a]
$A^{2,3,7,8H}$, Oe	2.178	2.52; 2.13[a]
$A^{1,4,6,9H}$, Oe	<0.15	<0.5
A^{13C}, Oe	1.650	1.77
$A^{13C'}$, Oe	2.708	3.27
Line width, Oe	<0.04	0.17; <0.08[a]

[a] Unpublished data of Yang and Pohland.

The esr spectrum of 2,3-dichlorodibenzo-*p*-dioxin in TFMS acid is shown in Figure 2. In concentrated sulfuric acid, this compound does not exhibit an esr spectrum unless an oxidizing agent such as KNO_3 is added, and hyperfine splittings were not observed. On the other hand, in TFMS acid a well resolved spectrum was observed without the addition of any oxidizing agent.

The more highly chlorinated dibenzo-*p*-dioxins were observed to be extremely insoluble in concentrated sulfuric acid. For instance, octachlorodibenzo-*p*-dioxin was found to produce no esr spectrum even in the presence of potassium nitrate.[4] In TFMS acid, however, a strong esr signal was observed, although in this case an oxidizing agent or uv irradiation was needed to generate the free radicals. The ability of TFMS

(1) A. Carrington, F. Dravinick, and M. C. R. Symons, *J. Chem. Soc.*, 947 (1959).

(2) M. Tomita, S. I. Ueda, and M. Narisada, *Yakugaku Zasshi*, 79, 186 (1959).

(3) T. N. Tozer and L. D. Tuck, *J. Chem. Phys.*, 38, 3035 (1963).

(4) M. Tomita and S. Ueda, *Chem. Pharm. Bull. (Tokyo)*, 12, 33 (1964).

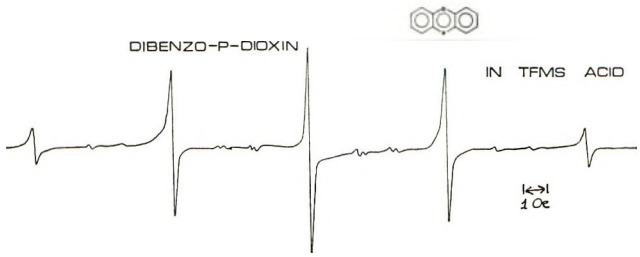

Figure 1. Esr spectrum of dibenzo-*p*-dioxin in TFMS acid.

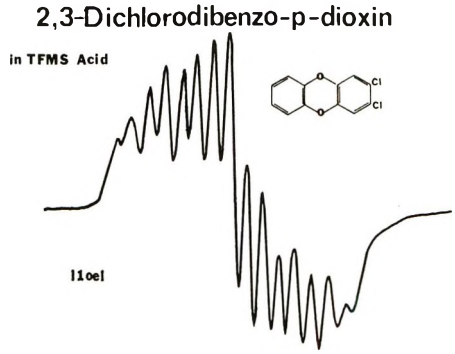

Figure 2. Esr spectrum of 2,3-dichlorodibenzo-*p*-dioxin in TFMS acid.

acid to dissolve this compound in sufficient quantity may be ascribed to its extremely high acidity.[5]

Other aromatic hydrocarbons were observed to yield well resolved esr spectra in TFMS acid. For example, anthracene and 9,10-dimethylanthracene cation radicals generated in TFMS acid solvent exhibited known spectra with line width comparable to the homogeneity of the electromagnet. We believe, therefore, that this solvent will become extremely valuable in the generation of cation radicals for esr spectral studies, not only because of its high acid strength, but also because of its other useful properties, such as low freezing point and low viscosity.

(5) T. Gramstad, *Tidsskr. Kjemi. Bergv. Met.*, **19**, 62 (1959); *Chem. Abstr.*, **54**, 12739 (1960).

DIVISION OF CHEMISTRY AND PHYSICS
FOOD AND DRUG ADMINISTRATION
DEPARTMENT OF HEALTH, EDUCATION, AND WELFARE
WASHINGTON, D. C. 20204

G. C. YANG*
A. E. POHLAND

RECEIVED JANUARY 17, 1972

Exchange of Water Molecules at Air–Water Interfaces

Publication costs assisted by C.S.I.R.O., Auslralia

Sir: It has been shown recently[1] that H_2O is absorbed initially at a steady rate into a sample of D_2O held in a small beaker supported above an extensive surface of H_2O contained in a large glass tank. Shah[1] postulated that this absorption is controlled by the equilibrium rate of exchange of water molecules at the interface. From the observed rate of uptake, 8.5 mg m^{-2} sec^{-1}, he deduced the average time of residence of a water molecule at the surface to be about $^1/_{60}$ sec. This is immensely greater than the residence time of about 10^{-7} sec estimated from kinetic theory.[2]

This discrepancy is explained readily. The vapor pressure of H_2O above pure liquid D_2O is zero, so that water vapor transfers from liquid H_2O to liquid D_2O at a rate per unit area of

$$R = C_0/(\Omega_A + \Omega_D + \Omega_H) \qquad (1)$$

Here C_0 is the concentration of water vapor in equilibrium with liquid H_2O, Ω_A is the resistance encountered in the vapor space between the two liquids, Ω_D is the resistance to transfer through the D_2O interface, and Ω_H applies to the H_2O interface. As in more conventional studies of evaporation and condensation,[3-5] specific surface effects may be detected experimentally only if Ω_A is sufficiently small to be comparable with Ω_D and Ω_H; this follows from (1). The resistance of a water surface is of the order of 0.1 to 1 sec m^{-1}, its actual value depending upon the debated[6] condensation coefficient for water. The resistance Ω_D should be of the same order. If the vapor traveled between the two surfaces by molecular diffusion along a path of length l, then

$$\Omega_A = l/D$$

where D is the diffusion coefficient. For Shah's apparatus, a diffusion path of 50 to 100 mm seems appropriate, so that Ω_A should lie between 2000 and 4000 sec m^{-1}. (From tabulated data, the diffusion coefficient of water vapor in air is about 2.5×10^{-5} m^2 sec^{-1}.) For these figures $\Omega_A \gg \Omega_H + \Omega_D$, so that the observed rate of absorption depends negligibly upon surface processes like equilibrium exchange rates.

Substitution into Shah's data gives 2700 sec m^{-1} as the summed resistance. This indicates $l \sim 70$ mm, entirely consistent with this discussion.

(1) D. O. Shah, *J. Phys. Chem.*, **75**, 2694 (1971).

(2) N. K. Adam, "The Physics and Chemistry of Surfaces," 3rd ed, Oxford University Press, London, 1941, p 6.

(3) I. Langmuir and V. J. Schaeffer, *J. Franklin Inst.*, **235**, 119 (1943).

(4) R. J. Archer and V. K. La Mer, *Ann. N. Y., Acad. Sci.*, **58**, 807 (1954).

(5) W. W. Mansfield, *Aust. J. Appl. Sci.*, **9**, 245 (1958).

(6) J. H. de Boer, "The Dynamical Character of Adsorption," 2nd ed, Oxford University Press, London, 1968, p 52.

CSIRO DIVISION OF APPLIED CHEMISTRY
MELBOURNE, VICTORIA 3001, AUSTRALIA

W. W. MANSFIELD

RECEIVED OCTOBER 15, 1971

Ultrasonic Relaxation in Calcium Nitrate Tetrahydrate Melts

Publication costs assisted by the National Science Foundation and the Office of Naval Research

Sir: Darbari and Petrucci[1] have reported ultrasonic absorption data for $Ca(NO_3)_2 \cdot 4H_2O$ melts which indicate a relaxation frequency of ~25 MHz. The relaxation frequency was found to increase with increasing water content but to be temperature independent over the range 30–60° for the tetrahydrate. The latter is rather surprising since other physical and chemical properties of such viscous hydrate melts are usually qutie temperature dependent. Some temperature dependence of the relaxation frequency has been reported by these authors for the melts containing more water but the difficulty in fitting a single relaxation curve to their data and the scatter of the data make the evaluation of the temperature dependence of the relaxation frequency quite dubious.

We have reexamined this system. When the measurements were carried out without precautions to remove bubbles, the α/f^2 values (α = absorption coefficient; f = frequency) were found to increase substantially at frequencies below 100 MHz as had been observed by Darbari and Petrucci[1] although the results did not agree. When steps were taken to remove bubbles, however, the results were quite different and are reported in this communication. Small bubbles can be readily observed by scattered light when the solid hydrate is melted. Further, even if the melts are heated to temperatures where the bubbles disappear, bubbles may reappear when the melts are cooled down to lower temperatures.

Reagent grade $Ca(NO_3)_2 \cdot 4H_2O$ (supplied by Matheson Coleman and Bell) was diluted with distilled water to a total of ~8 mol of H_2O/mol of $Ca(NO_3)_2$ to lower the melting point and viscosity so as to facilitate filtering through a Pyrex frit (4–5.5 μ max pore size). The sample was then transferred to a spherical flask and degassed under vacuum while exposed to 20-kHz high-intensity sound waves transmitted through the walls of the vessel with the total acoustical energy output of the transducer estimated to be 50–100 W. This vacuum–acoustic treatment was continued for 12 hr and served to degas the liquid while simultaneously reconcentrating the solution.

The composition of the melt was determined by two methods. One method involved drying the sample under vacuum while slowly raising the temperature to 200° and determining the amount of water by weight loss. The other method involved determining the Ca^{2+} content by titration with a standardized EDTA solution. The results by both methods agreed in all instances to at least ±0.5%.

One large sample of each composition was prepared and from this the ultrasonic absorption cells were filled a number of times with care to minimize redissolution of air or whipping of bubbles into the solutions. No detectable deviations were observed from filling to filling of the ultrasonic cells.

The ultrasonic absorption was measured with two separate sets of apparatus, both of which involved send–receive techniques with pulse-modulated ultrasonic waves. One apparatus, designed for measurements at elevated as well as room temperatures, covered the frequency range 5–85 MHz. This apparatus used two quartz delay lines of 8-in. length each, the unusual length a feature intended to provide thermal isolation between the liquid under study and the sending and receiving quartz transducers (5-MHz X-cut quartz crystals) attached to them. The path length within the liquid under study (between the opposing ends of the delay lines) was controlled with a precision micrometer to within $\pm 1 \times 10^{-4}$ cm. The attenuation was measured with increasing liquid path length using a comparison method with a Daven TS-497B signal generator operating in the pulse mode as a voltage substitution standard. Acoustic diffraction corrections[2] were found significant only at the lowest frequency (5 MHz).

The second ultrasonic system was the same as was used in prior work in this laboratory[3] and was used to cover the range 30–470 MHz. With either ultrasonic apparatus, temperature control was at least to ±0.3° over long periods (several hours) with the fluctuations over the time for a typical run not more than ±0.1°.

The results are indicated in Figure 1 in terms of α/f^2 where α is the absorption coefficient in cm^{-1} and f is the frequency in hertz. The values were measured in random order at various odd harmonies of the quartz transducers plus the fundamental. Also shown are some of the Darbari–Petrucci data. The present data indicate a much higher relaxation frequency than found by these workers at comparable compositions. Furthermore, the relaxation frequency apparently increases with temperature rather than being temperature invariant. Interpolating the Darbari–Petrucci data for α/f^2 to the compositions and temperatures of the present study indicates that their results at lower frequencies are also significantly higher than those obtained in the present study.

We propose that the explanation for this discrepancy is bubbles in the work of Darbari and Petrucci. These workers do not indicate in their publication any special steps to eliminate bubbles. Bubbles are known to increase ultrasonic absorption in liquids (see, *e.g.*, ref 4 and 5). Bubbles with radii in the range 10^{-4} to 10^{-5}

(1) G. S. Darbari and S. Petrucci, *J. Phys. Chem.*, **73**, 921 (1969).

(2) H. Seki, A. Granato, and R. Truell, *J. Acoust. Soc. Amer.*, **28**, 230 (1956).

(3) L. Jackopin and E. Yeager, *J. Phys. Chem.*, **74**, 3766 (1970).

(4) S. Devin, *J. Acoust. Soc. Amer.*, **31**, 1654 (1959).

(5) T. Hueter and R. Bolt, "Sonics," Wiley, New York, N. Y., 1955, pp 228–233.

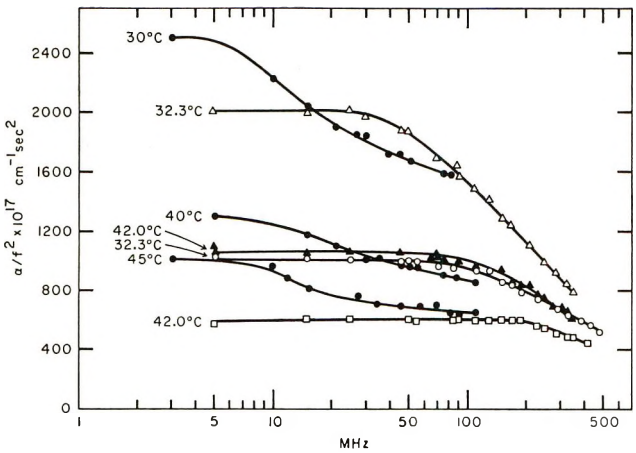

Figure 1. Plot of α/f^2 *vs.* frequency for various water concentrations of $Ca(NO_3)_2 \cdot xH_2O$ at different temperatures. Present work: △, ▲, $x = 3.73$; ○, □, $x = 4.14$. Reference 1 (Darbari and Petrucci): ●, $x = 4.0$

cm should have resonance frequencies in the range 5×10^6 to 5×10^7 Hz and could give rise to anomalous absorption in this frequency range.

Hydrolysis is unlikely as a possible explanation since small additions of concentrated nitric acid to the hydrate melts did not have any appreciable effect on the results. It is very unlikely that any appreciable sonochemical reaction was produced by the ultrasonic degassing. We know of no instance where *substantial* changes in chemical composition have been produced with ultrasonic treatment[6] other than in high molecular weight polymers which are sensitive to shear degradation and free radical chain reactions. If any trace amount of an impurity (*e.g.*, nitrites) was produced by the ultrasonic treatment, it certainly would not be expected to *decrease* by a *large* amount the ultrasonic absorption associated with the major components. Furthermore, vacuum filtering without the ultrasonic treatment also lowered the observed absorption but not by as much as the ultrasonic degassing. The degassing of viscous liquids is very difficult.

When the ultrasonically degassed melts were allowed to crystallize *several times in air*, the absorption coefficient was found to increase by an easily detectable amount at the lower frequencies. It was also noticed that the melts became turbid.

The relaxation frequencies corresponding to the present α/f^2 data cannot be evaluated accurately because of the lack of data at sufficiently high frequencies. An estimate has been made of the relaxation frequency for $Ca(NO_3)_2 \cdot 3.73H_2O$ at 32° on the basis that the data can be fitted to a single relaxation. The value so obtained is 170 ± 30 MHz. The validity of fitting these data to a single relaxation, however, is open to question.

Brillouin scattering experiments are now underway in an attempt to obtain absorption data at frequencies in the low gigahertz region.

Acknowledgment. This work has been supported by a contract with the Office of Naval Research and grants from NATO and NSF. The authors gratefully acknowledge helpful discussions with Dr. L. Jackopin, relating to the ultrasonic instrumentation.

(6) E. Yeager and F. Hovorka, "Ultrasonics," in "Encyclopedia of Chemical Technology," Vol. 14, Interscience, New York, N. Y., 1955, pp 407–422.

CASE WESTERN RESERVE UNIVERSITY
CLEVELAND, OHIO 44106

STUART SMEDLEY
C. HALL
ERNEST YEAGER*

RECEIVED OCTOBER 18, 1971

Ultrasonic Relaxation in Calcium Nitrate Hydrated Melts

Publication costs borne completely by The Journal of Physical Chemistry

Sir: In answer to the communication of Yeager, *et al.*,[1] we shall deal first with the reliability of Yeager's findings and the possible significance of them, and then we shall discuss the origin of the observed discrepancies.

We have repeated the experiment of Yeager starting with $Ca(NO_3)_2 \cdot 8H_2O$, and concentrating to $Ca(NO_3)_2 \cdot 3.62H_2O$ with simultaneously a high intensity 20-kHz ultrasonic field and vacuum for 5 hr. The melt was analyzed for Ca^{2+} by cation exchange and for NO_3^- by differential spectrophotometry at 3100 Å; there was a 0.5% (absolute) disagreement between the two independent analyses. Ultrasonic absorption data at 45° for this melt are shown in Figure 1. The dashed line shows Yeager's result for $Ca(NO_3)_2 \cdot 3.73H_2O$ at 42°. This experiment reproduces in substance his findings.

With the melt presumably so purified, we introduced bubbles into it by forcing N_2 for 0.5 hr at room temperature. The liquid stood overnight in a closed container. It froze and was remelted in the same sealed vessel. Some opacity was observed. Without precautions to avoid bubbles, the melt was transferred to an ultrasonic cell, and the experiment was repeated at 45°. The surprising result (Figure 1) is that, instead of obtaining a large absorption increase as claimed,[1] the same data were obtained as in the first experiment, within experimental error. Further trials of introducing gas into the melts were repeated by bubbling air for about 1 hr into it. The melt was now very turbid. Ultrasonic runs were repeated shortly thereafter, and again 4 days later at the same temperature, 45° (Figure 1); again, the same results were obtained. Because of the possible claim that bubble size distribution would affect the position of the claimed spurious relaxation, N_2 was bubbled into the melt at about 55° through a 1-mm

(1) S. Smedley, C. Hall, and E. Yeager, *J. Phys. Chem.*, 76, 1506 (1972).

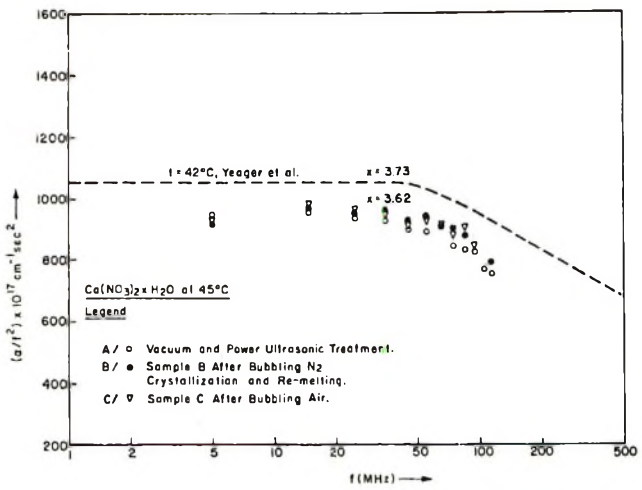

Figure 1. Plot of αf^{-2} *vs.* frequency, f, for $Ca(NO_3)_2 \cdot 3.62H_2O$ at 45°. Melts treated as indicated.

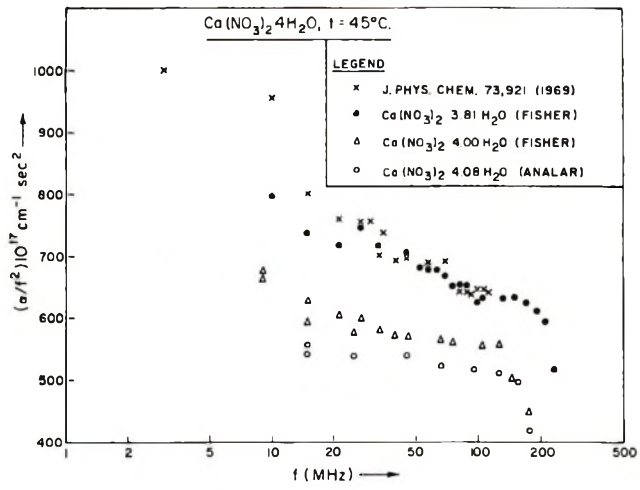

Figure 2. Plot of αf^{-2} *vs.* frequency, f, for $Ca(NO_3)_2 \cdot xH_2O$ at 45°, where x = 3.81, 4.00, and 4.08. For each composition, the same results were obtained whether the salt was simply melted or filtered (10-μm pore size) under a vacuum of 30 mm.

capillary and a 10-μm pore size glass frit, each for 72 hr. Once again, the sound absorption was unaltered.

Another argument against the thesis of the bubbles emerges when the problem of reproducibility is considered, since it is unlikely that two melts would contain similar concentration and size distribution of bubbles. On the contrary, when two melts of exactly the same composition (within ±0.02 mol of water/mol of salt) were recently prepared, we invariably obtained ultrasonic absorption results within experimental error. Also, temperature recycling of the melts should make the data, if they are influenced by bubbles, irreproducible, which is contrary to our observations.

The argument presented by Yeager, *et al.*,[1] that the resonance frequency of pulsating bubbles of 1-μm (10^{-4} cm) and 0.1-μm diameter is the cause of the excess sound absorption does not find substance if the shape of the sound absorption relaxation spectrum is considered.

From the quoted[1] paper of Devin,[2] it is true that for a bubble of 1-μm radius R_0, the resonance frequency $f_M \approx (3\gamma P_0/\rho)^{1/2}/2\pi R_0 = 6.6$ MHz, where $\gamma = C_p/C_v$, *i.e.*, the ratio of the specific heats at constant pressure and volume; here it is assumed to be 1.4; P_0 is the static pressure, about 1×10^6 dyn cm^{-2}; ρ is the density of the liquid. However, the viscous damping constant, $\delta_{visc} \cong (8\pi\eta f_M/3\gamma P_0)$, is proportional to the viscosity of the liquid. Therefore at 30°, η = 2 P and $\delta_{visc} \cong 66$. The number of cycles required for the amplitude of motion to be reduced to $\exp(-\pi)$ of its original value is the Q (quality factor) of the bubble system. Q may be defined as $\delta_{visc}^{-1} = f_M/\Delta f$, and in our case $\Delta f = 6.6 \times 10^6 \times 66 = 440$ MHz. $\Delta f = f_2 - f_1$, where f_1 and f_2 are the frequencies at which the sound absorption has been reduced to one half the value at f_M. Such a large value of $\Delta f/2 = 220$ MHz is not justified by the experimental data.[3]

From these results it appears that bubbles are not involved in the sound absorption differences and that some other factor must be. Perhaps it is the strong ultrasonic field treatment;[1] sonoration is known to cause structural degradation.[4] We will not inquire as to other possible reasons for the discrepancies of the data.

We have found that the application of vacuum alone to the molten salt did not have any measurable effect on the ultrasonic results. Salts from two different manufacturers were used (Figure 2). Whether the salt was simply melted or filtered under house vacuum (30 mm) at 50° through a 10-μm pore size glass frit was inconsequential with respect to the absorption. The composition of the clear fluids used here was nominally $Ca(NO_3)_2 \cdot 4H_2O$, but known in each case to ±0.01 mol of H_2O/mol of salt.

Examination of Figure 2 shows that fair reproducibility with our previous results can be obtained if the composition of the melt is $Ca(NO_3)_2 \cdot 3.8H_2O$ instead of the previously reported $4H_2O$. The difference in the sound absorption of the two melts is due to the great dependence of the viscosity upon their composition. An error of 0.5% absolute would change the molar composition by 0.1 mol of H_2O/mol of $Ca(NO_3)_2 \cdot 4H_2O$. Since in no way could we reproduce our 1969 data unless we adjusted the composition, we believe that a systematic chemical analysis error is the only cause of the discrepancy. Because the various physical treatments of our melts did not alter their ultrasonic characteristics, we conclude that the effect of any naturally occurring bubbles is nil and we feel that the bubble hypothesis should be rejected as irrelevant in this instance.

(2) C. Devin, Jr., *J. Acoust. Soc. Amer.*, 31, 1654 (1959).
(3) G. S. Darbari and S. Petrucci, *J. Phys. Chem.*, 73, 921 (1969).
(4) B. Carlin, "Ultrasonics," 2nd ed, McGraw-Hill, New York, N. Y., 1960, Chapter X.

Finally, Figure 2 reveals an onset of a relaxation, probably of viscoelastic nature, at high (>100 MHz) frequencies with the disappearance of the B contribution to the sound absorption as used in the equation $\alpha f^{-2} = [A/1 + (f/f_r)^2] + B$. Because of the proximity of the relaxation that we observed to the one at higher frequencies, it cannot be excluded that a mathematical description of both relaxations, as belonging to a continuous broad distribution of relaxation times, could be achieved provided data encompassing the requisite frequency range to cover all of the relaxation regions up to the pseudo-glass absorption were available.

DEPARTMENT OF CHEMISTRY
POLYTECHNIC INSTITUTE OF BROOKLYN
BROOKLYN, NEW YORK 11201

G. S. DARBARI
M. R. RICHELSON
S. PETRUCCI*

RECEIVED NOVEMBER 1, 1971

Temperature Dependence of the Drift Mobility of Electrons in Glassy 10 *M* Sodium Hydroxide Ice

Publication costs assisted by the Air Force Office of Scientific Research

Sir: The problem of electron transport and scattering mechanisms and the full interpretation of photoconductivity data in disordered systems requires a knowledge of the electron mobility. Recent measurements of electron drift mobilities in amorphous silicon[1] and in liquid hydrocarbons[2,3] show that the drift mobilities are temperature activated and suggest that transport involves transient trapping. In contrast, a recent measurement of the Hall mobility of electrons in glassy 10 *M* NaOH ice indicates that lattice phonon scattering dominates the transport process and suggests that the electron motion in this matrix can be treated in terms of a band model.[4] Here we report drift mobility measurements on electrons in glassy 10 *M* NaOH ice which confirm the applicability of a band model to this system. Also, the temperature dependence of the mobility in the high-field region shows that ionic species scattering as well as lattice phonon scattering occurs.

Glassy 10 *M* NaOH ice at 77°K efficiently traps electrons generated by γ irradiation.[5] These trapped electrons can be detrapped optically to produce photoconductivity.[6] The drift mobility is measured with a time-of-flight method,[7] using a high gain FET 148 B operational amplifier with a rise time of less than 20 μsec. A light flash produces mobile electrons near one electrode by optical detrapping of some of the trapped electrons produced by γ irradiation. These electrons drift under an applied field to the positive electrode and the time dependence of this current is observed on an oscilloscope. The cryostat used for measurements of the temperature dependence above 77°K has been described.[6] The variation of temperature below 77°K was achieved by transferring cold helium gas from a storage dewar to the experimental double dewar. The temperature inside the experimental dewar is varied by controlling the rate of gas transfer.

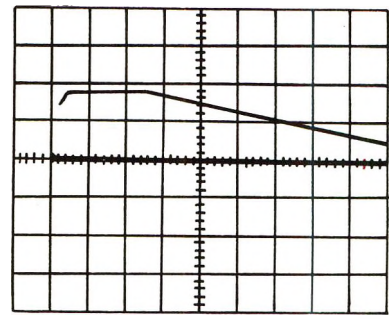

Figure 1. Oscilloscope trace of drift velocity of electrons in 10 *M* NaOH glassy ice at 77°K γ-irradiated to 0.18 Mrad at an applied field of 4 kV/cm. The vertical scale is 0.2 V/division and the horizontal scale is 20 μsec/division. The light pulse occurs where the base line trace begins. The base line trace was obtained with the light shutter closed.

After a xenon light flash, the scope signal rises to a maximum within the response time of the amplifier, is constant while the mobile electrons move across the sample, and decreases when they reach the opposite electrode. A typical oscillogram is shown in Figure 1. The time from the light flash to the break point for the decrease is taken as the transit time of mobile electrons. The transit time is determined most accurately by plotting the data on a log time scale. The drift mobility is calculated from $\mu_D = L^2/Vt$, where V is the applied voltage, t is the transit time, and L is the sample thickness (1 mm).

Figure 2 presents the temperature dependence of the drift mobility at 4 kV/cm for a γ-irradiation dose of 0.18 Mrad. All data in Figure 2 were taken on a single sample and the error in the relative drift mobility is shown by error bars which are approximately the size of the filled circles. Other samples give a similar temperature dependence and the reproducibility of the drift mobility at a given temperature is ±10%. At the field and dose used the electrons are somewhat above thermal energies and are described as "hot," as shown by photocurrents which are somewhat superohmic.[6] The drift mobility signals are too small to carry out a complete temperature dependence study at low fields, but even in the "hot" electron region the temperature

(1) P. G. LeComber and W. E. Spear, *Phys. Rev. Lett.*, **25**, 509 (1970).
(2) R. M. Minday, L. D. Schmidt, and H. T. Davis, *J. Chem. Phys.*, **55**, 3112 (1971).
(3) W. A. Schmidt and A. O. Allen, *ibid.*, **52**, 4788 (1970).
(4) I. Eisele and L. Kevan, *ibid.*, **55**, 5407 (1971).
(5) L. Kevan, *Actions Chim. Biol. Radiat.*, **13**, 57 (1969).
(6) I. Eisele and L. Kevan, *J. Chem. Phys.*, **53**, 1867 (1970).
(7) (a) R. G. Kepler, *Phys. Rev.*, **119**, 1226 (1960); (b) W. F. Spear and J. Mort, *Proc. Phys. Soc.*, **81**, 130 (1963).

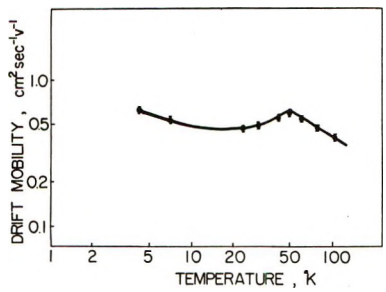

Figure 2. Temperature dependence of the drift mobility of electrons in 10 *M* NaOH glassy ice γ irradiated to 0.18 Mrad at an applied field of 4 kV/cm.

dependence, if observed, is characteristic of the type of scattering mechanism. For example, see the early results of Ryder on hot electrons in germanium.[8] At 20 kV/cm the electrons in glassy 10 *M* NaOH ice are hotter and the temperature dependence is much weaker than that shown in Figure 2. At 4 kV/cm the temperature dependence that is seen is characteristic enough to identify two different scattering mechanisms.

From 100 to 50°K the drift mobility increases as the temperature decreases. This is indicative of lattice phonon scattering and suggests that the electron motion can be treated in terms of a band model. This temperature dependence is also consistent with that found for the Hall mobility of electrons in this matrix.[4] For "ideal" bands acoustical phonon scattering leads to $\mu \propto \exp(\theta_0/T)$ for $T < \theta_0$ where θ_0 is the Einstein temperature for optical modes.[9] For 10 *M* NaOH ice $\theta \approx 151$°K.[4] The data fit a $T^{-0.7}$ dependence or an $\exp(53/T)$ dependence. This is somewhat weaker than the $T^{-1.3}$ dependence found for the electron Hall mobility at low fields. However, measurements of the drift mobility at other fields indicate that the temperature dependence becomes stronger at lower fields, and the superposition of a positive temperature dependence from an ionic species scattering mechanism, to be discussed next, also tends to weaken the measured temperature dependence for the drift mobility in the 50–100°K range. So the drift and Hall mobility data seem consistent and support a lattice phonon scattering mechanism.

Between 50 and 20°K the drift mobility decreases as the temperature decreases. This is indicative of an ionic species scattering mechanism which has a theoretical temperature dependence of $T^{1.5}$ as given by the Conwell–Weisskopf formula,[10] $\mu \propto T^{1.5}/\ln(1 + aT^2)$. The lattice phonon density decreases at lower temperatures and it appears then that ionic species scattering becomes dominant in the high-field hot electron region. The observed temperature dependence between 20 and 50°K varies only as $T^{0.54}$, but the deviation from the theoretically expected dependence is consistent with some remaining contribution from lattice phonon scattering and some deviation in the slightly hot electron region. The drift mobility temperature dependence below 15°K is also consistent with ionic species scattering and can be accounted for by the log term in the denominator of the Conwell–Weisskopf formula.

We can also identify the ionic species that serve as scattering centers as O^- and perhaps e_t^- which are produced by irradiation. Empty electron traps may also contribute as scattering centers. O^- is confirmed to be one scattering species as shown by a decrease in the drift mobility as the O^-/e_t^- ratio is increased for constant e_t^- concentration. It is also clear that the Na^+ and OH^- ions of the matrix do not serve as scattering centers because, according to estimates based on the Conwell–Weisskopf formula, such a high concentration of scattering centers is only consistent with mobility magnitudes 10^2 to 10^3 times lower than observed.

The drift mobilities in Figure 1 are about 10 times lower than the low-field Hall mobility of 4.7 ± 1.9 cm²/V sec at 80°K.[4] This is because Figure 1 applies to the hot electron region in which the drift mobility is field dependent. At 77°K we have been able to measure the field independent value of the drift mobility at 300 V/cm and obtain a value of 2 cm²/V sec. This is in good agreement with the Hall mobility and again supports the application of the band model to electron transport in 10 *M* NaOH glassy ice.

Acknowledgment. This work was supported by the Air Force Office of Scientific Research under Grant AFOSR-70-1852. Some of the instrumentation was supported by the U. S. Atomic Energy Commission under Contract AT(11-1)-2086.

(8) E. J. Ryder, *Phys. Rev.*, **90**, 766 (1963).

(9) F. J. Blatt, "Physics of Electronic Conductions in Solids," McGraw-Hill, New York, N. Y., 1968, pp 254–258. For "ideal" bands the conduction band minimum occurs at $k = 0$, where k is the wave vector.

(10) W. Shockley, "Electrons and Holes in Semiconductors," Van Nostrand New York, N. Y., 1950, pp 250–291.

DEPARTMENT OF CHEMISTRY
WAYNE STATE UNIVERSITY
DETROIT, MICHIGAN 48202

TIMOTHY HUANG
IGNATZ EISELE
LARRY KEVAN*

RECEIVED JANUARY 3, 1972

Journal of Chemical and Engineering Data

APRIL 1972, Vol. 17, No. 2

TABLE OF CONTENTS